UCRL 6376
Cy 110 A

UNIVERSITY OF CALIFORNIA

Ernest O. Lawrence Radiation Laboratory

AEC RESEARCH AND DEVELOPMENT REPORT

LIVERMORE SITE

DISCLAIMER

SECRET

UNCLASSIFIED

UCRL-6376
Nuclear Rocket &
Ramjet Engines, C-86
M-3679 (24th Ed.)

This document contains 194 pages.
This is copy 110 of 154 Series A.

CLASSIFICATION CANCELLED
Date 11-26-73
R B Martin
R. B. Martin, USAEC ORO
Research & Technical Support Div.

UNIVERSITY OF CALIFORNIA
Lawrence Radiation Laboratory
Livermore, California

Contract No. W-7405-eng-48

PLUTO QUARTERLY REPORT NO. 7*

(January – March 1961)

(Title: Unclassified)

by

The Nuclear Propulsion Division Staff

April 3, 1961

*Previous Quarterly Reports

No. 1, UCRL-5699
No. 2, UCRL-5829
No. 3, UCRL-5925
No. 4, UCRL-6036
No. 5, UCRL-6143
No. 6, UCRL-6258

UNCLASSIFIED

RESTRICTED DATA

This document contains restricted data as defined in the Atomic Energy Act of 1954. Its transmittal or the disclosure of its contents in any manner to an unauthorized person is prohibited.

SECRET

DISTRIBUTION OF THIS DOCUMENT IS UNLIMITED

DISTRIBUTION

Series A

	Copy No.
LRL Livermore,	
Information Division	1 - 15
John S. Foster	16
Forrest Fairbrother	17
C. M. Van Atta	18
Gerald W. Johnson	19
Theodore C. Merkle	20 - 24
Harry L. Reynolds	25
Richard P. Connell	26
James W. Bell	27
Roger E. Batzel	28
Albert J. Kirschbaum	29
Henry C. McDonald, Jr.	30
W. Blake Myers	31 - 35
Albert J. Rothman	36
James S. Kane	37
William C. Grayson, Jr.	38
Robert W. Westbrook	39
DASA Livermore Liaison Office,	
Norman G. Hunt	40
LRL Berkeley,	
R. K. Wakerling	41
Wallace B. Reynolds	42
Hayden S. Gordon	43
LRL Mercury, Nevada,	
James L. Olsen	44
Division of Military Application, Washington,	
Brig. Gen. A. W. Betts	45
U. S. Atomic Energy Commission, Washington,	
Irving Hoffman	46 - 47
Air Force Special Weapons Center	48
Air Research and Development Command (RDRAP)	49
Air Research and Development Command (RDRRA)	50

DISTRIBUTION (Continued)

Series A

	Copy No.
Air Technical Intelligence Center	51
Air University Library	52
Albuquerque Operations Office	53
Advanced Research Projects Agency	54
Argonne National Laboratory	55
Army Ballistic Missile Agency	56 - 57
Assistant Secretary of Defense, R&D (WSEG)	58
Atomic Energy Commission, Washington	59 - 62
Atomics International	63
Battelle Memorial Institute	64
Brookhaven National Laboratory	65
Bureau of Naval Weapons	66 - 69
Bureau of Naval Weapons (SPO)	70
Bureau of Ships	71
Chicago Operations Office	72
Defense Atomic Support Agency, Sandia	73
Defense Atomic Support Agency, Washington	74
duPont Company, Aiken	75
General Electric Company (ANPD)	76 - 78
General Electric Company, Richland	79 - 80
Lockland Aircraft Reactors Operations Office	81
Los Alamos Scientific Laboratory	82 - 83
The Marquardt Corporation	84
National Aeronautics & Space Administration, Cleveland	85 - 86
National Aeronautics & Space Administration, Washington	87 - 88
New York Operations Office	89
Oak Ridge Operations Office	90
Office of Naval Research	91
Office of the Assistant for Operations Analysis DCS/O	92
Office of the Chief of Naval Operations	93
Patent Branch, Washington	94
Phillips Petroleum Company (NRTS)	95

DISTRIBUTION (Continued)

Series A

	Copy No.
Pratt and Whitney Aircraft Division	96
San Francisco Operations Office	97
Sandia Corporation	98
School of Aviation Medicine	99
Union Carbide Nuclear Company (ORNL)	100
USAF Project RAND	101 - 102
U. S. Naval Postgraduate School	103
Wright Air Development Division	104 - 109
Office of Technical Information Extension	110 - 154

PLUTO QUARTERLY REPORT NO. 7

Table of Contents

	Page No.
CHAPTER I – TORY II-A	7
Section I – Neutronics	7
Section II – Aerothermodynamics	11
Section III – Engineering	13
CHAPTER II – MATERIALS DEVELOPMENT AND PILOT PLANT ACTIVITIES	34
Section I – Process and Materials Development	34
Section II – General Chemistry	63
CHAPTER III – TORY II-C	73
Section I – Neutronics	73
Section II – Aerothermodynamics	93
Section III – Engineering	109
TABLE OF CONVERSIONS	6

TABLE OF CONVERSIONS

°C	°F	°C	°F	°C	°F
0	32	650	1202	1250	2282
50	122	700	1292	1300	2372
100	212	750	1382	1350	2402
150	302	800	1472	1400	2552
200	392	850	1562	1450	2642
250	482	900	1652	1500	2732
300	572	950	1742	1550	2822
350	662	1000	1832	1600	2912
400	752	1050	1922	1650	3002
450	842	1100	2012	1700	3092
500	932	1150	2102	1750	3182
550	1022	1200	2192	1800	3272
600	1112				

Btu/second-in^3	=	1.82 megawatts/foot^3
Btu/second	=	1.0548 kilowatts
Btu/hour-ft^2-°F	=	5.676×10^{-4} watt/cm^2-°C
Btu/lb-°F	=	1.0 calorie/g-°C
calorie	=	4.186 joules or watt-seconds
pound	=	454 grams
inch	=	2.54 centimeters
cubic foot	=	1728 cubic inches
cubic inch	=	16.387 cubic centimeters
megawatt-day	=	1.05 gram U^{235} fissioned (200 Mev per fission)
pound/ft^2	=	0.4882 gram/centimeter^2
pound/in^2	=	70.30 grams/centimeter^2
barn	=	10^{-24} centimeter^2
gravity (g)	=	980.7 cm/sec^2 = 32.17 ft/sec^2

PLUTO QUARTERLY REPORT NO. 7

(January – March 1961)

Lawrence Radiation Laboratory, University of California
Livermore, California

CHAPTER I. TORY II-A

SECTION I. NEUTRONICS

TORY II-A-1

The measured vane angle for cold criticality was very nearly 64 degrees, a position which was exactly predicted on the basis of perturbation studies applied to the findings of the Livermore tests. It is pertinent to point this out since the absolute, computed effective multiplication factor is still nearly 4% higher than that which is experimentally measured.

This 4% difference between calculation and experiment takes into account the recently established resonance absorption integral of 0.9 barn per atom above 3 kev for R-235 Hastelloy material. The effect of this resonance from Hastelloy tension tubes and the shroud amounts to 2.8% in reactivity.

A 500-foil activation study was made. Figure I-1 shows the radial power distribution of the reactor. Each point represents an integration over the core length. Considerable scatter of measured data points up to ±7% is observed. Those points that fall above the average suggest the presence of hot spots in the reactor. The temperature of fuel tubes in the after end of the reactor will be raised beyond the design temperatures, and the corresponding channels in the base plate will be subject to air at somewhat higher temperatures than anticipated. No positive correlations have been established between the hotter channels and proximity to structural components in the core. Azimuthal variations at the core's radial periphery were clearly correlated with the poison of the control vanes. Variations of ±5% in channel power were seen. It is assumed that the apparent scatter is due to both the discrete allocation of fuel classes and the inherent variation of fuel concentrations per class. The latter may be as high as ±2.5%. The rise of power near the core center in Fig. I-1 is very likely due to 23 unfueled temporary tube columns in the central module.

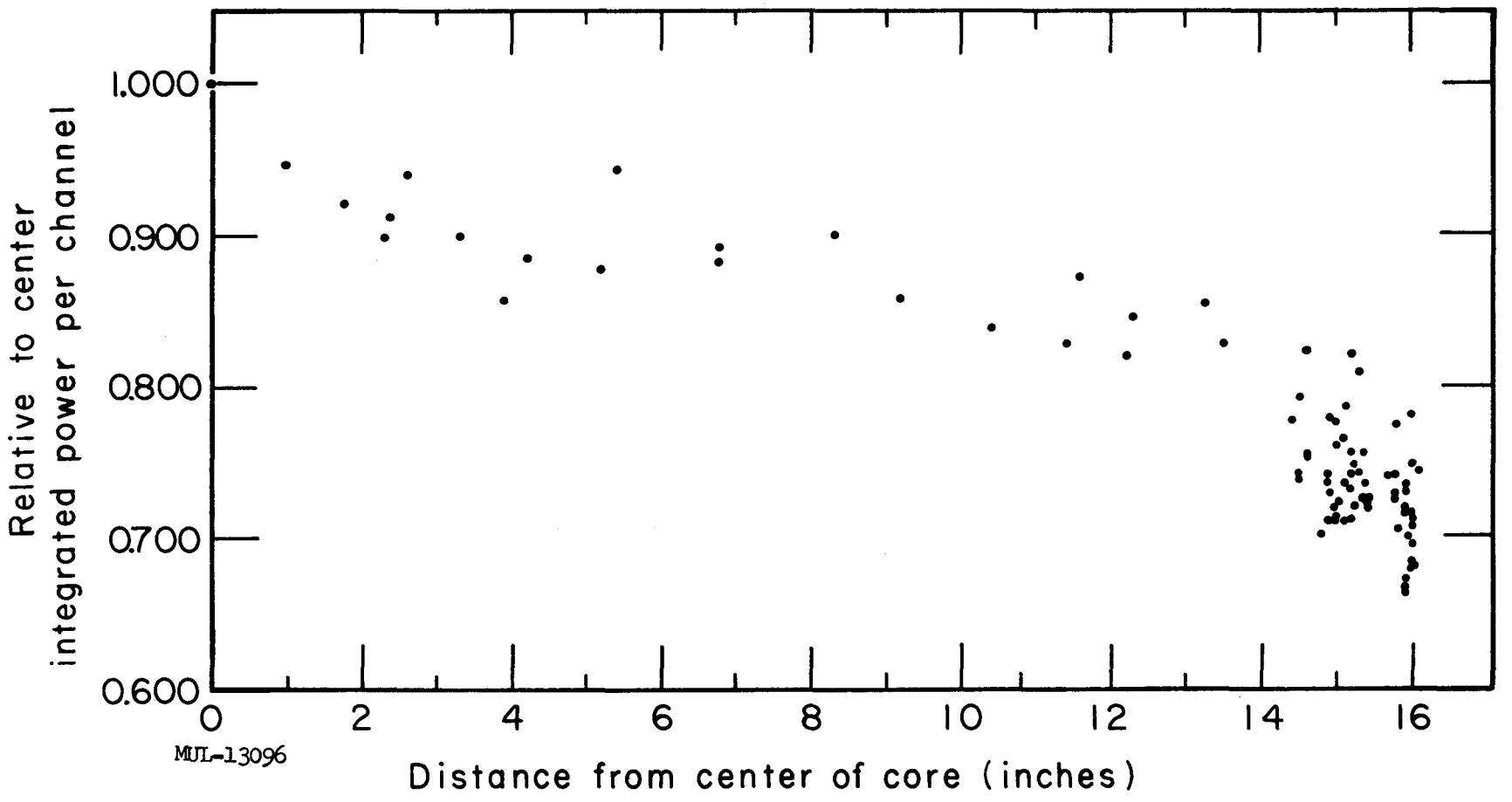

Fig. I-1. Tory II-A-1. Measured relative radial power distribution. (NTS, Dec. 9, 1960). Average core temperature about 300°K. Critical vane angle of 64 degrees.

A power profile, measured axially at the core center, is shown in Fig. I-2. Calculated values are in good agreement with experiment. In the front BeO reflector, where calculated power densities are somewhat higher, it must be noted that unshielded cross sections for uranium have been used, whereas the foils were 0.001 in. thick. Self-shielding is expected to decrease the calculated data, thus giving still better agreement with experiment.

On the basis of these fission traverses, and from results of machine calculations, a flat radial power distribution is presently predicted for high-temperature operation, for the vane angle of 105°. Contributions from gamma heating have been taken into account. This is the anticipated critical vane angle for high-power, high-temperature operation. The half-way insertion of two vernier rods has been taken into account in arriving at the 105° vane angle prediction.

It is of interest to note that recent measurements on simple, BeO-moderated, critical assemblies at Livermore have permitted a determination of the effective delayed neutron fraction as 0.0088. This value is considerably higher than the hitherto accepted number of 0.0065. Curiously enough, if one compares the 0.11% in k_{eff}, which is calculated for 1 degree of vane motion at the critical point, with the \$0.125 of measured change in reactivity due to the same perturbation, as reported from NTS, one obtains the same value of 0.0088. Besides the criticism that can be raised against the latter comparison of calculated to measured data, an experimental uncertainty of at least 10% must be considered. However, Zoom results bearing on the worth of the delayed neutron fraction in a typical Tory II-A-1 core configuration render a value of $\beta_{eff} = 0.0069$. This matter is being pursued further because of its significance for the Tory II-C reactor design.

TORY II-A-2

As to the Tory II-A-2 reactor, a 21.6% increase in the fuel mass above that of the A-1 core is recommended. This increase is based on subsequent assumptions:

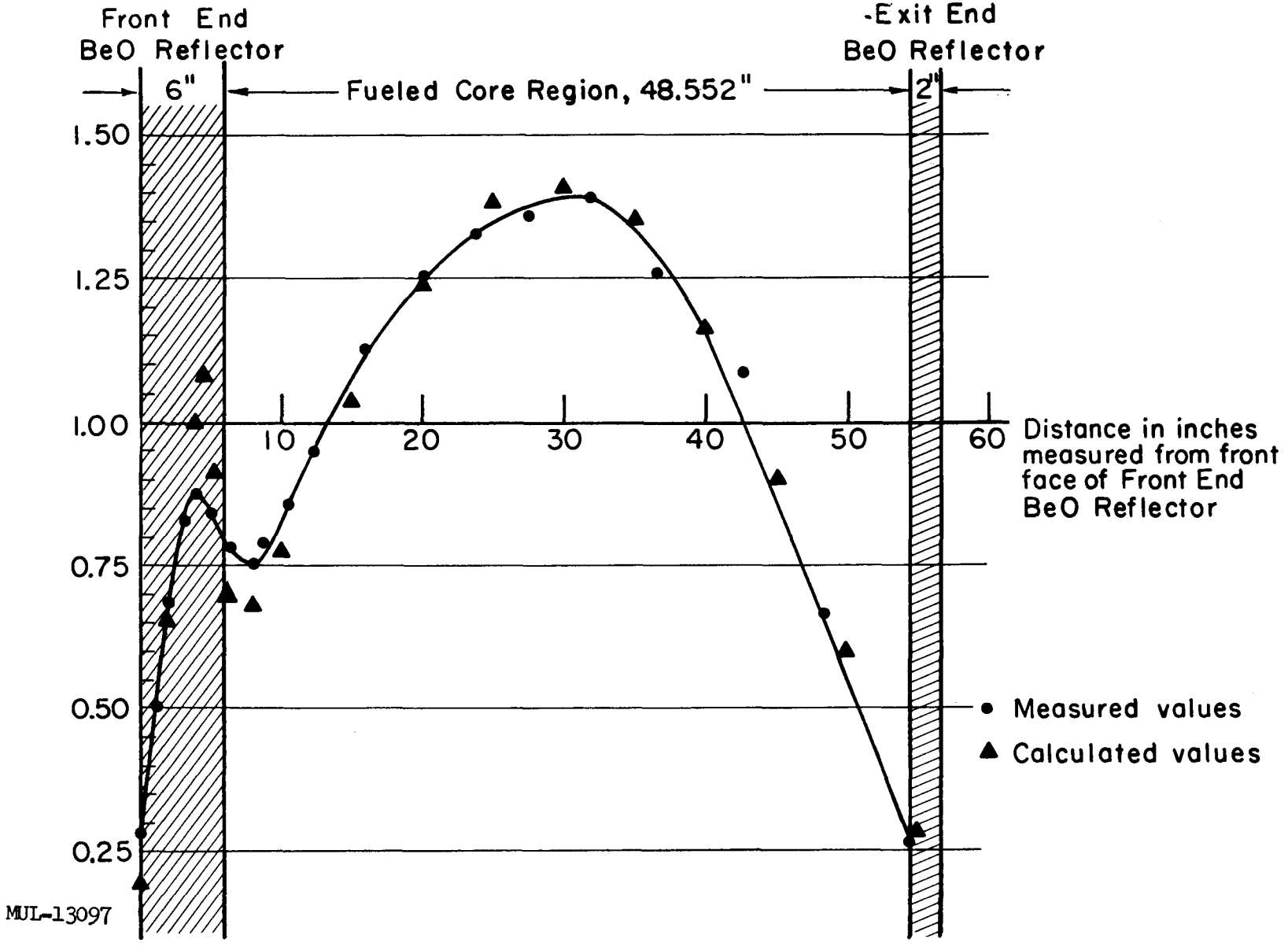

Fig. I-2. Tory II-A-1. Measured axial power distribution at core center. (Data taken from foil activation experiment, NTS, Dec. 9, 1960.)

	$\Delta k_{eff} \times 10^2$
a. A medium core length of 44.506 in. instead of 48.552 in.	- 1.71
b. An effective average fueled BeO density of 0.987 instead of 0.975 of the maximum theoretical value.	+ 0.90
c. An average cobalt content in tension tubes of 0.64 wt % instead of 0.14 wt %.	- 0.75
d. Heavy water coolant in the side reflector as it is now used with the A-1 reactor.	---
	- 1.56

A reactivity reserve of approximately 1.4% has been included to provide for unforeseen eventualities, e.g., for low densities in the central module prototype BeO plates. In case of overfueling, it should be noted that a - 1% adjustment in reactivity can be effected by a partial closure of the graphite reflector halves, e.g., by a 3-inch gap.

The fuel chart for the Tory II-A-2 reactor is taken over from its predecessor, the Tory II-A-1 core, except for a uniform 4 class increase in loading. The maximum fuel concentration for this core is then found to be 9.34 wt %.

SECTION II. AEROTHERMODYNAMICS

TORY II-A

Cold Blowdown Experiments. The Tory II-A-1 reactor was successfully cold-flowed in Nevada and the results of these tests can be summarized by stating that no reactor flow problems were encountered for flow rates up to 342 pps with cold inlet air. Measured pressure levels agreed with predicted values to within the limit of error of the transducers. Observed structural strains also agreed with the strains predicted.

As expected, acoustical trumpeting occurred during the interval in which the flow rates were greater than 81 pps and less than 187 pps. Although the absolute force levels induced into the reactor system by this flow phenomenon are not presently known, no test-induced damage to the reactor was noted at the conclusion of the experiments.

Stored-Energy Heater Analysis. The Tory II-A stored-energy heater was evaluated for several types of blowdowns. The analysis was performed using a five-zone lumped parameter model on the analog computers. The analog results were validated by application of the Hot-N-Tot IBM 7090 code developed for general stored-energy heater analysis. The computer programs, with typical Tory II-A heater results, are presented below.

Demonstration Run – 40 Mw. Three types of demonstration runs have been considered. These types are differentiated by the magnitude of the inlet gas temperatures employed. The three inlet gas temperatures are 80°F, 400°F, and 1060°F.

Expected reactor parameters for 40-Mw power, 2250°F maximum fuel-element wall temperature, and each inlet gas temperature are as follows:

Inlet Air Temperature = 80°F*

Maximum temperatures:

Fuel element	= 2266°F
Shroud	= 121°F
Tie rods	= 438°F
Dogbones	= 1900°F
Base plates	= 1987°F

Overall reactor parameters:

Flow rate	= 103 pps
Inlet total pressure	= 49 psia
Exit nozzle total pressure	= 28 psia
Exit nozzle total temperature	= 1493°F

Inlet Air Temperature = 400°F†

Maximum temperatures:

Fuel element	= 2266°F
Shroud	= 443°F
Tie rods	= 731°F
Dogbones	= 1920°F
Base plates	= 2022°F

---

*Minor reactor modifications are required for operations at this inlet air temperature.

†Present plans are that this inlet temperature will be the one used for the demonstration run.

Overall reactor parameters:

Flow rate	=	114 pps
Inlet total pressure	=	58 psia
Exit nozzle total pressure	=	31.46 psia
Exit nozzle total temperature	=	1655°F

Inlet Air Temperature = 1060°F

Maximum temperatures:

Fuel element	=	2266°F
Shroud	=	1096°F
Tie rods	=	1300°F
Dogbones	=	1950°F
Base plates	=	2079°F

Overall reactor parameters:

Flow rate	=	167 pps
Inlet total pressure	=	93 psia
Exit nozzle total pressure	=	49 psia
Exit nozzle total temperature	=	1880°F

SECTION III. TORY II-A ENGINEERING*

MARMAN CLAMP FAILURE

During an air-supply-system qualification run on January 11, the forged four-segment Marman V-band clamp joining the exit nozzle to the duct turning section parted. The nozzle was thrown some 480 ft, bouncing twice in soft sand and landing essentially undamaged (Fig. I-3). There was no reactor core in the duct. The alternate heat shield was severely warped by the hot supersonic flow following failure. Several pressure rakes were also deformed or carried away. There does not appear to be any further damage due to this cause.

Several factors seem to have contributed to the clamp failure, perhaps all of them necessary conditions.

---

*See page 33 for correction to last Quarterly Report (UCRL-6258) regarding double buggy springs.

Fig. I-3. Tory II-A nozzle, 480 ft from test vehicle, in landing position.

1. The clamp material was improperly processed in fabrication.
2. Sensitized material was converted to an unsafe condition by exposure.
3. Loads were concentrated due to low-order articulation, tolerance accumulation, and possible warping from the austenite to martensite transformation.

The clamp material, AM355, a precipitation-hardening stainless steel, was delivered to the fabricator as a forged ring in what was to be the overtempered martensite form for subsequent machinability. This form is stable below 1000°F and ductile, but does not have the potential strength for the composition. Due to abnormally large grains, the material was actually in mixed form, overtempered martensite plus austenite, and potentially brittle if cooled sufficiently to transform the austenite to martensite. The clamp was machined and delivered without the normal subsequent austenite-martensite-temper (SCT) cycle. Such a cycle only optimizes properties generally, in this instance it was crucial to the utility of the alloy. Figures I-4 and I-5 contrast the clamp material with the bolt material which was properly heat treated.

The broken clamp is shown in Fig. I-6. The sequence of failure as indicated primarily by the predominant bending mode of failure in the bolt (Fig. I-7) is believed to have begun near the top end of the upper (west) segment and continued through the parting of that segment, the top hinge and the (east) bolt as the clamp unfolded. Figure I-8 shows the final position of the upper (east) segment. Figure I-9 shows the three-segment assembly as it fell, probably executing a half turn to finish with the bottom up. The small triangular portion was found near the single segment on the east side of the building.

There were four forged 36-in. clamps on the duct for this run, and they all had a similar fabrication history.

Carrying of a sample from the broken clamp through the austenite-martensite-temper (SCT) cycle increased the room-temperature Charpy V-notch impact strength to a more acceptable 15 ft-lb in contrast with an unacceptable 2 ft-lb strength for an untreated specimen. As a result, all seven of the forged 36-in. clamps have been given the SCT treatment.

After the SCT treatment, three segments of the 28 processed were found to be cracked in the inner fillet near an end. These cracks may have been preexisting; it has been noted that the cracks seem to correlate with the abundance of delta ferrite in the material. This in turn has been correlated with variations in the nitrogen content. Samples are now being analyzed for nitrogen to

Fig. I-4. Forged Marman clamp, electro-etched after cathodic etching to bring out tempered martensite. Light area was retained austenite, subsequently transformed at NTS, darker area is the tempered martensite. (100×)

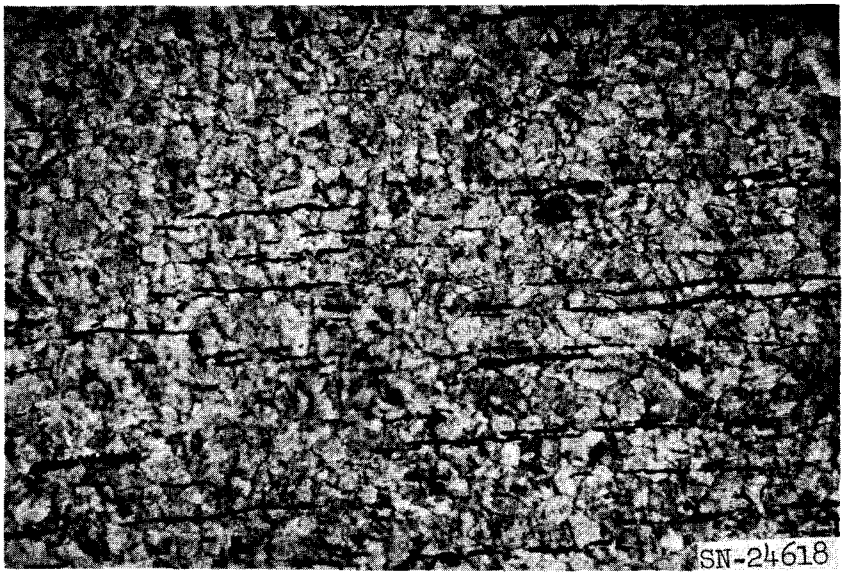

Fig. I-5. Marman clamp bolt, 100% tempered martensite. Electro-etched. (100×)

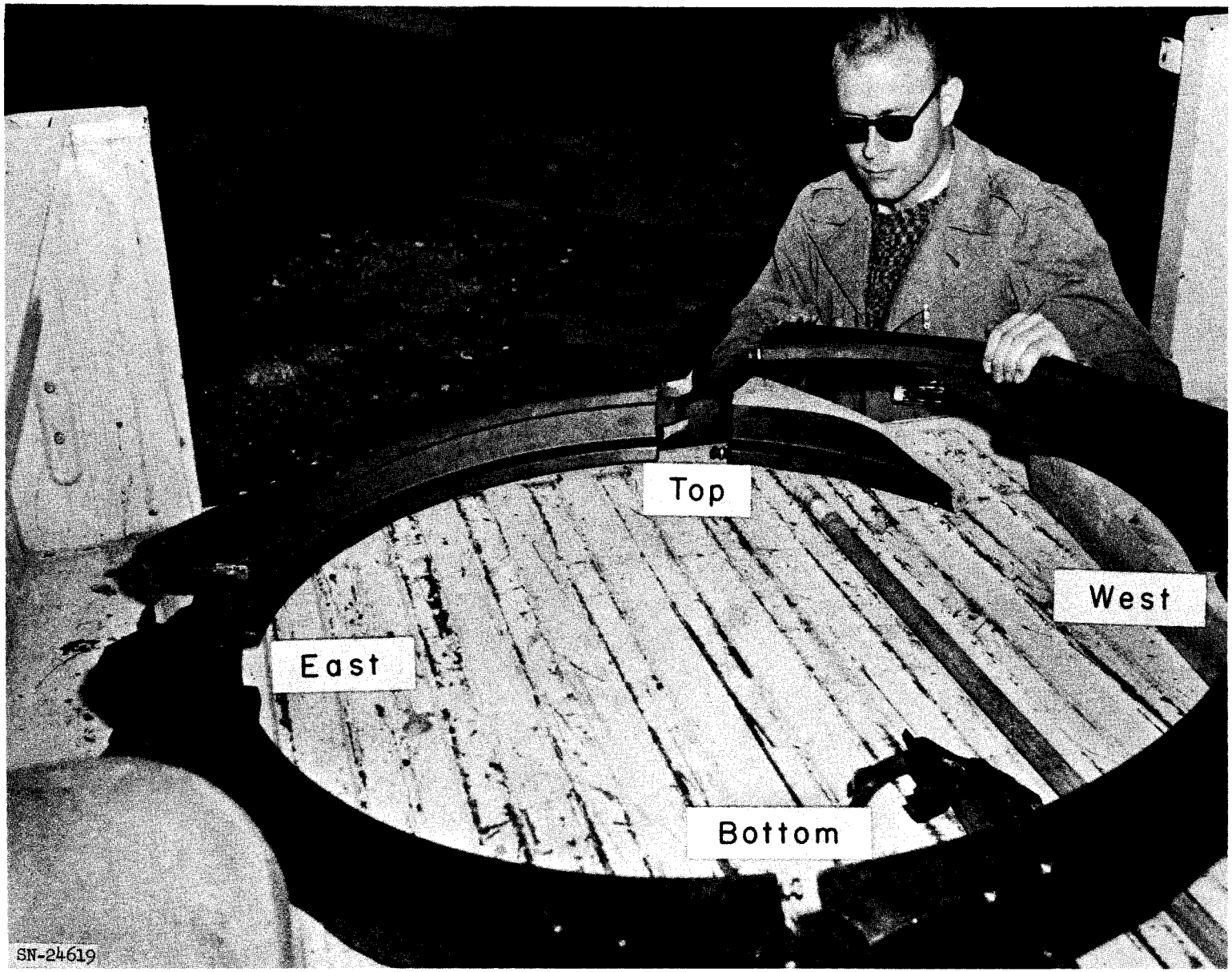

Fig. I-6. Broken Marman clamp.

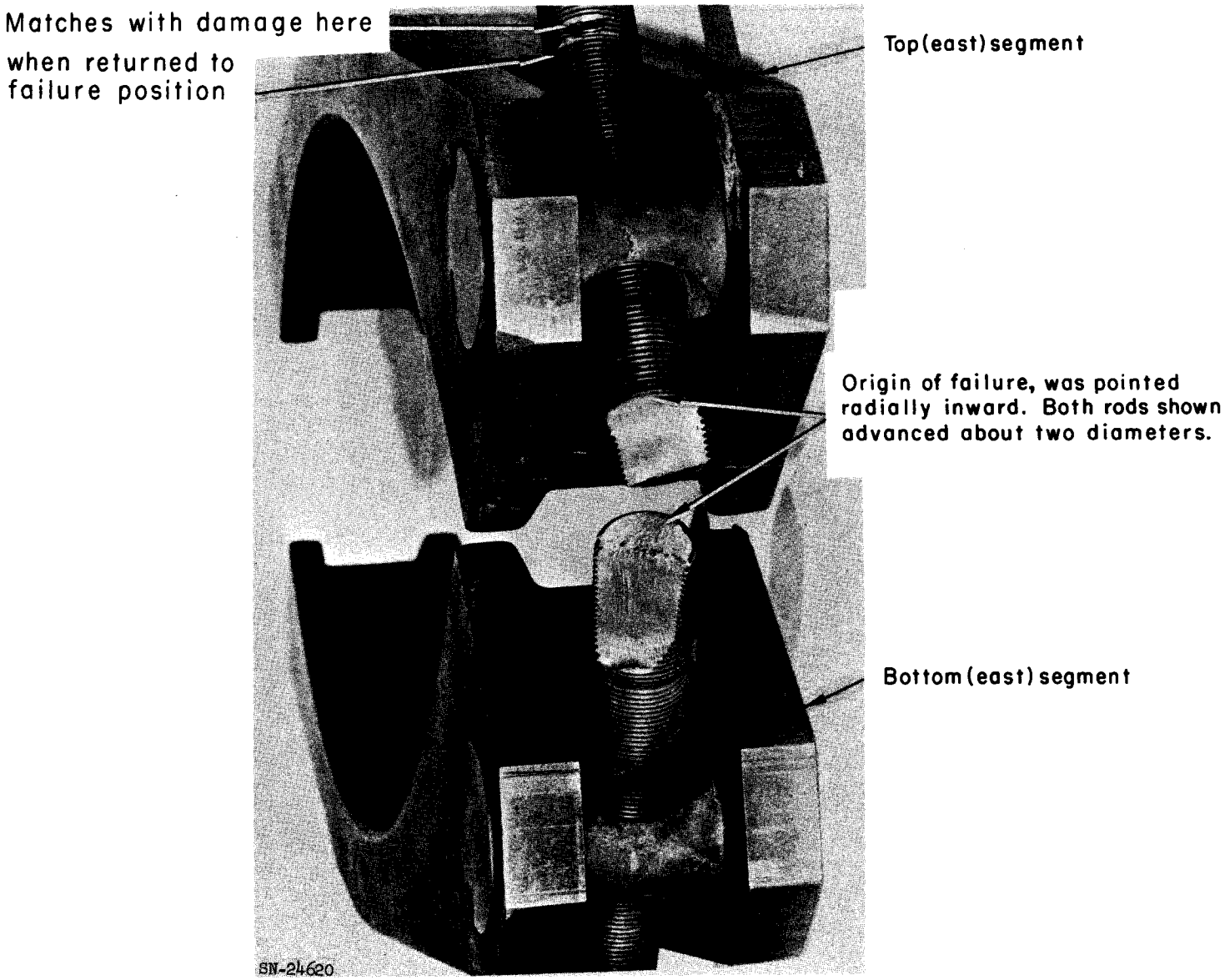

Fig. I-7. View of Marman clamp bolt after failure.

Fig. I-8. Segment of Marman clamp as it landed after failure.

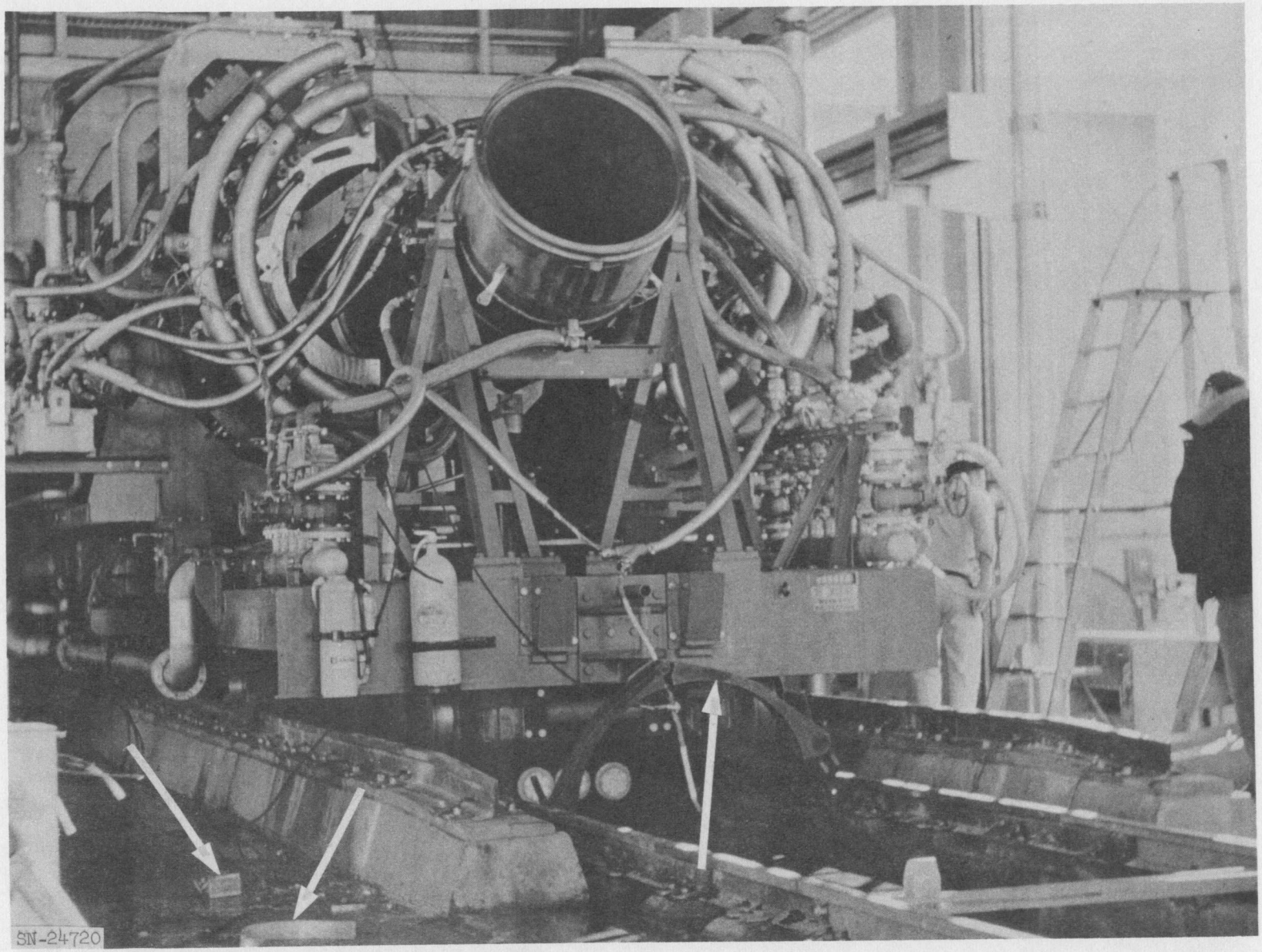

Fig. I-9. Three-segment assembly of Marman clamp as it fell.

allow a service recommendation. Table I-1 summarizes the properties for material from one of these three cracked segments and probably serves as an indication of the minimum properties to be expected from the forged parts. Figures I-10 and I-11 contrast the delta ferrite problem.

A total of six clamps have been realized from the SCT program. They have been further processed as follows:

1. Magnaglo inspected for cracks with negative results.
2. Remachined to reduce load concentrations in the conical contour and in the external fitments by a factor of about 2.
3. Zyglo inspected for cracks with negative results.
4. Electrofilmed to reduce the friction coefficient on the conical surfaces.
5. Hydrostatically tested once each to 800 psi at room temperature with a maximum recorded strain equivalent to 147,000 psi on an elastic basis and with a residual strain less than 5×10^{-5} in./in.
6. Hardness tested with a range of Rockwell C: 38-44.
7. Chemically analyzed (no results to date).
8. Fifteen strain gages have been placed on each assembly.

The balance of the clamps installed for the subject run (3-36-in. and 5-24-in., except the forged A182-F5a 24-in. remote disconnect clamp) were cast from AM355 material. They had been given the final austenite-martensite-temper cycle and a sample was actually reduced in Charpy V-notch strength by a repetition of this cycle (Fig. I-12).

Figure I-13 shows the properties of samples from a cast segment. The low impact strengths have been attributed to a coarse grain structure (1/8- to 1/4-in. grains at 1×) and have led to a service requirement of 300°F as the minimum operating temperature.

The entire stock of cast clamps (6-36-in. and 5-24-in.) were processed as listed for the forged clamps except that:

1. Magnaglo inspection revealed a prevalence of indications similar to those shown in Fig. I-14 in the inner cylinder between conical surfaces. These are believed to be magnetic as well as structural discontinuities (e.g., hot tears filled with stable austenite) which will substantially restrict service conditions.
2. Only the 36-in. clamps have been hydrostated. The 24-in. clamps are to be tested at NTS. The hydrostatic test pressure was limited by a

Table I-1.

An AM355 forged Marman clamp was given the SCT heat treatment. It cracked in a fillet at the thickest cross section. The following data are for this clamp.

Chemistry

	AM355 Heat treat crack	AM355 Composition range
Cr	15.44 ± 0.05%	15 - 16
Ni	4.0 ± 0.1%	4 - 5
Mn	0.95 ± 0.05%	0.50 - 1.25
C	0.11 ± 0.01%	0.10 - 0.15
N	0.07 ± 0.01%	0.07 - 0.13

Mechanical Properties (room temp)

Tensile: (Cross head 0.020-0.050 in./min)

	Yield (psi)	Ultimate (psi)	Elongation (%)
Transverse	165,300	176,800	9.75
	165,400	178,400	8.5
	164,800	177,500	9
Longitudinal	138,000	176,900	14.1
	137,300	177,000	14.2
	136,900	176,800	14.6

Charpy V-Notch Impact Strength (ft-lb)

	Room temp	300°F
Transverse	4	11-1/4
	4-3/4	13
	3-1/2	
Longitudinal	10-3/4	31-1/4
	11	29-1/4
	13-1/4	34-1/2

Fig. I-10. Forged AM355 Marman clamp which failed in Nevada. Later given the SCT heat treatment and exhibited 15 ft-lb transverse impact at room temperature. Longitudinal section, cathodically etched. (100×)

Fig. I-11. Forged AM355 Marman clamp which cracked during SCT heat treatment. Longitudinal section, cathodically etched. (100×)

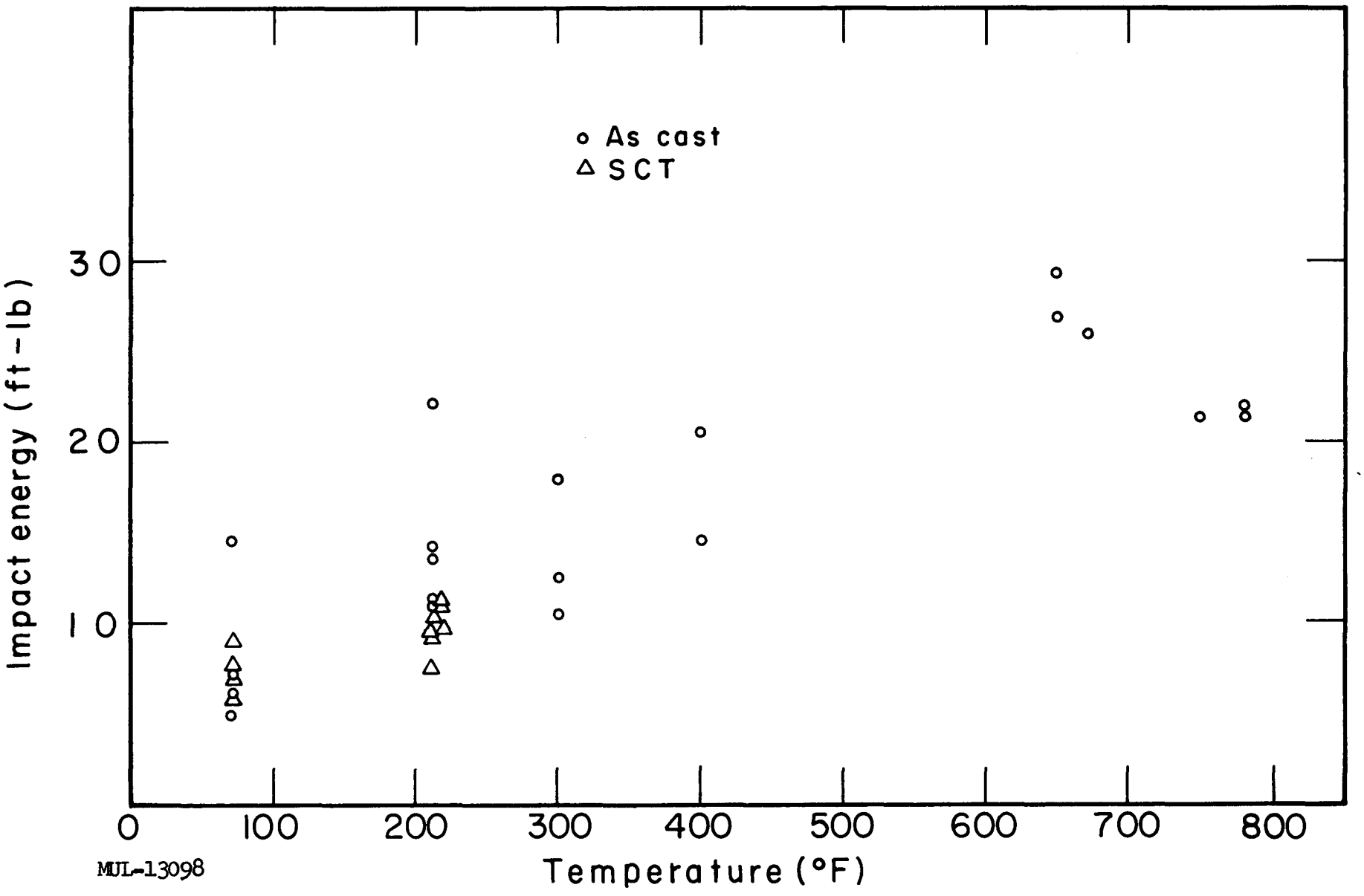

Fig. I-12. AM355 cast Marman clamp. Charpy V-notch, longitudinal and transverse.

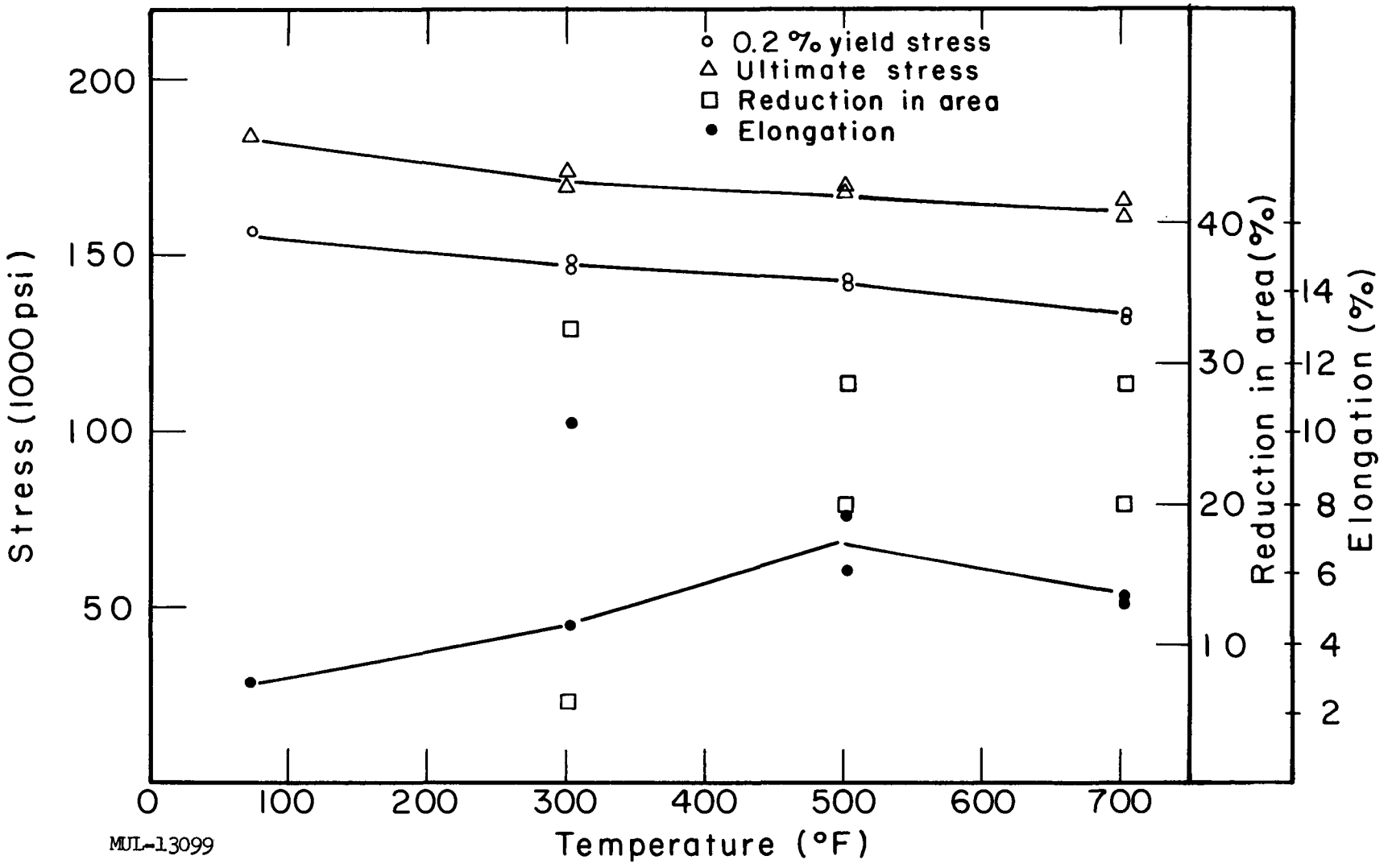

Fig. I-13. AM355 cast Marman clamp, as received. Longitudinal and transverse tensile test.

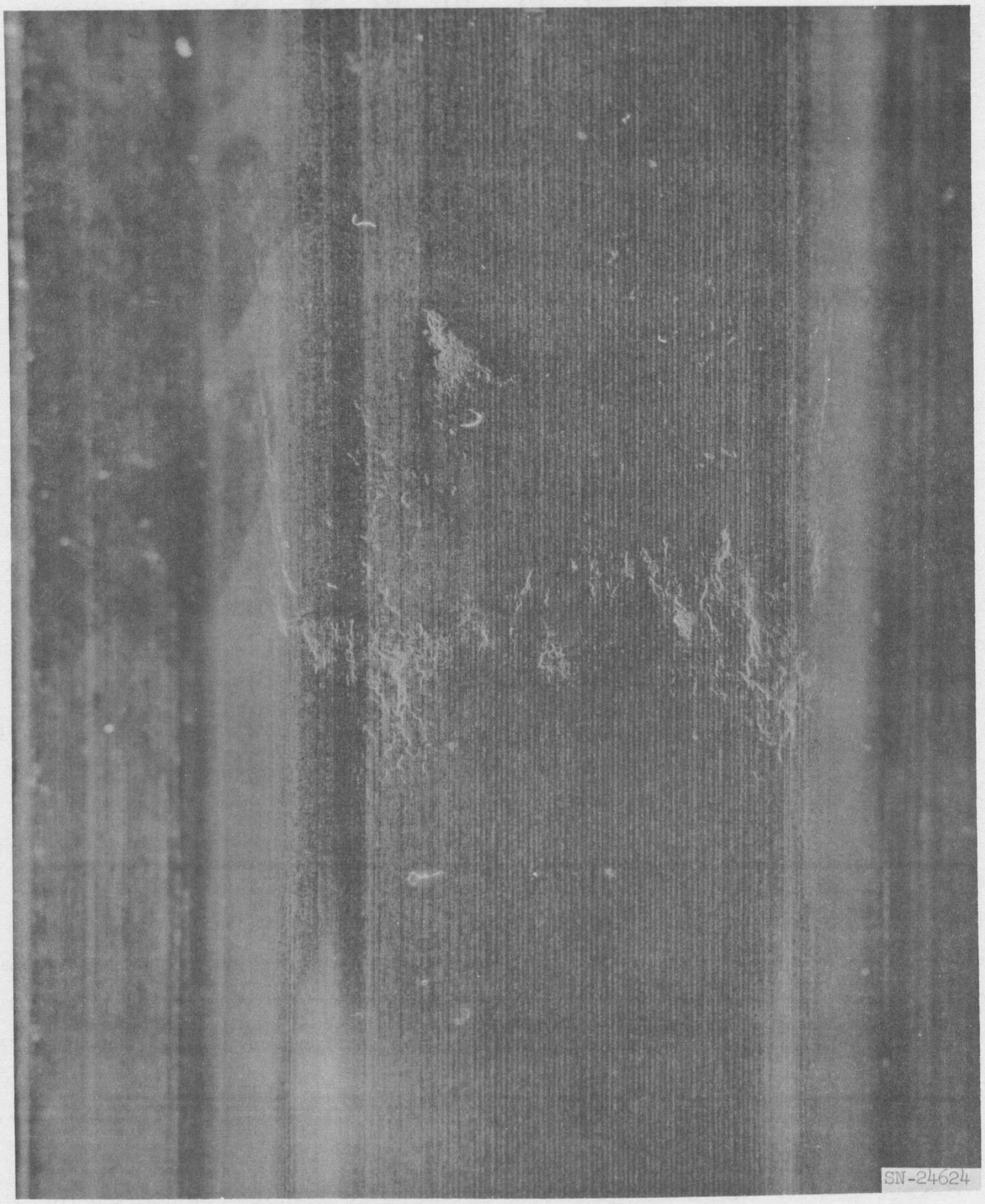

Fig. I-14. Magnaglo inspection of Marman clamp.

150,000-psi elastic stress indication; this gave a range of 620 to 750 psi and in one case a 5% overshoot on stress. The maximum residual strain was 2×10^{-4} in./in.

3. Hardness testing gave a range of 38-45 Rockwell C.

A program for total replacement of these clamps with a 16-segment V-band using 4340 Cr-Ni-Mo steel has been initiated to allow design-point operation of the Tory II-A reactor.

A reduced power run is planned following no-core qualification runs for the present clamps where strain indications will be the guide for serviceability.

A significant portion of the service loading can be attributed to differential expansion forces. Interim service will be restricted in temperature.

TEST VEHICLE RUNAWAY

As a step in the qualification of the Site 401 Facility for planned nuclear operations in January, a remote controlled withdrawal of Test Vehicle No. 1 from the test pad was accomplished at the conclusion of no-core blowdown operations on January 11. The vehicle became disconnected from the prime mover due to a loss of radio control signal prior to switching to the main line and rolled free to the bunker face. Failure safe-break equipment had not been replaced at that time which was during the vehicle modification program.

The energy gained in the 6-ft fall was absorbed principally in deforming the main air duct supports both in the bunker (Fig. I-15) and on the vehicle (Figs. I-16 and I-17). Subsequent hydrostatic pressure testing of the alignment section (Fig. I-18) caused it to fail at a crack which has been attributed to the vehicle runaway even though it had not been seen by penetrant inspection in the interim. Figure I-19 shows the vehicle being withdrawn from the test pad following the accident.

Comprehensive Magnaglo and radiographic inspection has revealed some damage to car air ducting.

Test Vehicle No. 2 was prepared for service without controlling the delay in nuclear operations.

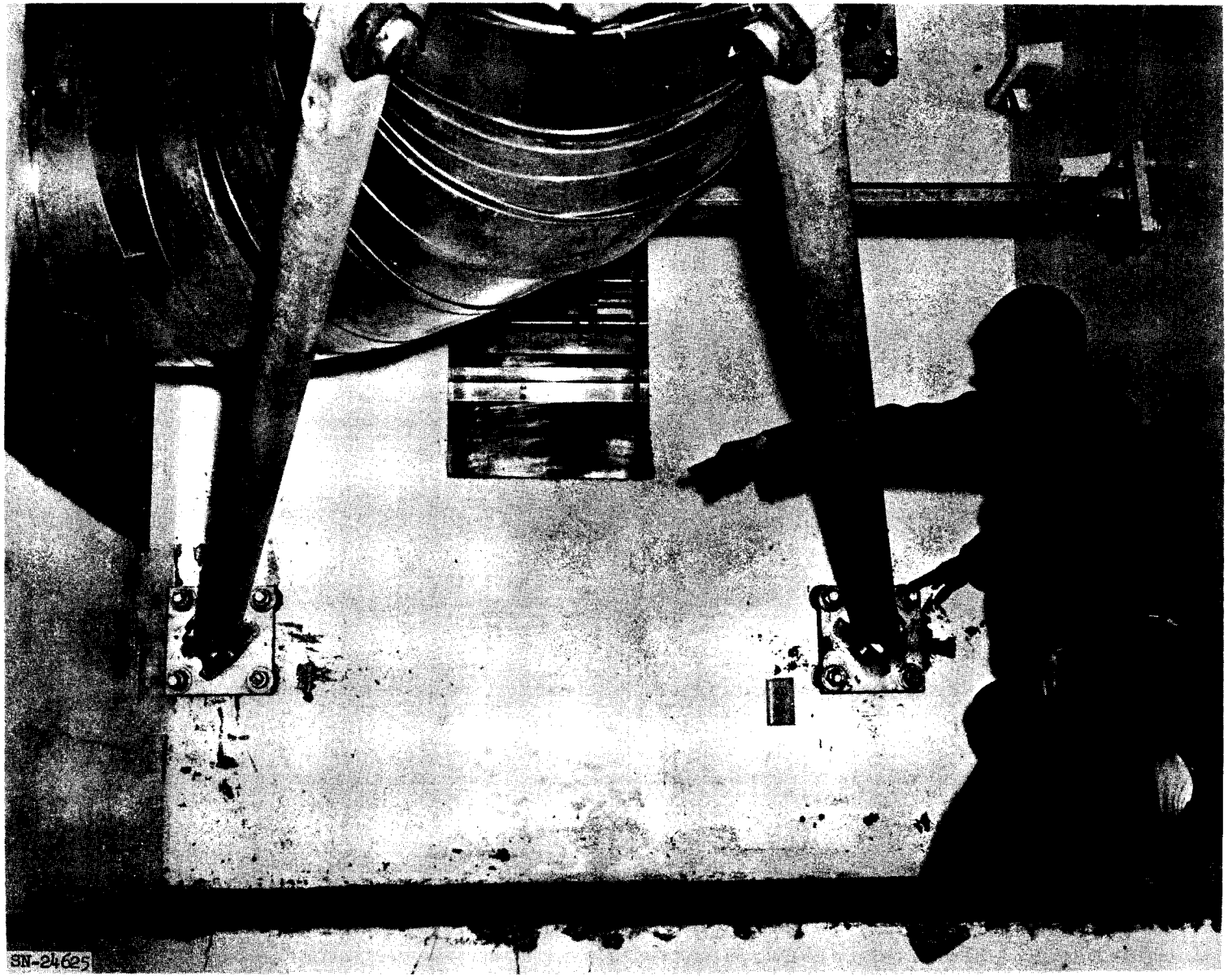

Fig. I-15. Deformation in main air duct supports in the bunker.

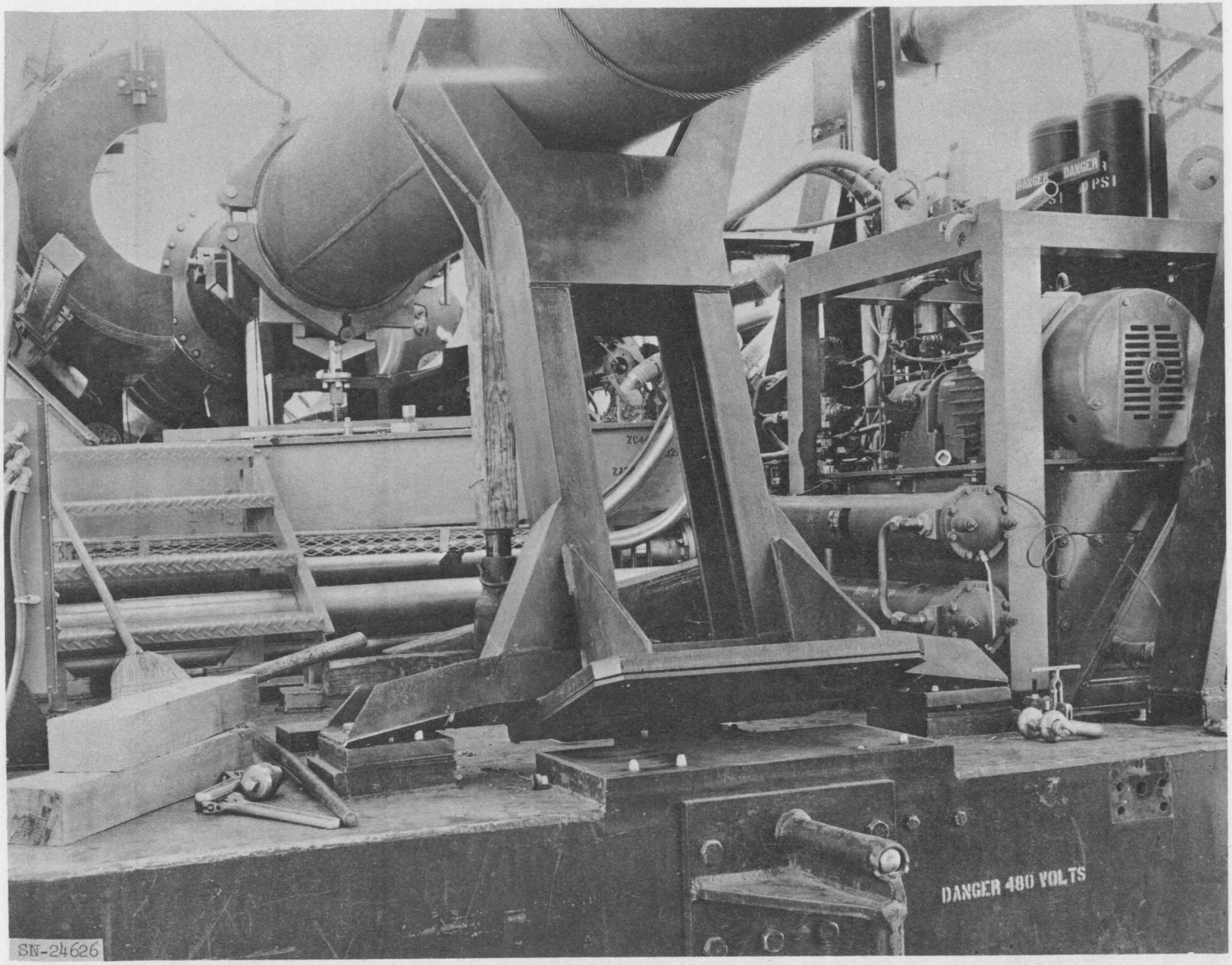

Fig. I-16. Deformation in the main air duct support on the test vehicle.

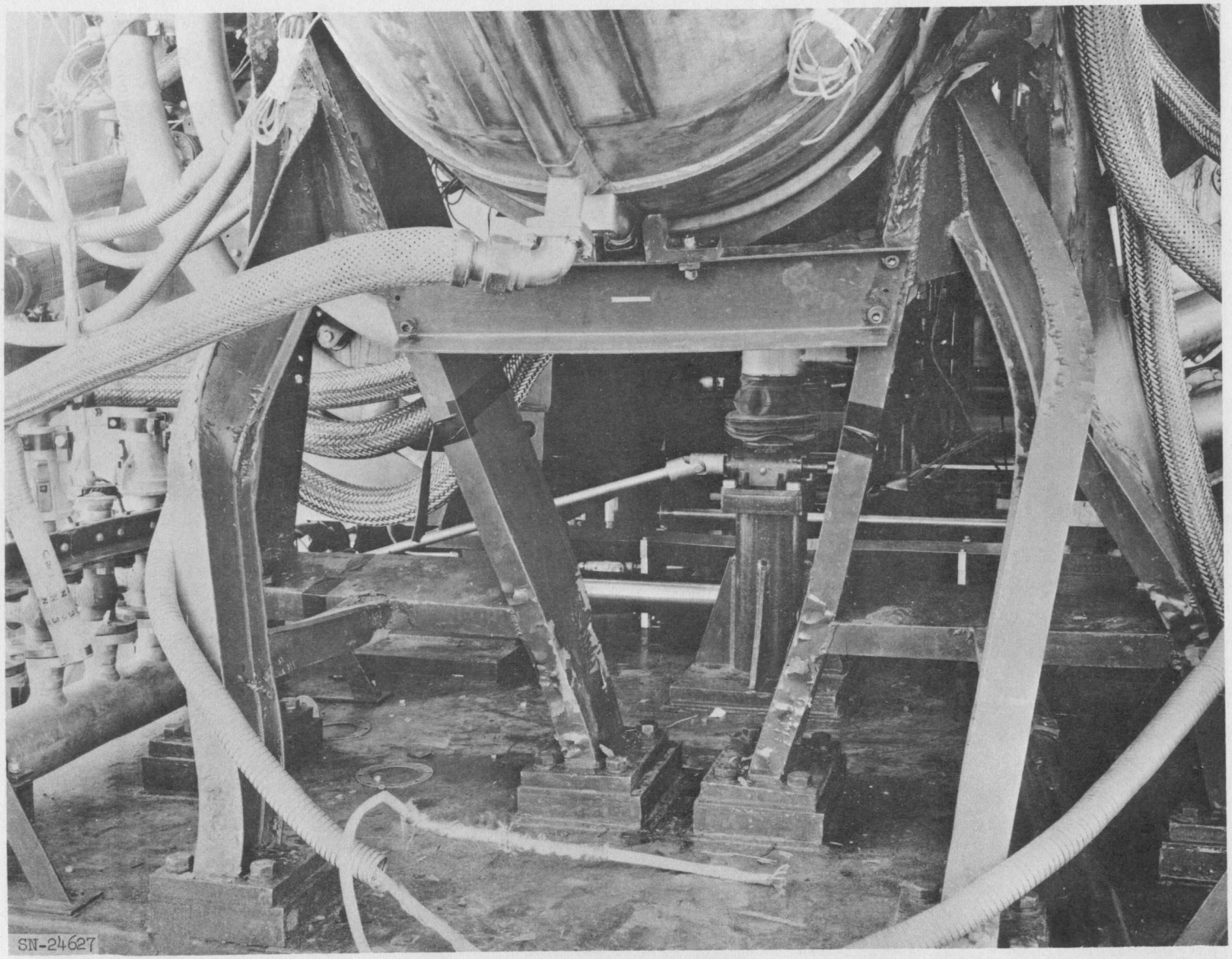

Fig. I-17. Deformation of the air duct supports on the test vehicle.

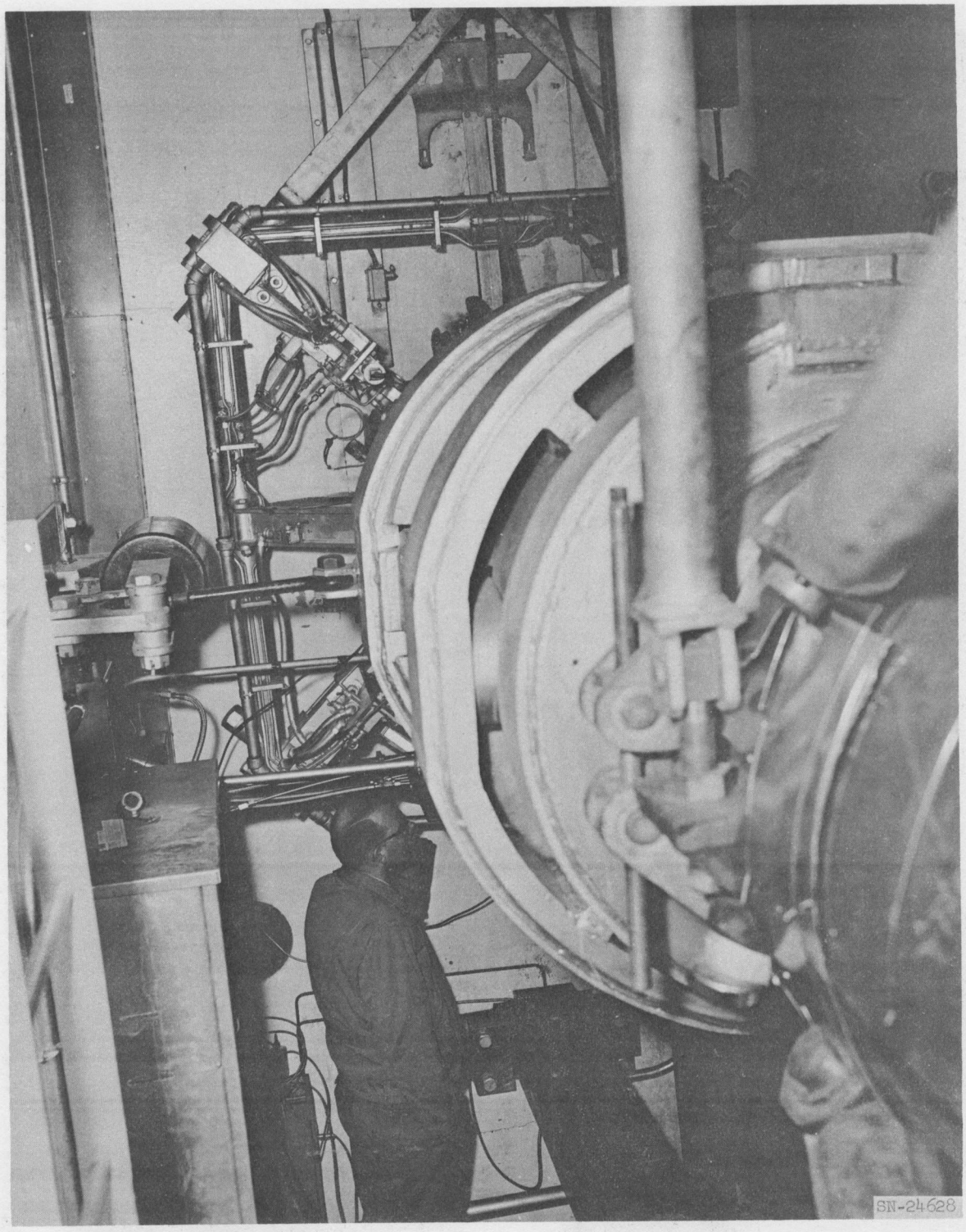

Fig. I-18. View of the alignment section.

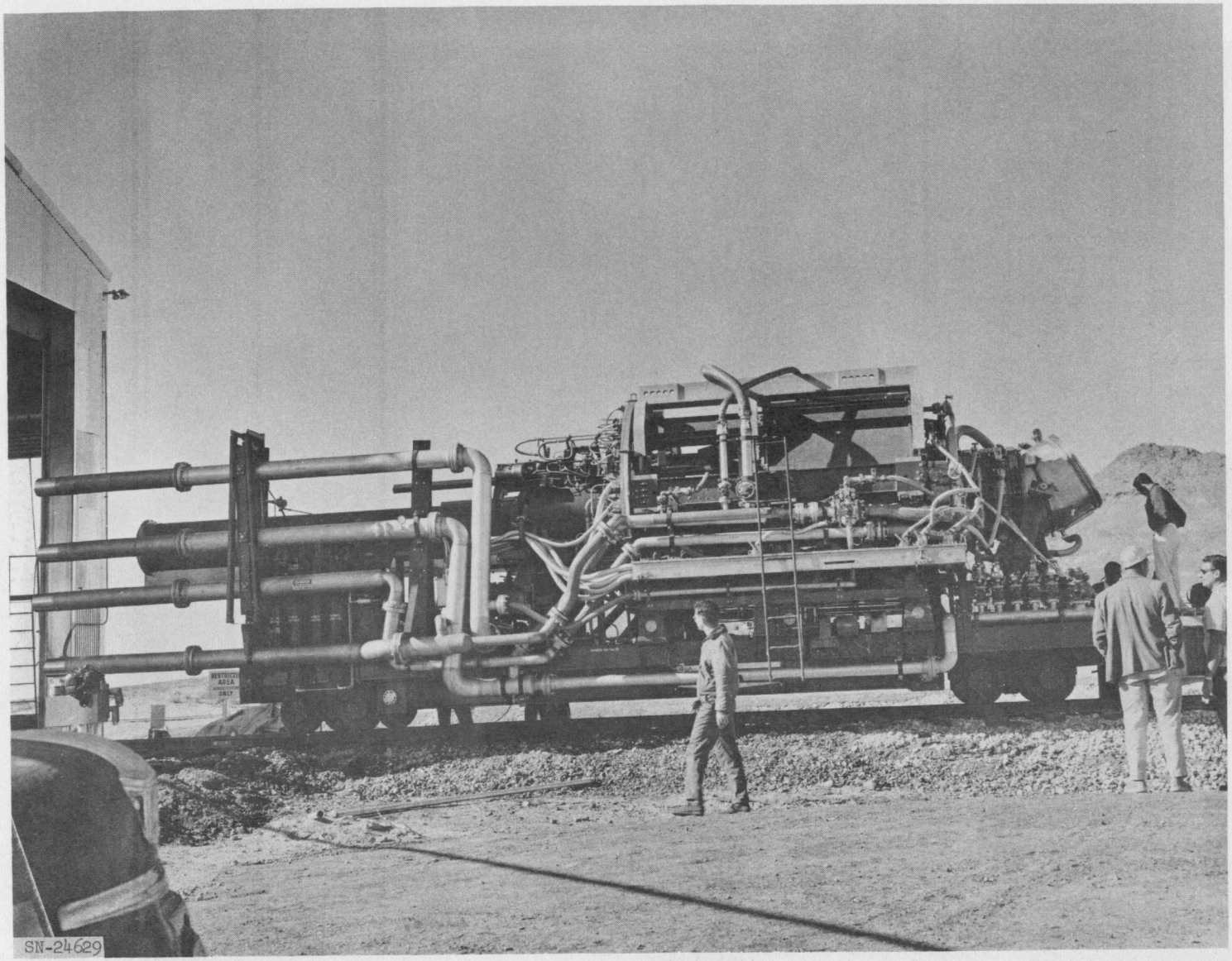

Fig. I-19. View of the Tory II-A test vehicle being withdrawn from the bunker after accident.

DOUBLE BUGGY SPRINGS

On page 55 of Pluto Quarterly Report No. 6 (UCRL-6258), Fig. I-32, dealing with Tory II-A double buggy springs, was incorrect. The difference in ordinates for the two curves was labeled as the load band width. The correct presentation of data is shown in Fig. I-20, where the lower curve represents the difference in load corresponding to the extremes of deflection (± 0.107 in.).

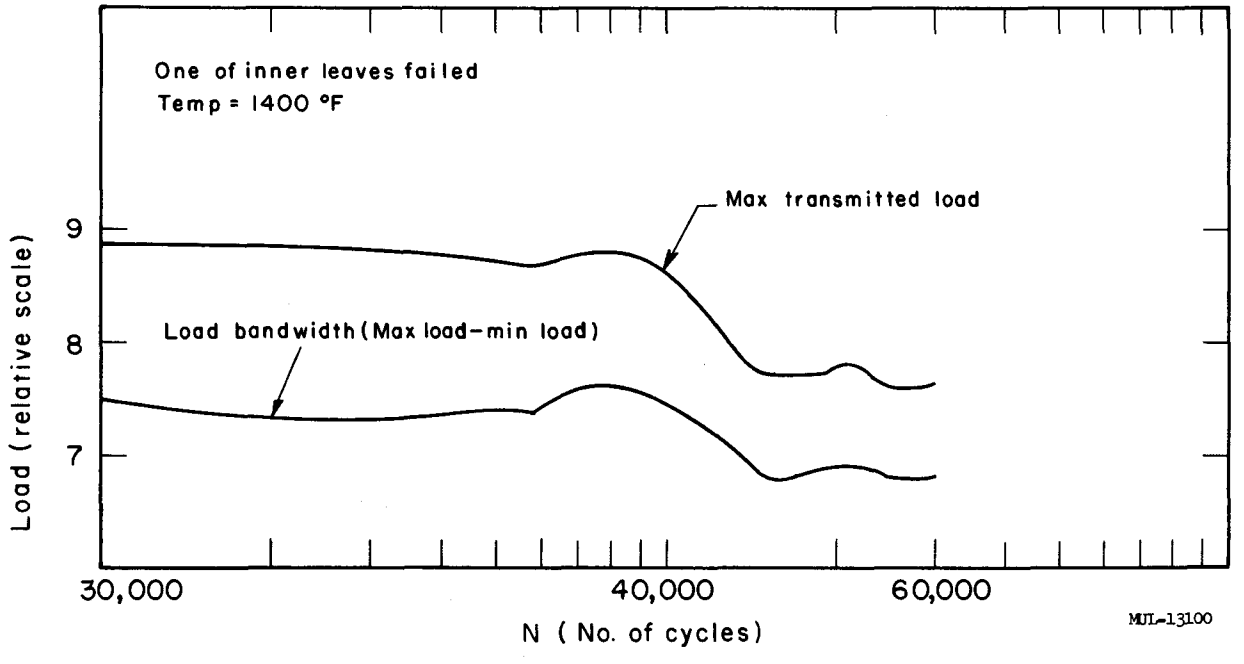

Fig. I-20. Load vs N for double buggy circle spring. Second run, 30,000 to 60,000 cycles.

CHAPTER II. MATERIALS DEVELOPMENT AND PILOT PLANT ACTIVITIES

SECTION I. PROCESS AND MATERIALS DEVELOPMENT

I. MATERIALS STUDIES

A. Basic Studies

1. Electrical Properties of BeO

The electrical resistivity and conductivity of BeO are being determined as part of a general program to obtain fundamental property data on oxide materials at high temperatures. Measurements are being made in vacuo on extruded samples, 97% of theoretical density, using the dc voltmeter-ammeter method. Results for sample No. 1 show that in the range 600-1600°C a plot of the ln σ is linear with 1/T. Values of conductivity vary from 10^{-16} $(\text{ohm-cm})^{-1}$ at 600°C to 10^{-5} $(\text{ohm-cm})^{-1}$ at 1600°C. The activation energy for the conduction process is calculated to be 58 kcal/mole (2.51 ev). Measurements on sample No. 2 were complicated by a variety of polarization effects such as the rapid decay in direct current from a high value which appeared immediately on application of a voltage. Careful work showed that values from the two samples agreed to within 5% at 821°C.

2. Oxidation of UO_2

Attention was directed to two phases of urania oxidation. The first was the possible conversion of U_4O_9 to U_3O_8 and the second the high-temperature (700-1500°C) oxidation of UO_2 pellets in air.

The first study required the verification of the U_4O_9 phase. Structural differences should exist between $UO_{2.25}$ in which the oxygen is randomly located and the U_4O_9 phase in which the oxygen is ordered at the 1/2, 1/2, 1/2 unit cell position. In an attempt to obtain the ordered structure, samples of UO_2 which had been oxidized to a O/U ratio of 2.25 were annealed at $\approx$ 900°C in an inert atmosphere. It was impossible by x-ray methods to observe any difference between the annealed and unannealed specimens. Complete verification must be accomplished by neutron diffraction methods.

Assuming that the annealed samples were U_4O_9, preliminary thermogravimetric examinations indicated that there was no difference in oxidation rates between the "U_4O_9" phase and the $UO_{2.25}$.

High-temperature oxidation work was carried out with sintered UO_2 pellets ($\approx$ 1.25 cm $\times$ 0.1 cm) in an air atmosphere. The pellets were cut from sintered UO_2 cylinders approximately 1.25 cm by 4 cm and then fired in hydrogen at 900°C before oxidation. These samples were then put into a helium atmosphere at the following temperatures: 700, 900, 1360, and 1525°C. Air was introduced and the samples were oxidized isothermally. At the lower temperatures the oxidation product (U_3O_8) fell away as a fine powder and no protective shell was formed around the pellet in the temperature range 900-1000°C as Peakall and Antill[1] found.

A linear rate was observed with no induction period evident (Fig. II-1). Therefore the rate-determining step is the formation of U_3O_8 at the surface of the pellet. The slopes of the lines in Fig. II-1 represent the rates since no change in surface area occurred during reaction. When the logarithm of the rate constant was plotted versus reciprocal of the absolute temperature as shown in Fig. II-2, an activation energy of 14 kcal was obtained. This compares with 26 kcal for $UO_2 \rightarrow U_3O_7$ and 35 kcal for $U_3O_7 \rightarrow U_3O_8$.[2]

The run at 1525°C was different from those at the lower temperatures. Only a slight weight gain was noted, followed by a loss in weight greater than the initial gain. No pellet disruption took place as occurs at lower temperature. X-ray examination showed the presence of U_2O_5 and U_4O_9. The weight gain is apparently the difference between the oxidation to U_4O_9 and the volatility of the urania. The presence of U_2O_5 probably occurred as the sample was taken from the furnace and passed through the temperature range in which U_2O_5 is stable.

3. X-Ray Diffraction: U-O and BeO-U-O

a. U-O

The phase equilibrium studies made on the high temperature x-ray diffraction equipment at reduced pressures have cast doubt on the possibility of determining the true equilibrium conditions at temperatures below 1000°C. Several runs using $UO_{2.0}$ as the starting material and a vacuum less than

---

[1] K. A. Peakall and J. E. Antill, Oxidation of Uranium Dioxide at 350-1000°C, J. Nuclear Materials 2, 194-195 (1960).

[2] S. Aronson, R. B. Roof, Jr., and J. Belle, Kinetic Study of the Oxidation of Uranium Dioxide, J. Chem. Phys. 27, 137-144 (1957).

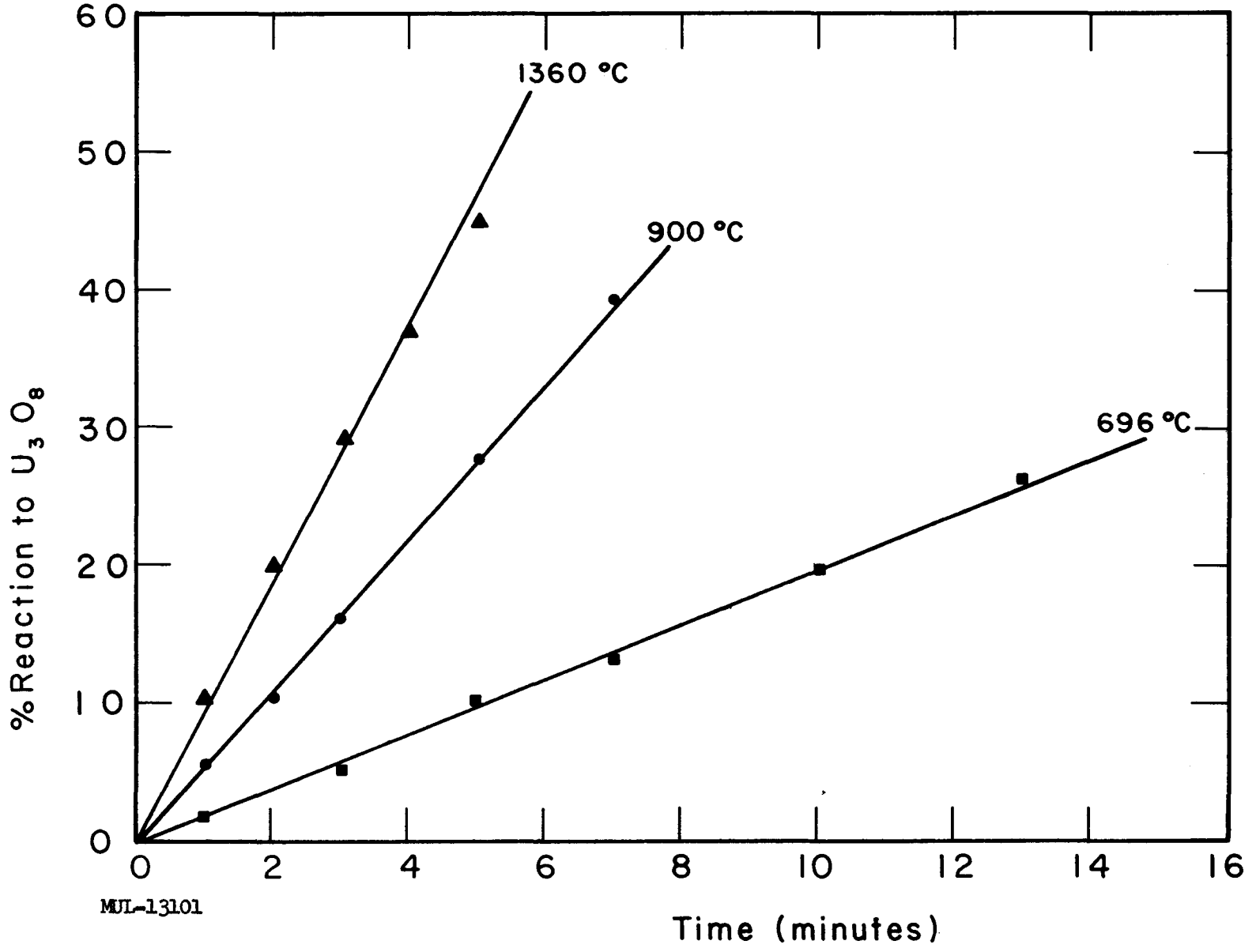

Fig. II-1. Oxidation of urania pellets.

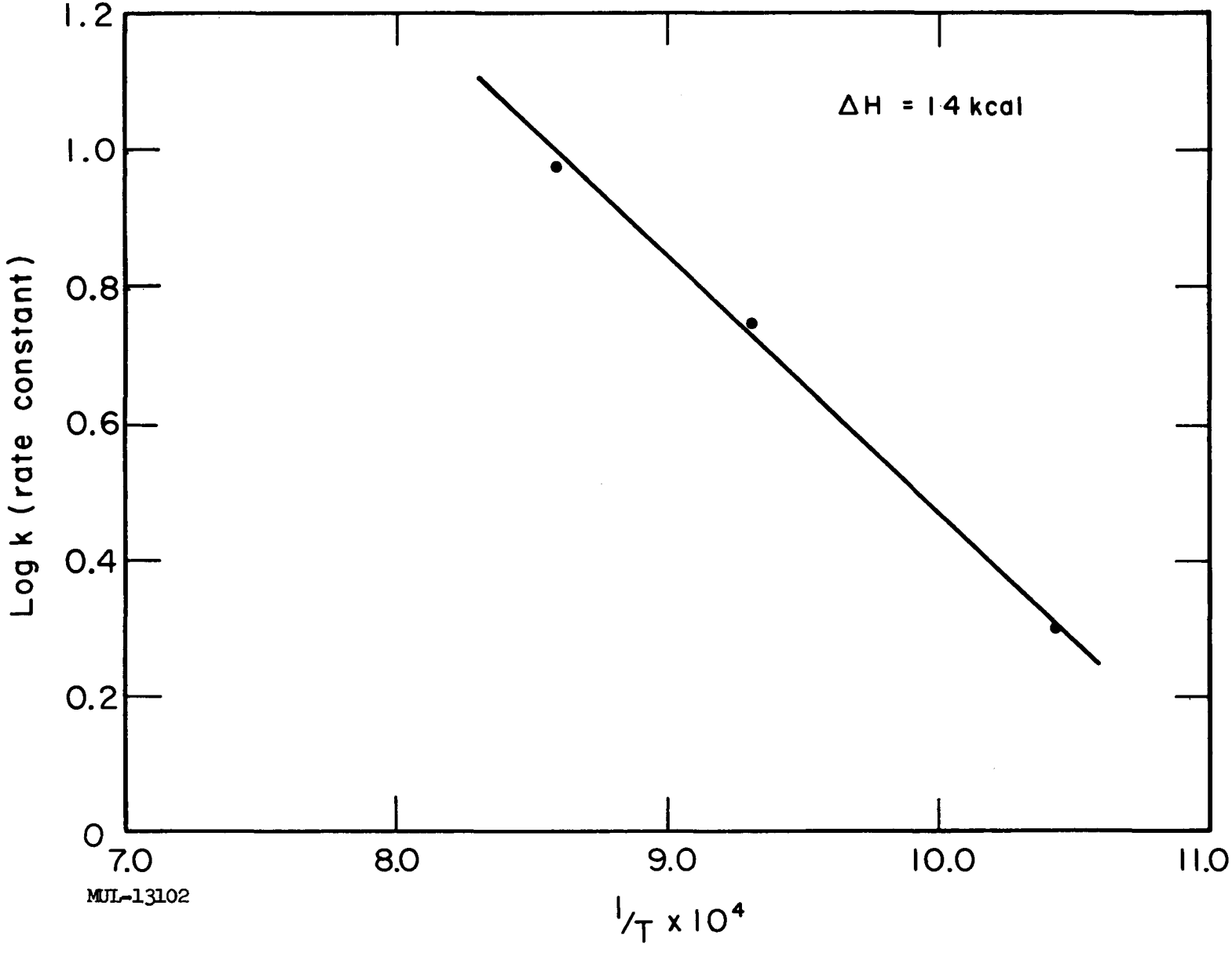

Fig. II-2. Oxidation of urania pellets.

10^{-4} mm Hg pressure show no change in phase up to 1000°C. On the other hand, U_3O_8 heated under the same conditions shows the gradual change toward the hexagonal form up to 400°C. Above 500°C, it appears to lose oxygen and transform to orthorhombic U_2O_5. This U_2O_5 is stable up to around 1000°C where it loses additional oxygen and changes to a $UO_{2.0}$. The formation of any intermediate U_4O_9 has not been detected.

Using a leak device consisting of a flattened copper tube, several runs have been made in the 175-200 μ Hg region. The U_3O_8 samples showed only the change to a hexagonal structure, but the change did not appear to be complete until the temperature was over 800°C. The 130-200 and 131-201 doublets are not resolved above 300°C but the second-order reflections 260-400 and 262-402 do not coalesce until 800°C. On the other hand, UO_2 under these conditions transforms into U_3O_7 above 315°C and does not oxidize further until the temperature is above 525°C where U_3O_8 forms. Both samples showed no further change up to 1000°C.

The dependence of the phase existent under a given set of pressure-temperature conditions on the starting material raises the question as to which phase is the equilibrium phase. At present no answer has been found. If it can be assumed that the oxidation reactions with UO_2 as the starting material are rapid, and go to completion, then a phase diagram might be inferred, but the existence of the tetragonal U_3O_7 (which is believed to be metastable) as an oxidation product of UO_2 questions this approach also.

b. BeO-U-O

Thin wafers cut from BeO-10% UO_2 tubes have been examined in several atmospheres of varying oxygen pressure. No new phases have been identified up to 5 atmospheres O_2 pressure and 1400°C. The first detectable oxidation of the UO_2 to U_3O_8 is a function of the O_2 pressure. At 0.2 atmosphere O_2 (1 atm air) the U_3O_8 is detectable slightly below 500°C, whereas at 5.0 atmospheres O_2 the first oxidation occurs slightly below 400°C. The nature of the surface exposed to the x rays also shows an effect on this temperature of oxidation. If the surface is the outer skin of the original hexagonal tube rather than a ground surface, the temperatures are as much as 100°C higher than quoted above.

Samples heated in air (0.2 atm O_2) showed loss of the U_3O_8 that had formed at lower temperatures. Significant amounts of U_3O_8 were present at 1000°C, but at 1200°C all of the U_3O_8 had disappeared. The concentration of

UO_2 at 1000 and 1200°C appeared to be essentially the same. This loss of U_3O_8 was not observed at 1.0 atm O_2 pressure. Significant amounts of UO_3 (hexagonal) were present on the cooler parts of the furnace after the 0.2-atm-O_2 runs, suggesting the formation of UO_3, and then volatilization of the species accounting for the disappearance of the U_3O_8. The presence of UO_3 in the sample could not be detected because of its structural similarity to U_3O_8. No UO_3 was detected in any of the higher O_2 pressure experiments.

4. Oxidation of UC

Uranium monocarbide is receiving a great deal of attention as a potential fuel material, but so far no data on the oxidation properties has appeared in the literature. The material used in this investigation consisted of approximately spherical grains, ranging in size from 140 to 180 μ in diameter.

Several isothermal runs have been made in the range from 300 to 395°C. At the lower temperature the rate data fit very well a $[1 - (1 - R)^{1/3}]$ versus time plot which represents reaction at a receding interface. Close to 400°C this rate equation was no longer valid. On a weight-gain basis the oxidation requires the formation of UO_3 and free carbon.

The presence of UO_3 has been confirmed by x ray, and also visually since it occurs as a reddish brown powder. Chemical analysis is now in progress to ascertain the presence of free carbon. Accepting the postulate of free carbon there exists the possibility of its oxidation to CO_2 which competes with the initial reaction. As the temperature is raised the oxidation of free carbon becomes more important due to difference in activation energies and may account for the lack of correlation of the run at around 400°C.

B. Fuel Retention and Stability

Further studies were made of fuel element stability in the presence of high pressure (5 atm) oxygen. A modulus of rupture furnace was enclosed in a shell capable of at least 60 psig pressure. Only one sample at a time can be subjected to bend testing. However, the space surrounding the bend specimen can be utilized simultaneously for pressure testing without load.

In each test the bend specimen was loaded to 7400 psi (3-point loading – 3-in. span) at room temperature. The system was purged for several minutes with flowing oxygen and then pressurized to 75 psia (5 atm). The following temperature schedule was reproduced in each test:

a) Room temperature to 1150°C in 1.5 hr.

b) 1150°C for 4 hr.

c) 1150°C to 600°C in 1.5 hr.

The furnace was depressurized at 600°C and cooled to room temperature slowly (about 2 hours). During the tests the bend specimen and the temperature were checked every 15 minutes. Temperatures were measured by thermocouple and blackbody pyrometry. Both temperature readings agreed within 15°C. Note that these tests are more rigorous than previous ones, viz., samples were heated and cooled for appreciable times while under pressure. Earlier testing indicated that this procedure exaggerated instability.

The results are grouped under (a) Uncoated LRL tubes; (b) Tory II-A-1 tubes; (c) Coated and annealed LRL tubes; (d) Miscellaneous tubes; and (e) Discussion.

1. Pressure Testing

a. Uncoated LRL Tubes

Values are listed in Table II-1. Several observations stand out. First, for UO_2 concentrations of over 5% the tubes lose considerable strength upon exposure to 75 psia oxygen at 1150 and 1250°C for four hours. Results for 5% UO_2 concentrations are less clear. A few tubes lost considerable strength (esp. Nos. 1-5, 2-13, 2-21), others lost strength moderately; and a few lost little or no strength. It is believed that the 4.93% UO_2 tubes which lost considerable strength as well as the 6.2% and 6.8% tubes are not truly representative. They were obtained from an early batch of tubes in which only a small percentage passed Zyglo inspection because of process difficulties (cracking during and after extrusion). Therefore these tubes may have been intrinsically defective even though they passed Zyglo inspection.

Note that pre-test modulus of rupture is about 20-30,000 psi in 3-point bend at room temperature. Fueled tubes containing 2.5% UO_2 showed no loss in strength after exposure to 1150 or 1250°C

Only the 5% UO_2 tubes were subjected to hot bending loads (7400 psi). These tubes successfully withstood the load. Modulus of rupture tests on the tubes after exposure indicated a moderate decrease in room temperature strength after testing (15,000 and 17,000 psi after exposure to 1250 and 1150°C, respectively), about the same decrease as that observed under pressure but without load.

Table II-1. Fuel Stability Tests – LRL Uncoated Tubes, 4 Hours at 75 psia O_2.

Test No.	Sample No.	Identification No.	Test temp (°C)	UO_2[a] (%)	Theo. density before test[b] (%)	Weight change (%)	Flex. resonance loss[c] (%)	Hot bend results (7400 psi)	Mod. rupture after test (psi)	X-ray analysis at break point[d]	Specimen appearance after test
4	9	V35 (round-Tu)	1150	2.5	98.7	0	0	No test	30,900		Surface brown
4	10	V35 (round-Tu)	1150	2.5	98.9	0	0	No test	31,600		Surface brown
4	11	V35 (round-Tu)	1150	2.5	98.8	0	0	No test	25,500		Surface brown
4	12	V35 (round-Tu)	1150	2.5	98.4	0	0	No test	22,000		Surface brown
5	21	V35 (round-Tu)	1250	2.5	98.7	0	0	No test	28,300		Surface brown
5	22	V35 (round-Tu)	1250	2.5	98.7	0	0	No test	32,300		Surface brown
5	23	V35 (round-Tu)	1250	2.5	98.7	0	0	No test	23,800		Surface brown
5	24	V35 (round-Tu)	1250	2.5	99.3	0	0	No test	28,500		Surface brown
1	5	1041 D SS #32 (hex-Oy)	1150	4.93 (4.99)	(98.2)	0	No test	No test	12,200	Trace U_3O_8	Center brown, black skin
2	13	1041 D SS #32 (hex-Oy)	1150	4.93 (5.02)	(98.6)	+0.07	No test	No test	5,900		Center black with brown specks
2	21	1041 D SS #32 (hex-Oy)	1150	4.93	98.6	+0.02	No test	No test	12,100		Center black to brown irregular
4	5	50 × 156 (hex-Tu)	1150	5.0	99.3	0	0	No test	21,400		Surface brown
4	7	50 × 156 (hex-Tu)	1150	5.0	99.0	0	0	No test	22,300		Surface brown
4	8	50 × 156 (hex-Tu)	1150	5.0	99.1	0	0	No test	18,300		Surface brown
4	6	50 × 156 (hex-Tu)	1150	5.0 (5.18)	99.2	0	0	Sustained load	17,000		Surface brown
5	18	50 × 156 (hex-Tu)	1250	5.0 (5.21)	99.3	0	0	Sustained load	14,900		Surface brown
5	17	50 × 156 (hex-Tu)	1250	5.0	99.3	0	0	No test	19,500		Surface brown
5	19	50 × 156 (hex-Tu)	1250	5.0	99.0	-0.02	0	No test	13,400		Surface brown
5	20	50 × 156 (hex-Tu)	1250	5.0	99.0	0	0	No test	16,700		Surface brown
1	6	1049J SS #20 (hex-Oy)	1150	6.25	98.3	+0.06	No test	No test	5,800		Center black
2	14	1049J SS #20 (hex-Oy)	1150	6.25 (6.18)	(98.6)	+0.13	No test	No test	3,700	Strong U_3O_8	Center black
2	22	1049J SS #20 (hex-Oy)	1150	6.25 (6.19)	(98.6)	+0.03	No test	No test	31,700	No U_3O_8	Center brown, thin black skin
1	7	42L (hex-Oy)	1150	6.87	99.5	+0.17	No test	No test	4,000		Surface black
2	15	42L (hex-Oy)	1150	6.87	99.2	+0.16	No test	No test	5,300		Surface black
2	23	42L (hex-Oy)	1150	6.87	99.3	+0.15	No test	No test	3,500		Surface black
1	8	42P (hex-Oy)	1150	7.88	98.2	+0.16	No test	No test	5,700		Surface black
2	16	42P (hex-Oy)	1150	7.88	98.7	+0.20	No test	No test	5,500		Surface black
2	24	42P (hex-Oy)	1150	7.88 (6.94)	99.2	+0.23	No test	No test	4,800		Surface black
7	1	80 × 164 (hex-Oy)	1150	8.0	>98	+0.11	4	No test	5,400		Surface black
10	1	80 × 164 (hex-Oy)	1150	8.0	>98	+0.17	13	No test	6,500		Surface black
6	9	80 × 164 (hex-Oy)	1150	8.0	99.0	+0.17	13	No test	8,400		Surface black
9	9	80 × 164 (hex-Oy)	1250	8.0	98.6	+0.22	15	No test	6,700		Surface black
12	1	80 × 164 (hex-Oy)	1250	8.0	98.6	+0.20	10	No test	5,700		Surface black
4	1	100 × 160 (hex-Tu)	1150	10.0	99.7	+0.27	37	No test	4,600		Surface black
4	2	100 × 160 (hex-Tu)	1150	10.0	99.7	+0.28	28	No test	3,600		Surface black
4	3	100 × 160 (hex-Tu)	1150	10.0	99.7	+0.29	25	No test	4,700		Surface black
4	4	100 × 160 (hex-Tu)	1150	10.0	99.7	+0.34	26	No test	4,100		Surface black
5	13	100 × 160 (hex-Tu)	1250	10.0	99.1	+0.32	20	No test	5,600		Surface black
5	14	100 × 160 (hex-Tu)	1250	10.0	99.9	+0.31	16	No test	6,000		Surface black
5	15	100 × 160 (hex-Tu)	1250	10.0	99.7	+0.31	15	No test	5,000		Surface black
5	16	100 × 160 (hex-Tu)	1250	10.0	99.7	+0.32	18	No test	5,200		Surface black

[a] Values are nominal. Obtained from vault records. Values in parentheses are wet chemical analysis after testing.

[b] Value in parentheses based on chemical analysis after testing.

[c] Changes less than 1% reported as 0%.

[d] All patterns indicated BeO + $UO_{2.0}$.

Note: Tu = tuballoy (normal uranium)
Oy = oralloy (enriched uranium)

MUL-13103

b. Tory II-A-1 Tubes

These tubes differ from LRL tubes in a number of respects. They are somewhat lower in density (generally 0.5 to 1.5% less); they had ground surfaces as produced; they were made by mixing powders instead of by precipitation, and have larger particles of UO_2; and they contain 0.1% CaO to increase their sinterability. They were sintered at lower temperatures (reportedly 1550 to 1650°C) than was the case for LRL tubes (1750°C).

Results are given in Table II-2. It is apparent that at 1150°C and 5 atm O_2 these tubes do not lose strength up to 8.2% UO_2 concentrations. However, the only tubes tested under load of 7400 psi (Nos. 14-16 and 16-7) broke before reaching test temperature while being heated in the furnace (at about 600°C). Interestingly, the broken halves from the post-tested broken tubes had good room temperature strengths.

c. Coated and Annealed Tubes

Results for coated tubes and vacuum-annealed tubes are given in Tables II-3 and II-4. The results are discussed in detail below (see C, "Coatings and Protective Treatments").

d. Miscellaneous Tubes

Some experiments have been made and will be carried out to determine the reasons for greater fuel stability at 1150°C at 5 atm O_2 (under no load) of the Tory II-A-1 tubes compared to LRL tubes obtained by precipitation from uranium solution. Interestingly, previous tests (UCRL-5699, p. 35) have shown that LRL tubes have much better fuel retention (losses are 1/5 to 1/10 those of the Tory II-A-1 tubes).

It is true, as shown in Tables II-2 and II-3 that both types of tubes containing 8% UO_2 failed under a load of 7400 psi at 1150°C. Furthermore, little testing of the Tory II-A-1 tubes has been done at temperatures above 1150°C.

The following variables are under study:

a. Density difference
b. Effect of surface grinding
c. Effect of flux addition (esp. CaO)
d. Effect of powder vs precipitation mixes
e. Effect of UO_2 concentration
f. Effect of test temperature.

Table II-2. Fuel Stability Tests – Tory II-A-1 Tubes, 4 Hours[f] at 75 psia O_2.

Test No.	Sample No.	Identification No.	Test temp (°C)	UO_2[a] (%)	Theo. density before test[b] (%)	Weight change (%)	Flex. resonance loss[c] (%)	Hot bend results (7400 psi)	Mod. rupture after test (psi)	X-ray analysis at breaking point[d]
1	1	700-470-1375	1150	4.93 (4.72)	(97.9)	0	No test	No test	28,000	No U_3O_8
2	9	756-470-624	1150	4.93	96.8	0	No test	No test	21,400	
2	17	756-470-624	1150	4.93	96.7	0	No test	No test	26,300	
1	2	742-625-008	1150	6.25	97.6	0	No test	No test	27,400	
2	10	744-625-003	1150	6.25	97.6	0	No test	No test	27,100	
2	18	744-625-004	1150	6.25	97.4	0	No test	No test	26,700	
1	3	747-652-056	1150	6.87	97.7	+0.02	No test	No test	30,100	
2	11	700-716-860	1150	6.87	97.5	+0.03	No test	No test	25,900	
2	19	700-716-860	1150	6.87	97.6	+0.02	No test	No test	30,300	
1	4	751-788-401	1150	7.88	98.1	0	No test	No test	23,000	
2	12	751-788-515	1150	7.88 (7.99)	98.1	+0.03	No test	No test	30,800	Trace U_3O_8
2	20	751-788-515	1150	7.88	98.1	+0.02	No test	No test	27,600	
14	6	745-827-330	1150	7.88	97.1	0	0	No test	31,300	
14	10	745-827-330	1150	7.88	97.1	0	0	No test	30,800	
16	8	745-827-330	1150	7.88	97.4	+0.03	0	No test	30,100	
16	7	745-827-330	1150	7.88	97.4	No test	No test	Broken at 600°C	26,700[e]	
14	18	745-827-325	1150	8.27	97.1	0	0	No test	24,000	
16	17	745-827-325	1150	8.27	96.8	0	0	No test	30,800	
16	19	745-827-325	1150	8.27	96.9	+0.02	0	No test	33,100	
14	16	745-827-325	1150	8.27	97.1	No test	No test	Broken at 600°C	26,100[e]	

[a] Values are nominal. Obtained from vault records. Values in parentheses are wet chemical analysis after testing.

[b] Value in parenthesis based on chemical analysis after testing.

[c] Changes less than 1% reported as 0%.

[d] All patterns indicated BeO + $UO_{2.0}$.

[e] This sample which failed during hot-bend testing was broken again on 1-1/2" centers.

[f] Test 14 stopped after sample broke at 600°C.

Note: All tubes are oralloy.

MJL-13104

Table II-3. Fuel Stability Tests — Coated and Annealed LRL Tubes, 4 Hours at 75 psia O_2.

Test No.	Sample No.	Tube description	Identification No.	Test temp (°C)	UO_2[b] (%)	Theo. density before test (%)	Weight change (%)	Flex. resonance loss[c] (%)	Hot bend results (7400 psi)	Mod. rupture after test (psi)
1	23B	Al coat[a]	119F 277-23	1150	5.4	98.8	0	No test	Unbroken	No test[d]
2	24B	Al coat	119F 277-23	1150	5.4	98.6	0	No test	Unbroken	28,300
3	2	Al coat	100 × 160	No test	10.0	97.5	---	---	---	22,000
3	4	Al coat	100 × 160	1150	10.0	98.5	0	-0	No test	24,600
3	5	Al coat	100 × 160	1150	10.0	99.0	0	No test	No test	19,400
3	6	Al coat	100 × 160	1150	10.0	98.9	0	-3.1	No test	21,400
3	8	Al coat	100 × 160	1150	10.0	98.6	0	0	No test	17,300
3	9	Al coat	100 × 160	1150	10.0	98.7	0	0	No test	22,400
3	10	Al coat	100 × 160	1150	10.0	98.7	0	0	No test	22,400
3	11	Al coat	100 × 160	1150	10.0	98.5	0	0	No test	17,300
7	2	Al coat	7P-B	1150	8.1	98.6	No test	No test	Broke at 1150°C	5,500[e]
8	1	Al coat	7P-B	1150	8.1	97.9	No test	No test	Broke at 1150°C	16,000[e]
10	2	Al coat	7P-B	1150	8.1	98.9	No test	No test	Broke after 1.5 hr at 1150°C	13,200[e]
6	10	Al coat	7P-B	1150	8.1	99.7	No test	No test	Broke at 1150°C	No test
12	3	Al coat	7P-B	1250	8.1	99.2	No test	No test	Broke at 1150°C	3,300[e]
9	15	Al coat	7P-B	1250	8.1	>99.5	No test	No test	Broke at 1150°C	No test
17	1	Al coat	80 × 169	1150	8.1	99.8	No test	No test	Broke at 1150°C	No test
22	1	Double Al coat	80 × 169	1150	8.1	99.5	No test	No test	Broken	No test
24	4	Double Al coat	80 × 169	1150	8.1	99.5	No test	No test	Broken	No test
3	7	Al coat	100 × 160	1150	10.0	>98.0	No test	No test	Broke at 1150°C	No test
8	2	Al coat	7P-B	1150	8.1	>98.0	+0.09	-23	No test	4,000
10	3	Al coat	7P-B	1150	8.1	>98.0	0	0	No test	28,600
9	10	Al coat	7P-B	1250	8.1	98.7	+0.22	-33	No test	2,800
12	2	Al coat	7P-B	1250	8.1	98.9	+0.21	-37	No test	2,900
17	2	Al coat	80 × 169	1150	8.1	99.8	+0.25	No test	No test	5,400
22	2	Double Al coat	80 × 169	1150	8.1	99.5	+0.01	No test	No test	30,300
24	3	Double Al coat	80 × 169	1150	8.1	99.5	+0.01	No test	No test	22,800
26	1	Feldspar glass coat	-----	1150	8.1	>99.0	---	---	Broken	---
19	2	Vacuum anneal	1109-282	1150	6.9	98.9	+0.02	0	No test	26,000
23	2	Vacuum anneal	1109-108	1150	6.9	98.9	+0.02	0	No test	22,900
25	2	Vacuum anneal	1109-272	1150	6.9	98.9	+0.04	-7	No test	8,700
19	1	Vacuum anneal	1109-167	1150	6.9	98.2	No test	No test	Broke at 1150°C	No test
23	1	Vacuum anneal	1109-137	1150	6.9	98.9	No test	No test	Broke at 1150°C	No test
25	1	Vacuum anneal	1109-263	1150	6.9	98.9	0	0	Unbroken	No test[f]

[a] These tubes were coated with Al paint and then H_2 fired a second time.

[b] Values are nominal. Obtained from vault records.

[c] Changes less than 1% reported as 0%.

[d] This sample broke during the unloading operation.

[e] This sample which failed during hot-bend testing was broken again on 1-1/2 centers.

[f] This sample saved for further evaluation.

MUL-13105

Table II-4. Fuel Stability Tests – Coated LRL Tubes (and Controls) – Additional Tests.

Sample No.	Type of test	Type & No. of coats	Sintering temperature (°C)	UO_2 (w/o)	Weight change (%)	% UO_2 lost (by gamma count)	M. of R. 3" span (psi)	Remarks
12-C	5 atm O_2 1200°C	Al paint 1	1725	5.41			Broke*	No crazing by Zyglo inspection.
13-C	5 atm O_2 1200°C 48 hr	Al paint 2	1725	5.41	0.00	0.45	24,000	" " " "
21-C	" " "	Al paint 3	1725	5.41	-0.10	0.18	20,250	" " " "
26	" " "	None (Control)		5.41	+0.09	0.37	11,750	Crazing by Zyglo inspection on one end only.
50 × 156	" " "	None (Control)		5.00	0.00		19,000	No crazing by Zyglo inspection.
100 × 160	" " "	None (Control)		10.00	+0.26		4,000	" " " "
Mix 151 #2	" " "	Al paint $MgO \cdot Al_2O_3$	1800	10.00	+0.24		9,000	" " " "
1	1 atm O_2 1525°C 120 hr	None (Control)		5.41	-0.58		22,750	" " " "
29-B	" " "	Al paint 1	1725	5.41	-0.45		19,000	" " " "
33-B	" " "	Al paint 3	1725	5.41	-0.42		20,250	" " " "
34-B	" " "	Al paint 2	1725	5.41	-0.48		20,750	" " " "
Mix 151 #1	" " "	Al paint MgO	1800	10.00	-3.44		2,750	Not checked by Zyglo. No crazing noted.
Mix 151 #3	" " "	Al paint $MgO \cdot Al_2O_3$	1800	10.00	-1.45		5,500	" " " "
#36	" " "	Al paint + Zr	1850	5.00	-0.68		9,250	" " " "
#37	" " "	Al paint + MgO	1850	5.00	-1.17		2,250	" " " "
#38	" " "	Al paint + MgO	1850	5.00	-1.66		2,250	" " " "

* This sample was loaded at 7400 psi while in the furnace. It broke when the furnace reached temperature. The broken tube was left in the furnace for 48 hours.

MUL-13106

Table II-5 shows a few of the effects examined to date. A few points are evident.

1. Refiring the Tory II-A-1 tubes to higher density did not grossly affect the stability of these tubes during oxidation at 1150°C, 5 atm O_2. However, the density increase was only 0.6 to 1.2%.

2. BeO-6% UO_2 tubes containing CaO (Tory II-A-1 mixes) and fired at high temperatures (1750°C in H_2) showed poor oxidation stability at 1250°C even though the tubes were stable at 1150°C. Similar mixes similarly fired, but containing no CaO did not show this poor stability at 1250°C.

3. The effect of grinding on stability of LRL tubes has not been adequately tested yet. Results at 5 and 10% UO_2 are listed in Table II-5. Conclusions as to the effect of grinding must be based on fuel concentrations of about 6 to 8% UO_2.

e. Discussion

In tests to date, LRL tubes have shown greater oxidation stability at lower fuel concentrations (5 to 6% and below). Samples which gained little or no weight at 1150°C had high strengths consistently. Zyglo observations after testing were difficult to make. In border line cases it seems difficult to judge a sample in which surface porosity may be confused with cracking.

A qualitative x-ray analysis on selected samples suggests a correlation between strength retention and the presence of U_3O_8. One Tory II-A-1 sample had high strength plus a trace amount of U_3O_8. Possibly longer times at temperature would have caused diminution of strength.

Specimens were virtually nonporous before the test. Those samples which lost strength showed in general a corresponding increase in open porosity. The open porosity was determined by difference between dry weight and weight saturated with kerosene.

In practice, fuel elements will see oxidizing conditions while subjected to a thermal stress (≈ 15,000 psi max Tory II-C condition). The tests described under 7400 psi steady load at temperature do not simulate the thermal stress in that stresses are lower and they are only applied over a small fraction of the tube's surface. More significantly, the bending stress continues to failure, unlike a thermal stress which may be relieved by creep-relaxation. The tests under load, consequently, have been used because they are currently available to screen protective coatings, rather than because they represent a true stress condition. The corrosion blowpipe will be used to simulate the latter.

Table II-5. Fuel Stability Tests — Miscellaneous Tube Types, 4 Hours at 75 psia.

Test No.	Sample No.	Tube description	Test temp (°C)	UO_2[a] (%)	Theo. density before test (%)	Weight change (%)	Flex resonance loss[b] (%)	Hot bend results (7400 psi)	Mod. rupture after test (psi)	% loss (γ count)
18	3	Tory II-A-1 tubes; Class 12 & 13 refired by LRL in H_2, 1750°C, 6 hr	1150	7.88	(97.4) 98.0[c]	0	0	No test	20,900	No test
18	5		1150	7.88	(97.4) 98.3	-0.02	0	No test	22,900	No test
18	14		1150	8.27	(96.8) 98.0	-0.01	0	No test	23,000	No test
18	15		1150	8.27	(97.1) 98.0	0	0	No test	25,800	No test
6	1	Round tubes with 0.1% CaO; received extruded and dried; fired by LRL at 1750°C	1150	6.0	98.1	0	-7	No test	24,700	No test
6	2		1150	6.0	98.3	0	0	No test	23,700	No test
6	3		1150	6.0	98.3	0	-2	No test	20,800	No test
6	4		1150	6.0	98.1	0	0	No test	20,000	No test
9	1		1250	6.0	98.0	+0.09	No test	No test	1,900	+0.09
9	2		1250	6.0	98.0	-0.05	0	No test	9,300	+0.16
9	3		1250	6.0	98.0	+0.03	-12	No test	5,300	+1.03
9	4		1250	6.0	98.0	+0.13	No test	No test	2,200	-0.22
6	5	Round tubes without CaO; received extruded and dried; fired by LRL at 1750°C	1150	6.0	98.3	0	0	No test	28,600	No test
6	6		1150	6.0	99.0	0	No test	No test	33,100	No test
6	7		1150	6.0	98.1	0	0	No test	29,600	No test
6	8		1150	6.0	99.3	0	0	No test	30,400	No test
9	5		1250	6.0	98.9	-0.02	0	No test	27,400	+0.25
9	6		1250	6.0	98.9	-0.01	0	No test	32,900	-0.07
9	7		1250	6.0	98.9	-0.02	0	No test	30,600	-0.53
9	8		1250	6.0	98.6	-0.03	0	No test	27,800	-0.53
6	15	LRL hex — all flats ground[d]	1150	5.0	98.3	0	No test	No test	21,700[e]	No test
6	16	LRL unground	1150	5.0	99.2	0	No test	No test	17,400	No test
6	17	LRL hex — all flats ground	1150	10.0	98.0	+0.27	No test	No test	4,000	No test
6	18	LRL unground	1150	10.0	98.1	+0.26	No test	No test	3,700	No test

[a] Values are nominal. Obtained from vault records.

[b] Changes less than 1% are reported as zero.

[c] Densities in parentheses are values as received before refiring.

[d] One-half of a 4-inch tube ground and the remaining half tested as is.

[e] Test on 1-1/2 inch span rather than standard 3-inch span.

MUL-13107

2. Corrosion Blowpipe

The blowpipe has been reassembled with a new test section. The present installation allows a SiC heater to radiate directly on the sample, giving a sample ΔT = 21°C (70°F) with the sample at 1175°C (outside). The maximum air pressure available (300 psia) requires that air flow be limited to about 0.071 lb/sec (85% of reactor flow) to prevent supersonic flow and choking below the sample.

Two trial runs have been made using 10% tuballoy samples coated with aluminum paint, and having 95.4 and 95.2% theoretical density, respectively. The first sample reached a uniform temperature of 1100°C for 30 minutes, then the run was terminated by a power failure. The sample had no change in weight, density, or appearance after cooling. The second run was terminated at 1100°C during the heat-up, when a sight glass cracked; this sample also showed no apparent damage.

Petrographic analyses were completed on two samples reported in Quarterly Report No. 6, UCRL-6258. Both were tested similarly at 1250°C and 225 psia air, with full details in the above report.

1. Sample 1030H-13,* vacuum-annealed prior to testing. The "skin" formed in the hole was quite dark, while the skin on the flats was clear, apparently depleted in urania. Both skins were just under 1-mil thickness, with the rest of the sample unaltered. Modulus of rupture was 28,500 psi at room temperature after testing.

2. Sample 42-1, no special preparation. Visibly black throughout, but with some unaltered UO_2 in the center of the BeO grains. There was considerable grain separation which, however, was too narrow to measure (thus $< 0.5\ \mu$). Fracture in modulus of rupture testing probably followed many loosened grain boundaries, accounting for loss of strength here, and presumably in other crazed samples. Modulus of rupture was 5200 psi after testing.

Efforts to determine any effects of SiC (heaters) on fueled BeO samples were not conclusive. Different results from earlier blowpipe preheater tests and DTA furnace tests suggested possible damage from SiC near the samples. A series of samples were tested in a DTA furnace with a uniform cycle of

---

* In Quarterly Report No. 6, UCRL-6258, p. 62, Table II-2, sample referred to as 1080H-13 should be 1030H-13.

heating and cooling in argon, and a 2-hour test at 1250°C in 45 psia O_2. Samples were placed on either SiC or Al_2O_3. In some cases changes in atmosphere were made by simply turning on the new gas (flushing), while in others the system was put under vacuum at the start and between each atmosphere change. A qualitative summary of the results is given in Table II-6. When atmosphere changes were made simply by flushing, crazing and loss of strength seemed to be associated with the presence of SiC. However, when atmosphere changes were preceded by a vacuum, none of the samples showed any apparent damage beyond a dark surface. The effects of residual oxygen during heating and cooling in the presence of SiC will be checked as time permits.

Table II-6. Effects of SiC and Al_2O_3 on Fueled Tubes.

No. of samples tested	Sample holder	Atmosphere changes by:	Weight changes	M/R range	Appearance
2	Al_2O_3	Flushing	Loss	High	Black skin, brown inside, no cracks
4*	SiC	Flushing	Gain	Low	Black or brown-black throughout, crazed
6	Al_2O_3	Vacuum	Gain and loss	High	Black skin, brown inside, no cracks
4	SiC	Vacuum	Gain and loss	High	Black skin, brown inside, no cracks

*Includes two samples from a blowpipe test.

C. Coatings and Protective Treatments

1. Vacuum Annealing

BeO tubes containing 6.87% UO_2 (99+% theoretical density) were vacuum annealed at 1800 to 2000°C and for 0.5 to 4 hours. Weight loss and fuel loss (by gamma count) were determined under the annealing conditions (Figs. II-3 and II-4). In general, fuel loss was appreciable (over 4%) at 2000°C and at 1900°C for four hours (Table II-7). No density changes were observed during the vacuum annealing.

The vacuum treated tubes were tested for oxidation stability at 1150°C for 4 hours at 75 psia O_2 pressure (Table II-7 and Fig. II-5). These tests

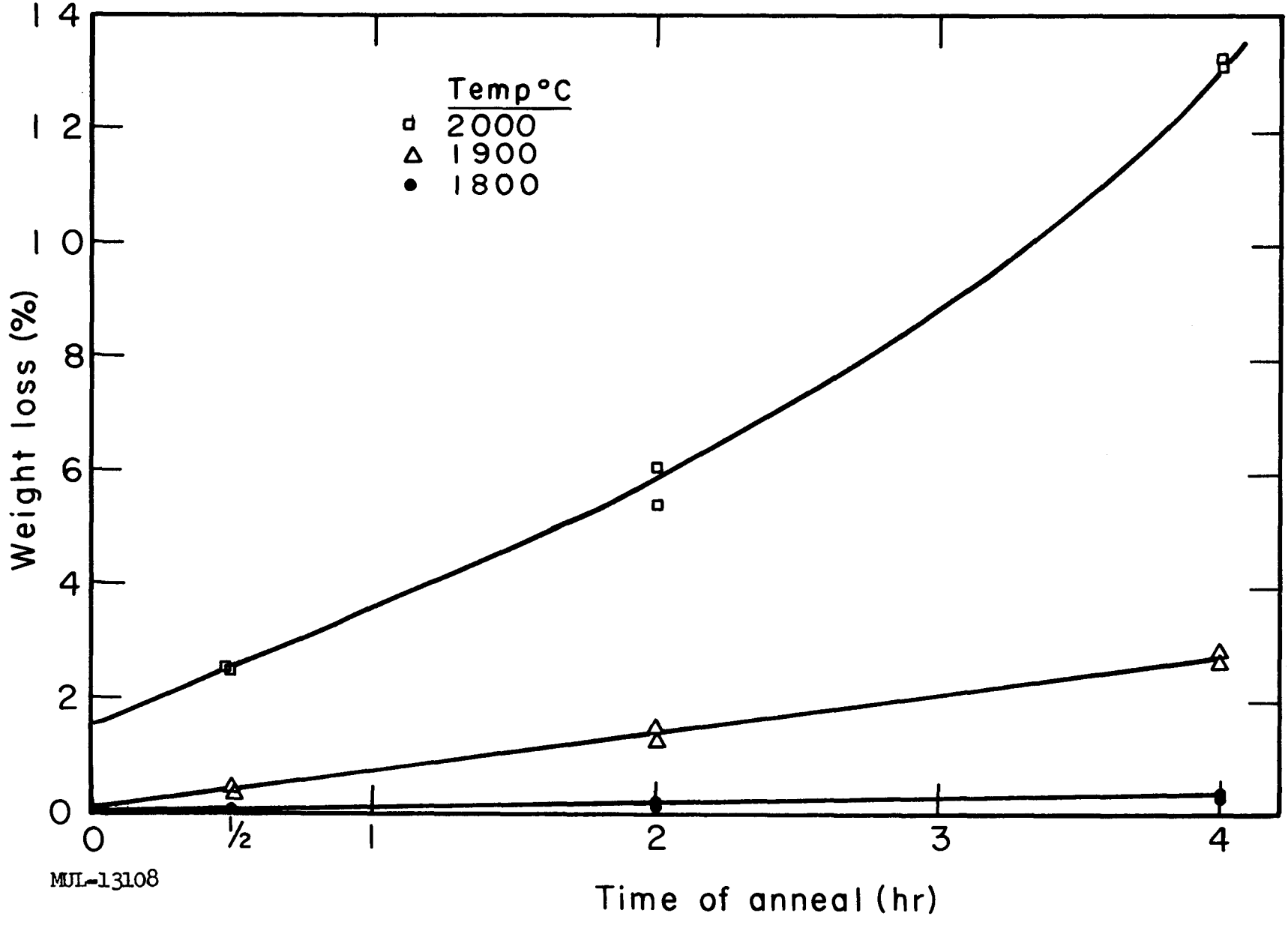

Fig. II-3. Weight loss of BeO-6.87 w/o UO_2 tubes during vacuum annealing.

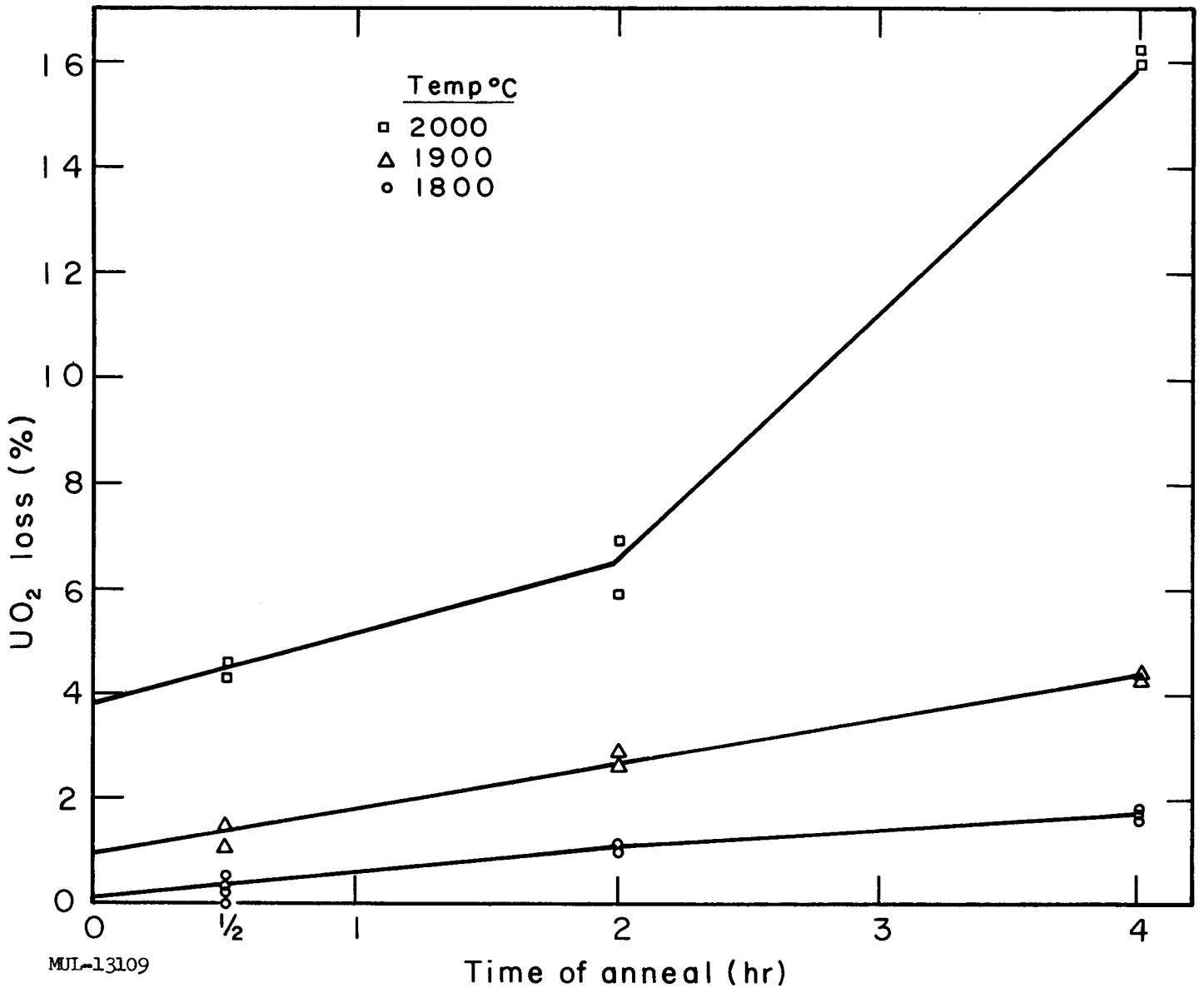

Fig. II-4. UO_2 loss in BeO-6.87 UO_2 tubes during vacuum annealing (as determined by γ count).

Table II-7. Vacuum Annealing.

Sample No.	Vacuum Annealing Conditions: T (°C)	Time (hr)	Weight loss (%)	UO_2 loss (w/o)	Oxidation, Testing[a]: Weight change (%)	E after[b] / E before	Modulus of rupture[c] (psi)	Remarks
1109-203	2000	1/2	2.54	4.64	+0.11	0.42	3,390	Crazed
1109-237	2000	1/2	2.54	4.39	+0.059	0.59	4,610	Crazed
1109-235	2000	2	6.16	5.92		1.00	21,000	
1109-159	2000	2	5.47	6.98		1.00	25,500	Not oxidized
1109-256	2000	4	13.33	15.95	+0.016		20,400	(usual observation)
1109-148	2000	4	13.12	16.25			22,800	
1109-283	1900	1/2	0.41	1.50	+0.12	0.47	3,820	Crazed
1109-273	1900	1/2	0.36	1.15	+0.13	0.50	1,050	Crazed
1109-182	1900	2	1.55	2.94		1.00	19,000	Not oxidized
1109-166	1900	2	1.33	2.66		1.00	25,200	Not oxidized
1109-207	1900	4	2.75	4.31		1.00	22,200	Not oxidized
1109-206	1900	4	2.91	4.35		1.00	24,800	Not oxidized
1109-136	1800	1/2	0.084	0.301		1.00	16,500	Not oxidized
1109-126	1800	1/2	0.086	+0.02		1.00	18,200	Not oxidized
1109-263	1800	1/2	0.087	0.39	0.0	1.00	Unbroken at 7400 psi	See Table II-3
1109-272	1800	1/2	0.092	0.61	+0.02	0.93	8,700	Crazed at one end
1109-93	1800	2	0.21	1.12		1.00	26,700	Not oxidized
1109-97	1800	2	0.22	1.14		1.00	26,100	Not oxidized
1109-167	1800	2	0.22	1.05			Broke, 7400 psi hot load	See Table II-3
1109-282	1800	2	0.21		+0.02	1.00	26,000	Not oxidized
1109-101	1800	4	0.44	1.72	+0.032	0.92	12,600	Crazed
1109-127	1800	4	0.48	1.67		1.00	24,800	Not oxidized
1109-137	1800	4	0.43	1.69			Broke, 7400 psi hot load	See Table II-3
1109-108	1800	4	0.41	1.78	+0.02	1.00	22,900	Not oxidized

[a] Four hours at 1150°C and 75 psia of O_2.

[b] Obtained by sonic method, using Elastomat apparatus.

[c] Made at 72°F ± 2° with 3-in. center and load rate of 30 lb/min.

MUL-13110

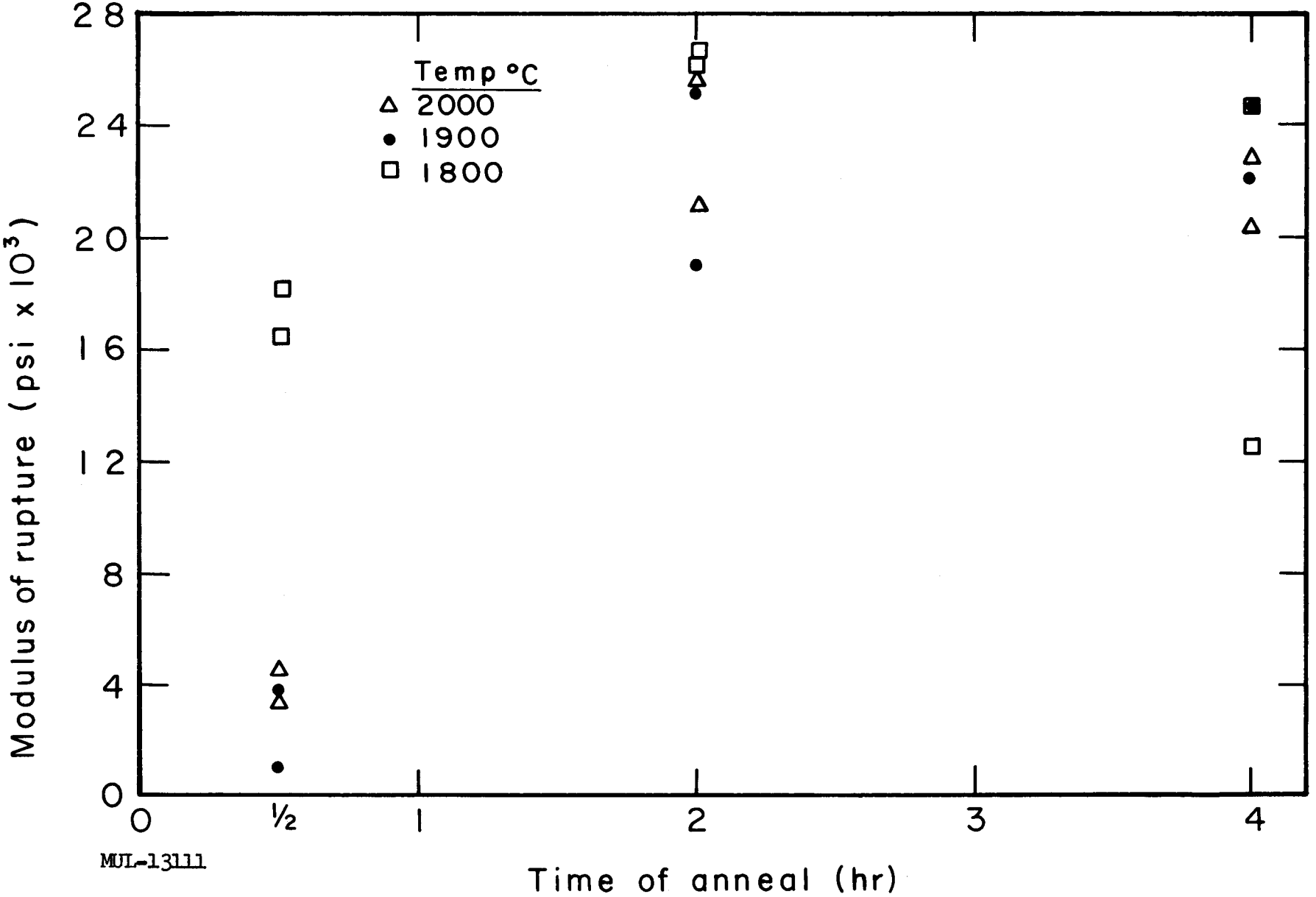

Fig. II-5. Room-temperature modulus of rupture (after oxidation) as a function of anneal time.

served as screening tests to choose the optimum annealing conditions. Oxidation test results showed that 0.5-hour anneal was insufficient. On the other hand, 2 to 4 hours gave rather high fuel and weight losses at 1900 and 2000°C. Based on these tests, a number of 1800°C-annealed tubes were given further oxidation tests, both under a load of 7400 psi and under no load (Tables II-3 and II-7). One of three tubes tested under load survived. The result was surprising since the successful tube was a 0.5-hour anneal and the failures were 2- and 4-hour anneals. The specimens tested with no load indicated somewhat lower post-test strengths for the 0.5-hour anneal than for the longer anneal times.

In particular, all the tubes but one annealed for 2 to 4 hours at 1800°C showed good stability under no load (5 out of 6).

An interesting effect was noted during vacuum annealing. Two samples that had been heated to 2100°C for 0.5 hour were found to be badly cracked when examined after being cooled to room temperature. A pure BeO tube was found to show the same effects under the same conditions. This was probably the same effect noted by Engberg and Zehms.[1]

2. Coatings

a. Al Coatings

Fueled BeO tubes were coated with aluminum paint and hydrogen fired to 1725°C for 30 minutes. They were tested for fuel stability at 5 atm O_2 at 1150 to 1250°C for up to 48 hours. In several cases they were tested at 1525°C under 1 atm O_2 for 120 hours. Results are given in Tables II-3 and II-4.

Tubes containing only 5.4% UO_2 showed little or no strength loss after testing. In addition they withstood a load of 7500 psi while at temperature and pressure in two tests (Nos. 1 and 2) but one failed in an earlier test (Table II-4, Sample 12-C). Al coated tubes containing 8% UO_2 showed erratic behavior. Three of them retained strength after oxidation exposure (no load), while three dropped to low strengths after exposure (3000 to 5000 psi). There is a question as to whether some of the coatings used for the 8% UO_2 tubes were of the

[1] Charles J. Engberg and Ernest H. Zehms, Thermal Expansion of Al_2O_3, BeO, MgO, B_4C, SiC, and TiC above 1000°C, Atomics International report NAA-SR-3086, Nov. 1958.

same quality as had been shown in earlier testing. For example, the 10% UO_2-BeO tubes coated with Al and tested earlier showed little or no loss in strength (Test No. 3, Table II-3). Based on previous observations, we would expect poorer oxidation behavior and greater strength loss with higher fuel concentrations.

Under a load of 7400 psi at 1150 and 1250°C, Al-coated tubes of high UO_2 concentration (8 and 10%) failed. In one case (Test 10, Sample 2, Table II-3) the tube withstood load for 1.5 hours at 1150°C before failure.

b. Other Oxide Coatings

Other coating materials were investigated such as Al paint with MgO added, $MgO \cdot Al_2O_3$ and CaO, MgO, Al_2O_3 (Table II-4). These coatings when fired to 1800°C and 1850°C appeared to have covered well and were very crystalline as observed under the microscope. However, these tubes did not hold up well in the oxidation test. Crazing was not evident but the tubes had poor strength and were black throughout the wall of the tube.

Other samples were coated using zirconium, zirconia, magnesium zirconate, zirconium silicate, and calcium zirconate. All of these coatings when fired in a hydrogen atmosphere to temperatures of 1700 to 1800°C had a black surface that would rub off easily. Consequently, tubes coated with material containing zirconium compounds were not tested.

c. Glassy Coatings

High-strength, high-temperature ceramic bonds are required in the Tory II-C reactor, to withstand 1200°F and 2000 to 2300°F. A high-temperature glaze was considered as a possible solution. After some preliminary work, a glaze consisting of 0.35 K_2O, 0.65 CaO, 0.57 Al_2O_3, 4.55 SiO_2 was applied to fueled and unfueled tubes. The fueled tubes were fired in air for 5 minutes at 1500 to 1550°C. Unfueled tubes were fired at the same temperature but for longer periods of time.

A number of pairs of unfueled tubes were glued together for testing the tensile strength of the glaze at 1200°F. Tensile strengths varied from 214 to 826 psi (mean of 24 samples was 550 psi). The contact between glaze and tube surface was only fair.

d. Water-resistance of Coatings

A number of the coatings described above were tested for resistance to water attack at 1525°C using 95°F dew point air. None of these coatings showed appreciable protection when compared with uncoated controls. Consequently tabular results are omitted.

D. Petrographic Studies of BeO-UO_2 Fueled Tubes

The first steps in the characterization of the petrographic properties of fueled BeO has been started. Samples have been selected and are being prepared in order that certain properties of the fueled tubes may be obtained. For any one sample, thin sections have been prepared: (1) perpendicular to the extrusion axis, (2) parallel to the extrusion axis and on the surface of the tube, (3) parallel to the extrusion axis but some distance in from the skin. The parameters of interest at this time are: the distribution of the fuel, and the size and shape of the fuel bodies and BeO.

Fuel concentration was measured by counting the number of fuel bodies in a fixed unit area of 74 μ^2. Each fuel particle was classified for its location by determining whether it was on the edge of two BeO grain boundaries, at a corner of through grains of BeO, or at the surface of a grain.

Size was measured by determining both the longest axis (r) which could be measured in a plane section of BeO, as well as the longest axis (p) perpendicular to r. Shape was estimated by the ratio r/p.

To date, only one thin section has been analyzed in detail. The results are summarized below.

		$\overline{X}$ (microns)	Standard deviation
Size :	BeO – r axis	15	≈ 10
	p axis	10	≈ 5
Shape:	BeO – r/p	1.5 (slightly tabular)	
Size :	UO_2 – r	1.30	≈ 0.45
	p	0.94	≈ 0.20
Shape:	UO_2 – r/p	1.4 (slightly tabular)	

Fuel Concentration:

50% of the BeO grains contained 1 to 3 UO_2 grains at the surface of the BeO.

53% of the grain boundaries contained 1 to 3 (maximum) particles of fuel.

60% of the unit areas (74 μ^2) examined had between 2 to 6 grains of fuel.

II. FABRICATION DEVELOPMENT

A. Fuel Element Fabrication

1. Raw Materials

We are looking for a possible correlation between BeO lots and tube quality. First indications are that some lots are superior to others.

2. Mixing and Precipitation

The efficiency of the mixers is still suspect. The current high incidence of low density inclusions raises the questions:

1. Whether the BeO is completely dispersed before precipitation.
2. Whether holdover from batch to batch is giving problems.

A pump-type mixer has been designed and fabricated in Lucite for preliminary evaluation. A duplicate of the bench-top mixer in use in the laboratory is being installed. This will be used to make smooth beryllia dispersions prior to precipitation in the existing mix tanks.

All batches are now being strained through vibrated 50-mesh screens before filtration. Unfortunately, it is not yet known whether a 50-mesh inclusion (0.011 in. diam) will produce a rejectable defect (0.030 in. diam).

No marked difference was noted among tuballoy fueled batches in which the beryllia was exposed to various pH environments in the slurrying step. The presence of free nitric acid or ammonium nitrate seemed to have little effect on the product. Chemical analysis indicates that BeO (UOX) is insoluble in dilute nitric acid.

3. Filtration and Drying

Filter cake is currently being dried and calcined at 1000°F. This temperature closely duplicates that used in the laboratory. The resultant dry filter cake, however, is of different color than that obtained in the laboratory, indicating different molecular species from the two operations. Judging by color, the laboratory material is approximately UO_3 while the other material in the Fabrication Facility is between $UO_{2.67}$ and UO_3. The calcined cake breaks up readily in the Simpson mix muller.

4. Binder Addition

Observable inhomogeneities in batches mixed only in the sigma blade mixer have prompted a return to the Simpson mix muller. We are currently mixing batches in similar fashion to the method used in the laboratory.

Recently, some extrusions have been made of material that was reworked in the mix muller after extrusion. Almost invariably, the material has re-extruded at a lower pressure, even though its water content has been reduced. The re-extruded material is not necessarily of better quality, but the change in extrusion properties indicates that our mixing methods are not reducing each batch to the same stable, uniform state of "complete" mixing.

5. Extrusion and Drying

During the quarter, straightness of extrusion has been brought under control by use of carefully designed, machined, and inspected die parts. The die parts are now properly mated, and extrusion is straight.

The glass fiber belt in the extruder line was identified as a cause of tube scratching. Better belt materials are in use, and further improvement is being sought.

A pneumatically driven tube cutter has been installed. It is at least twice as fast as the solenoid-operated cutter and is much more positive in action.

6. Sintering

Pacific Kiln. This kiln provided limited tube straightening data during the quarter. In its final run, 102 tubes were fired in 120° molybdenum grooves using molybdenum and tungsten mandrels. The tungsten mandrels produced 88% cambers under 3 mils; the molybdenum mandrels yielded only 69% cambers under 3 mils.

III. MECHANICAL PROPERTIES

A. Compressive Creep

High-temperature compressive creep data on LRL high-density-fueled extruded BeO is reported in the following table. All tests were conducted in air. The information on specimen L-103 has been reported in the last Quarterly Report (UCRL-6258).

Specimen	UO_2 (%)	% theo. density*	Temp (°F)	Stress (psi)	Secondary creep rate (in./in./hr)	Grain size (microns)
L-128	10	99.0	2500	1500	0.97×10^{-4}	To be determined
L-126	10	99.1	2500	3000	1.82	" " "
L-123	10	99.0	2500	4500	2.74	" " "
L-103	10	99.0	2500	6000	5.38	" " "
L-127	10	99.0	2700	3000	15.50	" " "

*Based on a value of 3.2425 g/cc.

Utilizing these preliminary results, a graph of stress versus strain rate at constant temperature can be obtained (Fig. II-6). It is interesting to note that the initial portion of the curve is approximately linear. This behavior might be interpreted in terms of the Nabarro-Herring type mechanism[1-3] of stress-directed diffusion of vacancies. Critical examination of the high stress region (viz., greater than 4500 psi) is currently in progress. Stress-strain rate relationships will be determined for other temperatures.

B. Elastic Modulus

The measurements and observations shown in Table II-8 have been made on round BeO-10 w/o UO_2 tubes, batch No. V-17. The observations were made in air, using the Elastomat apparatus.

From the data it appears that a phase change is occurring at some temperature below 650°C. This phase change is observed as the black bands about the sample, and also as a decrease in the elastic modulus of the sample. It appears that the sample requires a certain period of "gestation" at the transformation temperature to initiate the phase change, since the samples heated rapidly to temperature do not show any change. Once the phase transformation has been initiated, subsequent cycling of the specimen accelerates the transformation.

A similar test with BeO tubes containing 7.5% UO_2 did not show a decrease in the elastic modulus.

C. Thermal Stress

Three unfueled BeO specimens were tested in the modified thermal stress equipment (Fig. II-7). The data are presented in Table II-9.

The power to failure data for specimen A-4 is uncertain in that the reported value is the maximum power applied to the specimen; it is not known when failure occurred because the crack detection mechanism failed to operate.

---

[1] F. R. N. Nabarro, Deformation of Crystals by the Motion of Single Ions, Report of a Conference on the Strength of Solids, The Physical Society, London, 75-90 (1948).

[2] C. Herring, Diffusional Viscosity of a Polycrystalline Solid, J. Appl. Phys. 21, 437-445 (1950).

[3] J. Harper and J. E. Dorn, Viscous Creep of Aluminum Near Its Melting Temperature, Acta Met. 5, 654-665 (1957).

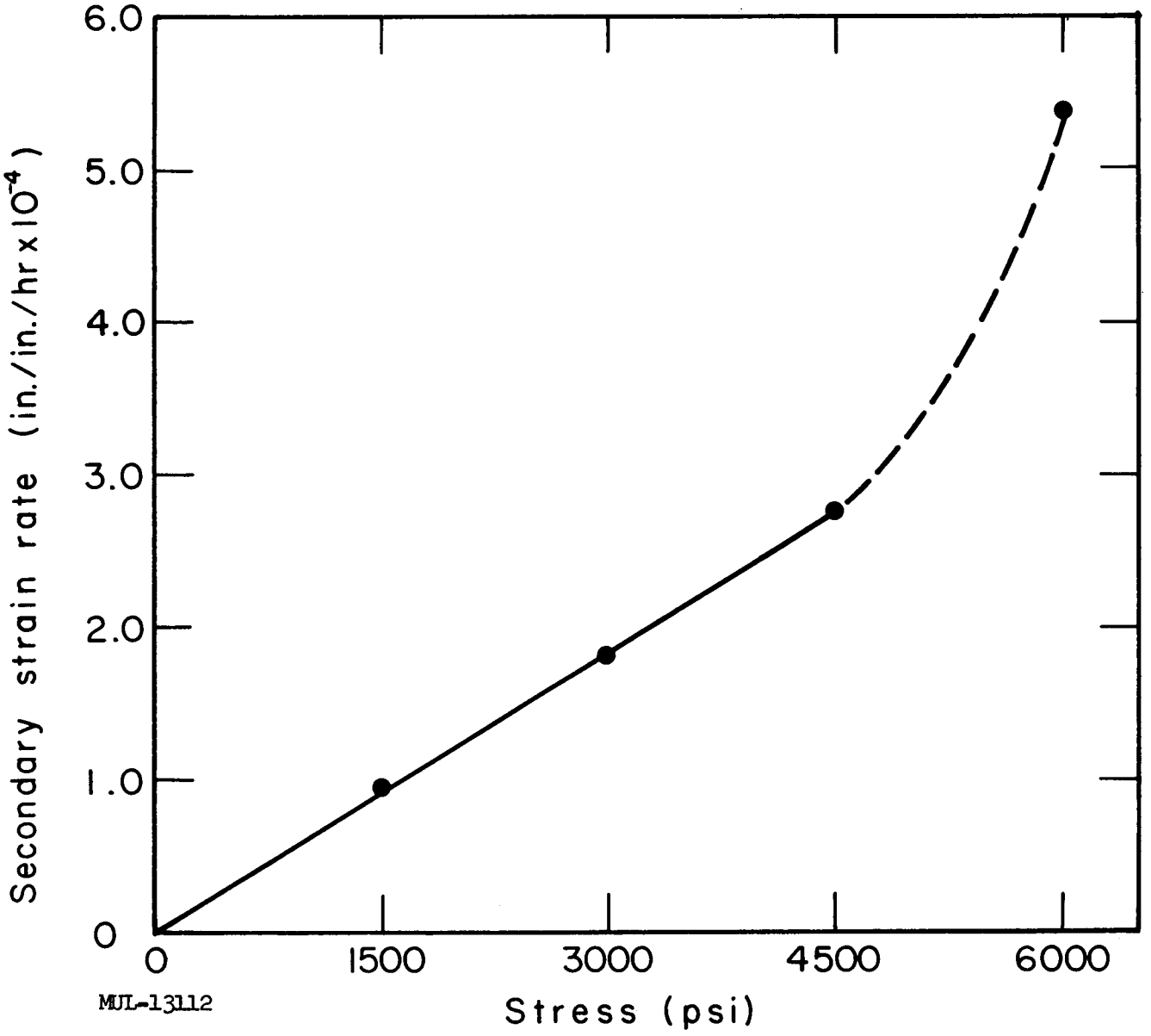

Fig. II-6. The effect of stress on strain rate for BeO-10 w/o UO_2 at 2500°F.

Table II-8. Elastic Modulus Measurements in Air On BeO-10 w/o UO_2 Tubes.
(Batch V-17)

Sample No.	Heat-up period (from room temp)	Max temp (°C)	Time at max temp (hr)	Observations
1	Slow – about 30 hr with intermediate soak at 300°C for about 16 hr	800	20	5% decrease in room-temperature elastic modulus. Sample had black bands about it.
2	Fast – about 3 hr to 750°C	750	16	No change in room-temperature elastic modulus. No bands about sample.
3	Cycle 1 – fast, about 3 hr to 750°C	790	19	No change in room-temperature elastic modulus. No bands about sample.
	Cycle 2 – slow, about 24 hr to 650°C with intermediate soak at 260°C overnight	650	16	2% decrease in room-temperature elastic modulus. Black bands present. Decrease in modulus with time at temperature observed.
	Cycle 1 – slow, about 26 hr to 750°C with intermediate soak at 440°C overnight	750	2	2-1/2% decrease in room-temperature elastic modulus. Black bands present. Decrease in modulus with time at temperature observed.
4	Cycle 2 – about 5 hr to 580°C	590	23	50% decrease in room-temperature elastic modulus. Decrease in modulus with time at temperature observed. Numerous resonant peaks appeared towards the end of the run.

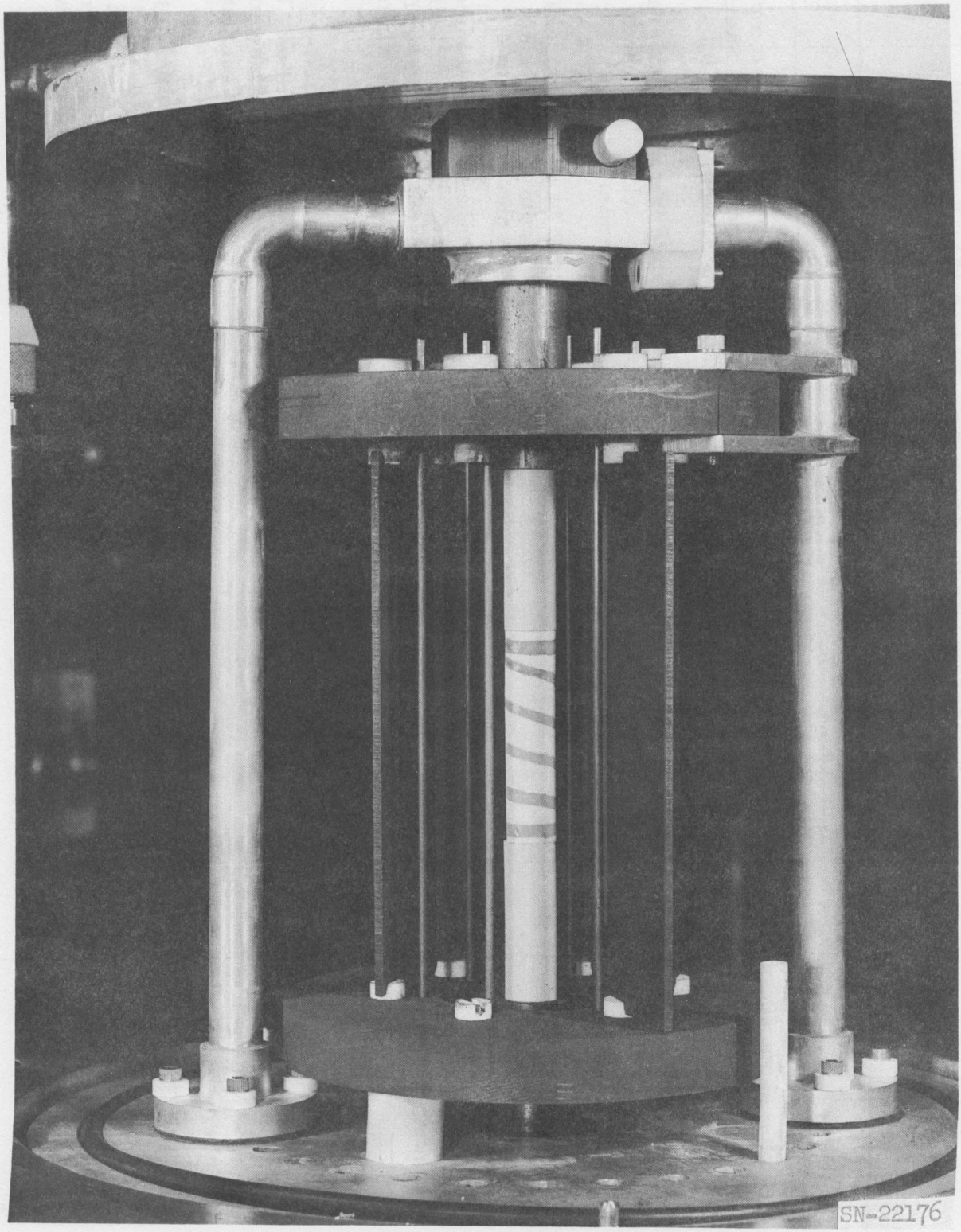

Fig. II-7. Equipment used in thermal stress tests of unfueled BeO specimens.

Table II-9. Steady-State Thermal Stress of BeO.
(BeO specimens: 3/4 in. o.d. × 1/4 in. i.d. × 3 in. long)

Specimen No.	ρ (g/cc)	Mean temp (°F)	Power to failure (watts/in.)	Time to failure (sec)	SK/E_a* (watts/in.)	Remarks
A-2	2.908	1890	826	52	80.9	Cracked
A-4	2.912	2600	1614	--	158†	Cracked
A-10	2.902	1900	550	--	53.8	Uncracked

*Maximum SK/E_a for Tory II-C is ≈ 25.5.

†Specimen cracked during test but crack detection mechanism failed to operate.

SECTION II. GENERAL CHEMISTRY

I. MATERIALS DEVELOPMENT – PLUTO

A. Vapor Pressure of Scandium Metal

The third and final series of vapor pressure measurements of Sc was completed. As before, the Knudsen cell method was used to determine the rate of effusion of Sc into high vacuum from a Ta cell at high temperatures. The orifice of the cell was a cylindrical channel of 0.0993 cm diameter and 0.019 cm long. Results of the measurements are summarized in Table II-10.

Table II-10. Series III Scandium Vapor Pressure Determinations.

Run No.	Temperature (°K)	Time (min)	Weight loss (g)	Pressure of Sc (g) (atm)
2	1723	126	0.00886	2.09×10^{-5}
3	1691	152	0.00592	1.15×10^{-5}
4	1598	338	0.00307	2.60×10^{-6}
5	1761	60.5	0.00659	3.27×10^{-5}

The most recent results confirm the Series II measurements, but differ by ≈ 25% from the Series I vapor pressures. It is felt that blackbody conditions were not attained in the Series I determinations. For the Series III measurements special care was taken in construction of the cell to insure

temperature uniformity and blackbody conditions. The cell lid was machined to fit all the way down around the outside of the cell body to insure good thermal contact. A conical protrusion was machined on the bottom of the inside of the cell to reflect radiation from the interior surfaces out through the orifice. This undoubtedly helped to achieve blackbody conditions.

B. Heat of Sublimation of MgO

The Birge-Sponer extrapolation method of obtaining dissociation energies has been applied to the extensive $MgO_{(g)}$ spectroscopic data of Mahanti. The least-squares fit obtained on the IBM 650 yields a dissociation energy of ≈ 85 kcal/mole for the lowest $^1\Sigma$ state of gaseous MgO. If the $^1\Sigma$ state dissociates to ground-state Mg and O atoms, the heat of sublimation for $MgO_{(s)} \rightarrow MgO_{(g)}$ $^1\Sigma$ ought to be ≈ 155 kcal/mole.

Transpiration experiments were performed by passing oxygen gas over solid MgO in an oxyacetylene combustion furnace at temperatures as high as 2175°K. From the MgO weight loss the ΔH for the reaction $MgO_{(s)} \rightarrow MgO_{(g)}$ was computed by means of the third law. The heat thus obtained was 150 to 165 kcal/mole. Unfortunately, even at the highest temperature the weight loss was less than a milligram, and in addition the flow rate of oxygen was rather high. A precise value of ΔH therefore cannot be obtained, and it is probable that the value obtained is high, since saturation of the gas stream may have been incomplete.

If the $^1\Sigma$ state of MgO does dissociate to the atoms in their ground states, as our data seem to indicate, this is a violation of the Wigner-Witmer correlation rules. An abstract (UCRL-6307) describes these results.

C. Beryllides of Re and the Pt Group Metals

A study was started to establish the phases existing in the binary systems of M-Be, where M is one of the following metals: Re, Ru, Rh, Pd, Os, Ir, and Pt. Samples were prepared by weighing out the powdered metals and blending them into mixtures which were then heated until it appeared reaction was complete. For Re, mixtures corresponding to Re_2Be, ReBe, $ReBe_3$, $ReBe_6$, $ReBe_9$, $ReBe_{11}$, and $ReBe_{20}$ were used. For the Pt group metals, mixtures corresponding to MBe, MBe_3, MBe_6, and MBe_{12} were used. The reacted sample was crushed and ground to a fine powder. X-ray diffraction powder patterns were then obtained which showed a number of phases that are isomorphous with beryllides previously identified. There was also evidence

of numerous phases whose identity and structure are not yet known. The results are given below.

Re-Be. The composition Re_2Be showed the presence of Re, $ReBe_2$, and a phase which is thought to be ReBe. The compositions ReBe and $ReBe_3$ indicated $ReBe_2$ plus "ReBe." $ReBe_6$ and $ReBe_9$ gave $ReBe_2$ plus lines indicating the presence of an unknown phase or phases. $ReBe_{20}$ showed a phase whose approximate stoichiometry is believed to be $ReBe_{22}$. $ReBe_{11}$ showed a small amount of $ReBe_{22}$ plus an unknown phase or phases.

Ru-Be. RuBe showed the presence of Ru metal plus an unidentified phase or phases. $RuBe_6$ showed a pattern similar to that of $OsBe_6$. $RuBe_9$ and $RuBe_{12}$ showed the presence of unidentified phases.

Rh-Be. All mixtures gave indications of a phase or phases which are not identified.

Pd-Be. PdBe showed a body-centered cubic phase plus some Pd metal. $PdBe_3$ gave an unidentified phase or phases. $PdBe_6$ showed a phase of the $AuBe_5$ type. $PdBe_{12}$ showed a phase which appears to be isomorphous with Nb_2Be_{17} plus additional material.

Os-Be. OsBe gave Os metal plus an unidentified phase or phases. $OsBe_6$ showed two phases. The predominant one could be indexed as body-centered cubic. The other, tentatively identified as $OsBe_{22}$, could be indexed as face-centered cubic. The other mixtures showed unidentified phases.

Ir-Be. The mixture IrBe showed a phase of the CsCl type identified as IrBe, plus some Ir metal. $IrBe_{12}$ showed a phase isomorphous with Nb_2Be_{17}. The other mixtures showed unidentified phases.

Pt-Be. Both $PtBe_6$ and $PtBe_{12}$ showed a phase of the $AuBe_5$ type plus small amounts of an unidentified phase or phases. The other mixtures all showed unidentified phases.

D. Oxidation of Niobium Base Alloy

Oxidation rate curves were obtained for supplier's alloy SM Cb 291, at temperatures of 1100, 1200, and 1300°C in static air using the thermobalance. The results are given in Fig. II-8. The composition of the alloy is 80% Nb, 10% Ta, and 10% W. It is one of the most oxidation-resistant Nb alloys developed by the supplier. Its tensile strength for stress-rupture in 100 minutes is given as 8300 psi at 2970°F, 6900 psi at 2850°F, 5200 psi at 2970°F and 4000 psi at 3200°F. The room-temperature ultimate tensile strength for the forged alloy is 80,000 psi with 31% elongation.

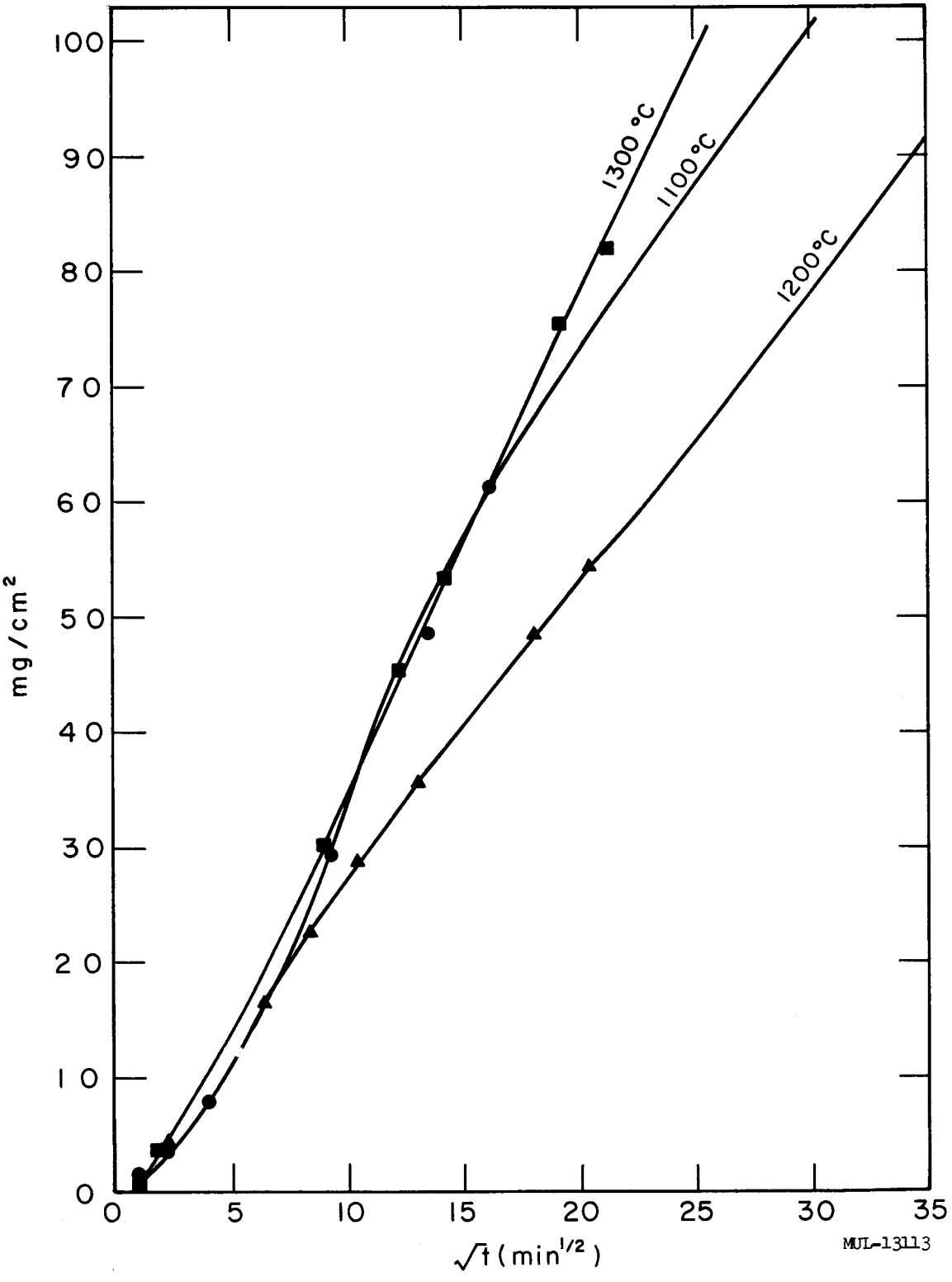

Fig. II-8. Oxidation rate curves for supplier's alloy SM Cb 291 in static air.

E. Lubricant Coating for Inconel X

A high-temperature lubricant coating for Inconel X was prepared. The coating consists of CaF_2 in an enamel frit matrix. The composition of the frit was CoO-60%, B_2O_3-20%, and BaO-20%.

Five Inconel X test specimens were coated. The initial cleaning step for each was as follows: No. 1 — sandblasted; No. 2 — abraded with Al_2O_3 powder; No. 3 — abraded with crocus cloth; No. 4 — chemically cleaned by first boiling in alkaline cleaner, then in HCl-$FeCl_3$ solution; and No. 5 — ground on SiC lapping board.

The metal specimens were first pre-oxidized at 2000°F for ≈ 2 minutes, and allowed to cool to 200-300°F. At this temperature, a slurry of the powdered CaF_2-frit in water was brushed on the sample. The pieces were then heated in air at 2000°F until the violet color of the coating turned black. CaF_2 was subsequently rubbed over the coatings to fill the remaining pores.

F. Stability of Fueled Tubes in High Pressure-High Temperature Environments

The effect of different pressures of oxygen on LRL fueled tubes at high temperatures has been further investigated. During the quarter the work was concerned mainly with determining the conditions under which the tubes cracked, and the effects of such cracking on thermal diffusivity.

1. Cracking of Fueled Tubes During Irradiation

Irradiations were made in the Livermore Pool-Type Reactor in ≈ 2.5 atm O_2 on a supplier's tube containing 8.23 wt % OyO_2 and on two LRL tubes containing 7.92 wt % OyO_2. After irradiation, the tube surfaces were found to be blackened and extensively cracked. Measurement of the relative thermal conductivity after irradiation showed that all three tubes had been adversely affected. These experiments are summarized in Table II-11.

Table II-11.

Sample	OyO_2 (wt %)	P_{O_2} (atm)	T (°C)	t (hr)	$flux_{(th)}$	$nvt_{(th)}$	R/R_0
G-1	8.23	≈ 2.5	1400 ± 25	23.5	3×10^{13}	2.4×10^{18}	1.62
L-16	7.92	≈ 2.5	1375 ± 25	24.0	3×10^{13}	2.4×10^{18}	2.20
L-8	7.92	≈ 2.5	1330 ± 30	115	3×10^{13}	1.2×10^{19}	2.60

It was not clear, however, that the observed results were due to the effects of irradiation or just to heating in oxygen. To resolve this question, a series of heatings in oxygen was performed to determine the effect on R/R_0. In the first set of these experiments, the thermal conditions of the irradiation were not duplicated exactly; the samples were heated in 1-atm room air; only after reaching temperature was the pressure raised to 2.5-atm O_2. The conditions of the heatings and the results are given in Table II-12.

Table II-12.

Sample	OyO_2 (wt %)	T (°C)	t (hr)	p_{O_2} (atm)	$\frac{\Delta m}{m(UO_2)} \times 10^3$	R/R_0	Comments
G-6 (supplier's)	8.23	1400	23.5	2.5	-38.8	1.22	Uncracked
L-7 (LRL)	7.92	1400	23.5	5.0	-189	1.14	Uncracked
L-10 (LRL)	7.92	1375	24	2.5	-22.3	1.17	Uncracked
L-28 (LRL)	7.92	1375	23.75	2.5	-19.7	1.13	Uncracked

It is seen that none of the above experiments showed the increase in R/R_0 found after reactor irradiation. A second set of measurements was done in which the specimens were introduced at differing rates into the hot, pressurized furnace. The sample thus went from room temperature to ≈ 1400°C. A thermocouple in the center of the sample tube was used to obtain the temperature-time history of each sample. The rate of heating was varied over a range which included the rate actually used in the reactor irradiations. The results of the measurements are shown in Table II-13 and Fig. II-9. $\Delta m/m(UO_2)$ is the ratio of the observed weight change to the amount of UO_2 originally present, and $\Delta T/\Delta t$ is the rate (per min) of heating from 1000°C to 1100°C.

Table II-13.

Sample	UO_2 (wt %)	$\frac{\Delta m}{m(UO_2)} \times 10^3$	$\Delta T/\Delta t$ (deg/min)	p_{O_2} (atm)	R/R_0	Comments
L-11 (LRL)	7.92	+11.6	50	2.5	2.96	Badly cracked
L-15 (LRL)	7.92	-0.2	53.5	2.5	2.21	Badly cracked
L-19 (LRL)	7.92	-113	142	2.5	1.24	Cracked
L-20 (LRL)	7.92	-11.6	163	2.5	1.27	Cracked
L-26 (LRL)	7.92	-24.2	~500	2.5	1.39	Cracked

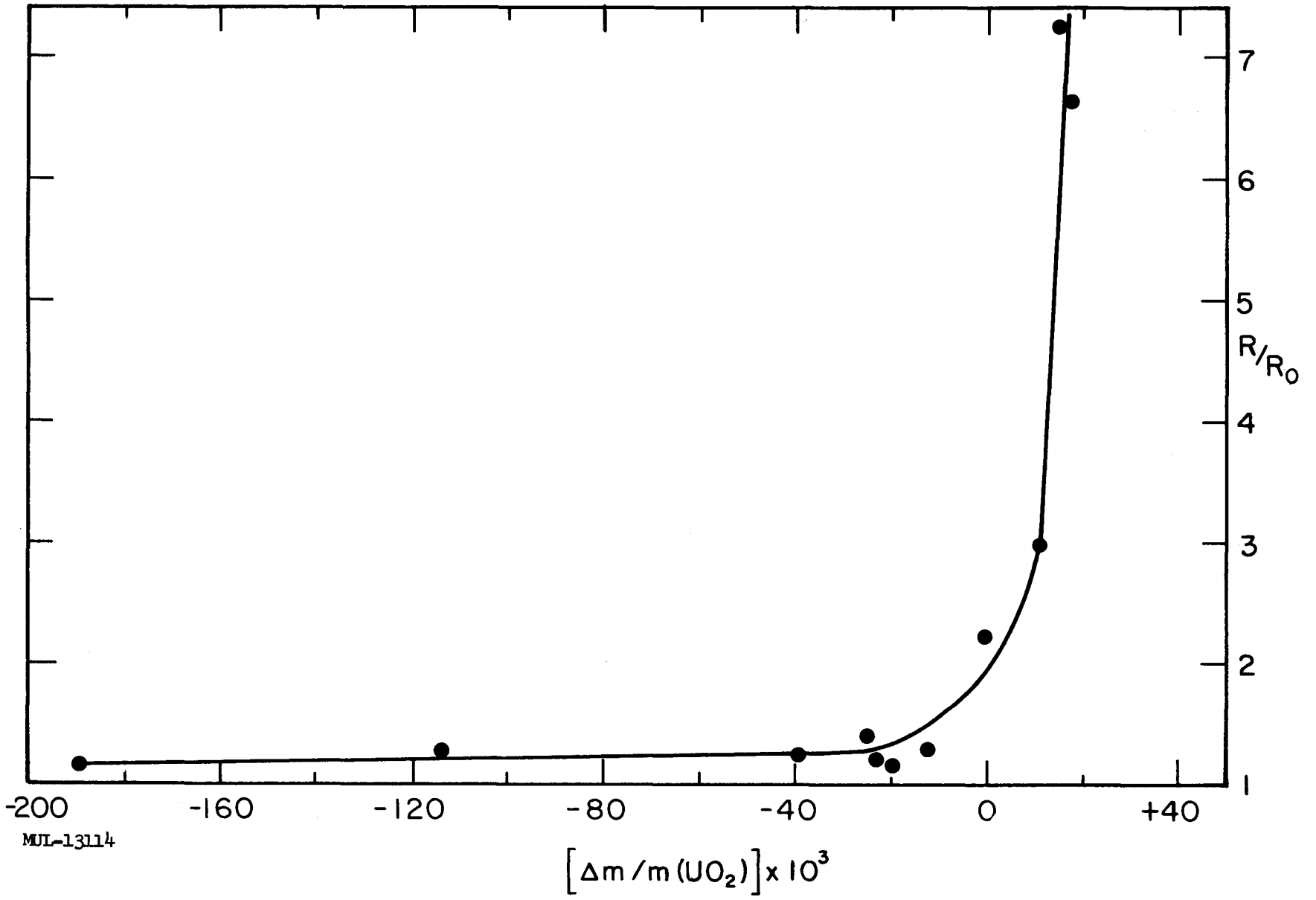

Fig. II-9. Correlation of weight change with change in thermal resistivity.

Cracking was determined by (1) microscopic examination, (2) Zyglo penetrant, or (3) sectioning, followed by examination, or all three. The value of R/R_0 roughly corresponds to the extent of cracking as seen on surface examination. A gain in weight is always associated with extensive cracking and a high R/R_0. In Fig. II-9, $\Delta m/m(UO_2)$ is plotted against R/R_0 for the specimens of Tables II-12 and II-13. The correlation is clear.

At this time, therefore, no further irradiation experiments can be planned until tubes become available which do not undergo serious deterioration on heating in oxygen, since it is not possible to separate irradiation effects (if any) from the changes in properties discussed above.

2. Occurrence of Cracking

During the quarter, a large number of experiments were performed to define further the conditions under which cracking of the fueled tube takes place. The experimental procedure was to weigh the sample, expose it to the desired conditions of oxygen pressure, temperature, and time, reweigh it, microscopically examine the surface, section the piece by cutting on a diamond saw, and finally examine the cut section. The detailed results of the work will be published in complete form. A summary of the results is as follows:

a. Ten-Minute Heatings on Round, 7.5 wt % Tuballoy Fueled Tubes. A plot of the pressure-temperature field in which cracking occurs in a 10-minute period is given in Fig. II-10. A contour plot of weight change vs pressure-temperature was constructed from the data of Fig. II-10. From the closeness of the contours it was found that the effect of increasing oxygen pressure is most pronounced at ≈ 1075°C.

b. Ten-Minute Heatings on Hexagonal, 7.29 wt % Oralloy Fueled Tubes. Work is now under way on locating the pressure-temperature field in which cracking occurs for hexagonal tubes. Results taken so far indicate that this field is similar to that given in Fig. II-10, but that the pressure of O_2 required to bring about cracking is less. Between ≈ 1050 and 1200°C these tubes are observed to crack with only 0.2 atm O_2.

c. Heatings on Tubes Containing 5.00 wt % and 2.5 wt % Urania. Two hexagonal tubes of 5.00 wt % OyO_2 were heated for four hours at 1235°C in 5-atm O_2. Both showed evidence of slight cracking, but much less than is

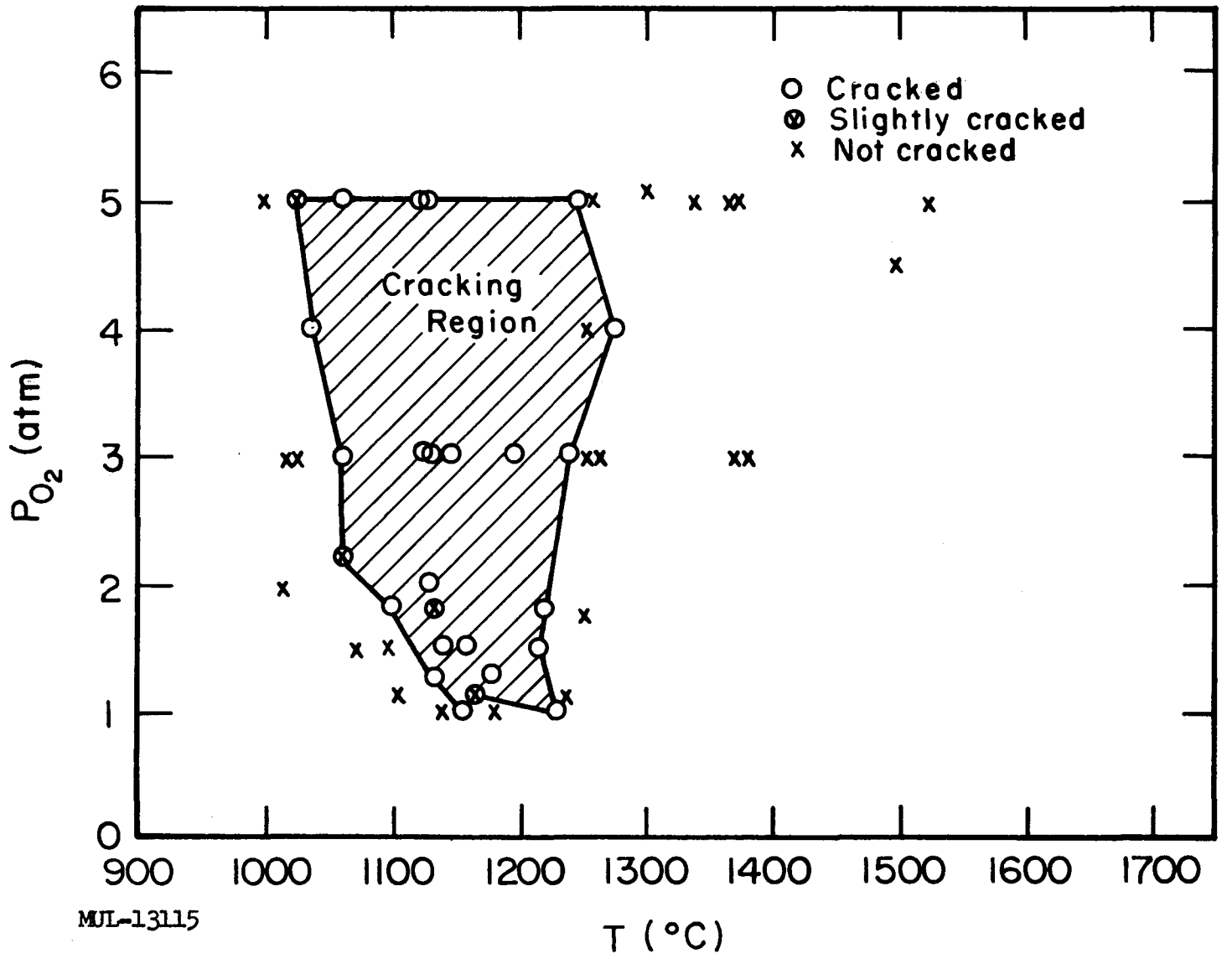

Fig. II-10. Correlation of cracking with temperature and pressure.

ordinarily seen on ≈7 wt % tubes. Twenty-three round, 2.5 wt % OyO_2 specimens were run in O_2 for 10 minutes at pressures of 1 to 5 atm and temperatures of 1000 to 1350°C. None of these specimens cracked.

d. Time Required to Cause Cracking. In an attempt to see how rapidly the cracking phenomenon takes place, a series of experiments was performed in which the sample was heated rapidly under constant pressure. The samples were hexagonal LRL tubes, containing 7.9 wt % OyO_2. The pressure of oxygen was ≈2.5 atm. The time which the sample spent between 1000 and 1250°C was then varied and the sample behavior noted. It was found that exposures as short as 40 seconds were sufficient to cause cracking.

CHAPTER III. TORY II-C

SECTION I. NEUTRONICS

CRITICAL MASS OF TORY II-C

The present discussion pertains to the Tory II-C reactor prior to the decision to reduce the fuel-tube hole size to 0.227 in. i.d. Minor changes are anticipated that will alter the conclusions now documented.

Some important parameters employed in the neutronic calculations follow.

Core length (cold)	50.70 in.
Core radius (cold)	23.625 in.
Side refl. thickness (cold)	3.00 in.
Front refl. thickness (cold)	10.00 in.
Rear refl. thickness (cold)	2.00 in.
Average reactor temp	1550°K (2330°F)
Fractional linear expansion, in all dimensions	1.27%

Volume Fractions

Core:	
Fueled BeO	0.4207
Unfueled BeO	0.0454
Tie tubes	0.005145
Void	balance

End reflectors:	
Unfueled BeO	0.4661
Tie tubes	0.005145
Side reflector:	
Unfueled BeO	0.8946
Tie tubes	0.005145

The fueled and unfueled BeO were assumed to be at 98% of theoretical density in the calculations. Also the tie tubes were assumed to be of René 41 (66.7% of tubes) and R-235 Hastelloy (33.3%), uniformly mixed throughout the reactor.

Newly-determined absorption cross sections thought to be due to high-energy resonance absorption by the tie-tube materials have been included. In the base calculation, the fuel mass was taken to be 50.0 kg of OyO_2, and it was dispersed axially and radially to achieve uniform power density in the radial direction. Also, the power density was uniform within the forward half of the active core. In the after half, the loading did not vary axially and so

the power density dropped approximately as $\cos(\pi Z/Z_{eq} + 2\Delta)$. The calculated multiplication constant for the hot (i.e., 1550°K = 2330°F) reactor was

$$k_{eff} = 1.0034.$$

Figures III-1 and III-2 illustrate radial and axial power density variations within the core. Figure III-3 is a map of the fuel loading in each zone of the Angie problem (based on a critical mass of 50 kg OyO_2. Figure III-4 shows the number of fuel tubes required in each class. The latter figure is to be considered as approximate, and subject to change.

Several effects were not included in the above Angie calculation:

1. Control rod holes
2. Side support structure
3. Neutron streaming
4. Actual density of BeO in front reflector
5. Xenon poisoning
6. Fuel burnup
7. Base plates

These will be considered in order.

1. The control rod holes for the shim rods are twelve in number and are approximately 8 inches from the reactor axis. Two additional holes farther out radially accommodate the vernier and safety rods. A Zoom calculation showed that the 12 shim rod holes cost:

$$\Delta k/k \simeq -0.022.$$

The total cost should be about

$$(\Delta k/k)_{holes} \simeq -0.025.$$

2. The side support structure has also been treated by several Zoom calculations. An earlier design had an areal density of 16.9 g/cm^2 of metal external to the side reflector. Extrapolations from experiments would indicate a $\Delta k/k \simeq +0.040$. A conservative Zoom representation (i.e., "Smear technique") gave

$$(\Delta k/k)_{ss} \simeq +0.032.$$

The latter value will be used.

3. Neutron streaming has been estimated by the Behrens method [Proc. Phys. Soc. (London) 62, 607 (1949)]:

$$\Delta k/k \simeq -0.010.$$

4. The front reflector will have a lower BeO volume fraction because of spacing problems involving the tie tubes. Final values are not yet available.

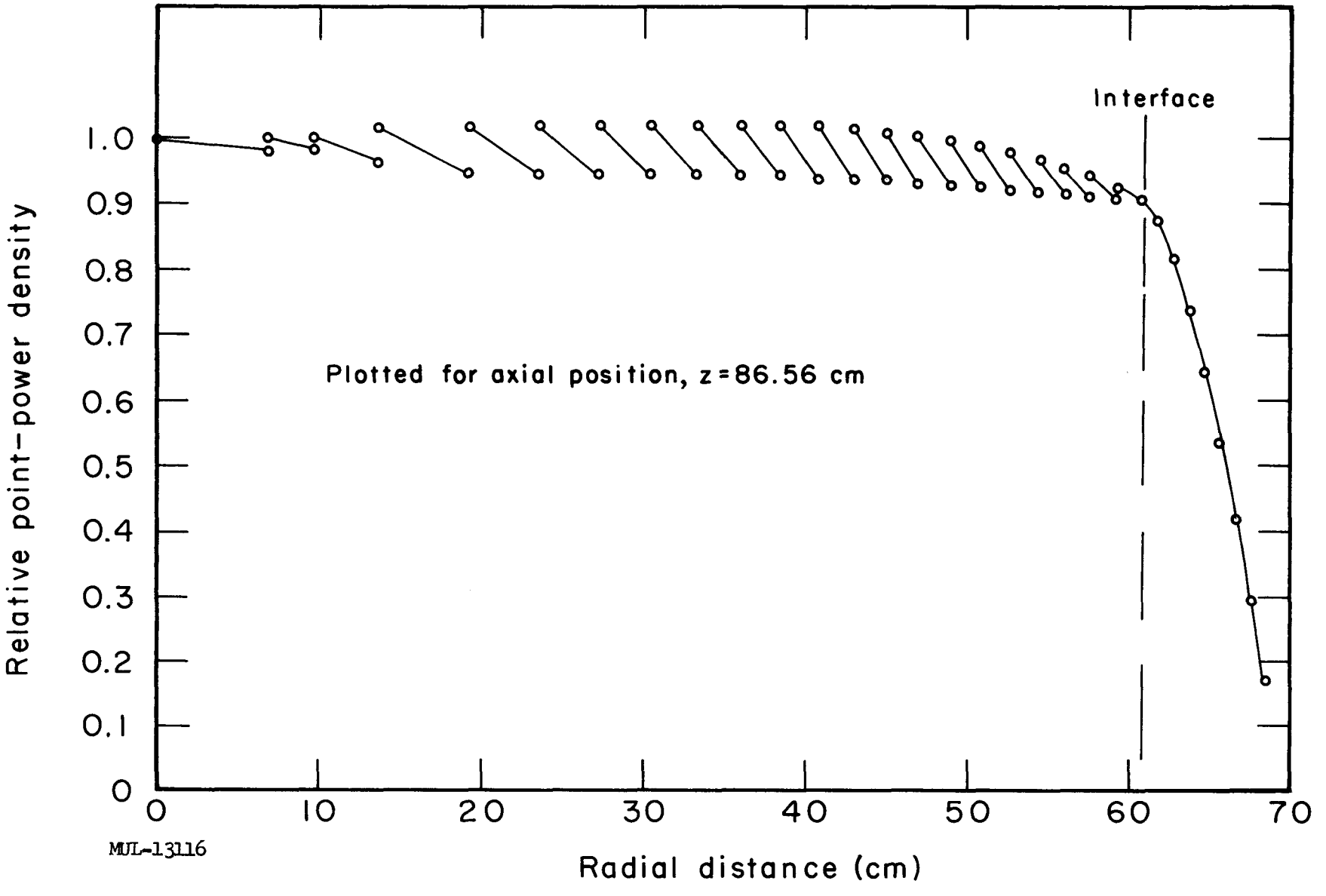

Fig. III-1. Radial power profile, Angie.

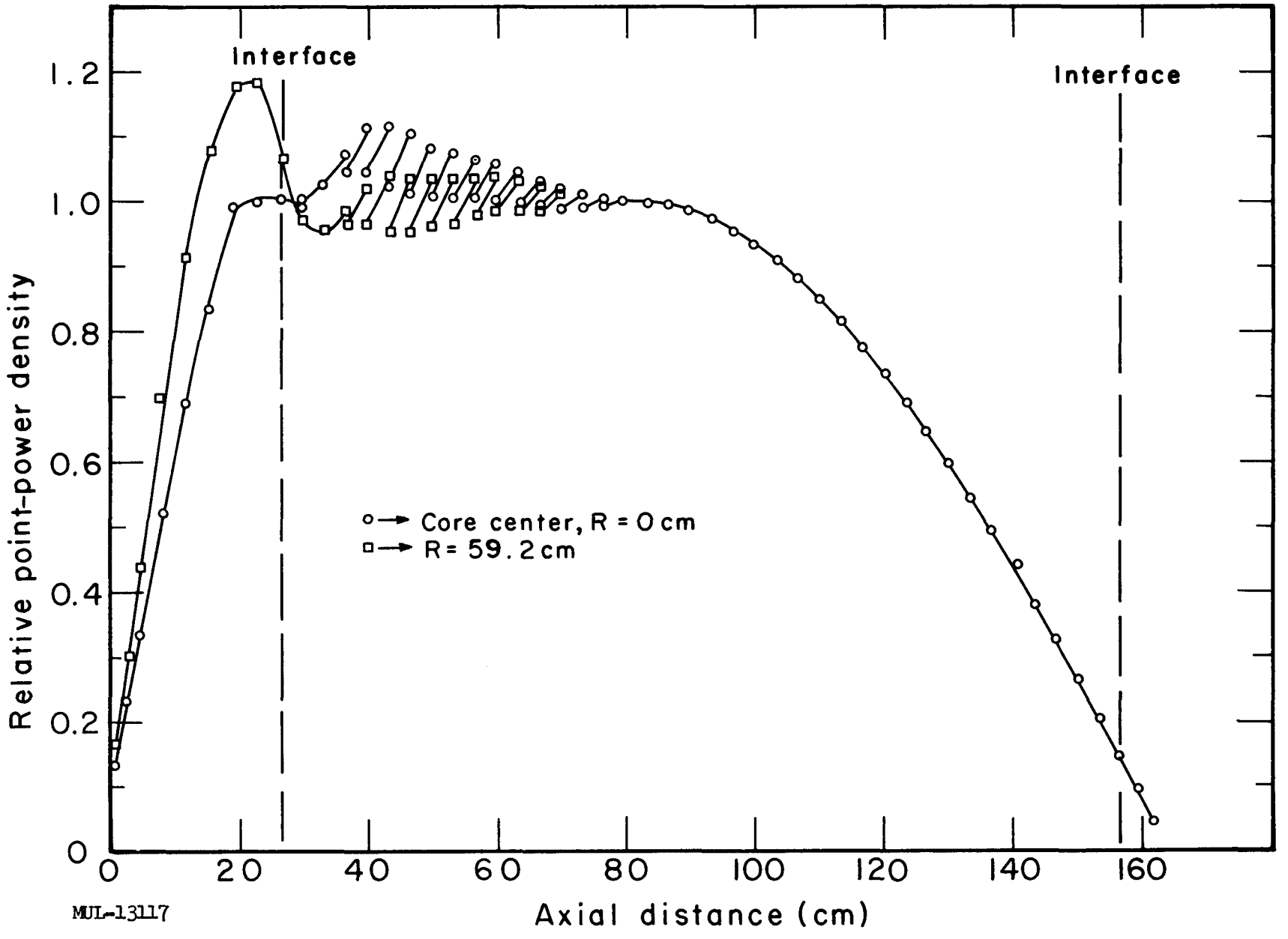

Fig. III-2. Axial power profiles, Angie.

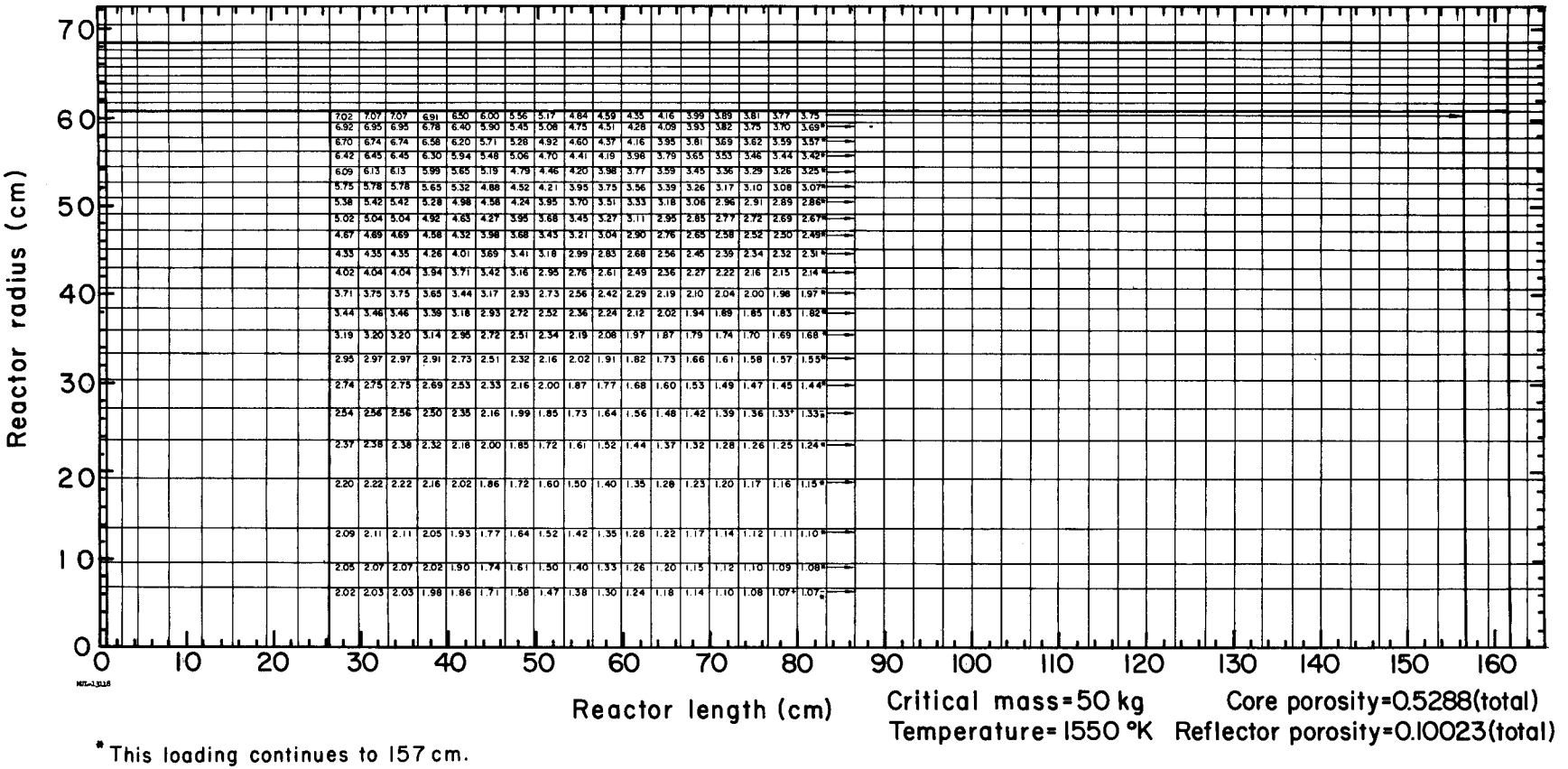

Fig. III-3. Weight percent of OyO_2 in fueled tubes.

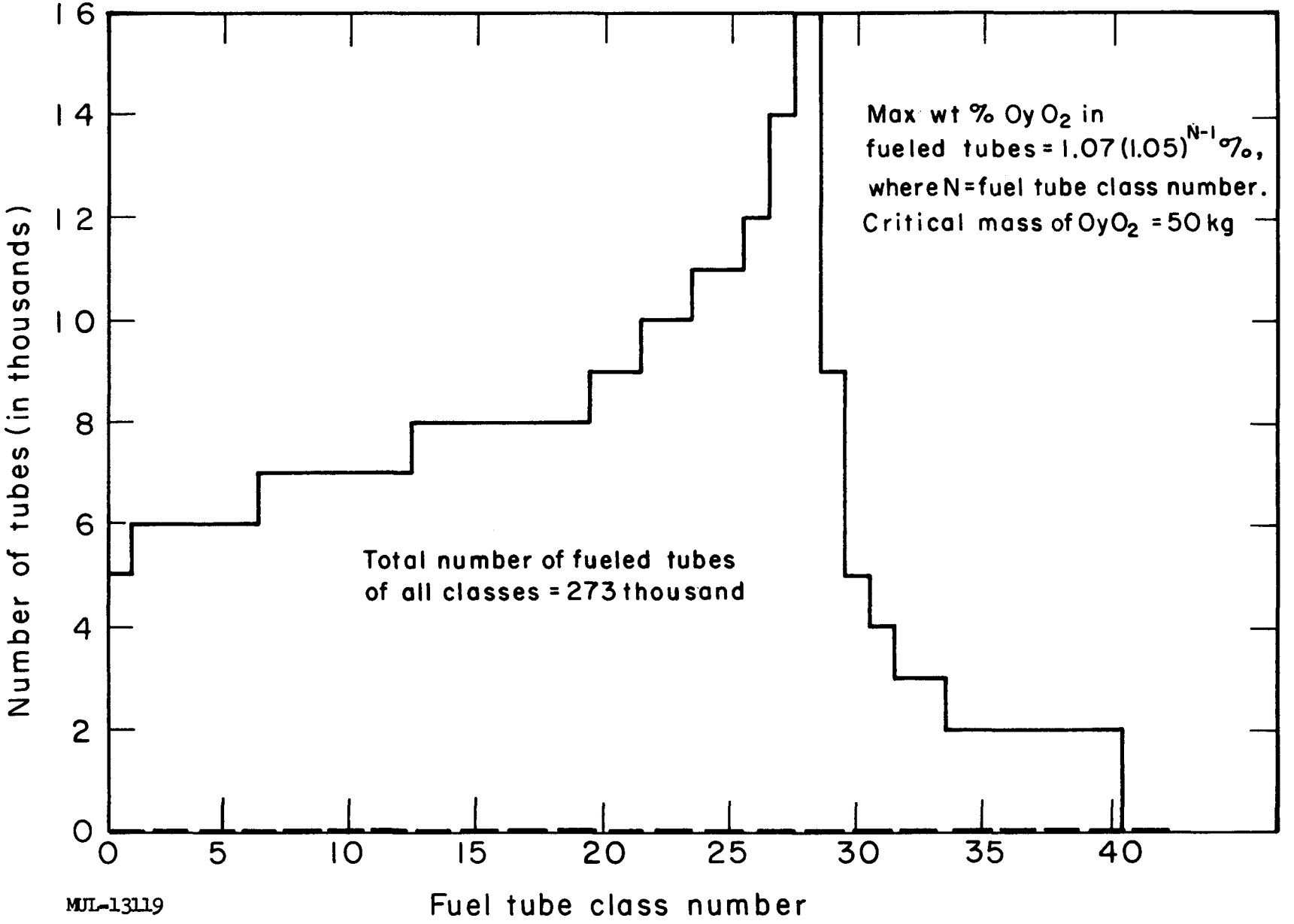

Fig. III-4. Number of fueled tubes vs class number for Tory II-C.

A 10% reduction in density may occur, which is found from Zoom calculations to imply that

$$\Delta k/k \simeq -0.003.$$

5. Xenon poisoning effects were estimated by Zoom calculations to be

$$(\Delta k/k)_{Xe} = -0.025.$$

A 10-hour operating period (which is appropriate to a Pluto reactor but not for Tory II-C) was assumed.

6. Fuel burnup is completely negligible. Even for a Pluto vehicle operating at 600 Mw for 10 hours, only 250 g of U^{235} are consumed. For a 50-kg OyO_2 loading, this is 0.5%, or $\Delta k/k \simeq -0.001$.

7. The niobium base plates are approximately equivalent to 0.4 in. of BeO at the core density. The additional length is shown by Zoom to be equivalent to

$$\Delta k/k \simeq +0.002.$$

The calculations showed that $\frac{\Delta k/k}{\Delta Z} \simeq 0.0054/\text{inch}$.

The final tally gives, for a 50-kg OyO_2 fuel loading,

$$k_{eff} = 0.974.$$

Zoom calculations show that a 7.6% increase in fuel loading is required to change k_{eff} by 1%. Therefore, the fuel loading must be increased by 19.5% to achieve a value of $k_{eff} = 1.00$.

The present required critical mass for the Tory II-C would be 60 kg OyO_2, from the above considerations. To maintain a critical mass near 50 kg OyO_2, a reduction in fuel-tube hole diameter to 0.227 in. (from 0.229 in.) was recommended. Upon acceptance, the critical mass was reduced to $M_c = 52$ kg OyO_2.

TORY II-C CONTROL RODS: NEUTRONIC ASPECTS

Neutronic control of Tory II-C is to be achieved by 12 hafnium control rods which are inserted axially into the core through the forward reflector. The axes of these "shim" rods are all approximately 8.9 in. from the core axis and are equally spaced. Two additional vernier rods are found 17.2 in. from the core axis.

A design currently in favor has a cross section of asterisk shape (i.e., six blades emanating from the center). Each blade is 0.5 in. in length,

0.080 in. thick, and makes an angle of 60° with its neighbors. The rod tips fall on a 1.0-in. circle.

The reactivity swing required in Tory II-C is: $\Delta k \simeq 0.13$. The following items account for the large value:

1. Temperature			
Nuclear	$\Delta k = -0.050$		
Geometry	-0.025		
Total		-0.075	
2. Xenon override		-0.025	
3. Shutdown		-0.025	
4. Excess at operating temp		-0.005	
	Total	-0.130	

In the event that the magnitude of the temperature effect is greater than $\Delta k = 0.075$, a greater swing would be required. It is sensible therefore to design for the largest reactivity swing allowable within limits set by matters such as maximum permissible power loads of the rods.

Two series of experiments have been performed to estimate the worth of such a system of shim rods. One involved the Spade facility, where simple hafnium strips were inserted into the center of a bare BeO assembly. The fuel-to-moderator molar ratio was: $BeO:U^{235} = 247$. A pulsed-neutron technique was employed. (See UCRL-6258.) Here, the initial dimensions were left unchanged and the degree of subcriticality (in dollars) was determined. In addition, experiments were performed relating the decrease in assembly height to its reactivity (dollar) cost.

The second series made use of the Snoopy facility, and a bare graphite assembly ($C:U^{235} = 600$) was used. An actual Tory II-C prototype hafnium rod of cruciform design was studied (i.e., four arms, 7/16 in. × 1/16 in. sheet of absorber in each arm, and overall dimensions of 1-1/8 in. × 1-1/8 in.). The graphite assembly was chosen here to represent more closely the Tory II-C scale of dimensions. That is, if one recalls from comparison of bare Spade and Snoopy experiments that 1.115 g of graphite is neutronically equivalent to 1.000 g of BeO, then the Snoopy assembly of density $\rho = 1.64$ g/cc is equivalent to one of BeO with $\rho(BeO) = 1.47$ g/cc. In Tory II-C, the density of BeO in the cold configuration is approximately 1.40 g/cc. Therefore, a

slight correction is required in scaling the Snoopy findings to the Tory II-C case, whereas a large correction is necessary in the case of the Spade experiments.

A. Spade Experiments

The major portion of the series was described in UCRL-6258 (Pluto Quarterly Report No. 6), pp. 88-92. In addition, it was found that a 1.00-in. decrease in height (from 20.0 to 19.0 in.) reduced the system reactivity by -$3.02. A Zoom calculation for this same change gave $\Delta k/k = -0.0263$. Therefore,

$$\beta_{eff} = \frac{0.0263}{3.02} = 0.0087.$$

This value is surprisingly large, since the value for β (i.e., delayed neutron fraction) is 0.0064.* However, β_{eff} is a sensitive function of the high-energy scattering cross sections and slowing-down character of the moderator. These constants at present are poorly known. Zoom calculations yield values for β_{eff} for the following cases:

Tory II-C	:	$\beta_{eff} = 0.0068$
Tory II-A	:	$\beta_{eff} = 0.0069$
Spade (247:1):		$\beta_{eff} = 0.0070$

These were found by removing 0.158 fission neutrons from the fission spectrum and replacing that same number at energies appropriate to the delayed neutrons. The removal reduced k_{eff} by 0.0064, whereas replacement raised k_{eff} by (β_{eff}/β) 0.0064, or simply β_{eff}.

The discrepancy between experiment and calculation is significant and warrants further study.

The issue of β_{eff} can be overlooked if the effect of a control rod is expressed in terms of changes in assembly height rather than dollars. If this is done, the worth of a Tory II-C control rod can be determined after several adjustments are made. These are listed below.

1. Spectrum differences
2. Density differences
3. Geometry of rod
4. Effect of void around rod
5. Partial rod insertion
6. Radial worth of rod
7. Interaction effects

*ANL-5800, p. 25 (1958).

Items 1, 5, and 6 were evaluated with the Zoom code. Item 2 involved a simple argument from mean free paths. Item 3 considered an experiment at LRL which showed that a cruciform, 1 in. × 1 in., was 1.7 times as effective as a 1-in. slab of the same thickness. Item 4 was estimated to be almost negligible. Item 7 is currently under study. The control rod worth in Tory II-C (i.e., 1 in. diameter, 6 blades, 0.080 in. thickness) is:

$$\Delta k \text{ per rod} = 0.018$$
$$\Delta k \text{ for 12 rods} = 0.216$$

The Spade experiment therefore indicates that the present rod design is adequate.

B. Snoopy Experiments

The Snoopy experiments also related control rod effects to change in assembly height. An actual prototype rod of cruciform shape was studied. The adjustments required to relate the finds to Tory II-C are:

1. Spectrum differences
2. Density and material differences
3. Geometry of rod
4. Partial rod insertion
5. Radial worth of rod
6. Rod interactions

Considerations similar to those in the Spade case give, for the Tory II-C control rod (i.e., 1 in. diameter, 6 blades, 0.080 in. thickness):

$$\Delta k \text{ per rod} = 0.011$$
$$\Delta k \text{ for 12 rods} = 0.133$$

Here the rods are seen to be barely adequate for Tory II-C requirements. The discrepancy between Spade and Snoopy extrapolations is not understood. However, the more conservative finding is found to be in slight excess of the minimum swing of $\Delta k = 0.13$.

In addition, fission traverses were taken normal to the prototype rod. It was worth $\Delta k = 0.0145$, as found from the assembly height change. An approximate value of \$2.60 was found by a rod "bump" experiment. The former value is thought to be of higher accuracy. A traverse along the prototype rod axis was also taken. The combined data are shown in Fig. III-5. Depressions of 20% in power density may therefore be anticipated in Tory II-C in the fuel elements closest to the control rods.

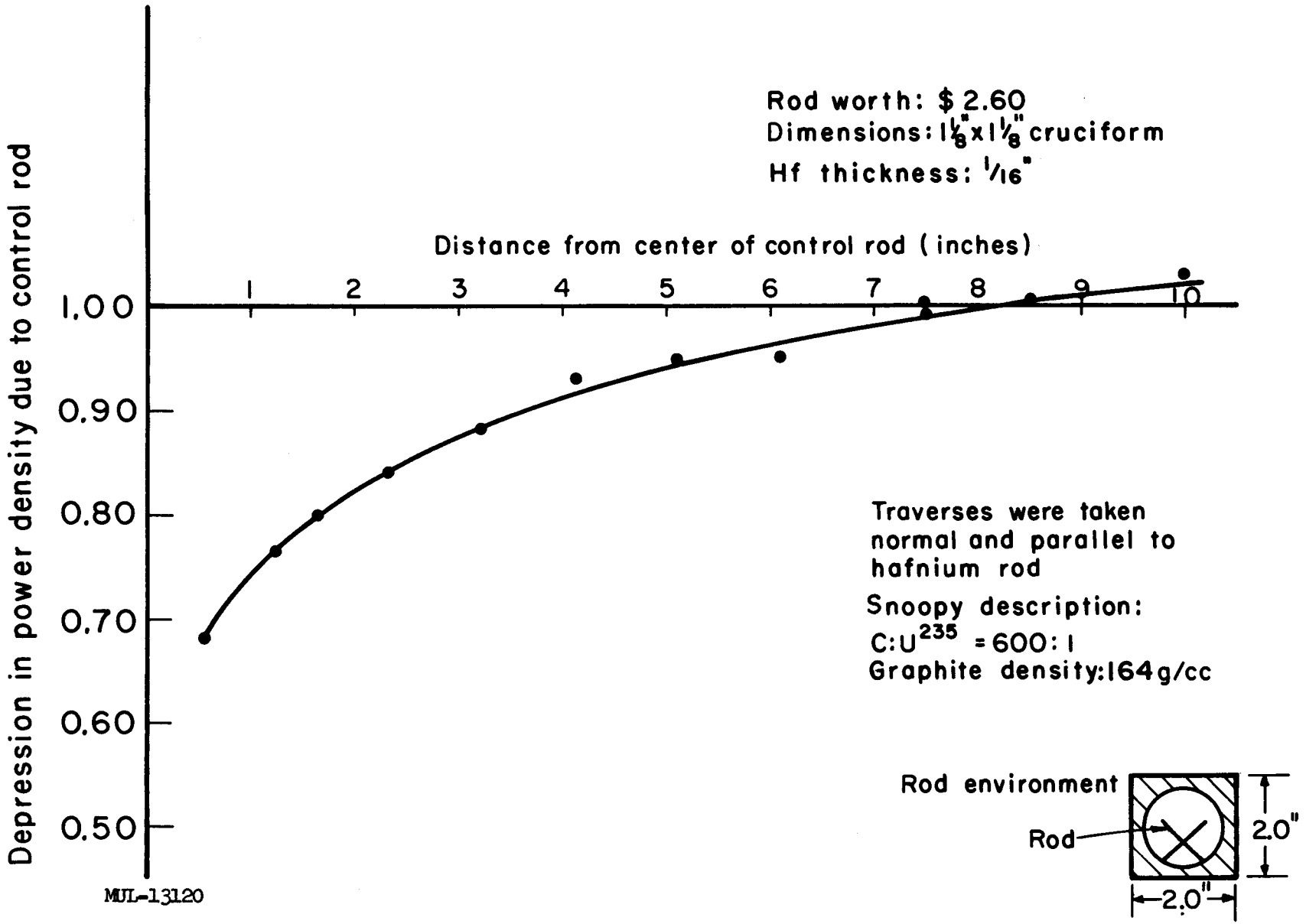

Fig. III-5. Effect on power density of hafnium control rod in Snoopy assembly.

NUCLEAR HEATING OF TORY II-C TIE RODS

Radiation heating of the Tory II-C tie rods has been calculated as a function of axial position for seven radial stations, from R = 0 to R = 26.7 in. The heating calculations were performed for both R-235 and René 41 tie rods of 0.58 in. i.d. and 0.67 in. o.d. surrounded by 12 unfueled BeO tubes in the fueled core region.

Gamma heating calculations are based on a source of ≈ 15 Mev/fission, which assumes that the fission-product gammas have reached saturation. Neutron heating due to (n, γ) and (n, n) reactions has been calculated from the Angie neutronics code output.

The total heating power density distribution for both R-235 and René 41 tie rods is given in Figs. III-6 and III-7, respectively. The following peak heating values were found for the two considered materials:

R-235: 0.89 Mw/ft^3 per Mw/ft^3

René 41: 1.15 Mw/ft^3 per Mw/ft^3

These power density values are given in Mw/ft^3 and are normalized to 1 Mw/ft^3 of average core power density based on the fueled core volume.

Summary of Calculations

1. Gamma Heating

The gamma heating power density distribution in the fueled core was obtained in the following manner:

(a) Infinite medium heating values for Hastelloy R-235 were computed by means of the Trikl code* for various medium compositions having uranium loadings representative of the Tory II-C loading. The effective loading, which is the average loading seen by gamma rays of average energy at a specific location in the core, was correlated to the Trikl heating values yielding a uranium-loading-dependent gamma heating distribution for the Tory II-C core.

---

*Trikl, which has been Fortraned for the IBM 7090, is designed to evaluate gamma energy deposition in an infinite source medium. The code computes event probabilities and follows the energy degradation history of photons born in the infinite source medium. The results are expressed in the form of an enhancement factor, a dimensionless ratio of actual heating to heating realized if only the Compton process prevailed, and in the form of absorbed energy density in each material. The code, designed for 30 energy groups and 9 materials, can be conveniently applied to calculate the heating of individual materials in a source medium in regions which are far removed from boundaries.

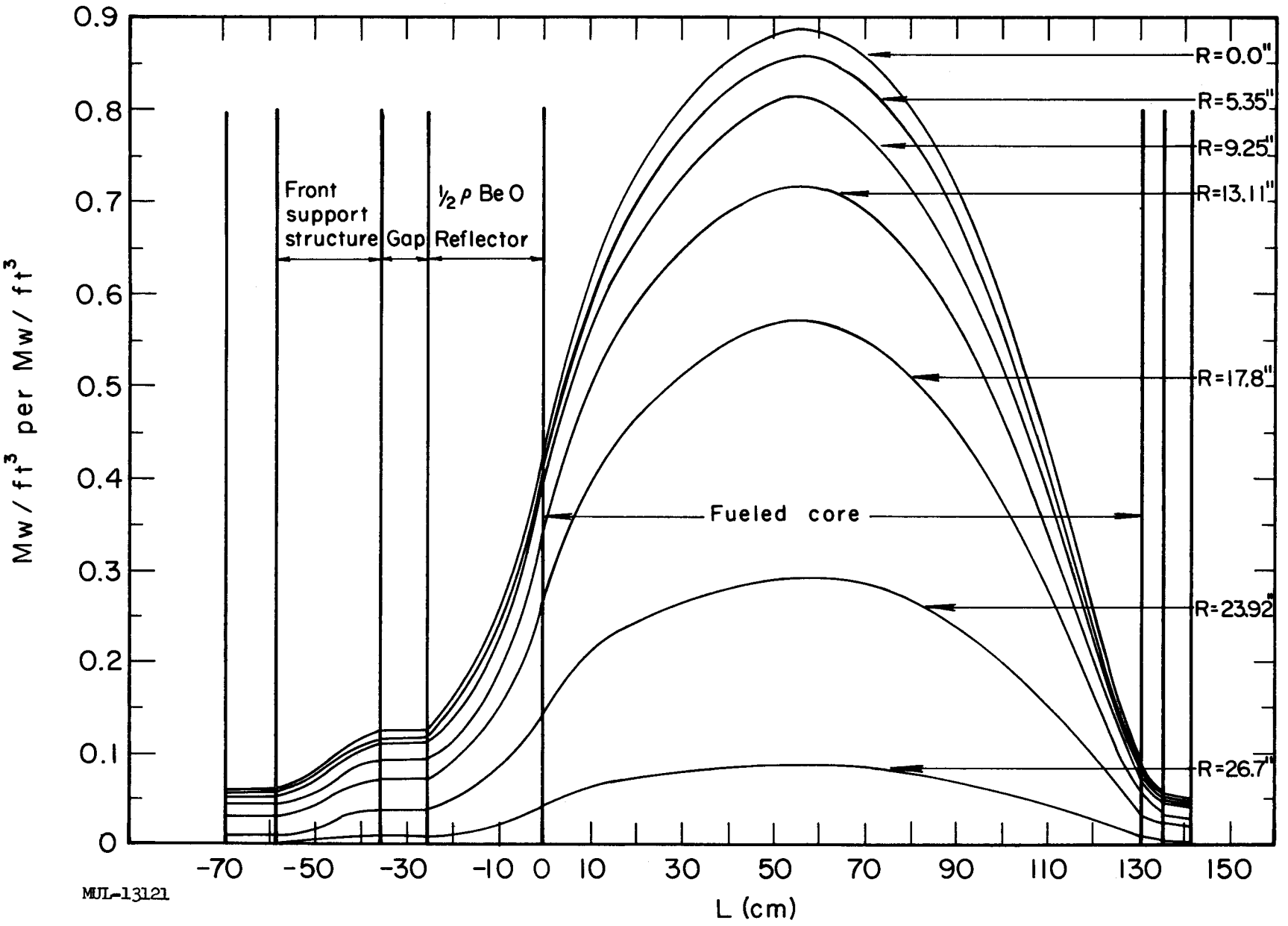

Fig. III-6. Nuclear heating power density in Tory II-C R-235 tie rods.

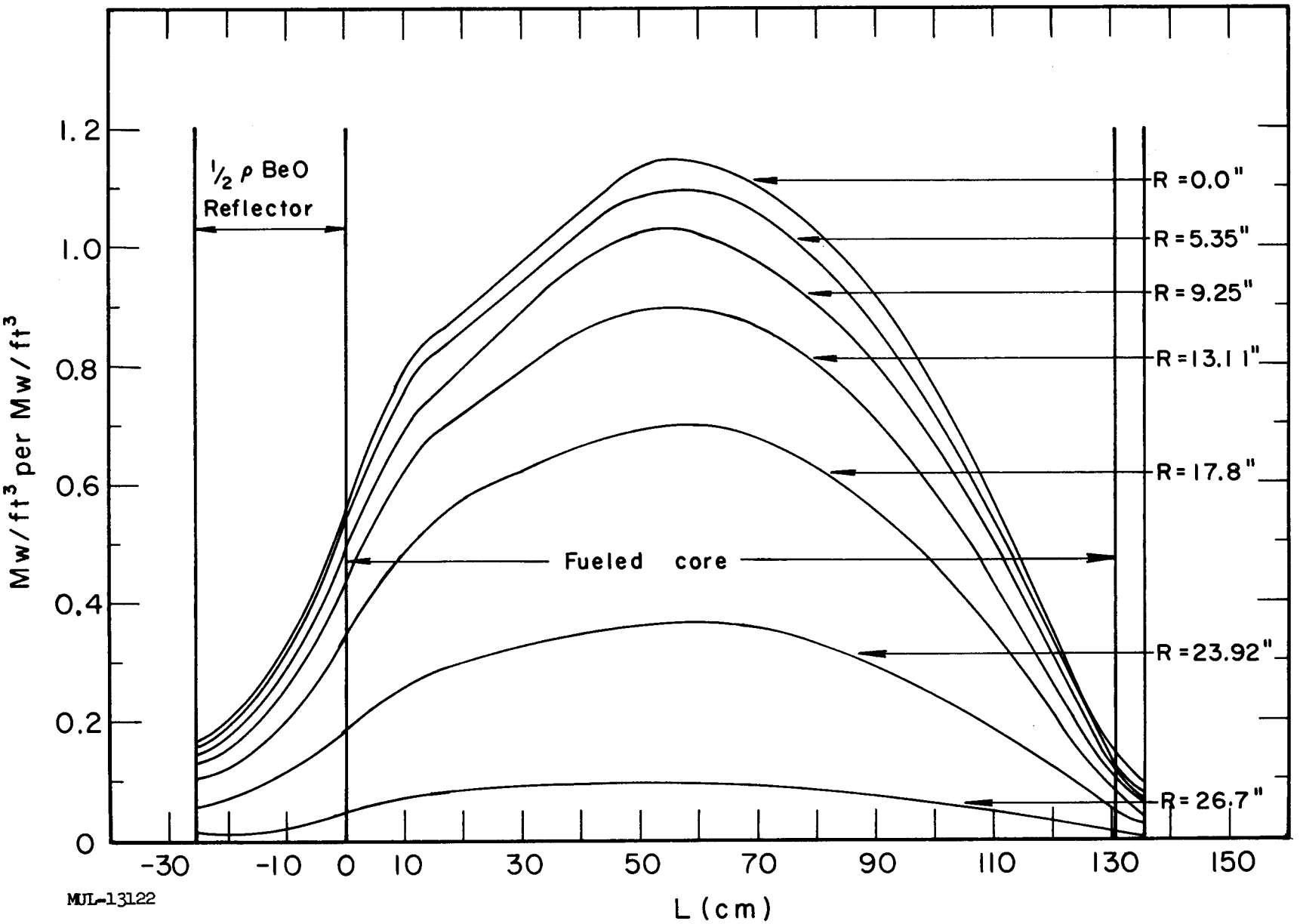

Fig. III-7. Nuclear heating power density in Tory II-C René 41 tie rods.

(b) The effects of tie-rod self-shielding, and shielding due to the unfueled BeO surrounding the tie rods, were incorporated into the above Trikl calculations by correcting the photoelectric cross section of the tie-rod material. The self-shielding factors were calculated from KAPL-1262, "Self-shielding factors for infinitely long, hollow cylinders." The shielding factor was shown to be proportional to the exponential integral of the second order E_2 (μx), where (μx) was considered to be the photoelectric mean-free-path thickness of the unfueled BeO. Both of these factors tend to reduce the photoelectric cross section of the tie-rod material in the energy range of most heating importance (see Figs. III-8 and III-9).

(c) The self-shielded and shielded uranium-loading-dependent gamma heating distribution was then superimposed upon the axial Tory II-C power density profile normalized to unity over the fueled length of the core, and the axial and radial gamma-ray energy absorption intensity functions for a uniformly loaded flat power cylinder of Tory II-C core dimensions.

To summarize, the gamma heating density dependence in the core incorporates the following factors:

1. Uranium loading variation
2. Self-shielding of the tie rods
3. Shielding of tie rods by the surrounding BeO
4. Axial power density profile
5. Axial and radial geometry effects

The infinite-medium Trikl results for the case of unshielded and shielded R-235 tie rods (as described above) and the corresponding BeO heating are given in Figs. III-8 and III-9, respectively. It can be seen that for a uranium loading factor of 1 (average BeO:U) a reduction of 25% in tie-rod R-235 heating is realized by including the shielding effects.

The fission gamma heating of René 41 was assumed to be the same as that of R-235 on the basis of a few sample Trikl calculations, and is reasonable to assume since their densities and Z's are similar.

2. Neutron Heating

Neutron heating of both R-235 and René 41 was calculated from the Angie results. Neutron heating results from two separate processes: absorption of low-energy neutrons or (n, γ) interactions, and loss of energy from elastic scattering or (n, n) interaction.

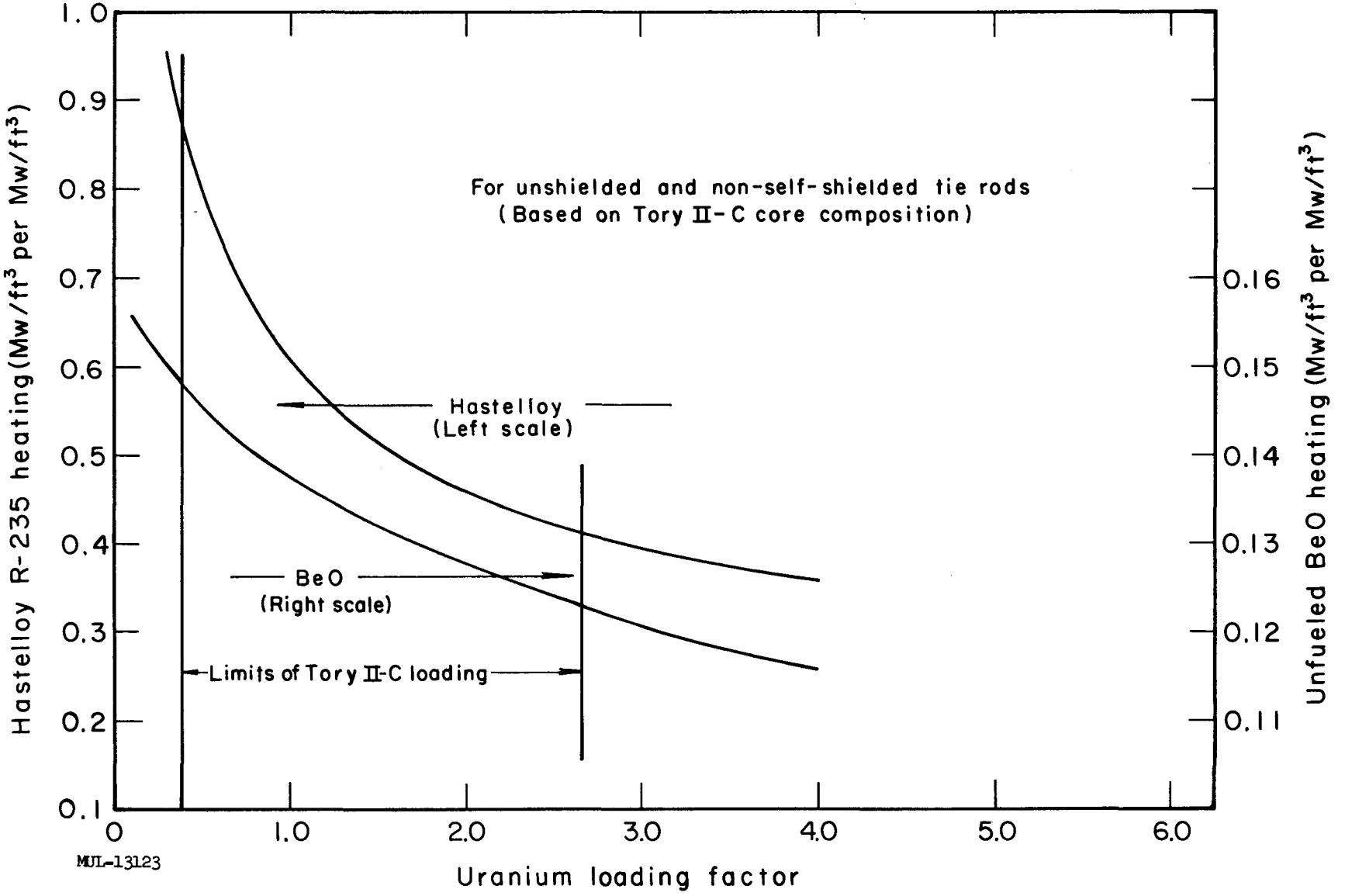

Fig. III-8. Infinite medium Hastelloy R-235 and BeO gamma heating as a function of the fuel loading factor for the Tory II-C core.

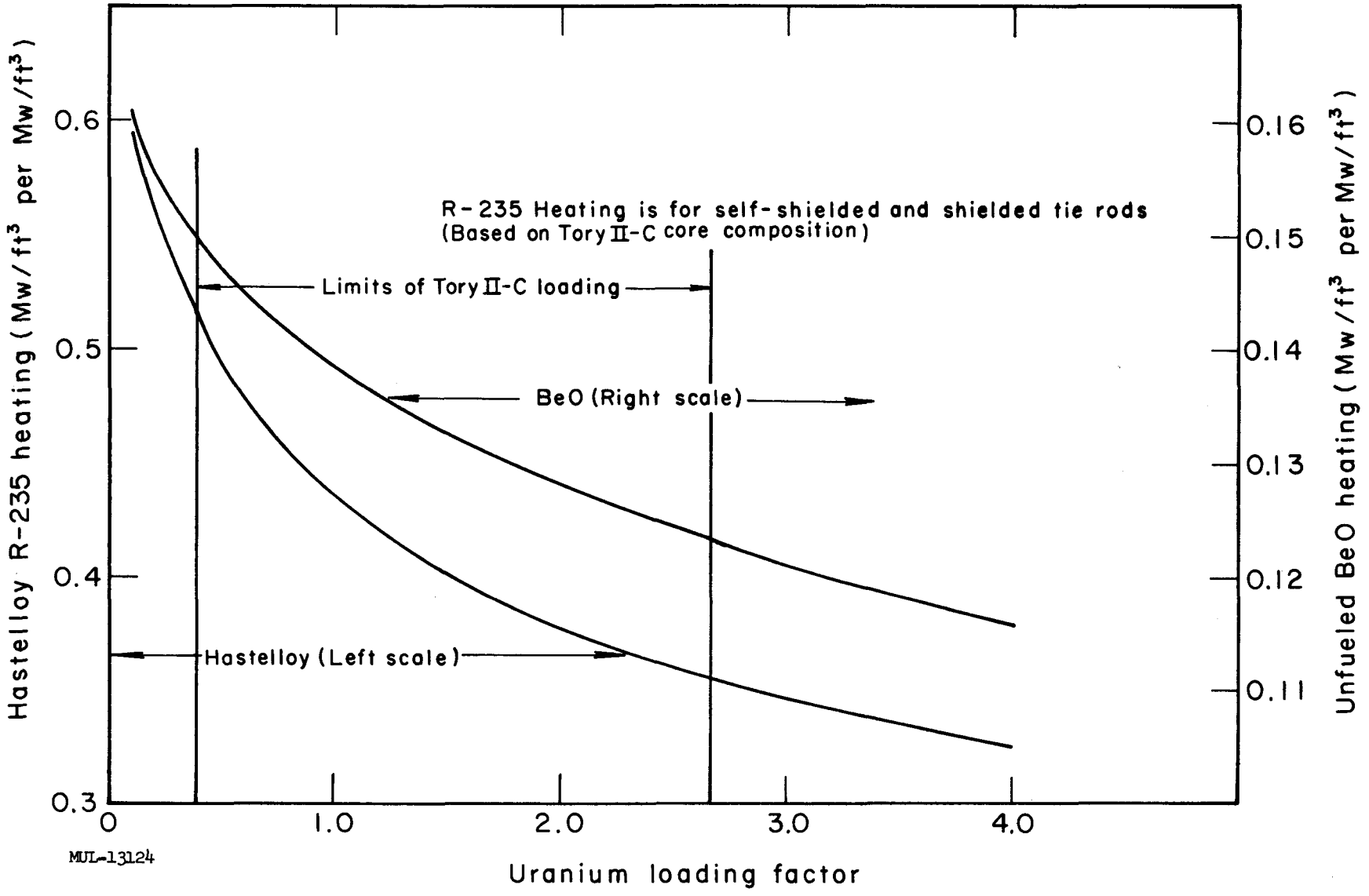

Fig. III-9. Infinite medium Hastelloy R-235 and BeO gamma heating as a function of the fuel loading factor for the Tory II-C core.

For the (n, γ) process, a summation of $\Sigma_a \phi$ was performed over the twelve bottom groups (which includes the resonances of R-235 in groups 8 and 12 and that of René 41 in group 9) along the length of the reactor at various radii; the Σ_a used were self-shielded for the considered tie rods. The spatial dependence of (n, γ) heating of tie rods was obtained from the calculated neutron capture density in the tie rods and the determination of the fractional gamma energy (from the (n, γ) process) absorbed by the tie rod per neutron captured.

The fraction of energy generated and absorbed by the tie-rod material can be shown to be equivalent to the self-shielding factor of the tie rod defined in KAPL-1262. A self-absorption fraction of 0.14 was calculated by considering an average gamma energy absorption coefficient ($\mu_a \rho$) of 0.2 cm^{-1} (for R-235 $\mu_a \rho$ is relatively flat in the 1 to 10 Mev range) and a total of 8.84 Mev released per capture.

The (n, n) heating was calculated by summing $\Sigma_{sc} \phi \Delta E$ (where ΔE is the average energy loss for elastic collision) over the six top energy groups along the axis of the reactor and scaled radially with the normalized flux dependence.

3. Heating Outside of the Fueled Core

Neutron heating in the reflector regions was calculated from the Angie problem in the same way as it was done for the core region.

Gamma heating dependence in the front, side, and back reflectors can be shown to fall off as the E_2 (μx) function, if one assumes the model of an infinite source plane having a cos θ emission shielded by an infinite slab.

The heating of the tie rods is enhanced in the region of the front support structure because of the (n, γ) process in the front support structure material. A conservative estimate of this secondary heating was made by assuming that (a) the neutron flux falls off exponentially in the front support structure, (b) all of the gamma energy released by the (n, γ) process contributes to the gamma flux, and (c) the gamma heating flux at the aft surface of the front support structure (facing the reactor) assumes half of the nonleakage value. The resulting dependence of this secondary heating is one that assumes a maximum at approximately t/3 (where t is the front support structure thickness) and which falls off exponentially from that point on.

NUCLEAR HEATING OF TORY II-C HAFNIUM CONTROL RODS

Control rod heating was calculated for two types of control rod configurations:

a) Twelve 1/8 in. by 1 in. cruciform rods at R = 20 cm

b) Twelve 1/16 in. by 1 in. cruciform (or asterisk-shaped) rods at R = 20 cm which have a neutron absorption capacity corresponding to a minimum required reactivity swing as determined from neutronics considerations.

Both calculations were done for fully inserted control rods at equilibrium conditions, i.e., saturation of fission-product decay gammas and steady-state neutronics.

The peak heating density values for each considered case are as follows:

a) 1/8 rod : 3.44 Mw/ft^3 per Mw/ft^3

b) 1/16 rod: 2.66 Mw/ft^3 per Mw/ft^3

The heating power density values are given in Mw/ft^3 and are normalized to 1 Mw/ft^3 of average core power density based on the fueled volume of the core.

Summary of Calculations

1. Gamma Heating

Fission gamma heating of the hafnium control rods was determined from infinite-medium values calculated by the Trikl code superimposed upon the Tory II-C power density profile and the axial and radial gamma-ray absorption intensity dependence due to geometry. The following features were included in the Trikl calculations:

(a) The medium uranium loading considered at each axial location was found by averaging the composition within a radius of one mean free path (λ = 20 cm), taking into account the axial and radial uranium loading dependence.

(b) The hafnium photoelectric absorption cross sections were corrected for self-shielding appropriate to each considered rod thickness (the self-shielding was calculated for a slab model), and were further modified to simulate the shielding effect of the R-235 shell around the control rod. The effect of the surrounding layer of unfueled BeO tubes was neglected.

2. Neutron Heating

For each neutron absorbed by the control rods $\approx$ 6.6 Mev are released in the form of high-energy gamma rays. A fraction of these gamma rays will be absorbed by the hafnium upon first collision. The balance of the energy is

assumed to escape into the surrounding medium. Some of that energy may re-enter the control rod material and be absorbed in it.

The neutron capture density in the 1/8 in. by 1 in. hafnium control rods was calculated from the Zoom output by summing over $\Sigma_a \phi$. It was found that 0.02147 neutrons per fission were absorbed by one cruciform rod.

The fraction of gammas from the (n, γ) process that is absorbed by the control rods was calculated by averaging over the (n, γ) source spectrum,* assuming that the gammas are made uniformly in a rod simulated by a cylinder of cross-sectional area equal to that of the cruciform. It was found that 24% of the (n, γ) energy is absorbed by a 1/8-in. blade.

The axial dependence of (n, γ) heating was obtained from the neutron flux distribution given in the Angie output.

In order to estimate the secondary (n, γ) heating, the escaped 76% of the (n, γ) energy was used as input for a Trikl problem which distributed this energy among the materials in the medium, using the same assumptions and corrections as those outlined above under "Gamma Heating."

3. Effect of Reducing Rod Thickness to 1/16"

The number of neutrons per fission absorbed per 1/8-in. rod is given above as 0.02147. However, from neutron economy considerations and from a realistic reactivity swing requirement it can be shown that the number of neutrons absorbed per rod need not be larger than 0.0127. From Zoom calculations it was found that

$$\frac{\Delta k/k}{\Delta n/\text{fiss.}} \cong 0.85 \pm 10\%.$$

In order to have the minimum necessary reactivity swing one needs a $(\Delta k/k) \cong 0.13$,† which implies a (Δn/fiss.) of 0.1525 for 12 rods and 0.0127 for 1 rod.

If one then considers control rods of smaller cross-sectional area to comply with the minimum reactivity requirement, it follows that the (n, γ) heating will be reduced by the fact that less neutrons will be absorbed and by the higher escape probability of the (n, γ) energy. The thickness of blades of such a rod was considered to be 1/16 in. In particular, six blades, each 1/2 in. wide, assembled to give an asterisk-like cross section, comprise the rod.

---

* L. V. Groshev et al., Atlas of γ-Ray Spectra from Radiative Capture of Thermal Neutrons (Pergammon Press, 1959).

† See p. 80, line 13.

Although a reduction in rod thickness reduces the (n, γ) heating of hafnium, the gamma heating per cubic foot on the other hand is shown to increase; this can be explained by the decrease of the self-shielding effect.

The latest proposed control rod design is one which has six 80-mil-thick by 1/2-in. blades arranged in an asterisk configuration. Available data indicates that the peak heating of such rods may assume approximately 3.0 Mw/ft^3 per Mw/ft^3.

A more precise analysis method for the control rod heating is presently being developed in the form of a Monte Carlo machine code. Results of these calculations should yield more accurate heating values.

SECTION II. AEROTHERMODYNAMICS

TORY II-C PERFORMANCE

During this reporting period, the final dimensions of all BeO tubes were determined. Preliminary reactor performance characteristics are as follows:

Flight parameters at the design point are:

a. Missile vehicle Mach number = 2.8
b. Missile altitude = 1000 ft
c. Ambient temperature = 311°K = 100°F
d. Diffuser angle of attack = 0 deg

The inlet design point parameters have been chosen to be the following:

a. Pressure recovery = 0.80
b. Bleed fraction = 0.04
c. Momentum recovery of bleed = 0.80
d. Supersonic spillage = 0
e. Diffuser operation ≃ critical

Reactor design parameters are taken to be the following (cold conditions):

a. Active core diameter = 47.25 in.
b. Side reflector thickness = 3 in.
c. Missile body diameter = 57.00 in.
d. Active core length = 50.7 in.
e. Exit reflector thickness = 2 in.
f. Entrance reflector thickness = 10 in.
g. Total fuel element flow area 848.5 in^2 (Γ_{FE} = 0.530)

h. Total side reflector tube flow area = 25.1 in^2 ($\bar{\Gamma}_{SR}$ = 0.054)

i. Tie rod flow area = 30.4 in^2 (Γ_{TR} = 0.749) (core and reflector)

j. Tie rod peripheral tube flow area = 13.29 in^2 (Γ_{TP} = 0.1481)

k. Control rod flow area = 14.8 in^2 (14 control rods)

l. Side support flow area $\simeq$ 120 in^2 (function of several temperatures)

Major fuel element parameters are the following:

1. Axial power shape as shown in Fig. III-10, flat radial power density at any axial station integrated over length of tube.

2. Maximum fuel element wall temperature = 2500°F.

3. Maximum fuel element internal temperature = 2568°F. (Use this for thermal expansion.)

4. Fuel element hole radius (cold) = 0.1135 in.*

5. Fuel element conduit L/D = 281 (includes end reflectors and 1-in. base plate).

The exhaust nozzle of the system is assumed to have the following characteristics:

a. Fixed nozzle throat area (cannot be dimensioned until the reactor structural design is complete).

b. Expansion ratio variable such that gas exhaust pressure always equals atmospheric pressure.

c. Velocity coefficient = 0.98.

d. Divergence factor = 1.00.

Results of optimization calculations indicate the following fuel element parameters at the design point (Γ_{FE} = 0.530) (see Table III-1):

a. Maximum fuel element material power density = 27.41 Mw/ft^3

b. Maximum volumetric power density = 12.88 Mw/ft^3

c. Hole radius (hot) = 0.1146 in.

d. Entrance Mach number = 0.225

e. Exit Mach number = 0.520

f. Maximum wall temperature = 2500°F

g. Entrance stagnation temperature = 946°F

h. Exit stagnation temperature = 2150°F

---

* The calculated optimum fuel element radius is 0.118 inch (hot). The decrease in hole size to 0.1135 inch (cold) caused a 0.08% loss in thrust coefficient (negligible).

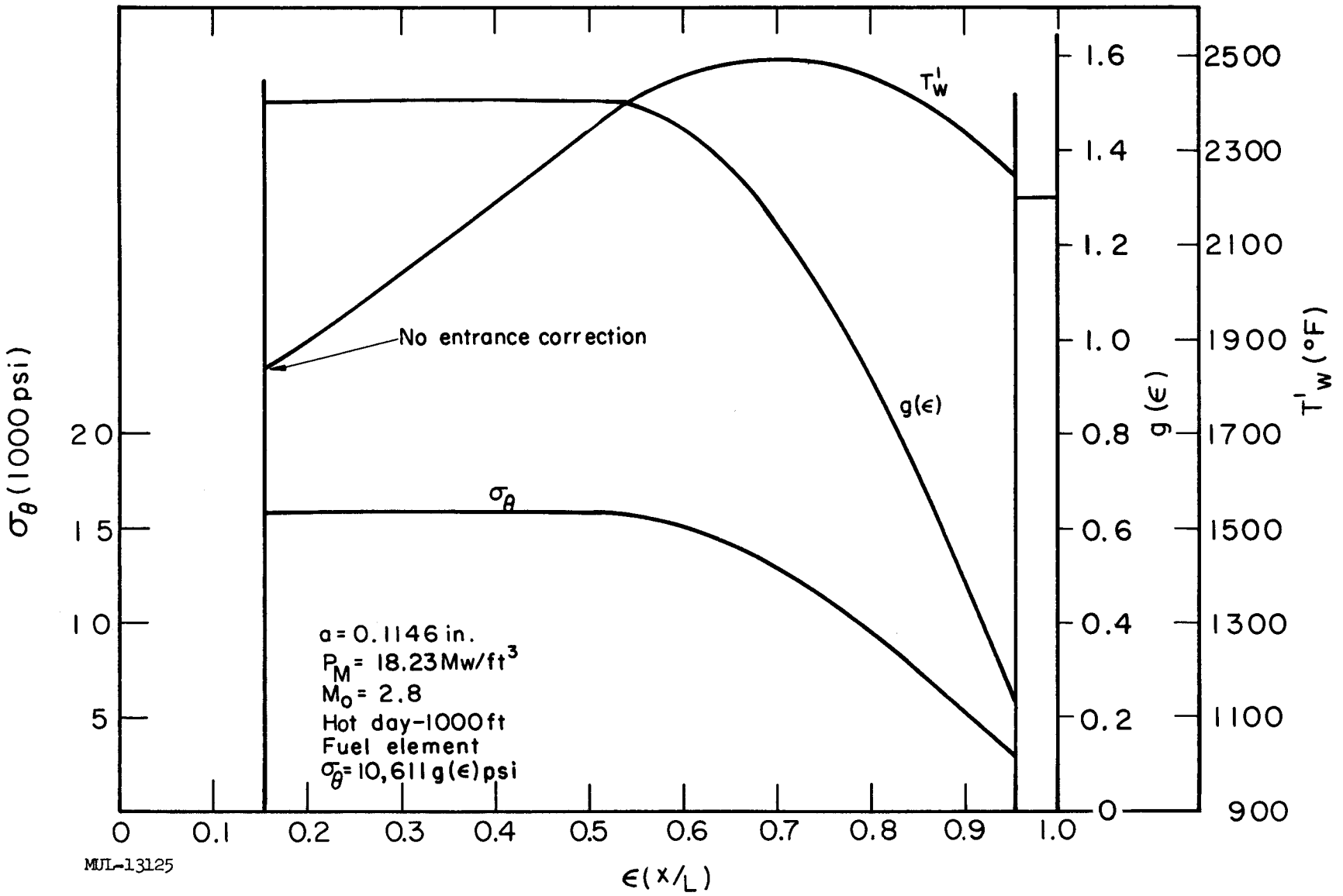

Fig. III-10. Tory II-C design parameters.

Table III-1. Fuel Element Parameters.*

Condition	P_{mat} max (Mw/ft^3)	P_{vol} max (Mw/ft^3)	M_1	M_2	T_w max (°F)	T_1^0 (°F)	T_2^0 (°F)	p_1^0 (psia)	p_2^0 (psia)	C_F (base)
Design M = 2.8	27.41	12.88	0.225	0.520	2500	946	2150	322	218	0.320
Limit M = 3.0	27.21	12.79	0.234	0.520	2500	1063	2172	347	235	0.240
T_1^0 = 600°F	36.61	17.21	0.202	0.520	2500	600	2049	350	244	---

*Hole radius = 0.1146 in. (hot).

i. Entrance stagnation pressure = 322 psia

j. Exit stagnation pressure = 218 psia

k. Single tube thrust coefficient (base) = 0.320

The true single tube thrust coefficient of Tory II-C is calculated to be 0.273 when the following corrections are made:

Thrust Coefficient

	Loss (%)
1. Boundary layer bleed	-4.0
2. Entrance losses (0.4% loss in pressure, some tapering of entrance assumed)	-0.7
3. Offset (misalignment) in air flow tubes	-3.0
4. Tube exit losses (5% loss in pressure, some tapering assumed)	-5.0
5. Power depression due to rods	-1.0
6. All others	-1.0
Total	-14.7

The predicted pressure, temperature, and Mach number profiles of a typical fuel element are presented in Figs. III-11 and III-12.

Gross design point parameters of Tory II-C have been estimated to be the following:

a. Total reactor power = 560 Mw (20,970 fueled conduits)

b. Total reactor flow rate = 1746 pps (1.5% for side reflector cooling, 2.3% for control rod cooling, 5% for tie rod cooling, 6.5% for side support cooling, 1.0% for tie rod tube cooling).

c. Average exit stagnation temperature $\simeq$ 2000°F

d. Reactor thrust coefficient based upon missile diameter of 57.00 in. = 0.171

Figure III-13 presents the results of an attempt at off-design performance analysis. When the diffuser is operating supercritical, the system is flow limited; hence, the thrust coefficient decreases for Mach numbers greater than 2.8 (hot day, 1000 ft altitude). For Mach numbers less than 2.8, the system becomes pressure limited and performance suffers accordingly. As shown in Fig. III-13, the performance curve for sub-design Mach numbers is incorrect, since losses due to flow spillage have not been included. The net result of this correction reduces the Mach margin. In addition, the drag coefficient,

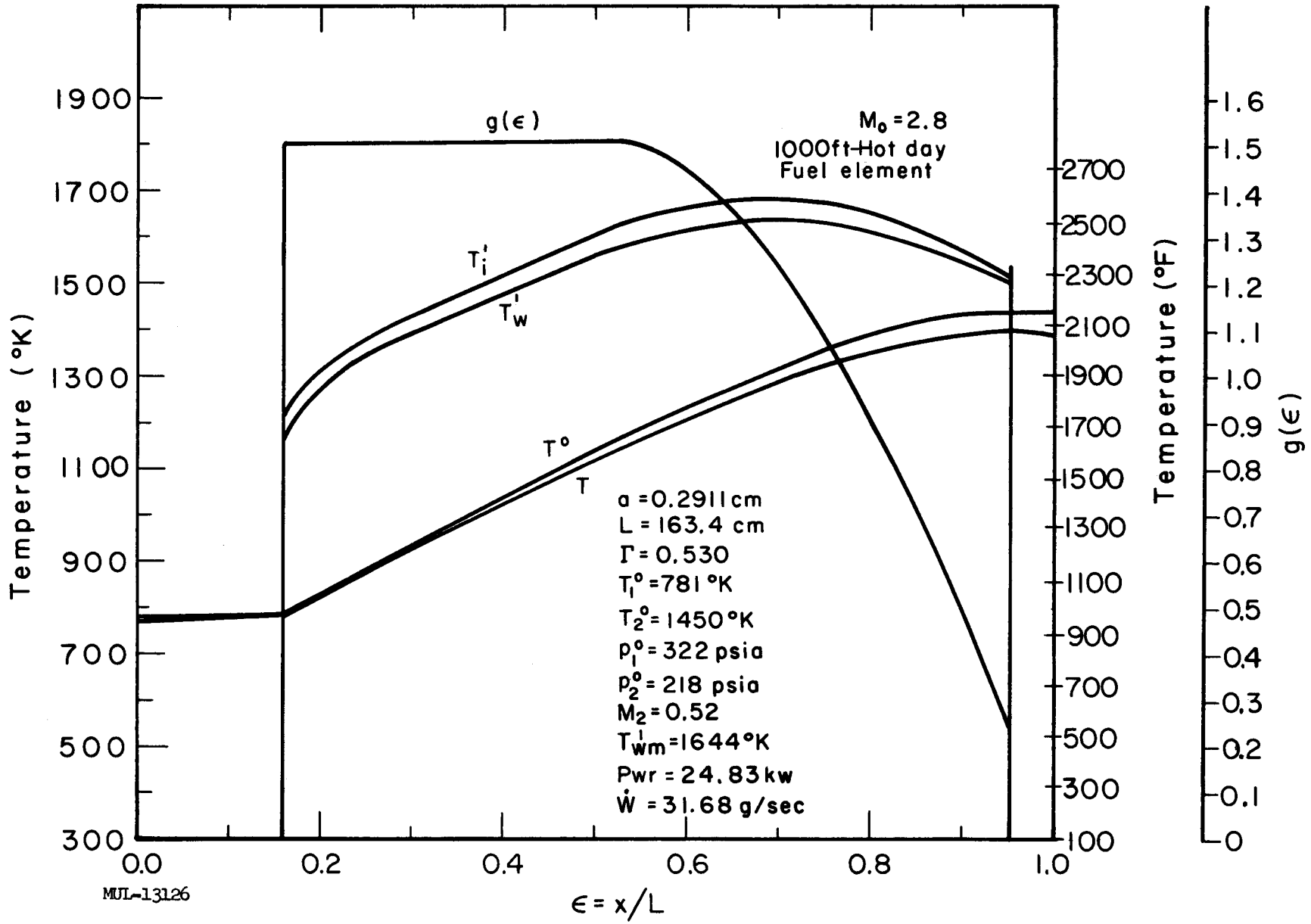

Fig. III-11. Tory II-C design point.

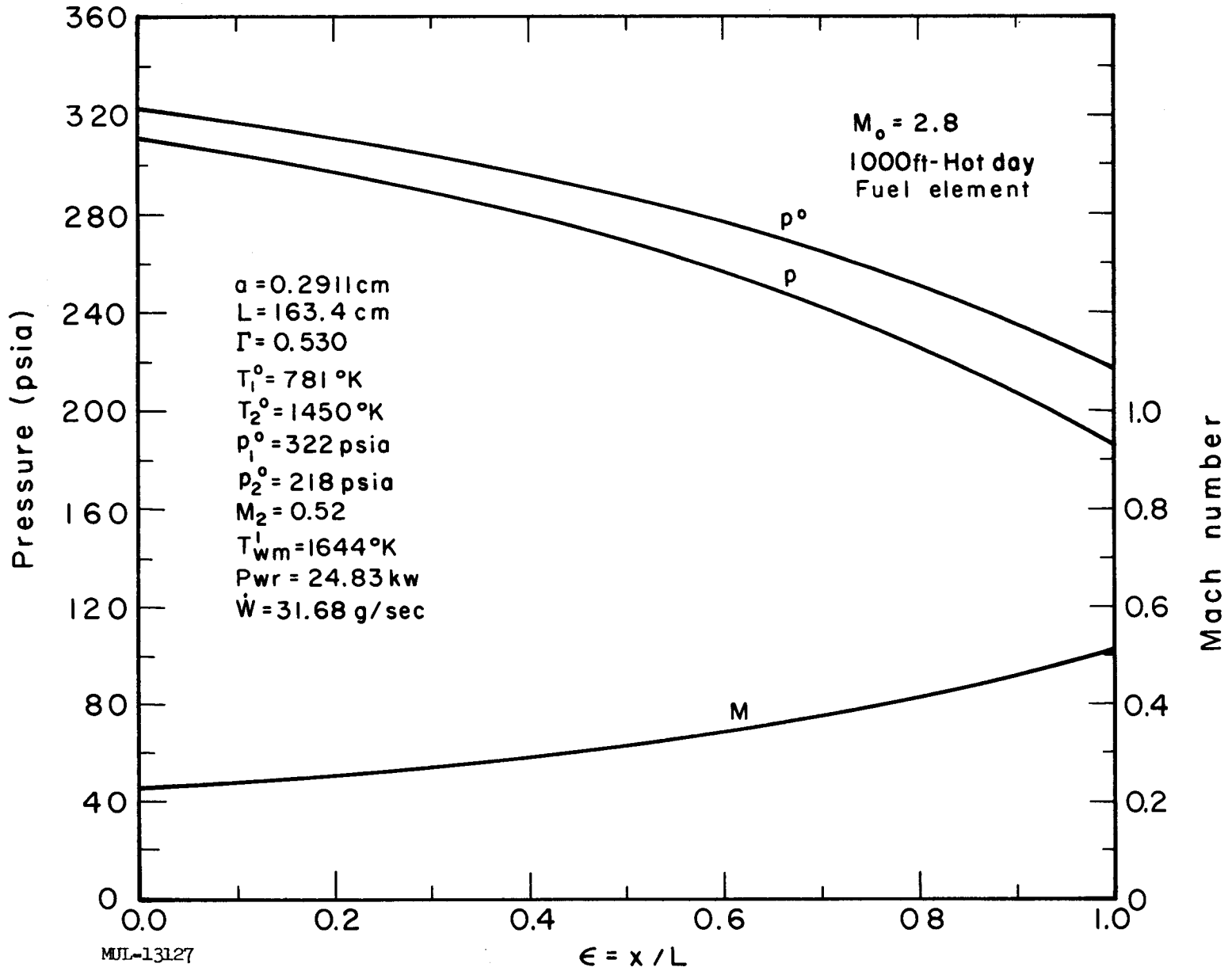

Fig. III-12. Tory II-C design point.

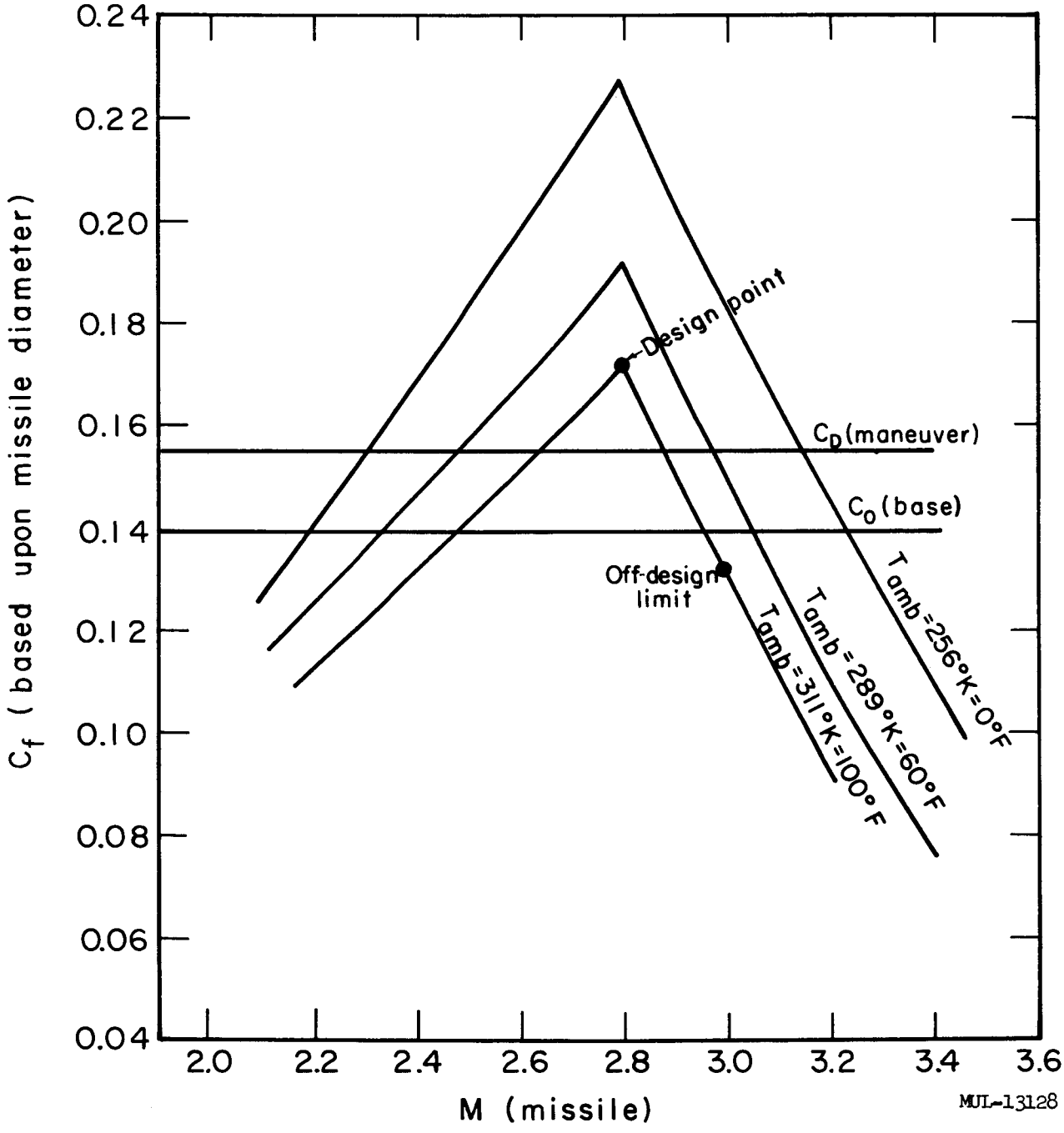

Fig. III-13. Thrust coefficient vs Mach number.

C_D, has been assumed to be constant. In truth, C_D will increase as the flight Mach number is decreased. This in turn will tend to lower the Mach margin.

As shown in Fig. III-13, Mach 3 operation with a 2500°F maximum wall temperature would not be possible with the present configuration (hot day, 1000 ft). Since some of the base parameters cannot yet be firmly fixed, it appears reasonable to assume a Mach limit to 3.0 for the device. The reactor structural limit is now established by this Mach limit. Since a great amount of effort will be expended on structural design of the reactor, an early specification of the structural loading limit is required. It is proposed that the aerodynamic loading of the reactor shall not exceed, under any circumstances, that which is present at the following flight conditions:

a. Flight Mach number = 3.0
b. Diffuser critical at flight Mach number = 2.8
c. Altitude = 1000 feet (P_a = 14.226 psia)
d. Atmospheric temperature = 100°F

At the upper Mach limit of 3.0, some pertinent fuel element parameters are as follows (Γ_{FE} = 0.530) (see Table III-1):

a. Maximum fuel element material power density = 27.21 Mw/ft^3
b. Maximum volumetric power density = 12.79 Mw/ft^3
c. Entrance Mach number = 0.234
d. Exit Mach number = 0.52
e. Maximum wall temperature = 2500°F
f. Entrance stagnation temperature = 1063°F
g. Exit stagnation temperature = 2172°F
h. Entrance stagnation pressure = 347 psia
i. Exit stagnation pressure = 235 psia
j. Single tube thrust coefficient = 0.240

The predicted pressure, temperature, and power profiles of a typical fuel element are presented in Figs. III-14 and III-15. Base fuel element thrust coefficient as a function of maximum wall temperature is presented in Fig. III-16.

Gross reactor parameters for Mach 3 operation are as follows:

a. Total reactor power = 556 Mw
b. Total reactor flow rate = 1872 pps
c. Average exit stagnation temperature $\simeq$ 2019°F

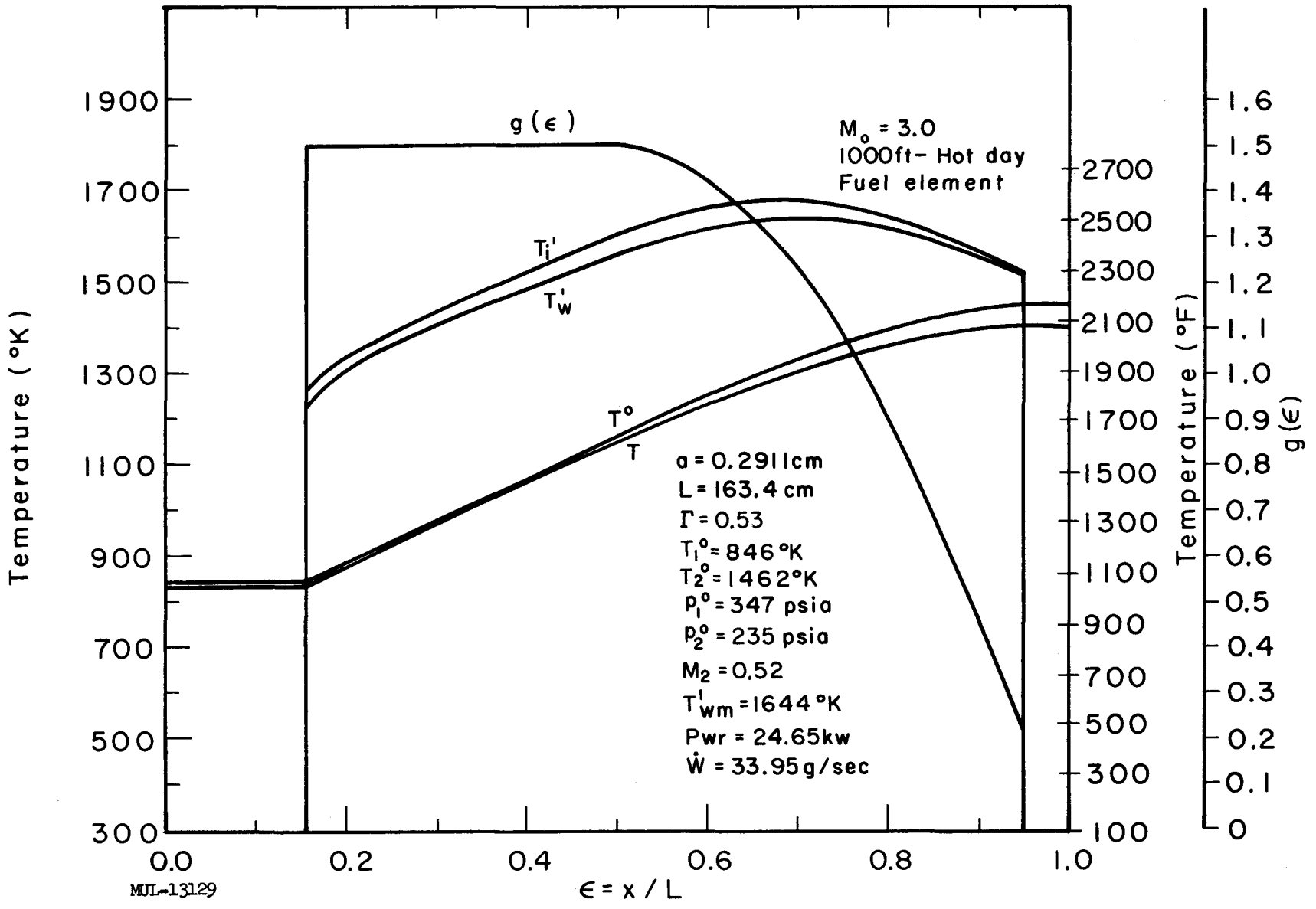

Fig. III-14. Tory II-C limit.

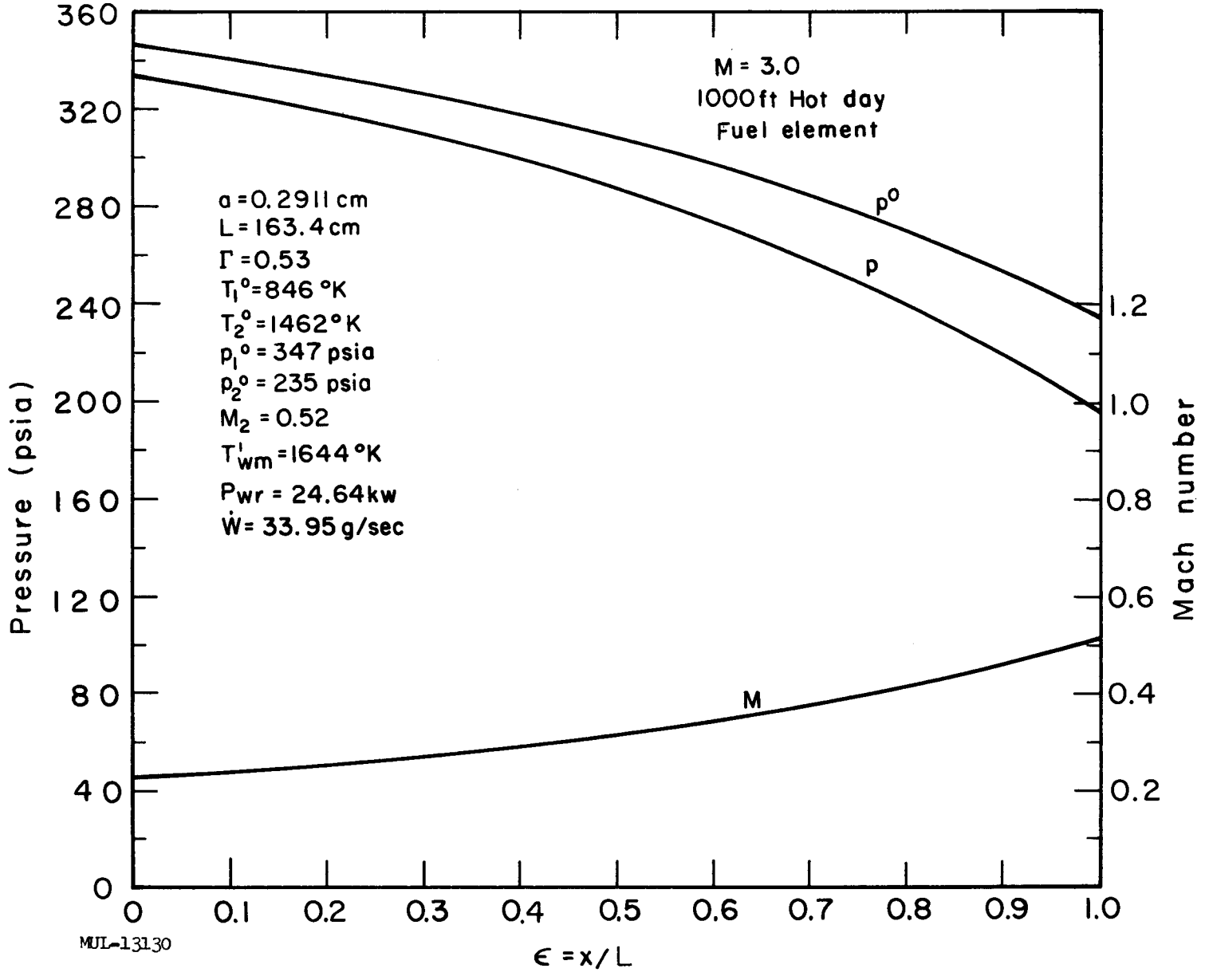

Fig. III-15. Tory II-C limit.

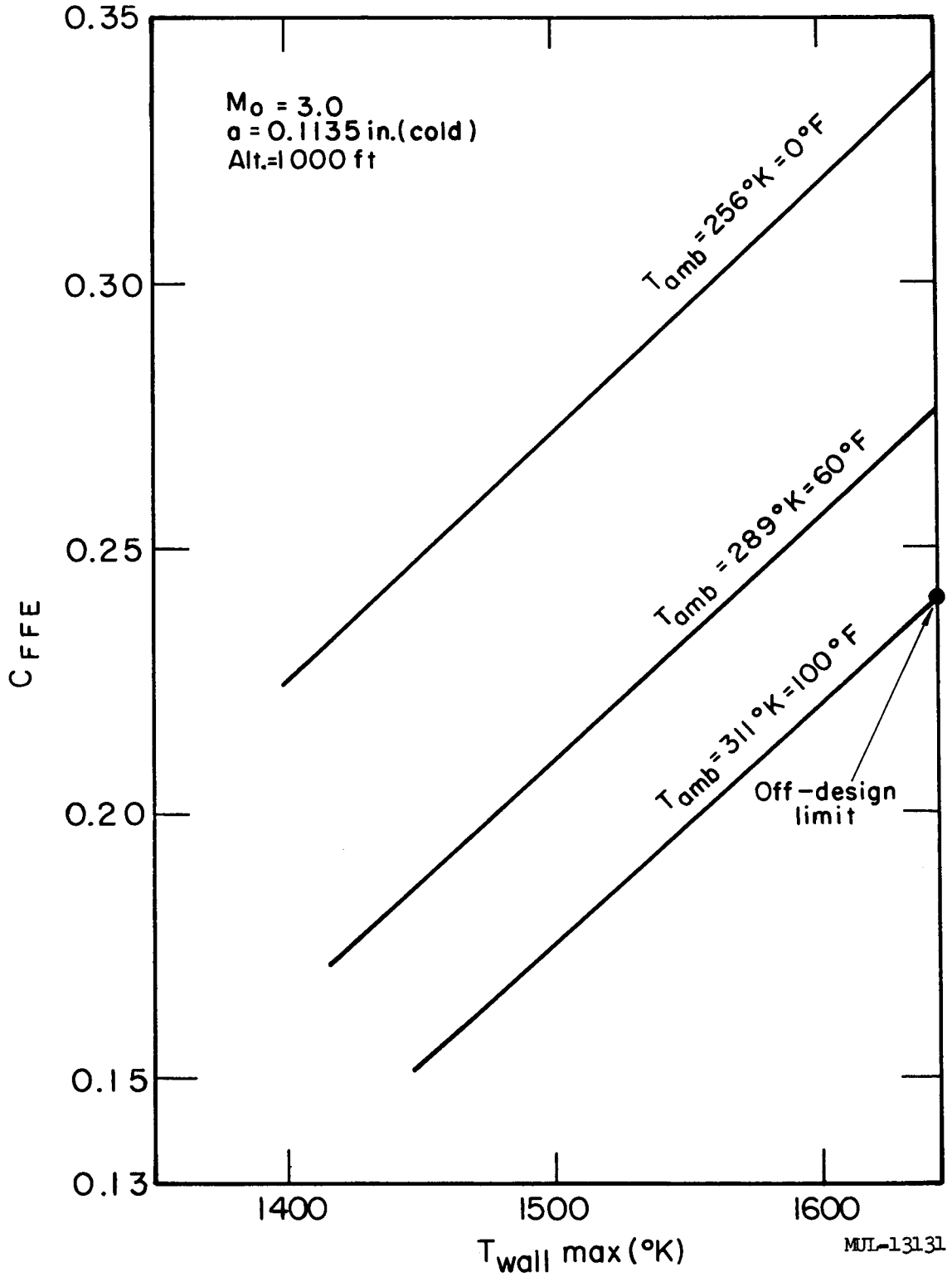

Fig. III-16. Tory II-C off-design.

The azimuthal fuel element thermal stress parameter, σ_θ, is plotted as a function of axial position in Fig. III-10. No correction was made for shape effects.

In the fabrication of fuel elements, some geometrical tolerance must be specified. The effect of fuel-element hole-size variation on the thrust coefficient is presented in Fig. III-17. The reference area used is that of a single fuel element. In making the perturbation calculations, it was assumed that only one full-length fuel element of the reactor had a flow-channel diameter different than that desired.

In computing the axial force acting on the reactor, pressure losses due to expected exit, entrance, and offset conditions must be included. An exit stagnation pressure loss of 5%, an entrance loss of 0.4%, and an offset loss of 1.8% will probably be experienced. Including these effects, the axial thrust loading on the active core is estimated to be less than 131 psi. The total axial force on the 54-inch reactor is expected to be 300,000 pounds. The gross thrust at the design point is about 35,000 pounds.

Since the friction factor of the fuel tubes may be higher than presently anticipated, the reactor axial loading may be found to be greater than 131 psia by as much as 6%. The flow channels of entrance and exit reactor sections must be carefully tapered to insure the low parasitic losses used in the calculations.

Expected fuel element conditions for a design pressure drop and design wall temperature run are presented in Figs. III-18 and III-19 for an inlet temperature of 600°F. A tabulation of pertinent fuel element parameters is presented in Table III-1.

NOMAC II

The original Nomac code[1] proved to be of such value in the analysis of the Tory II-A aerothermodynamic system that it was considered reasonable to expand this program so that it may be used for more general configurations. The resulting code (Nomac II) is capable of considering up to 30 independent varieties of flow channels having as many as 5 exit planes within the duct. Conservation of momentum is computed at each exit plane on the basis of a calorically imperfect gas. The nozzle calculations are identical to those employed

---

[1] See UCRL-6146, Pt. II.

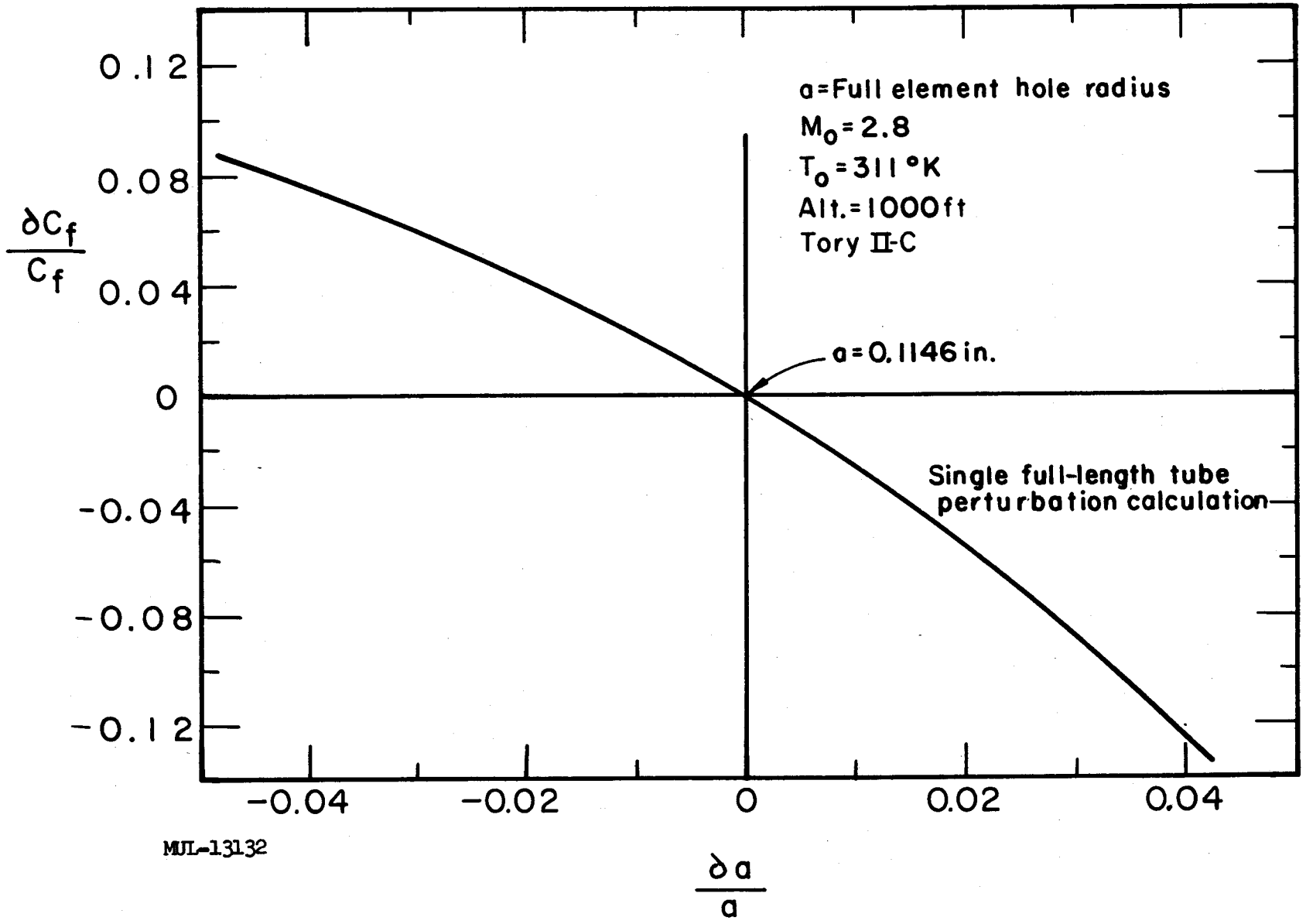

Fig. III-17. Thrust coefficient vs fuel element radius.

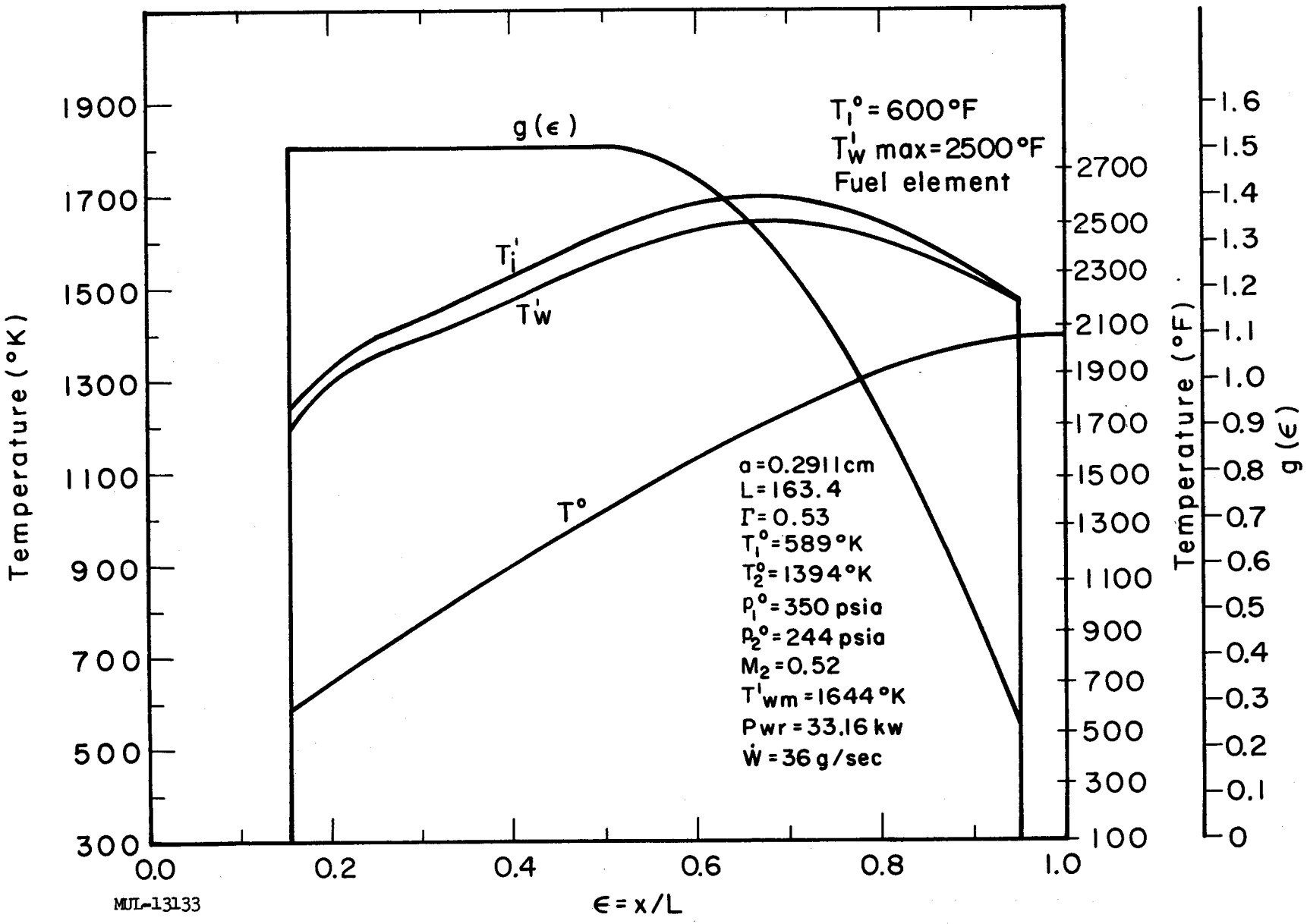

Fig. III-18. Tory II-C limit.

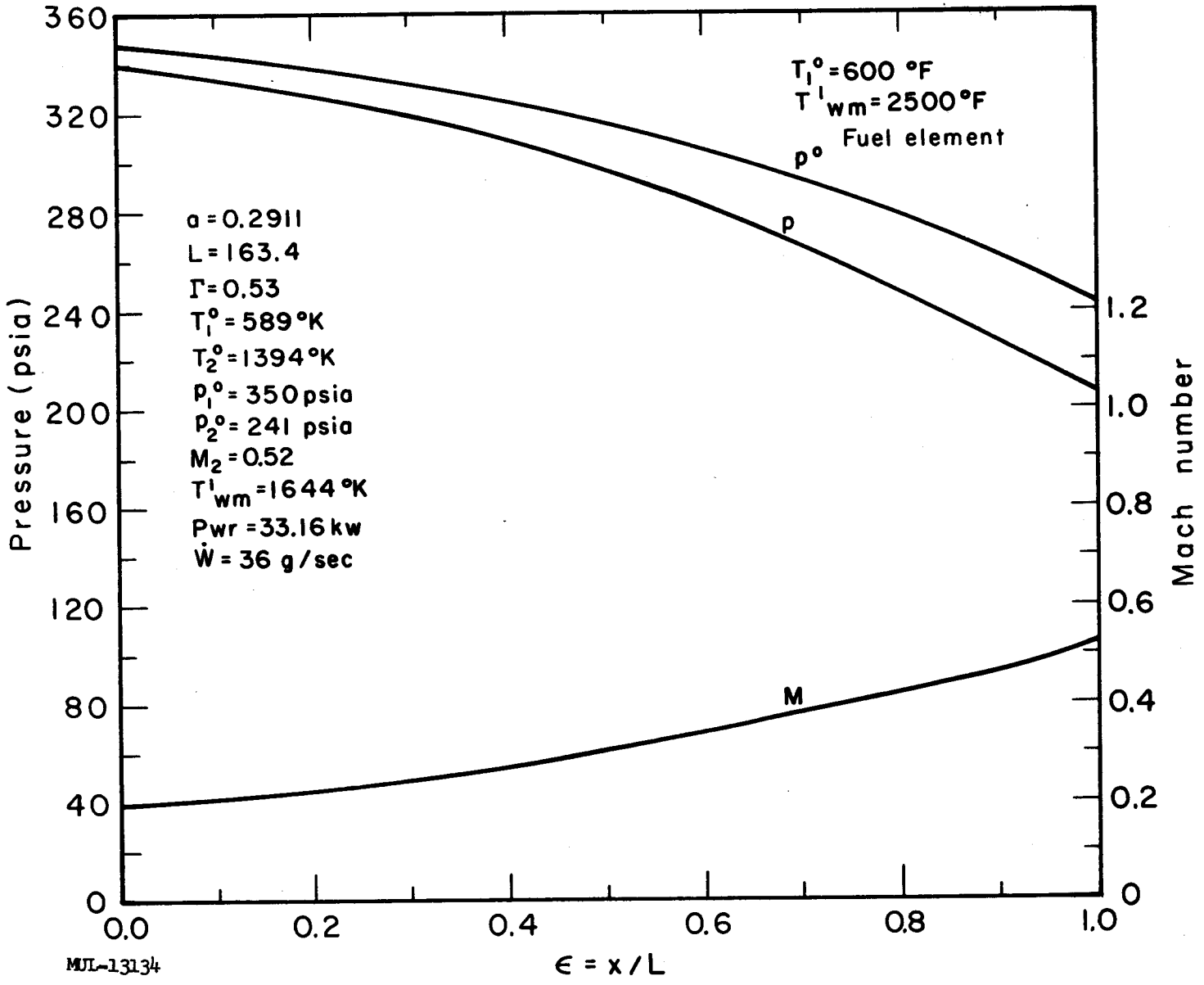

Fig. III-19. Tory II-C limit.

in the original code. As in the previous version of Nomac, the heat transfer momentum and friction effects within the individual flow channel are analyzed by means of the basic Floss III subroutine.[1]

The theory upon which Nomac is based is presented in its entirety in UCRL-6146, Part I and will, therefore, not be repeated here.

BASE PLATE HOT SPOTS

A perturbation calculation to predict the hot-spot temperature of a base plate has been performed. The assumptions used were as follows:

(a) One fuel element passage was completely plugged.

(b) Inlet total pressure nonuniformity was 1%.

(c) Exit static pressure nonuniformity was 5%.

The effect of each of these conditions as regards base plate temperature was computed. When the temperature effects are linearly added, the resulting temperature is 2503°F. The magnitude of this temperature is such that the Tory II-C base plate metal, F-48, should not fail if such a condition occurs. The maximum fuel element temperature for this condition is 3914°F, which is still below the melting point of BeO.

SECTION III. ENGINEERING

I. REACTOR DESIGN

During this quarter the structural arrangement of the reactor was refined. A preliminary analysis of all components indicates that the refined design is very nearly the final design. An assembly drawing of this design is presently nearing completion. Progress was made in materials testing and in component development and testing.

A. Materials Testing

1. Hastelloy R-235 (Tie Rod)

The creep-rupture tests reported in UCRL-6258 were continued. Figure III-20 shows the creep-rupture values obtained during this quarter. Complete creep data were obtained for each specimen so that curves for intermediate

[1] See UCRL-6146, Pt. II.

MASTER RUPTURE CHART

Alloy Hastelloy R-235	C	Temp.	Stress	Time	Elong.	P
Test	Fe	°F	1000 PSI	Hours	%	
Heat	Cr	1400	62	9	10	
Vendor	Ni	1500	32	250	7	
Requestor	Co	1720	32	1	5	
Date 3-14-61	Mo	1600	32	10	12	
By	W	1500	52	5	2.5	
	V	1500	50	1	10	
Temp.	Ti	1500	50	1	9	
T.S.	Al	1400	50	27	2.5	
Y.S.	Mn	1600	32	15	2	
Elong.	Si	1600	50	1	4	
R.A.						
Charpy						

Treatment: 1975 °F ½ hr water quench
1400 °F 16 hr air cool

Remarks: 0.080 in. thick sheet

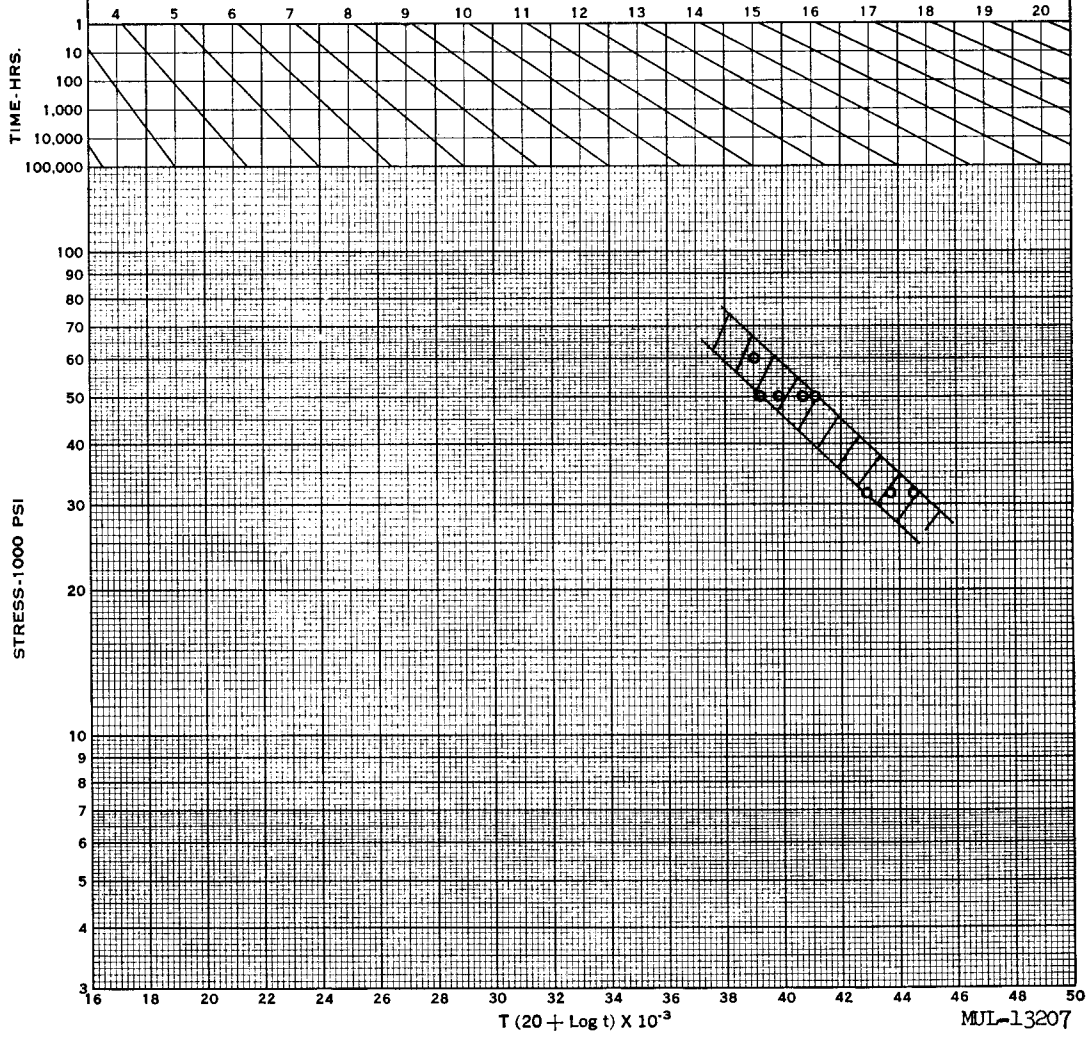

Fig. III-20. Creep rupture properties of Hastelloy R-235.

values of creep elongation may be prepared. The heat treatment used for this program has been found at LRL to provide maximum ductility and short-time yield strength since these are the properties considered most important in the tie rod design. There does not appear to be a great difference in creep rupture data regardless of the heat treatments involved.

2. René 41 (Tie-Rod and Side-Support Springs)

A comprehensive creep program on 0.120-inch sheet stock (applicable to spring material) is half complete. Figure III-21 reports the creep-rupture data obtained from 20 specimens. The heat treatment (HT No. 2 below) used is recommended by the vendor for maximum creep-rupture stress as this property is important in design of the side-support springs. Complete creep data were again obtained.

The mechanical properties of René 41 vary widely with the heat treatment used. Figures III-22 and III-23 show the effect of three different heat treatments on tensile properties. Figure III-24 shows a typical specimen used to obtain these values. Three groups of six specimens each were given the following different heat treatments:

HT No. 1	30 min at 1950°F – ac	(air cool)
	16 hr at 1400°F – ac	
HT No. 2	30 min at 2150°F – ac	
	4 hr at 1650°F – ac	
HT No. 3	10 min at 2150°F – ac	
	30 min at 1950°F – ac	
	16 hr at 1400°F – ac	

HT Nos. 1 and 2 are recommended for maximum tensile strength and maximum creep rupture strength, respectively. HT No. 3 is the heat treatment that the material would receive during the brazing operations anticipated for both the tie-rod and the side-support spring fabrication. The initial heating to 2150°F for 10 minutes would be the brazing cycle. There is a significant decrease in the ultimate strength when the brazing cycle is used; however, yield strength is not affected to a large extent. It is expected that decreasing the brazing time at 2150°F will reduce the loss in ultimate strength. It further appears that the ideal brazing alloy for René 41 would flow at near 1950°F.

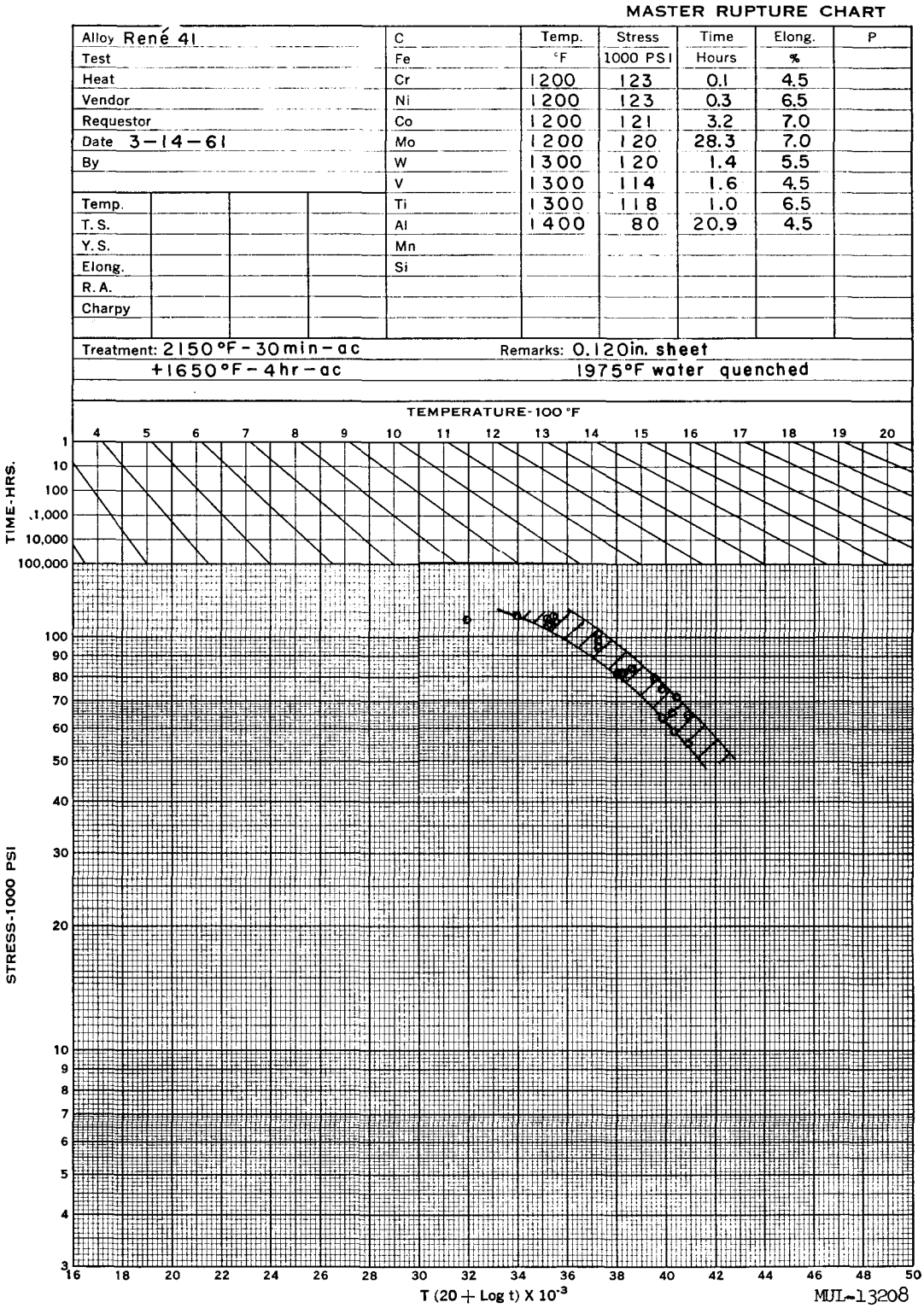

Fig. III-21. Creep rupture properties of René 41.

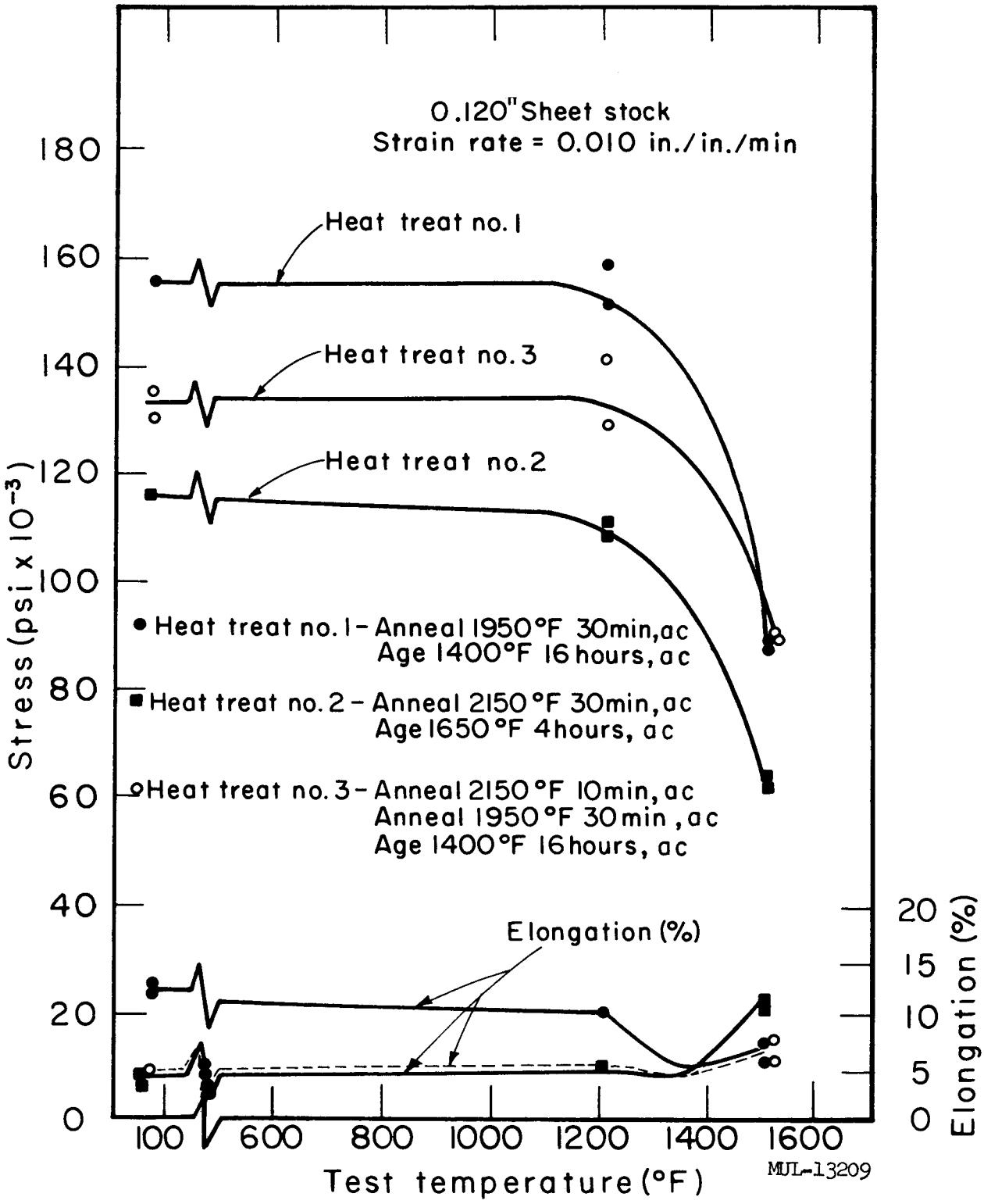

Fig. III-22. Effect of heat treatment on ultimate tensile strength and ultimate elongation of René 41 sheet.

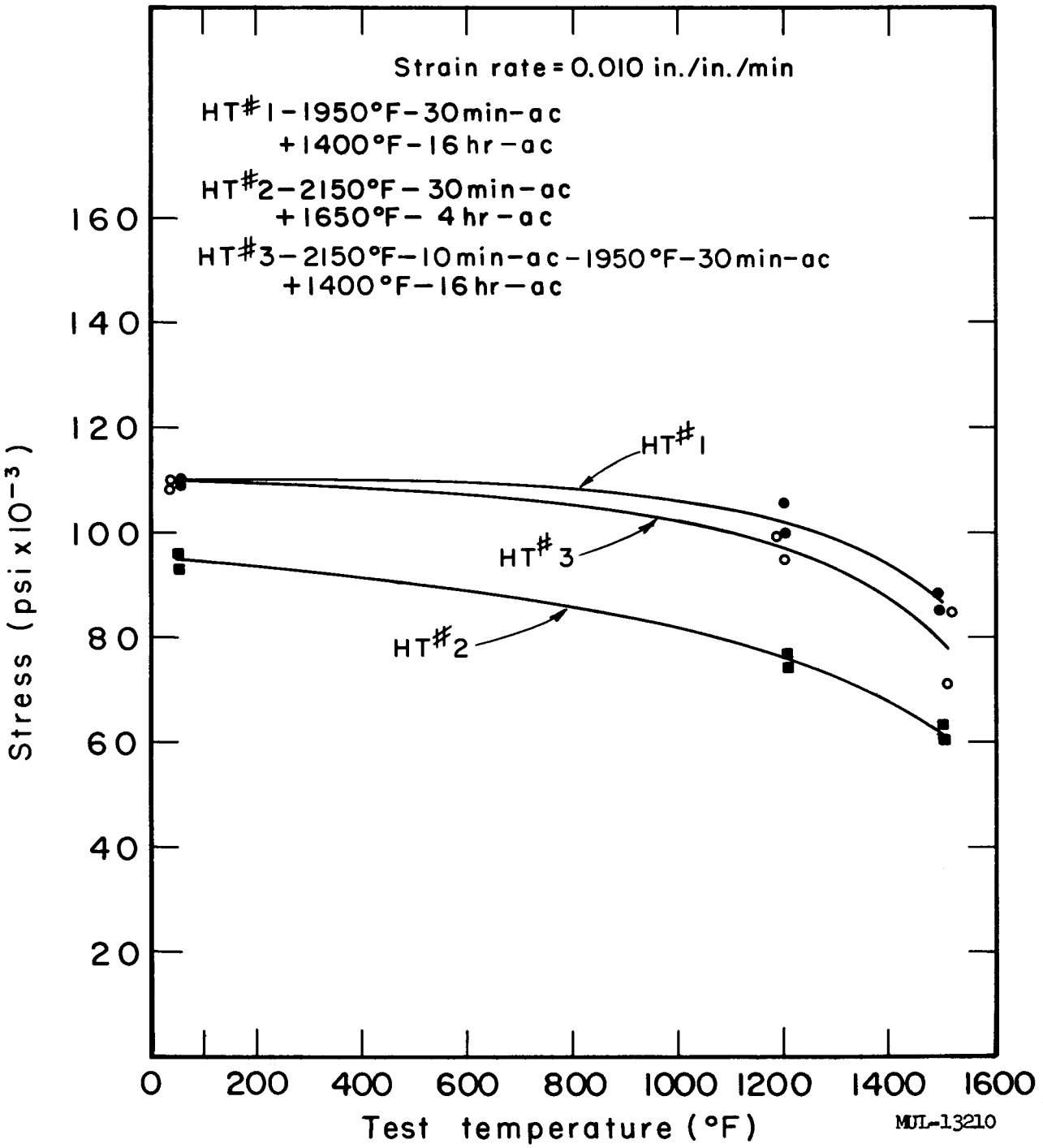

Fig. III-23. Effect of heat treatment on yield strength of René 41 sheet.

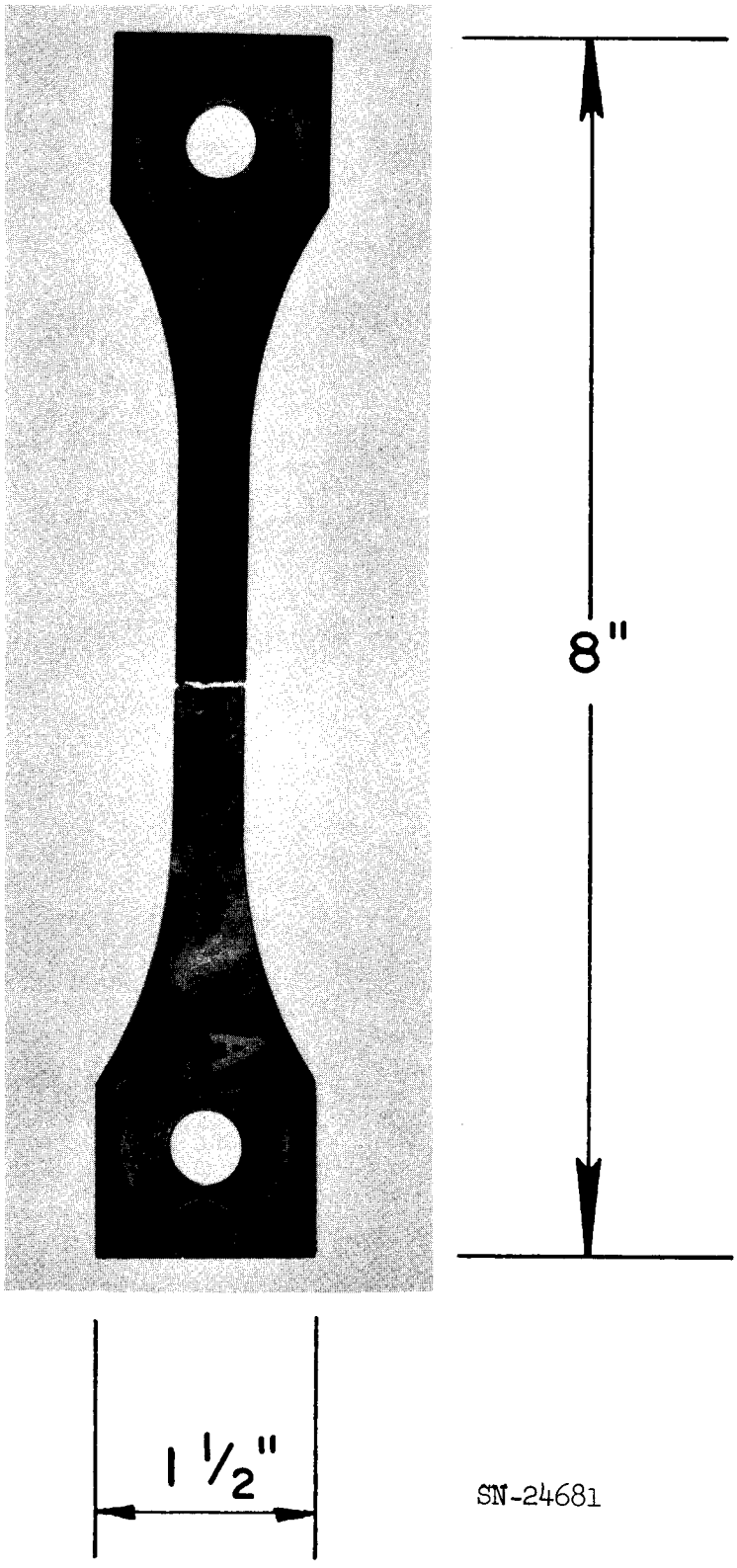

Fig. III-24. René 41 tensile test coupon after failure. Sheet, 0.120 inch thick. Typical of the specimen used to obtain curves of Figs. III-22 and III-23.

3. Hastelloy C (Reactor Duct)

Hastelloy C is a nickel-chromium-molybdenum alloy widely used in the chemical industry. Work thus far at LRL on this material shows it to have excellent ductility and weldability, combined with adequate strength at operating temperatures. Also, its low coefficient of expansion benefits the side support springs which support the front reflector.

A test program is now under way to determine the tensile properties of the base metal, welded base metal, and the weld metal itself. Fifteen of a total of 121 specimens planned have been tested. Table III-2 presents the available results. These results are also plotted in Fig. III-25.

Table III-2. Hastelloy C Tensile Properties.

Type of specimen	Test temp (°F)	Yield strength, 0.2% offset (kpsi)	Ultimate strength (kpsi)	Elongation in 1.5" (%)
All weld, as welded	70	84.0	127.0	28
	1200	58.8	90.0	31
	1350	52.9	80.0	32
All weld, solution heat treat (See Note 3)	70	55.5	118.7	44
	70	51.0	118.5	37
	1200	34.8	84.3	52
	1200	31.0	84.0	42
	1350	36.0	82.0	46
Base material, solution heat treat (See Note 3)	70	58.1	120.4	55*
	70	68.9	118.5	50*
	1200	33.1	81.2	44
	1200	34.0	86.8	53
	1350	36.0	78.8	40
	1500	33.1	65.9	33
	1500	45.9	75.2	33

*Based on 2.0 inch gage length.

Notes: 1. Strain rate controlled at 0.005 in./in./min through 0.2% offset.

2. Soak time at temp before test: 5 min.

3. Solution heat treat at 2225°F to 2250°F, water quench.

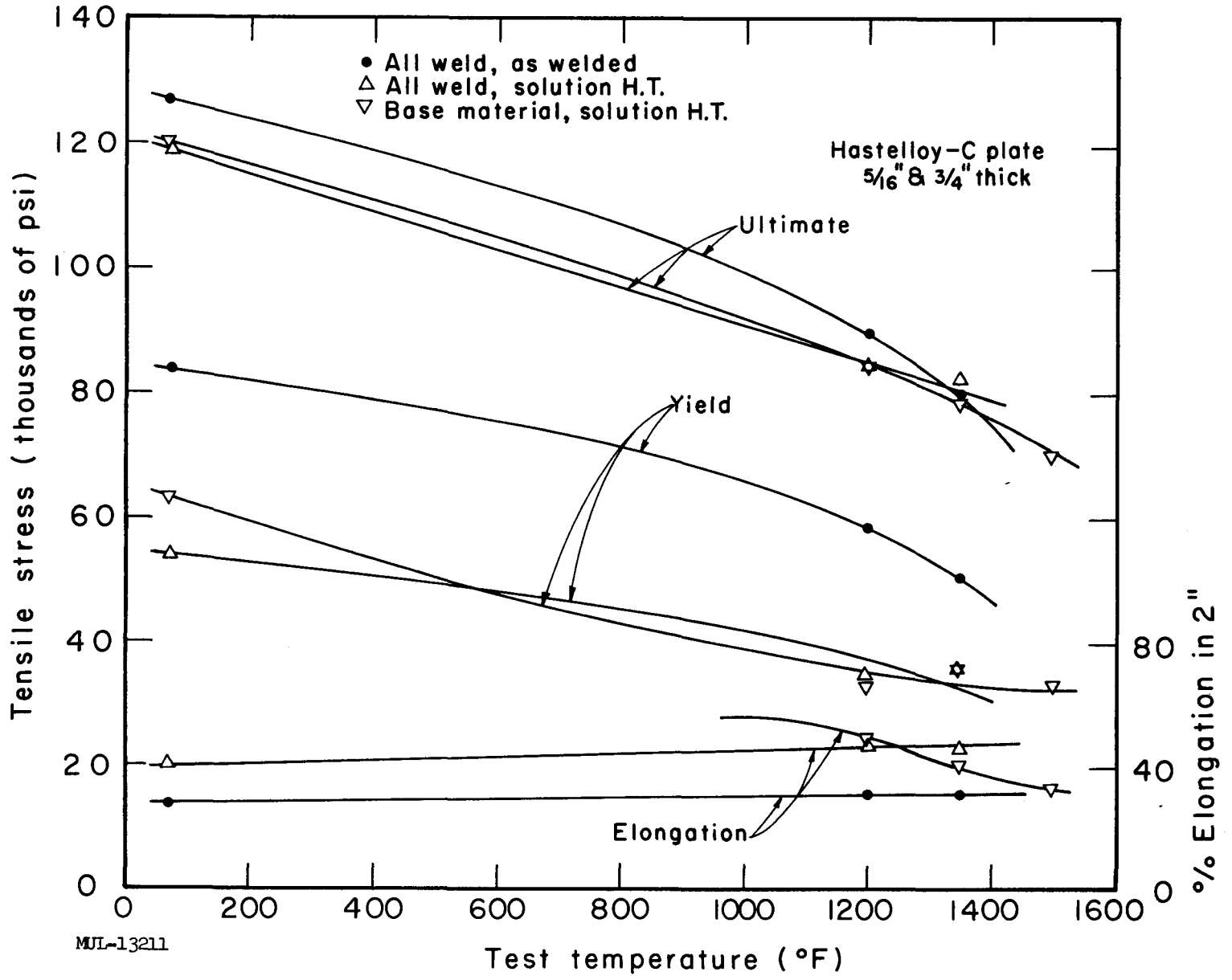

Fig. III-25. Comparison of tensile properties of Hastelloy-C weld material with base-metal properties.

The data given here show the excellent ductility of this material and the absence of "hot shortness" at the maximum expected operating temperature (1400°F). The weld metal in as-welded condition shows some loss in ductility over the base metal because of its cast structure. Solution treating at from 2225 to 2250°F for one hour appears sufficient to return the weld metal to base-metal ductility.

Welding details used for these Hastelloy C specimens are as follows:

Weld method	dc inert-gas shielded tungsten arc
Tungsten size	3/32 in.
Filler rod	3/32-in. -diam Hastelloy C
Current	95 to 150 amperes
Number of passes	9 to 12 for 5/16-in. plate 41 for 3/4-in. plate
Reference spec.	RMWS-7, ORNL

Welding data and nondestructive test results have been recorded for all specimens.

Figure III-26 shows the appearance of the all-weld metal specimens after failure. The rough texture developed well past the yield point. Metal "cry" could be heard from these specimens after large deformations had been reached.

4. Hafnium (Control Rod)

Hafnium has been chosen as the absorber material for the control rod. One method of control rod fabrication being considered uses hafnium sheet formed into a six-bladed cross-section configuration. Ultimate tensile strength and elongation of 0.050 inch sheet was determined at 1500 and 1800°F for a rapid strain rate. Results are plotted in Fig. III-27. The tests were performed in air after a 15-minute soaking period at temperature.

Susceptibility of hafnium sheet to oxygen embrittlement at elevated temperature was evaluated. Six test strips 3/8 × 4-1/2 in. were cut from the 0.050 sheet. Three were held at 2000°F in oxygen at atmospheric pressure for 10 hours and three were maintained as received from the vendor. Simple bend tests were performed with the strips supported on 4-in. centers and loaded in the middle. Results of these tests are given in Table III-3 and the tested specimens are shown in Figs. III-28 and III-29. It was not possible to break the as-received specimens before they slipped through the supports.

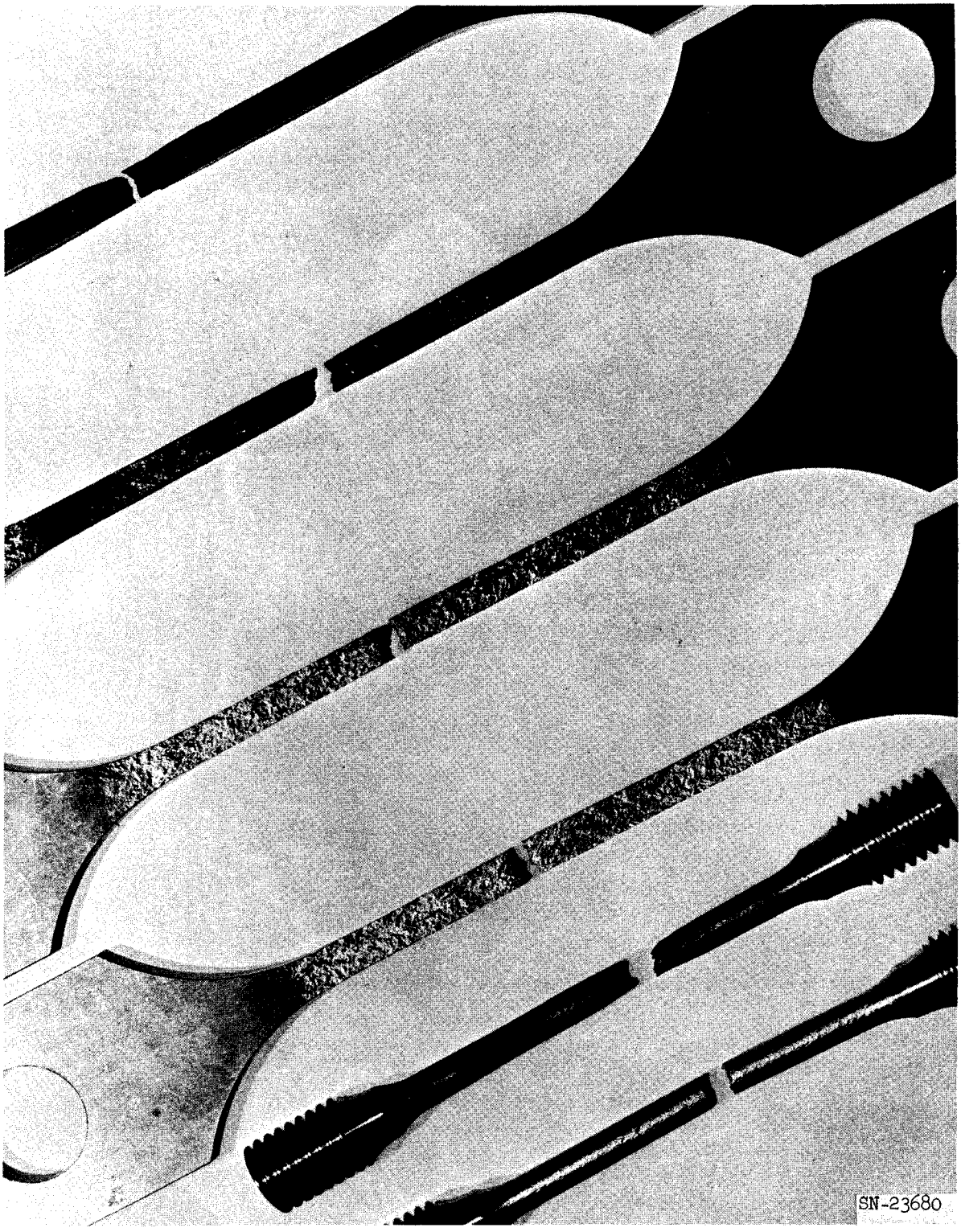

Fig. III-26. Hastelloy-C weld metal test specimens after failure. Typical of the specimens used to obtain curves of Fig. III-25.

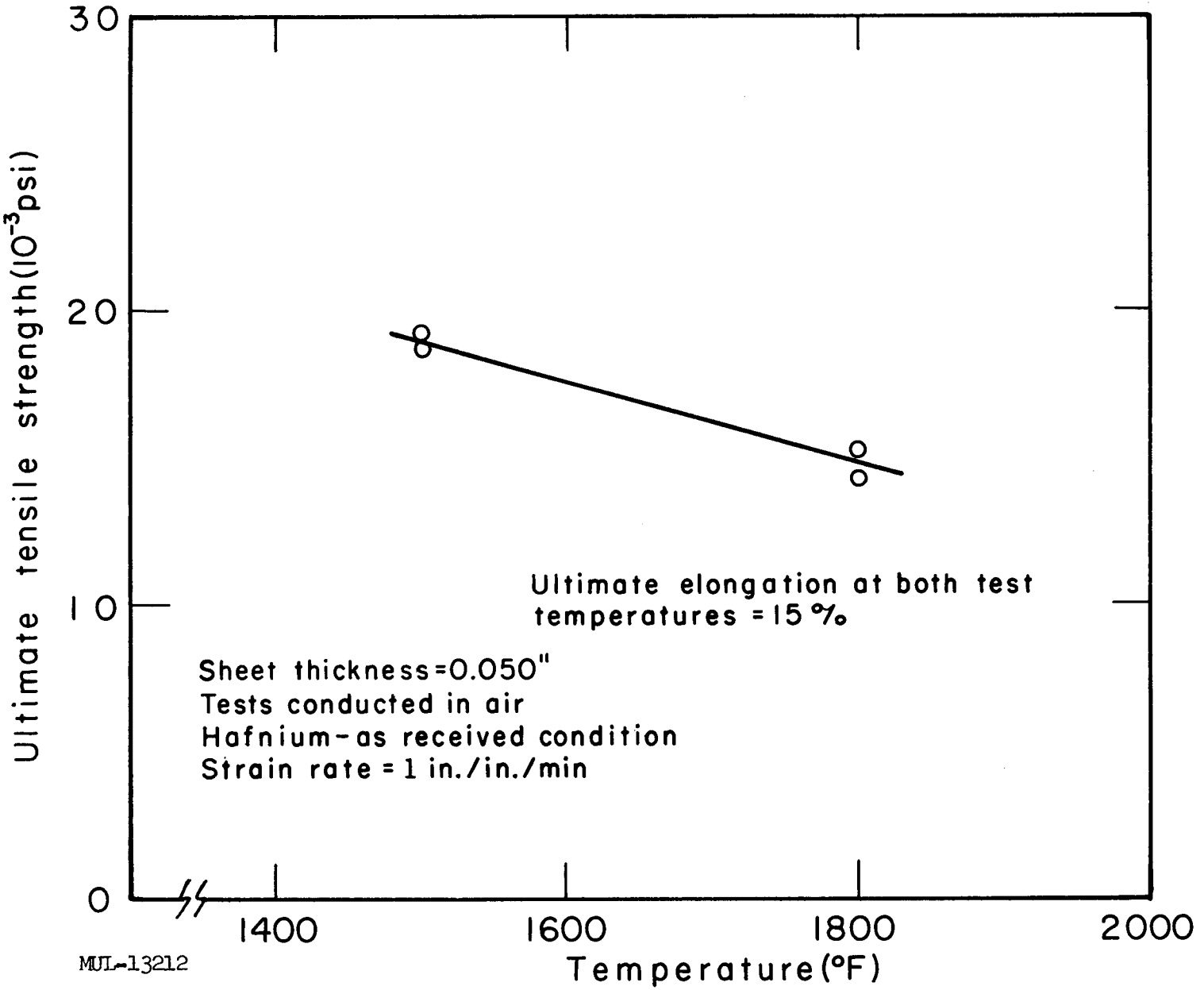

Fig. III-27. Tensile strength of hafnium sheet.

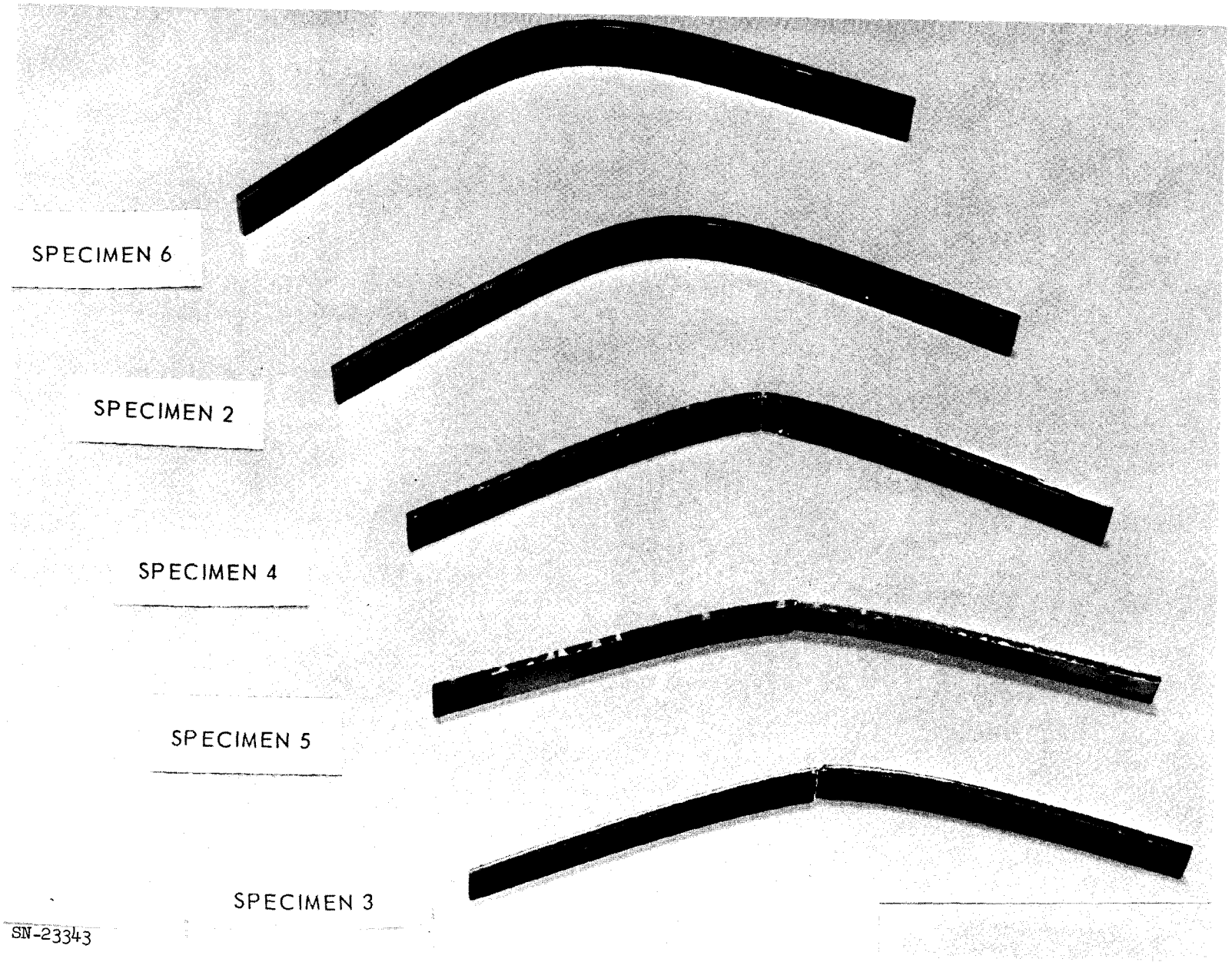

Fig. III-28. Effect of oxygen contamination on ductility of hafnium. All specimens tested in simple bending. Specimens 3, 4, and 5 were soaked in O_2 at 2000°F for 10 hr. Specimens 2 and 6 were tested as received. Specimens are 4-1/2 × 3/8 × 0.050 in.

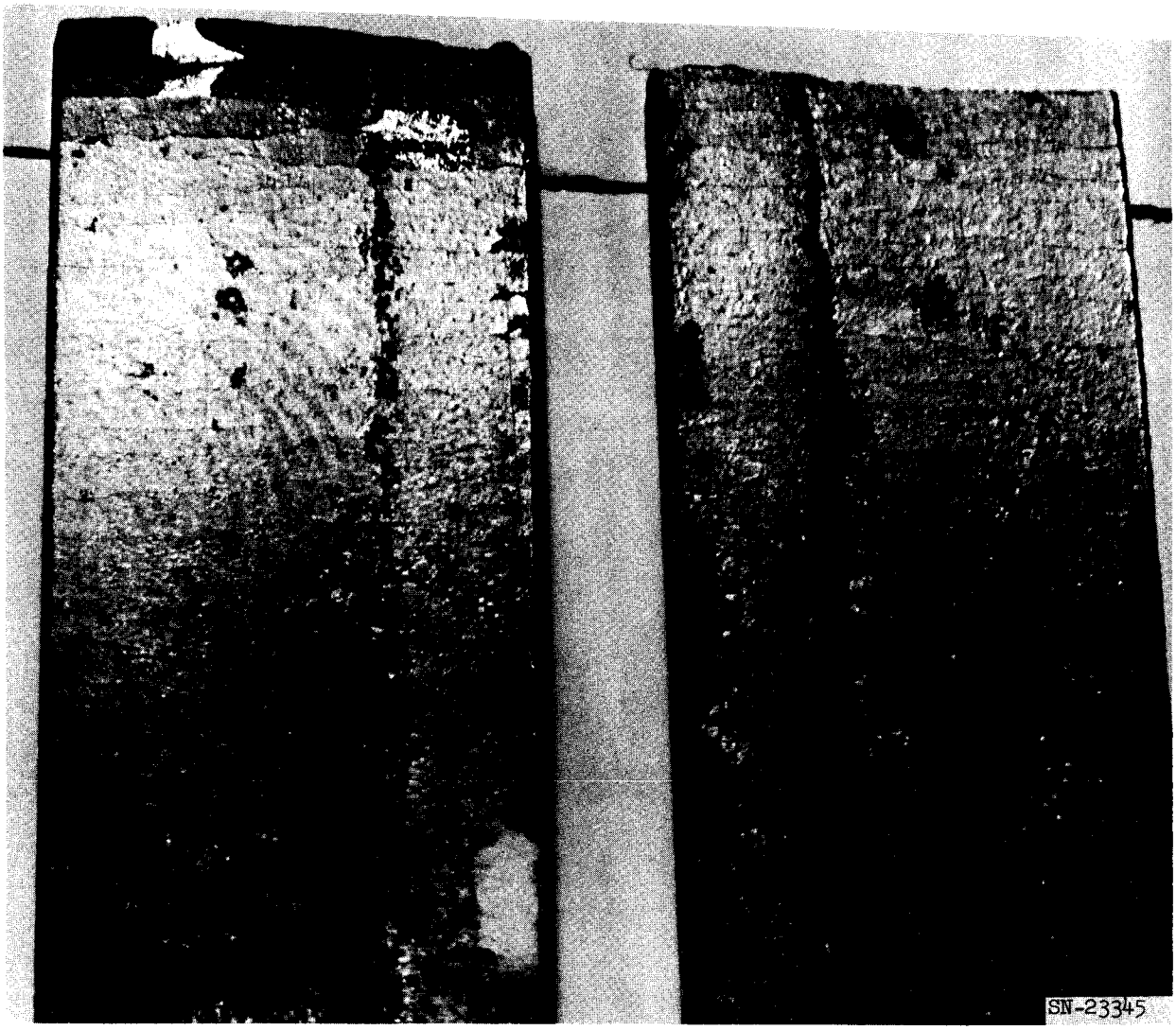

Fig. III-29. Tension surface at location of fracture of hafnium specimen 4 shown in Fig. III-28.

Although oxygen contamination has occurred, Fig. III-28 shows a comfortable level of ductility remaining even after this severe exposure. Effects of the oxygen contamination are clearly seen in Fig. III-29. The maximum calculated temperature of the control rod is 1500°F.

Table III-3

Bend Test Results of Oxygen-Contaminated Coupons of Hafnium.

Specimen No:	1	2	3	4	5	6
Condition*	AR	AR	O	O	O	AR
Dimensions (inch)	0.050 0.390	0.050 0.387	0.052 0.398	0.051 0.390	0.051 0.391	0.050 0.388
Section modulus (10^4 in^3)	1.625	1.670	1.793	1.690	1.695	1.615
Maximum load (lb)	13.5	13.8	16.4	17.4	15.45	13.2
Failure	No	No	Yes	Yes	Yes	No
Permanent set (inch)	--	0.80	0.43	0.40	0.50	0.82
Ultimate bending moment (in-lb)	--	--	16.4	17.4	15.45	--
Modulus of rupture	--	--	91,500	103,000	91,100	--

*AR: as received. O: oxidized.

5. Rare-Earth-Oxide Spray Coatings (Possible Control Rod Material)

Nine specimens of Inconel X were spray coated with a 25 w/o mixture of gadolinium oxide in a matrix of nichrome powder. These specimens have been tested and evaluated to determine coating adherence. This material assembly is no longer being considered for application in Tory II-C control rods.

The coated Inconel X bars (size 1/8 × 1 × 6 in.) were tested as follows:

Specimen No.	Coating thickness (mils)	Test	Test temperature (°F)
1	15	Bend	RT
2	16	Bend	RT
3	16	Bend	1400
4	16	Thermal shock	1500-RT
5	24	Bend	1400
6	30	Bend	RT
7	30	Bend	1400
8	47	Thermal shock	1500-RT
9	0	Bend	1400

The bend test consisted of a specimen simply supported at each end with load applied at midpoint. Specimens were brought to temperature and then loaded until the coating cracked or until a small increase in load produced a large increase in deflection. Loads and cross-head motion were recorded as well as temperature.

The thermal shock test consisted of heating a specimen to 1500°F and holding until the bar was at a uniform temperature. Then the specimen was given an agitated quench in cold water.

Test results are as follows:

Spec. 1: The coating was slightly separated from the specimen on one side at the center prior to test. The coating cracked at strains of 0.00176 and 0.00101 in./in. These cracks could have formed because of the slight separation described above.

Spec. 2: No cracks were found. Specimen took a permanent set of approximately 0.1 inch.

Spec. 3: No cracks were found. Specimen took a permanent set of approximately 0.32 inch.

Spec. 4: No cracks were found.

Spec. 5: The coating cracked at strains of approximately 0.00367 and 0.00389 in./in.

Spec. 6: The coating was slightly separated from the specimen on both ends prior to the test. No detectable increase in separation or cracks were observed. Specimen took a permanent set of approximately 0.14 inch.

Spec. 7: The coating separated slightly from the center of the specimen. No cracks were observed. The specimen took a permanent set of approximately 0.21 inch.

Spec. 8: The coating separated from the ends of the specimen.

6. Columbium-1%Zr (Early Base Block Material)

Creep testing coated 1%Zr-Cb alloy in air was completed. Specimens were described in the previous Pluto Quarterly Report and the test apparatus is shown in Fig. III-30. Coating was the same Al-Cr-Si pack diffused type planned for use with the base blocks.

A typical creep curve is shown in Fig. III-31. The initial straight line position in this plot is due to thermal expansion of the specimen under no-load conditions. Upon reaching test temperature, 2200°F, the load was applied

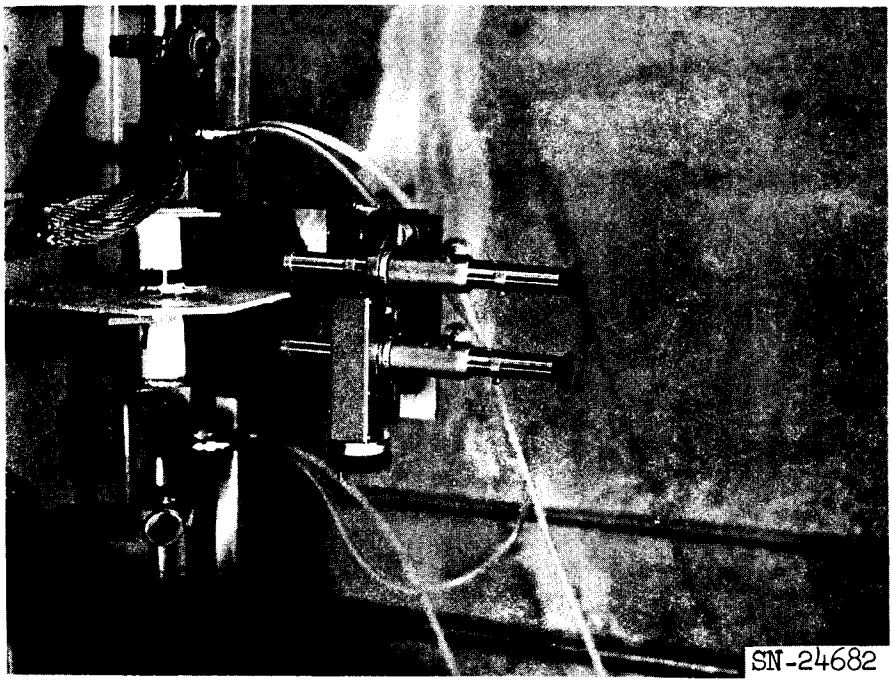

Fig. III-30. Optical extensometer used in creep testing 1Zr-Cb material. Specimen is inside the alundum tube. Heating is by conduction.

which produced rapid elongation, i. e., elastic deformation and first-stage creep. The reference line is used as a basis for reporting creep elongation to eliminate primary effects.

Stress for 1/2% creep and creep-rupture at 2200°F as a function of time are plotted in Fig. III-32. These results complete the present work on this material.

7. F-48 Columbium Alloy (Base Block)

The base blocks will be made from the F-48 columbium alloy. Photoelastic studies of base block stresses, verified by strain gages on a loaded metallic model, reveal stress levels beyond the capacity of the 1Zr-Cb alloy. The superior oxidation resistance of F-48 is also an important consideration.

Creep and tensile test specimens have been cut from an extruded bar of F-48 (see UCRL-6258, p. 144). Thirty-six specimens of each type have been coated using the process to be used on the base blocks, and will be tested in air by means of induction heating. Two special creep frames have been fabricated for use in these tests.

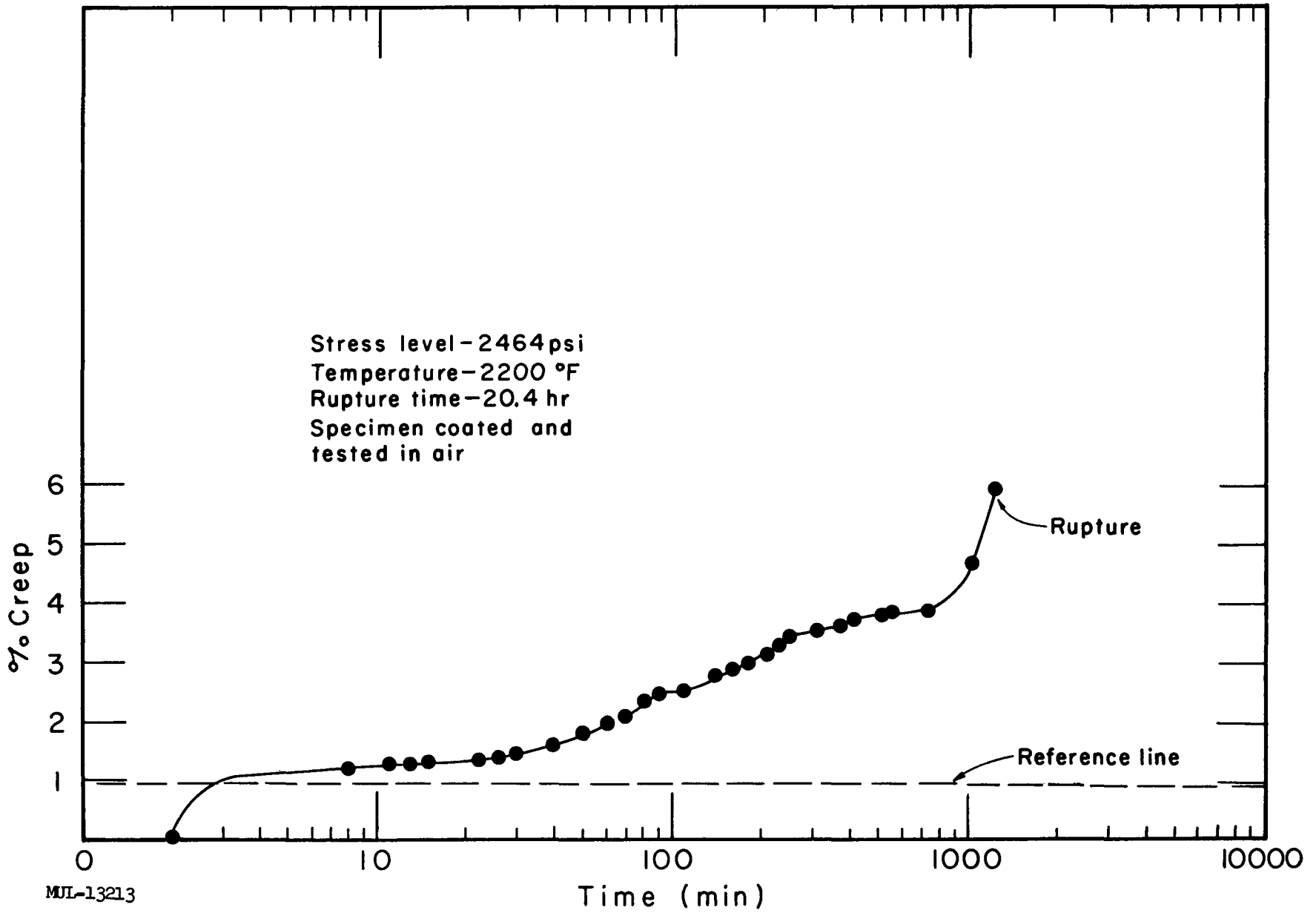

Fig. III-31. Typical creep curve for 1Zr-Cb. Data obtained in the apparatus shown in Fig. III-30.

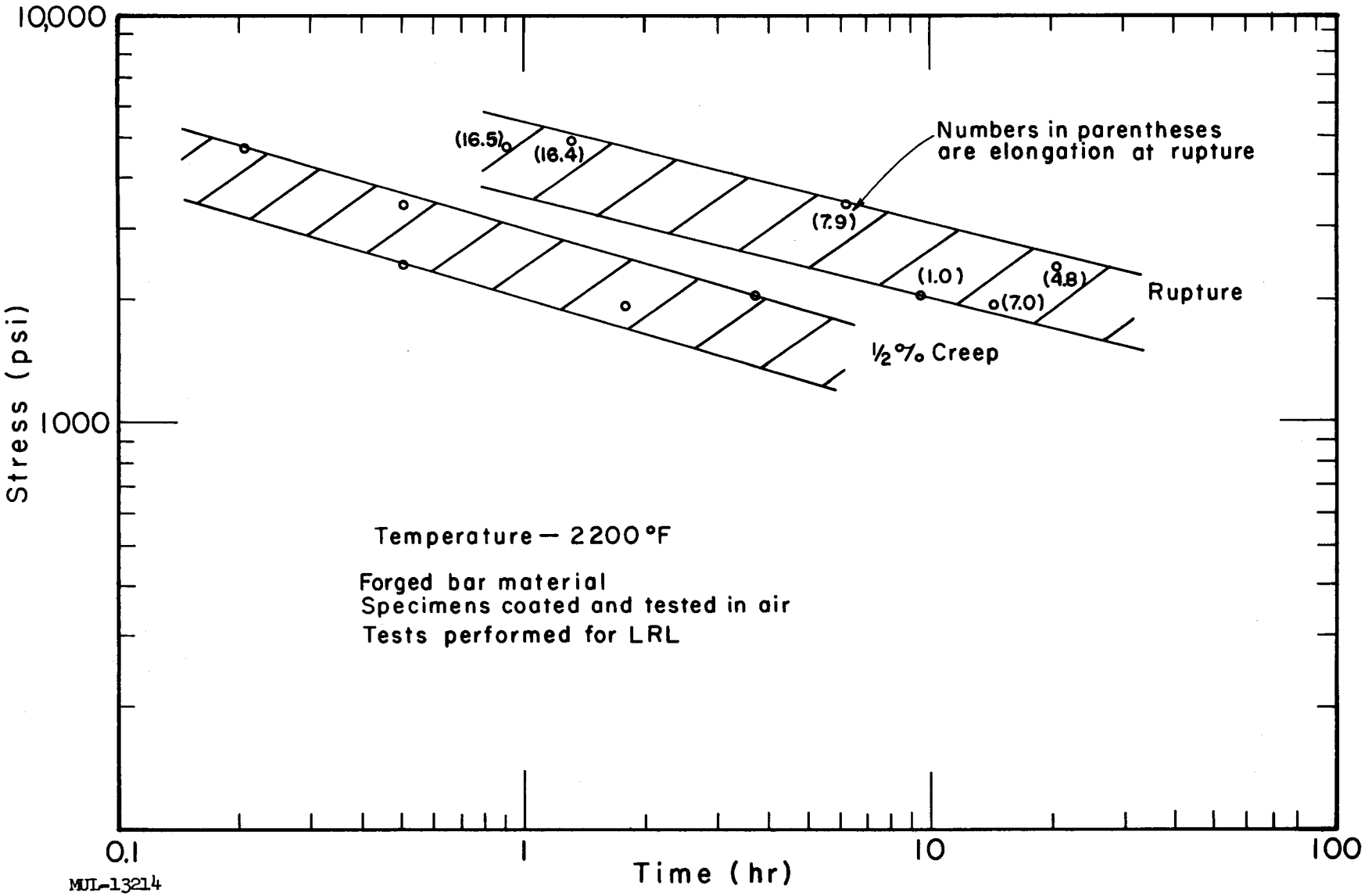

Fig. III-32. Creep properties of 1Zr-Cb. Testing performed in the apparatus shown in Fig. III-30.

Preliminary results from short-time tensile tests are shown in Fig. III-33. These values agree very well with those reported by other investigators for F-48 of similar chemistry.* Composition has been determined for the starting billet and is as follows:

	Top	Bottom
Zirconium	0.99 w/o	1.10 w/o
Molybdenum	5.2 w/o	5.2 w/o
Tungsten	15.7 w/o	15.3 w/o
Oxygen	210 ppm	150 ppm
Carbon	443 ppm	320 ppm
N	13 ppm	57 ppm

This analysis is within specification limits for the material.

Apparently, the thermal treatment received by this material in the coating process does not cause a loss in strength.

Ignition testing reported last quarter was continued. The test apparatus was that used for environmental testing on coated base plate specimens and is shown schematically in Fig. III-34. Previous tests on bare F-48 columbium alloys had produced two apparent temperatures where ignition occurred, 2670°F and 2770°F. The difference was attributed to a small thermal lag or response time at temperature before ignition proceeds. That is, a test specimen will be at its ignition temperature for a short time before it ignites. Raising the stream temperature at a given rate would, therefore, allow passing of the ignition point by a finite amount as a function of the rate of rise and delay ignition until a higher temperature was reached.

Previous tests were performed at two different rates of rise, 8.3 and 3.3°F/sec. If it is assumed that both specimens had the same true ignition temperature T_{ig}, then T_{ig} can be calculated from the test results:

$$2770 - 8.3t = T_{ig}$$
$$2670 - 3.3t = T_{ig}$$

which gives T_{ig} = 2600°F and time (t) to ignition failure after reaching T_{ig} of 20 seconds. Running at a gas temperature somewhat less (say 2570°F) should not produce ignition, while running at 2600°F should produce catastrophic failure at the end of 20 seconds.

---

*Data reported by Crucible Steel Company of America in AMC Interim Report 7-784 (II).

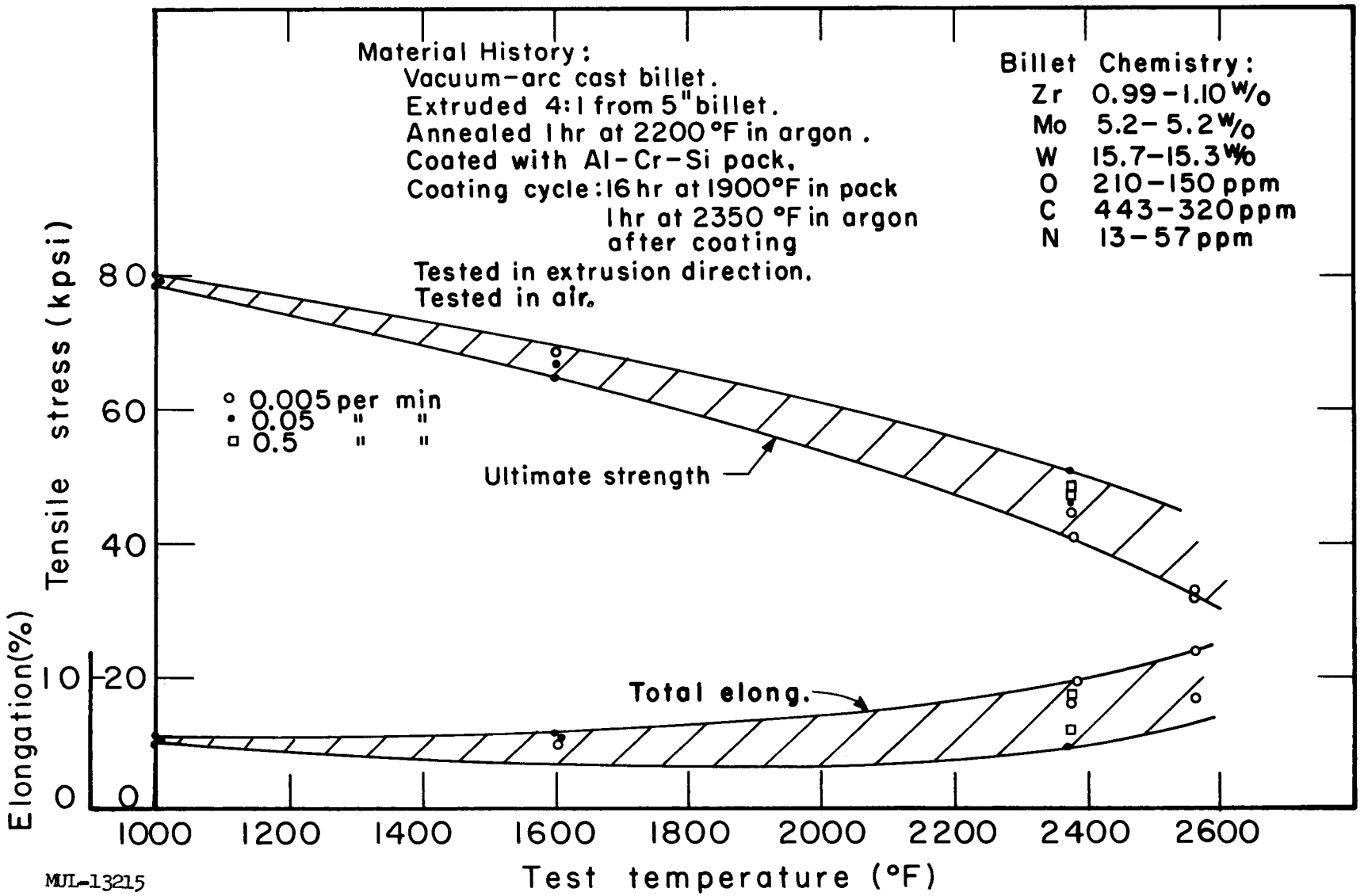

Fig. III-33. Tensile properties of coated F-48 columbium alloy tested in air.

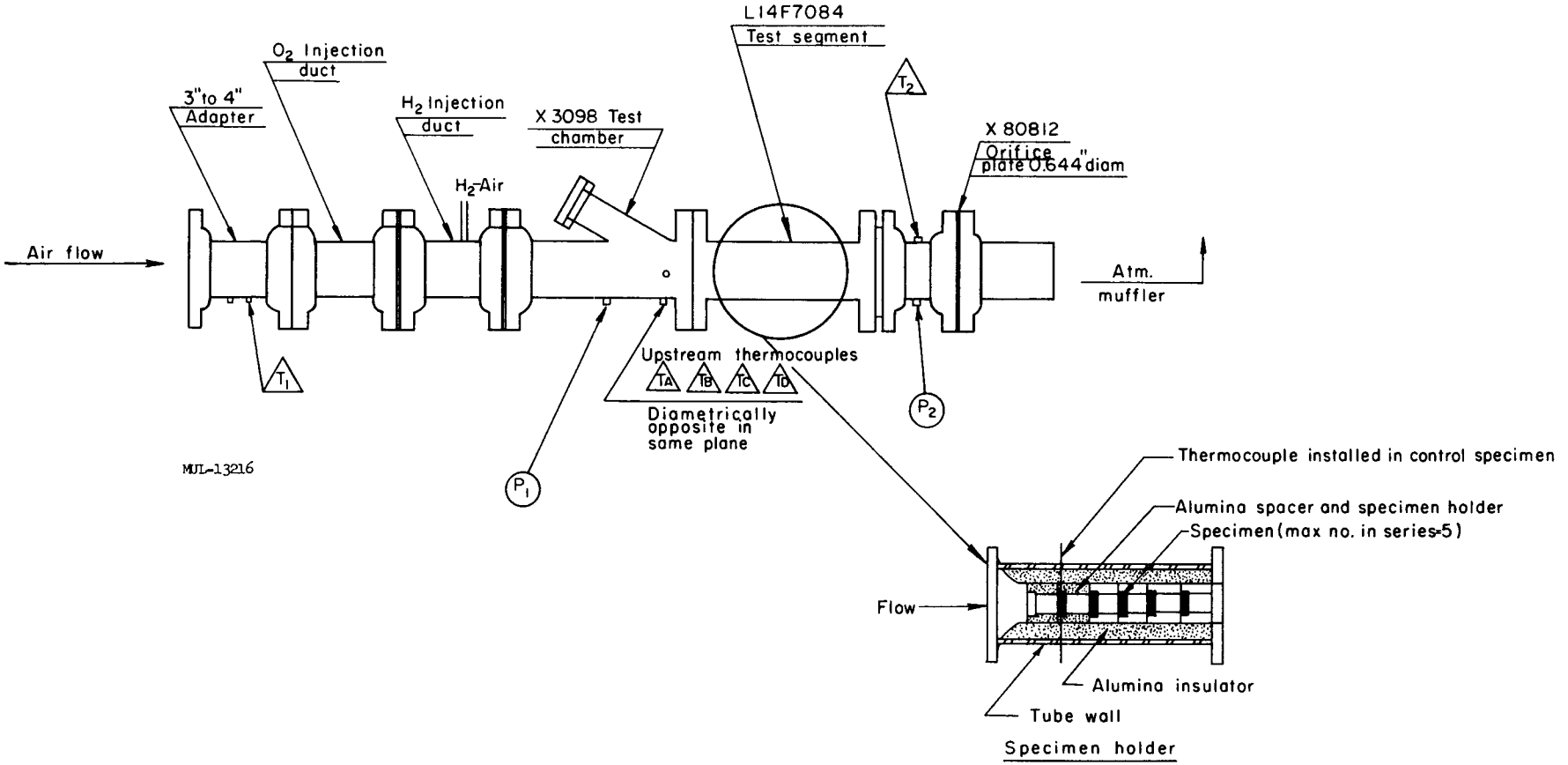

Fig. III-34. Schematic of high pressure – high temperature flow apparatus used for environmental testing of Tory II-C-1 base plate coating.

A test was set up using a bare F-48 specimen instrumented with thermocouples. The system was brought to equilibrium at 2480°F and increases of approximately 30°F per step were selected. At each new temperature level the temperature level was maintained for approximately 2 minutes to eliminate the effect of rate change and to allow the system to come into balance. At a steady 2590°F catastrophic failure occurred in something less than 60 seconds. The time lag (t) could not be determined with precision. The ignition temperature of 2590°F in the latter test confirms with reasonable precision the predicted value of 2600°F.

8. High-Temperature Lubricants (Side Support System)

Static coefficient of friction tests were performed on René 41 coated with the commercial compound Electrofilm #1000, sliding on bare René 41. A total of 14 tests were made at various temperatures to determine the static coefficient of friction for this combination. At the conclusion of the tests, the electrofilmed piece was examined and it was found that the electrofilm coating was almost completely gone from the René 41 piece. This, plus the test results shown below in Table III-4, indicates that Electrofilm #1000 will not be a satisfactory lubricant in the side support system.

The friction test apparatus used here was reported last quarter.

Table III-4. Static Coefficient of Friction for René 41 Coated with Electrofilm #1000 Sliding on Bare René 41.

Test temp (°F)	Test load (lb)	Static coefficient of friction	
		On reaching temperature	After 10-minute soak
72	6.05	0.178	0.173
250	"	0.123	0.167
450	"	0.181	0.228
600	"	0.273	0.280
800	"	0.299	0.300
1000	"	0.514	0.520
1200	"	0.646	0.742

B. Component Development and Testing

Base Block Fabrication

The 75-lb billet of F-48 columbium alloy received from supplier has been successfully extruded. The chemical composition of this material was reported last quarter. Figure III-35 shows the billet after it is welded into a molybdenum sheet metal can. The can protects the F-48 from oxidation during extrusion and subsequent forging or rolling operations. The molybdenum cladding is removed by pickling after the final sizing operation.

Figure III-36 shows the canned billet being loaded into the extrusion press. Handling time was 40 seconds from furnace to container. A press force of near 1100 tons was required to extrude the 5-1/8-in.-diam billet at a 3.08:1 reduction ratio. Figure III-37 shows the bar after extrusion and cooling in Vermiculite. Material for two Tory II-C base blocks will be removed for further processing by rolling and forging. Remaining material will be used for properties testing.

C. Coating Development

1. Environmental Testing of Coated Specimens

Significant progress has been made toward optimizing the coating selected for the Tory II-C environment. Evolution of the coating process during the last quarter has produced coated specimens that have adequately survived environmental testing at 2275°F for 5 hours.

The most recent test was one in which four coated specimens were tested simultaneously at a pressure of 100 psia and a flow rate of 288,000 $lb/ft^2/hr$ of high velocity gas containing 20% O_2. See Table III-5 for specimen description.

The specimens were placed in the facility in series (see Fig. III-34) with an Fe-Cr-Al-Y clad chromium control specimen occupying the first upstream position. The control specimen was drilled for thermocouple instrumentation and was used to set and monitor specimen temperatures. Because of a temperature gradient of approximately 100°F from the first to last specimen, individual specimens were exposed at the following temperatures:

Control	2300°F
CR	2275
CU	2250
CS	2225
CT	2200

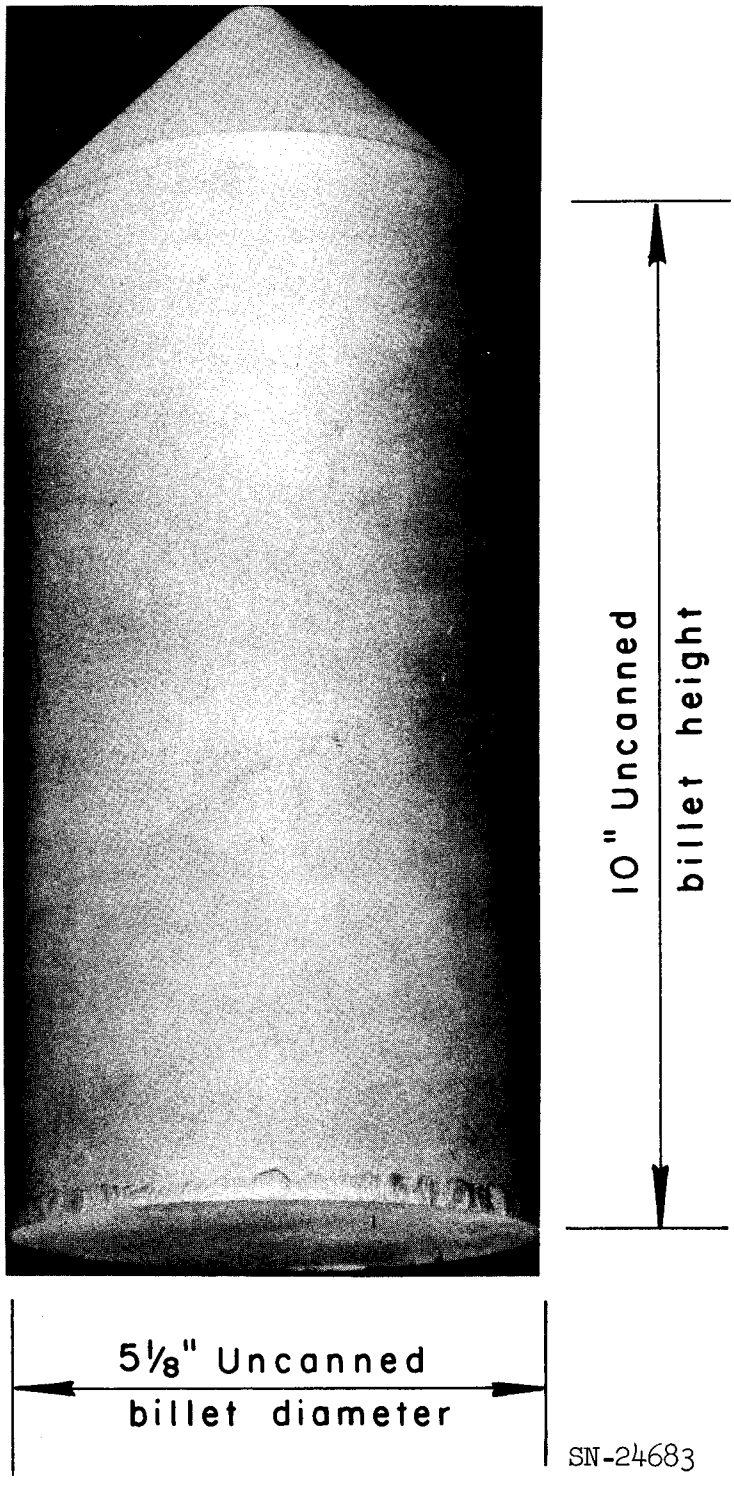

Fig. III-35. Billet of F-48 prepared for extrusion. The 5-1/8-in.-diam × 10-in.-high billet is placed in a molybdenum can for oxidation protection. The conical nose is solid molybdenum and leads the F-48 billet into the extrusion die.

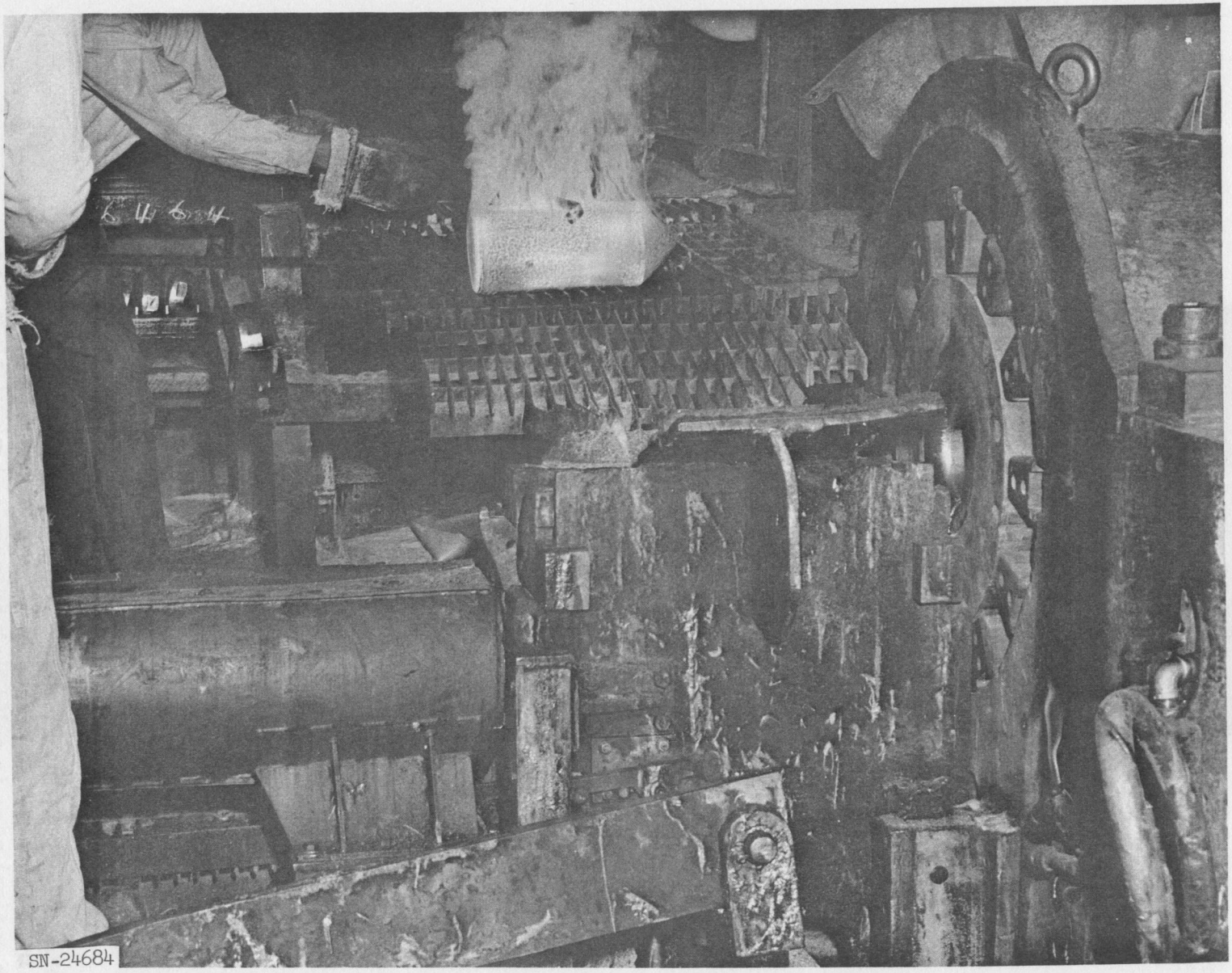

Fig. III-36. F-48 billet being loaded into extrusion press. Extrusion temperature is 2800 to 3000° F.

Fig. III-37. F-48 bar after extrusion and cooling in Vermiculite. Extrusion ratio is 3.08:1. Extrusion force for the 5-1/8"-diam billet was 1100 tons. Useful bar length is ≈ 30 in.

Table III-5. Coated Specimen Description.

Ident.	Alloy	Diam (in.)	Thick (in.)	Flow holes	Radius all corners (in.)	Coating	Previous testing
CR	F-48	1-1/2	3/8	4 ea. 3/8" diam	0.060	Cr-Al-Si	None
CU	F-48	1-1/2	3/8	"	0.060	Cr-Al-Si w/Zr silicate	None
CS	F-48	1-1/2	1/2	10 ea. 0.220" diam	0.030	Cr-Al-Si	None
CT	F-48	1-1/2	1/2	"	0.030	Cr-Al-Si	3 hr 2300°F static

The 2200°F specimen, CT, after the 5-hr run showed virtually no detrimental effects from the exposure. The beginning of coating attrition appeared on only a small area of the upstream face.

Specimen CU, which had a supplementary Al_2O_3 spray coating sealed with zirconium silicate over the base coating, showed no attrition after 5 hr at 2250°F.

The 2275°F CR specimen after the 5-hr run showed coating attrition over about 30% of its total area. Subsequent sectioning of this specimen and hardness traversing showed little oxygen penetration, however. The coating had done an adequate job at 2275°F and a very good job at 2200°F. Use of Al_2O_3 supplementary coat over the base coating appears to offer further protection. Assuming further statistical verification, the coating can be used reliably for this type of environment. Photographs of the test specimens after test are shown in Figs. III-38 through III-44. The hardness traverse curve for four of the tested specimens is given in Fig. III-45.

A pictorial description of part of the coating process is provided in Figs. III-46, III-47, and III-48. In Fig. III-46 two columbium alloy base blocks are being packed in a stainless steel retort for one phase of the Al-Cr-Si coating process. The piece with small holes is made from 1%Zr-Cb alloy. This piece will be used in the unit cell test. The other block is made from F-48 alloy with details very near those of final reactor parts. It will be tested in a high temperature flow environment.

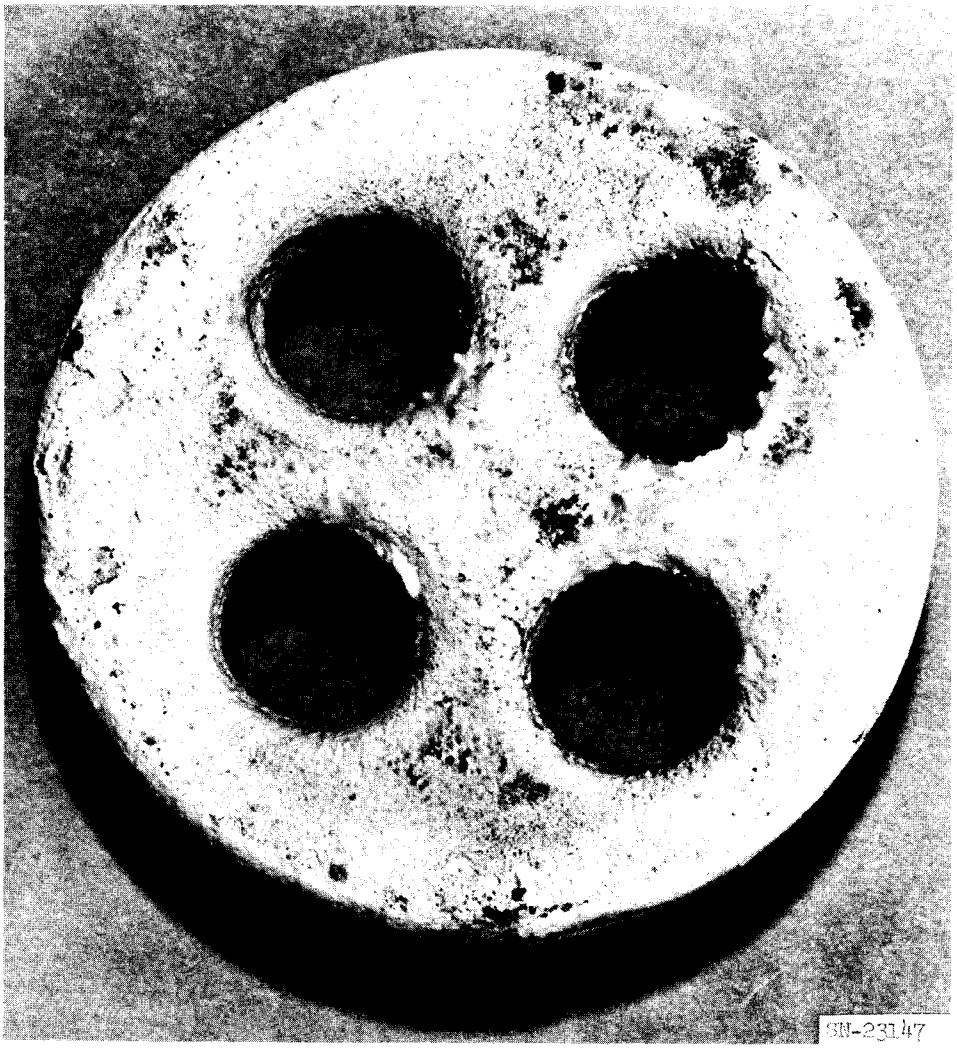

Fig. III-38. Downstream face of specimen CU after 5 hours' testing at 2250°F. Slight softening and flow of the supplementary coating may have occurred to produce the shiny surface at the center of the part. (Mag: 4×)

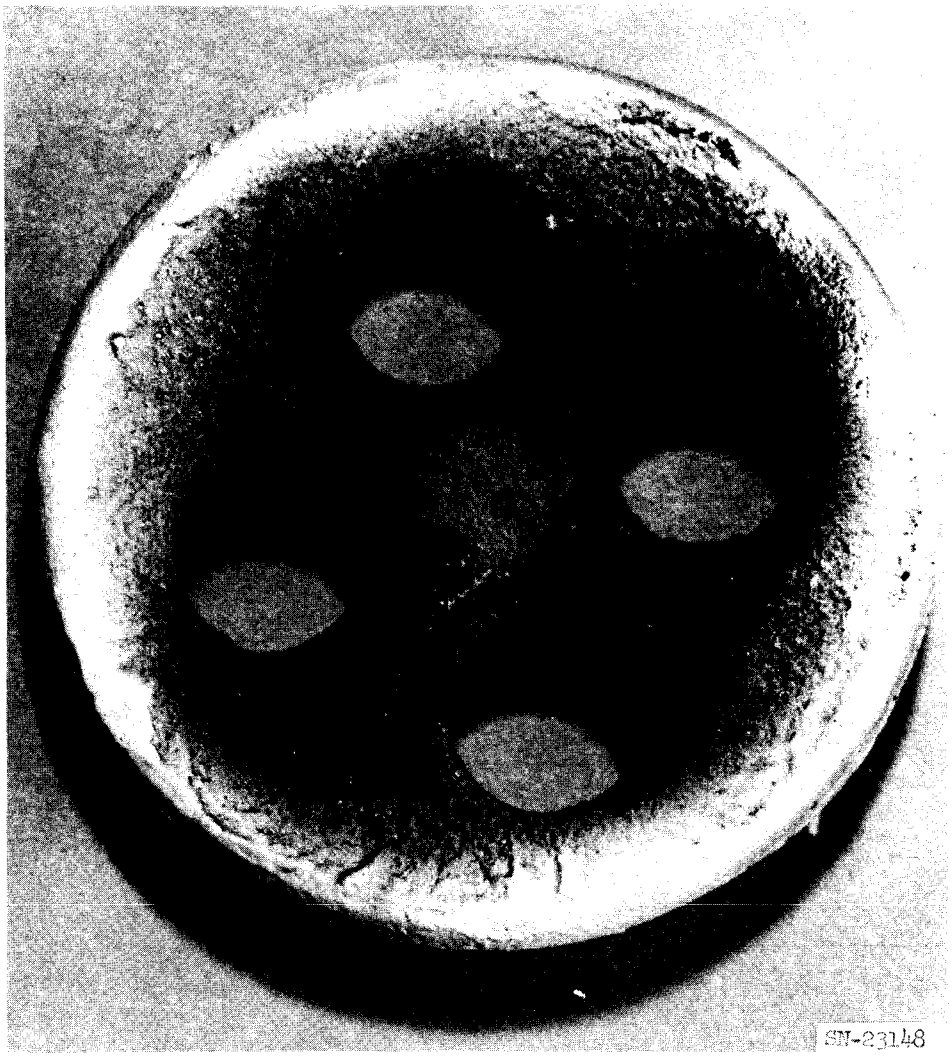

Fig. III-39. Upstream face of specimen CU after 5 hr at 2250°F. No loss of coating can be detected. The brown discoloration is believed to be due to combustion products. The alumina spray supplementary coating produced the irregular surface. Production parts using automatic spray equipment rather than manual would have a smooth surface. (Mag: 4×)

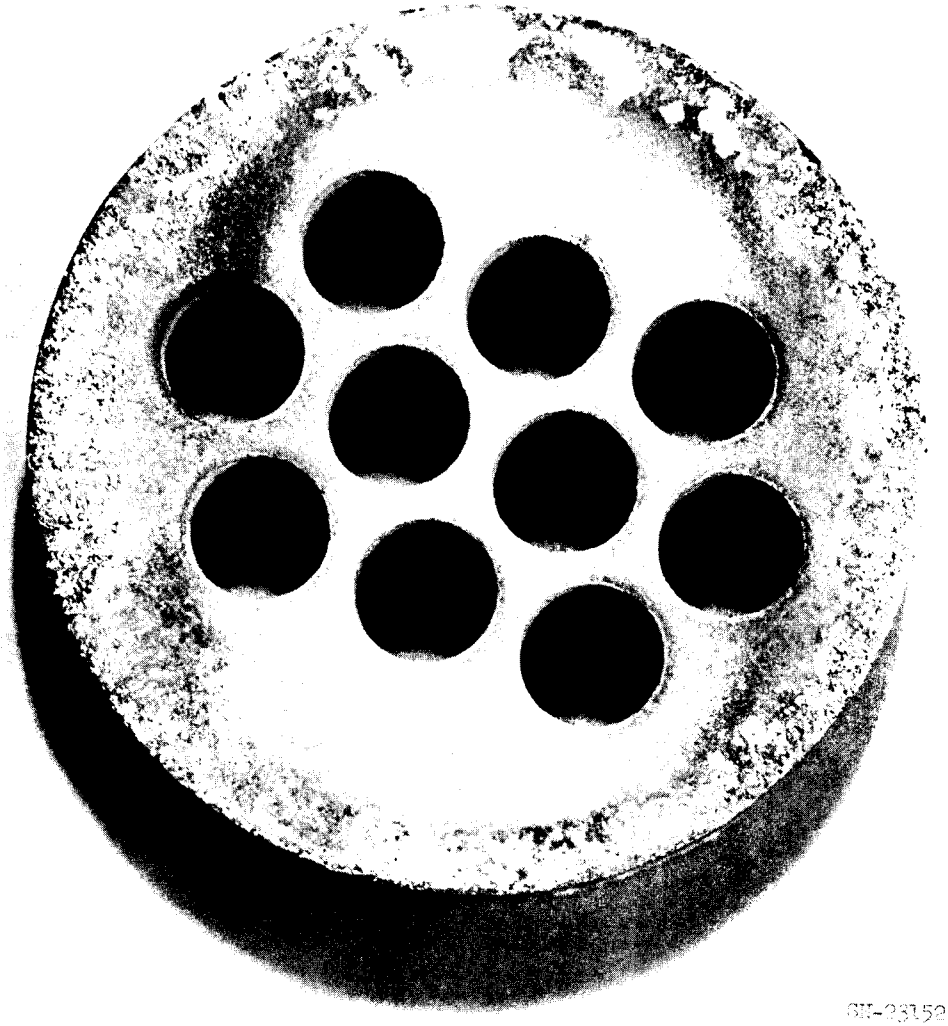

GM-23152

Fig. III-40. Downstream face of specimen CS after 5-hr exposure at 2225° F. The difference in appearance around the outer edge of the part is due to seating on the alumina holder and subsequent abrasion. (Mag: 4×)

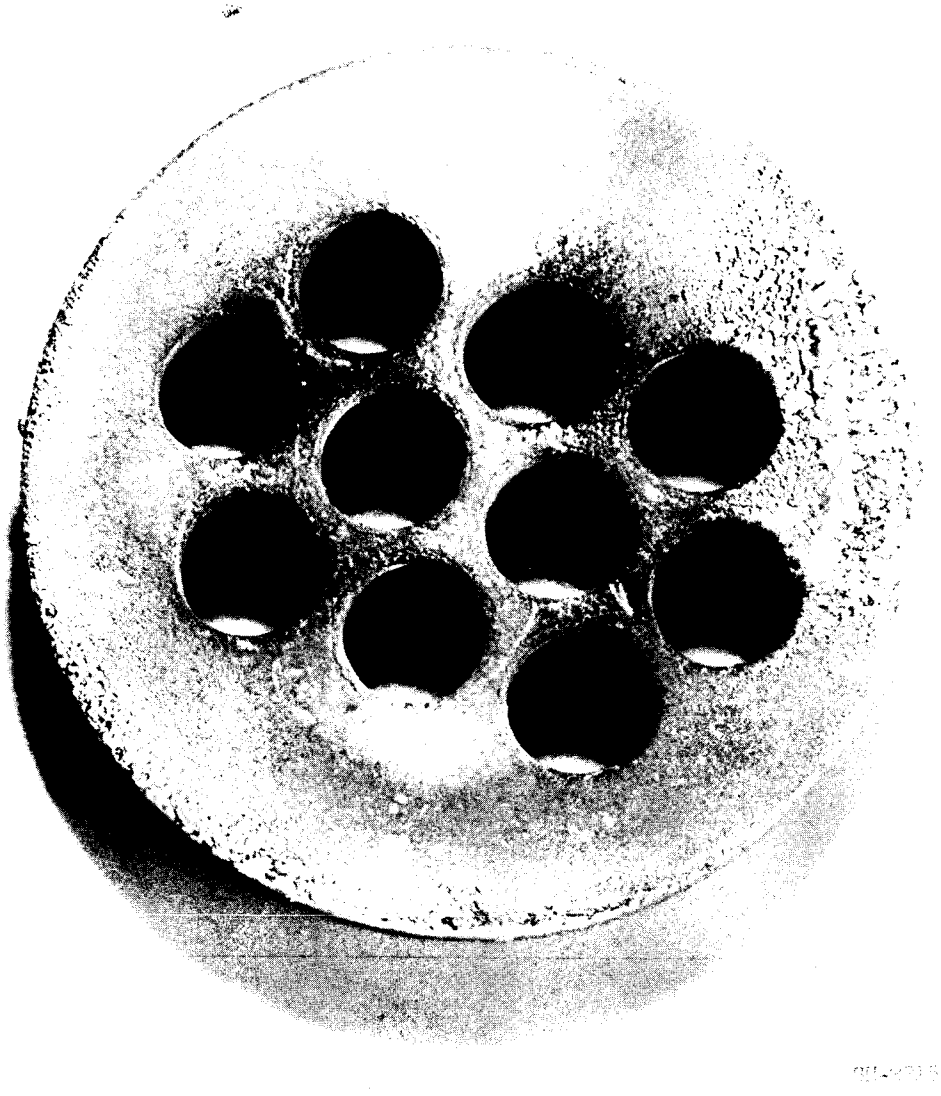

Fig. III-41. Upstream face of specimen CS after 5-hr exposure at 2225°F. Coating shows some loss on periphery of part at 3 o'clock. (Mag: 4×)

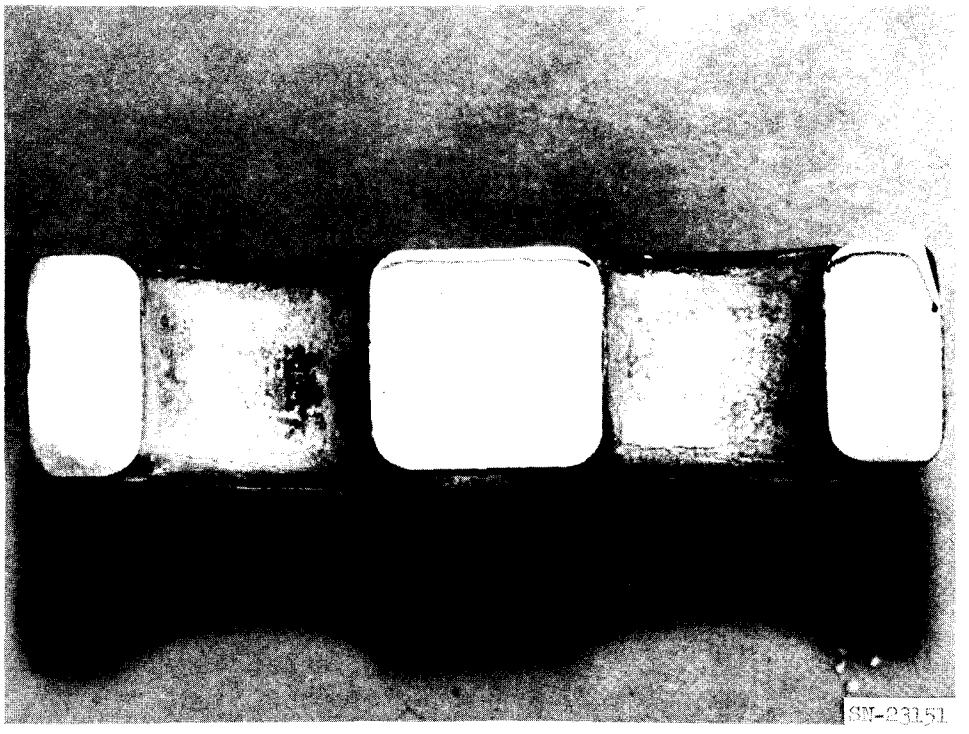

Fig. III-42. Section view of specimen CR after its 5-hr exposure at 2275°F. Upstream face is at the top. Hardness traversing showed no significant change in hardness although ≈ 30% coating attrition had occurred. Note the good retention of coating on inside of holes. (Mag: 4×)

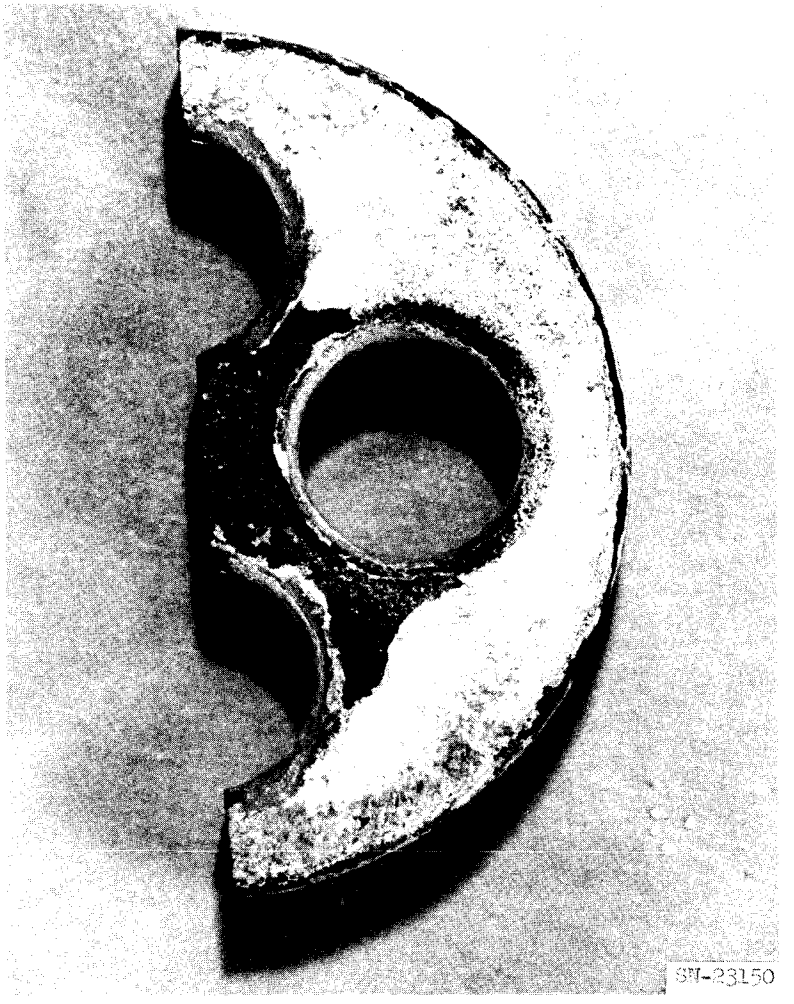

Fig. III-43. Downstream face of specimen CR after 5-hr exposure at 2275°F. Loss of coating is significantly less than on upstream face. (Mag: 4×)

Fig. III-44. Upstream face of specimen CR after 5-hr exposure at 2275° F. Some attrition of the coating is apparent in the lower half of the specimen. (Mag: 4×)

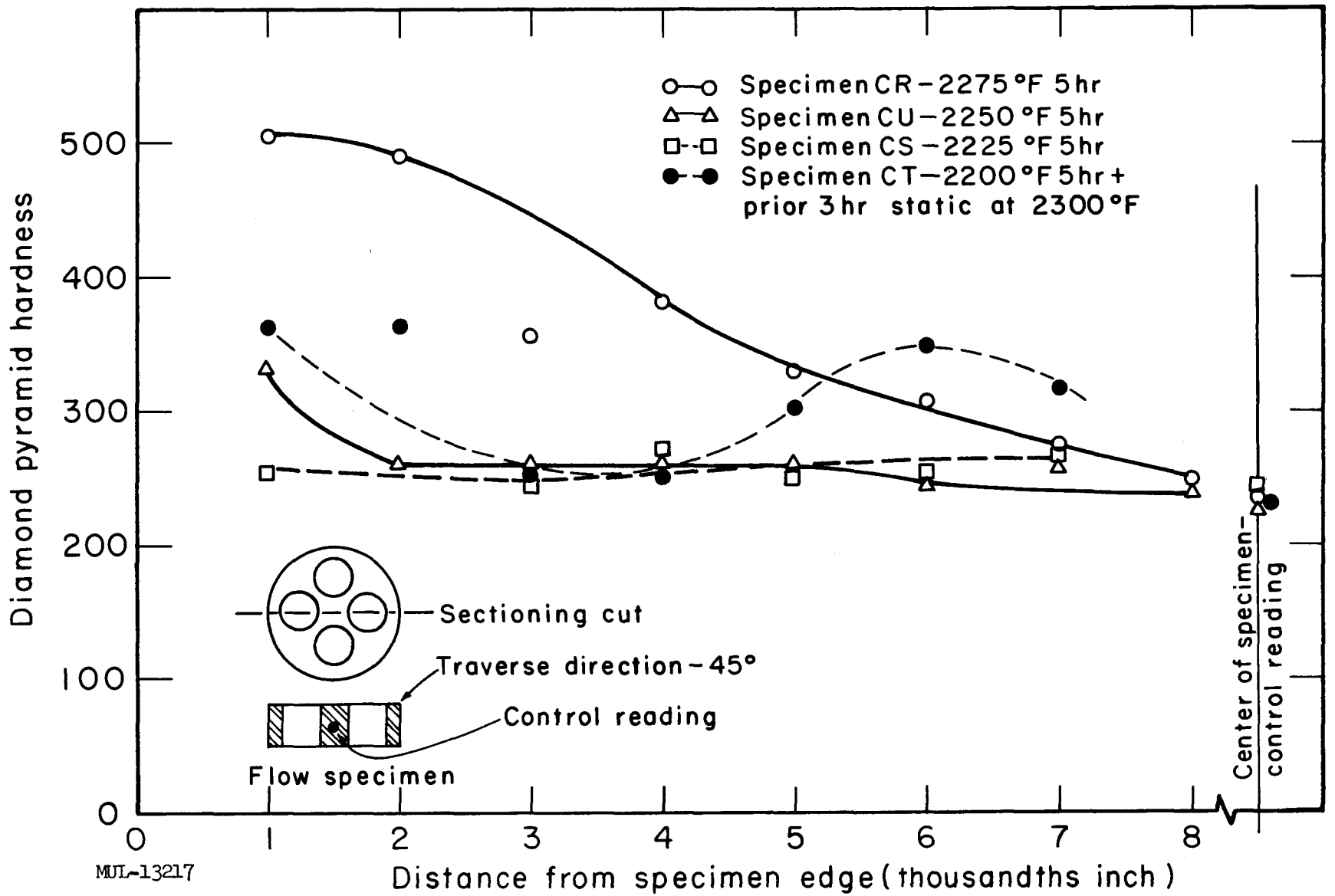

Fig. III-45. Hardness traverse of base plate coated specimens after flow testing. Low level of oxygen contamination of base metal through coating is revealed by small change in hardness near surface.

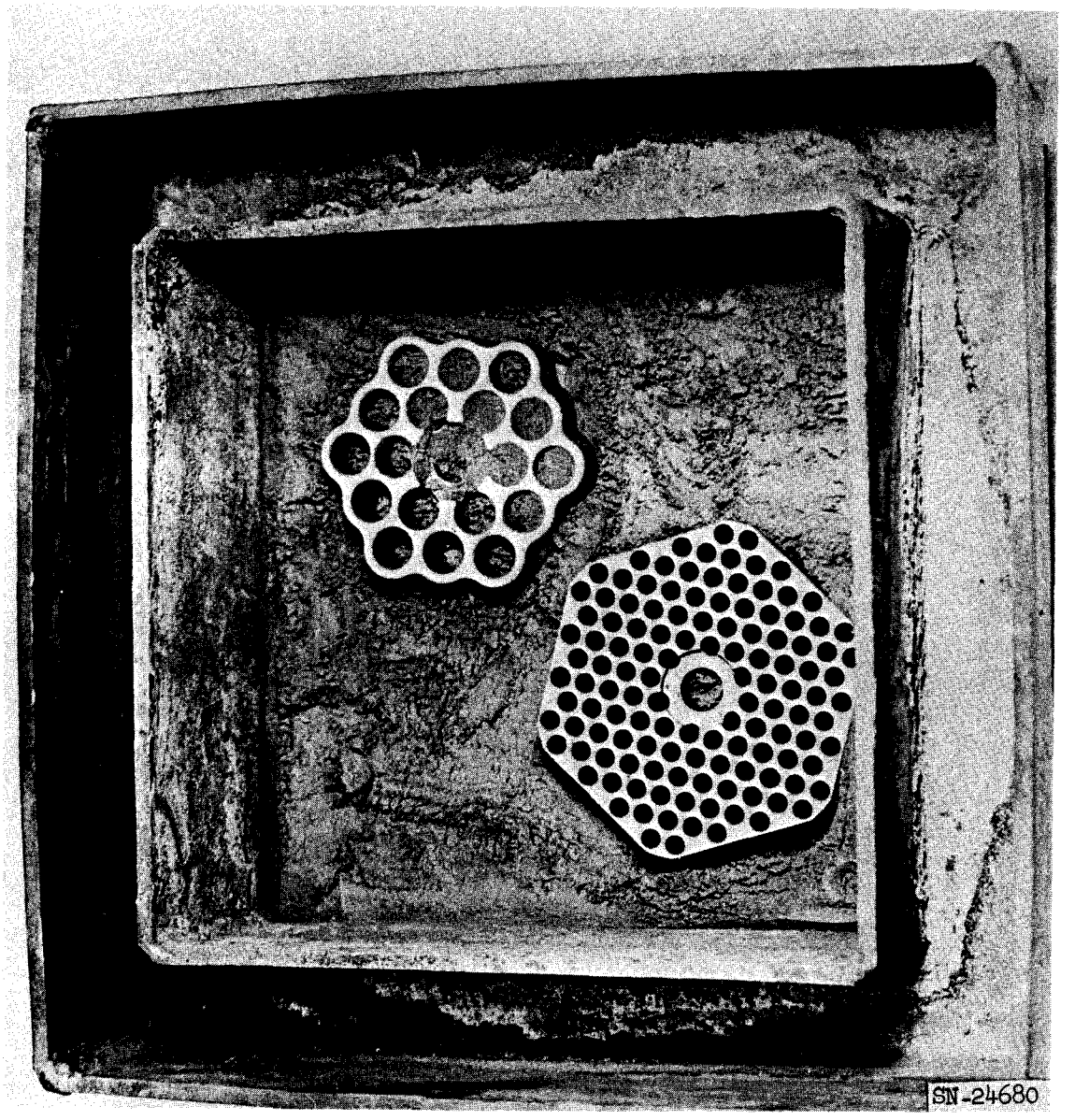

Fig. III-46. Base plate and hot module flow test plate loaded in stainless steel retort. After filling with pack material, retort will be sealed and placed in 1900°F furnace for processing.

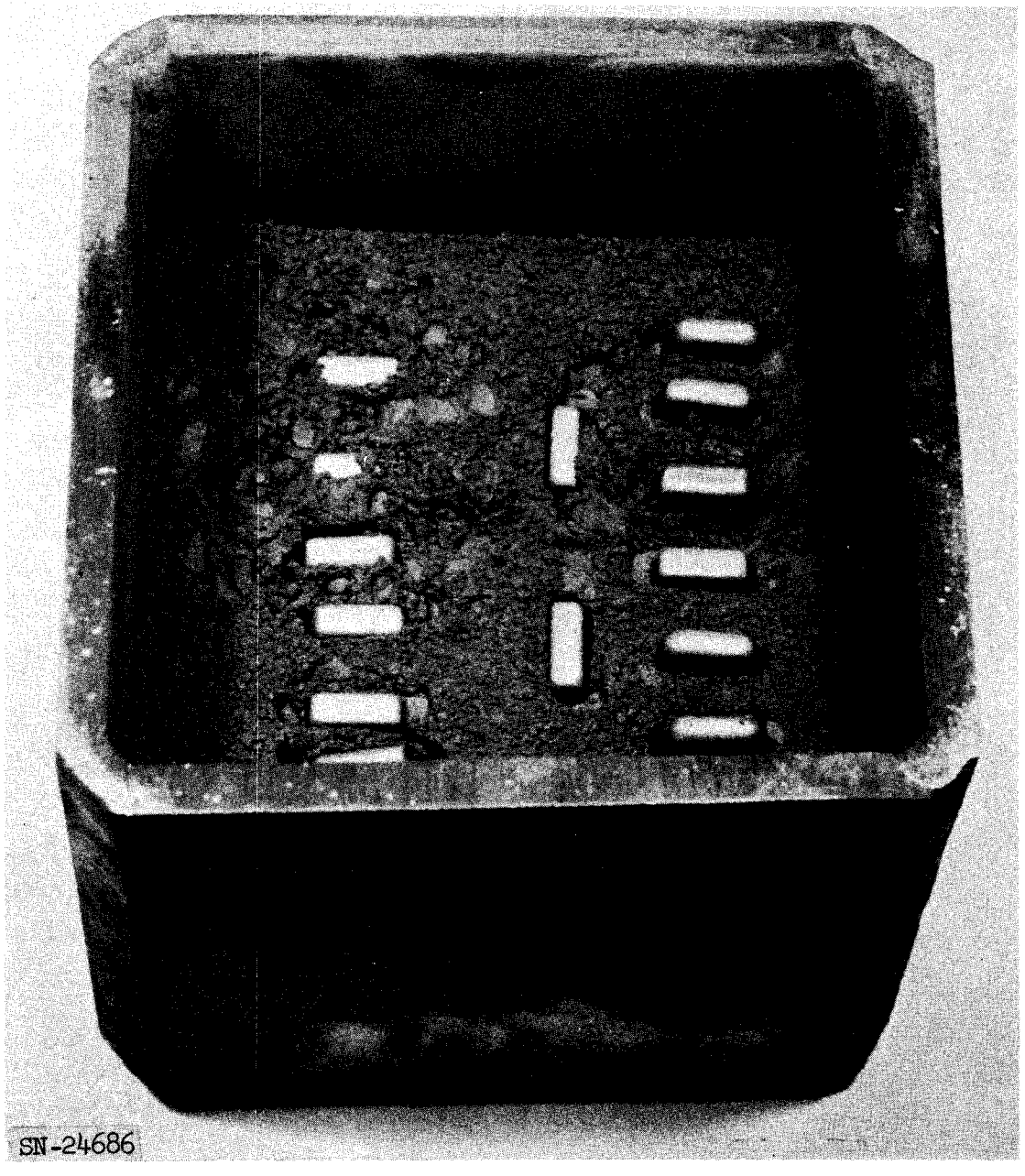

Fig. III-47. Test specimens loaded in stainless steel retort. Pack material will be compacted on top of specimens, retort covered and sealed. Retort will then be placed in furnace for 16 hr at 1900°F.

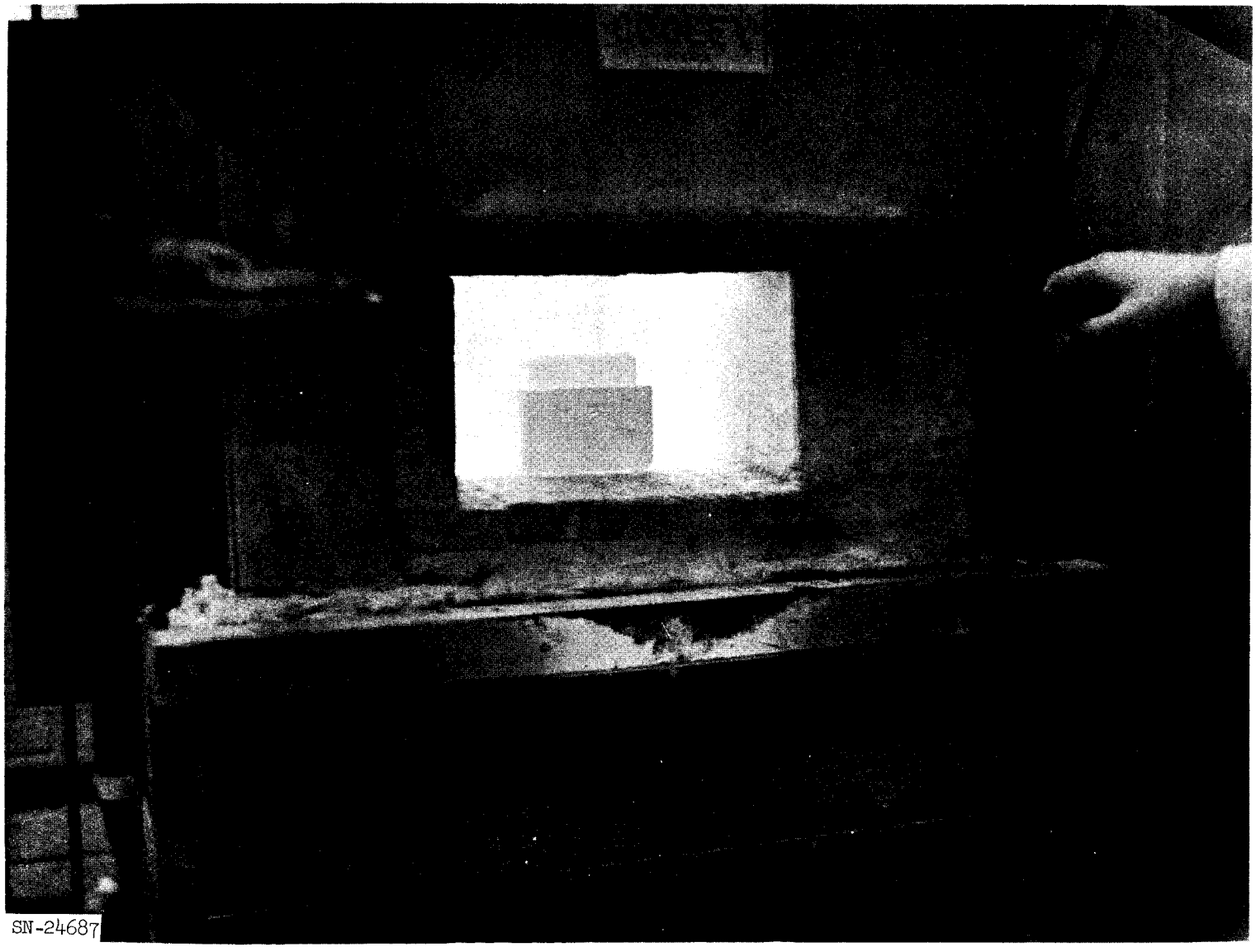

Fig. III-48. Loaded retort containing base plate and hot module flow test plate. Furnace is at 1900°F. Specimens will be processed for 16 hr as one cycle of the silicon-chromium/aluminum pack coating methods.

2. Coating Pack Atmosphere Evaluation

After selecting the pack type coating, it was necessary to review the process variables and tailor them to Tory II-C conditions. Pack atmosphere evaluation is the first step in this process. Pack type coatings are applied by immersion of the part to be coated in a suitable metal powder which is confined in a retort. The retort is then placed in a furnace at the appropriate temperature and the part fired for the correct amount of time. The principal objective of the pack is to coat the part, and the secondary objective is to displace residual oxygen and enhance the cementation reaction. Both objectives are accomplished by the addition to the pack of a material, which, in its gaseous form at elevated temperatures, will drive off residual oxygen and also provide for the transport of metal ions to the part to be coated. For example, the normal pack atmosphere for the chromium-aluminum pack incorporates potassium iodide for atmosphere control. The reaction is thought to be as follows:

$$Cr + Al + KI \rightarrow CrI_2 + AlI_2 \rightarrow$$
$$CrSi_2 + CrAl_2 + CrAlSiCb \text{ (intermetallic)}.$$

This would apply to a part that has a previous silicon coating so that its surface is principally a columbium disilicide. The one possible drawback to this normal atmosphere is a slight oxidation. Therefore, other pack atmospheres were tried.

The addition of urea to the normal pack composition resulted in a coating of inferior oxidation resistance. Urea was added in order to provide a reducing gas which, in theory, should have displaced residual oxygen. The use of ammonium chloride in lieu of the potassium iodide resulted in a coating of inferior oxidation resistance. The ammonium was also intended to provide the reducing gas atmosphere.

Vacuum degassing and argon purging to remove residual oxygen was attempted. The oxidation resistance of specimens coated in the degassed atmosphere showed promise of being superior to the normal pack atmosphere specimens. The procedures for degassing and purging, however, need to be improved. The following table compares the various pack atmospheres:

	Average weight gain of specimen
Urea in pack	0.65%
Ammonium chloride in pack	0.45%
Degassed pack	0.15%
Normal pack	0.27%

D. Photoelastic Stress Analysis

A three-dimensional photoelastic full-scale model of the base block shown in Fig. III-46 was made for stress determination. The model was supported through the center hole at the downstream face and an equally distributed 20-lb load was imposed on the upstream face.

Four horizontal slices have been taken through the model and the highest stressed ligament has been evaluated. The maximum shear stress distribution and a plot of the hoop stress through the depth of the plate is given in Fig. III-49. The maximum hoop stress in this (model) ligament is 48 psi.

To apply the model stresses to the prototype the following equation may be used:

$$\sigma_p = \sigma_m \times \frac{L_m}{L_p} \times \frac{(t_m)^2}{(t_p)^2}$$

where σ = stress at a given point, psi

W = distributed load lb

L = typical length dimension

t = typical thickness dimension.

The maximum stress in the full-scale model base block is therefore

$$\sigma_p = 48 \times \frac{2250}{20} = 5400 \text{ psi.}$$

This value is based on a 1.5-inch-thick plate and a total pressure load of 2250 lb. For a 1-inch plate the stress level is:

$$\sigma_p = 5400 \times \frac{(1.5)^2}{(1)} = 12,100 \text{ psi.}$$

E. Ceramic Parts

Figures III-50 and III-51 show details of BeO parts which have been received for the Tory II-C flow module assembly. These parts were fabricated to LRL specification. A total of 6 BeO hexagonal plates and 150 of the 7-tube inserts are on hand.

F. Tie Rod

Evaluation quantities of Hastelloy R-235 tie-rod tubing have been received from two sources using different fabrication techniques. This tubing was nominally 9/16 in. o.d., with a 0.045 in. wall thickness. One group of tubing was

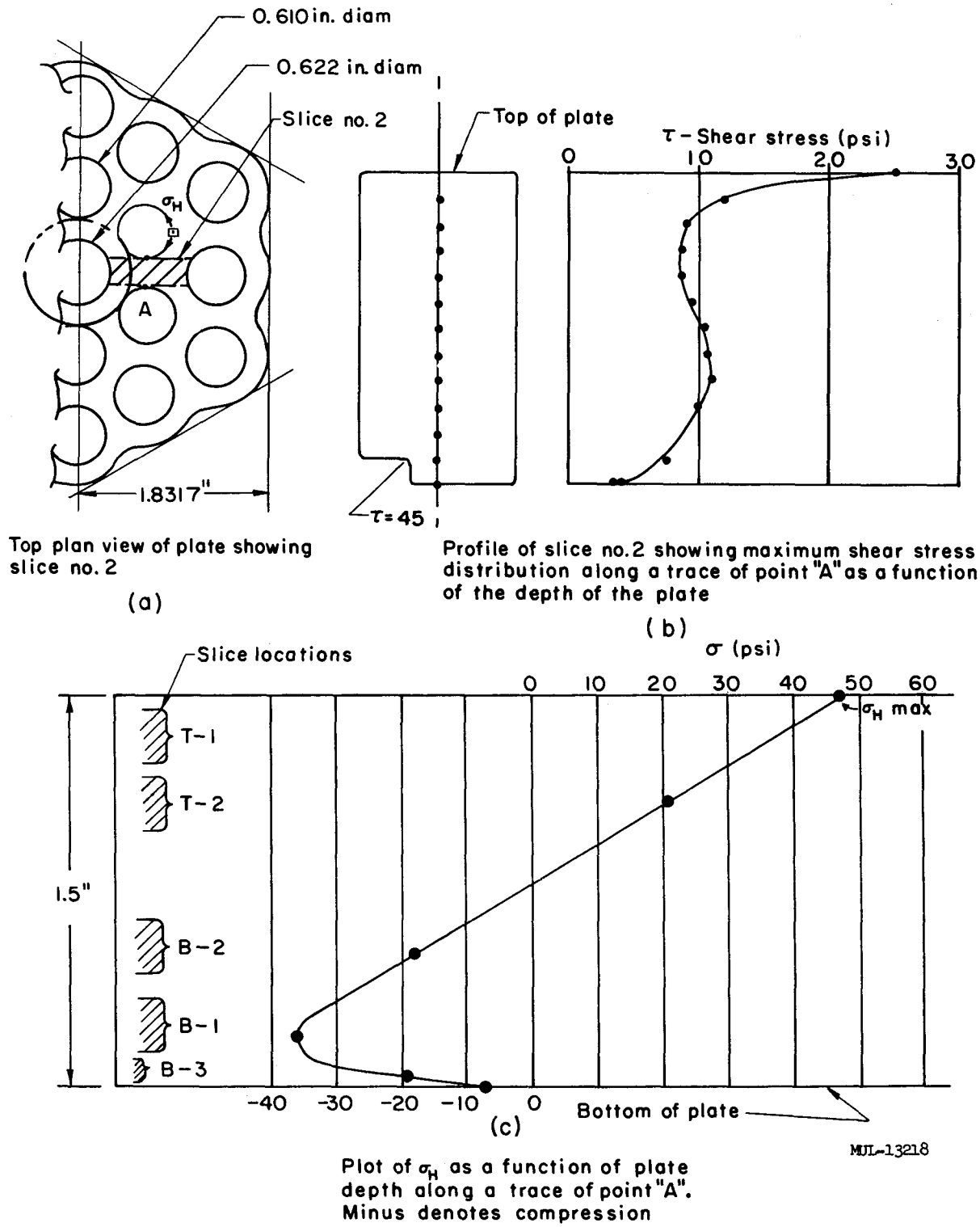

Fig. III-49. Photoelastic analysis of Tory II-C base plate stresses. The metal prototype for this model is seen in Fig. III-46.

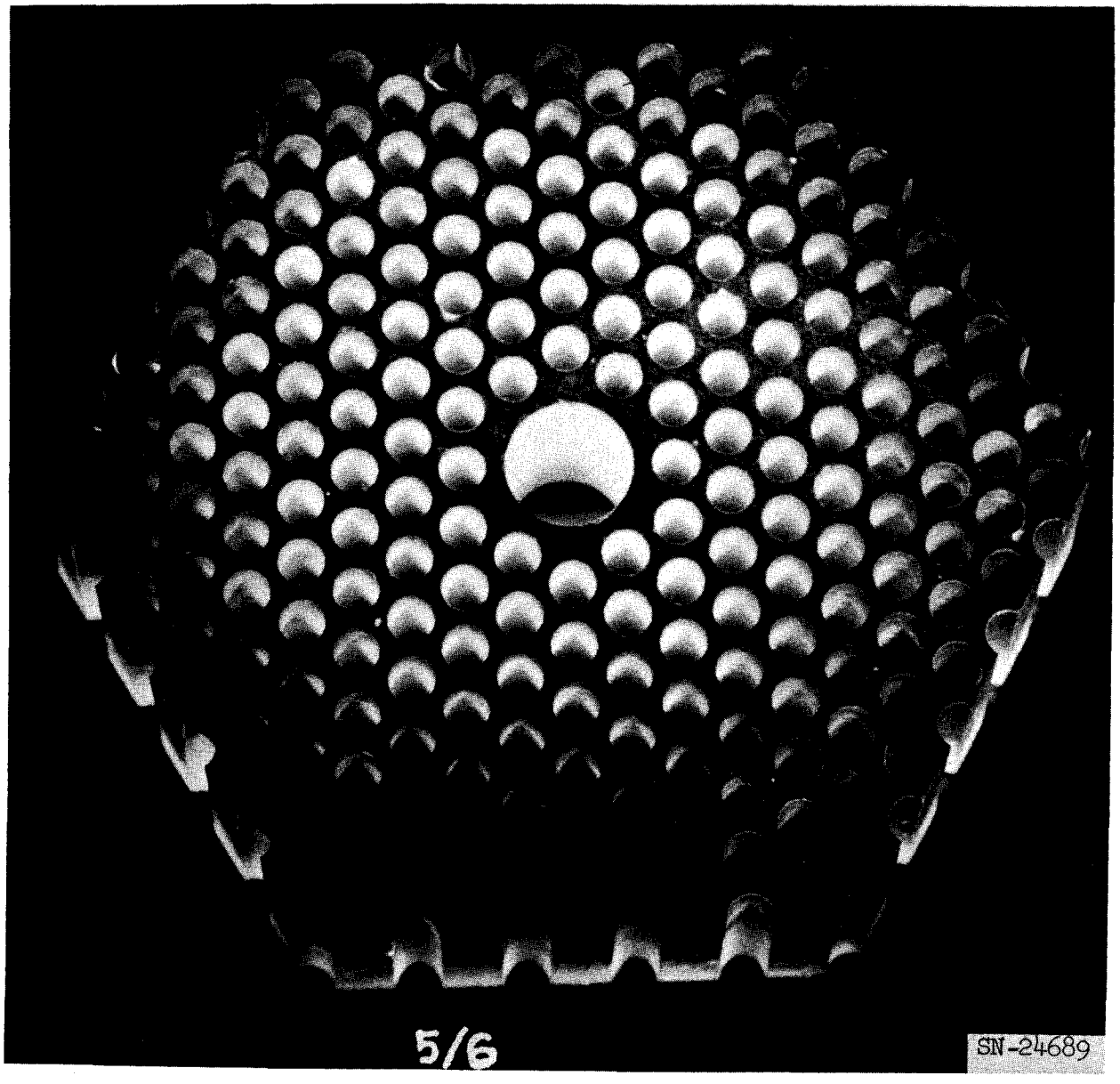

Fig. III-50. BeO plate for Tory II-C hot flow module assembly. Fabricated from a hot-pressed and sintered blank by diamond grinding and core drilling. Plate is 1 in. thick and 4.45 in. across flats.

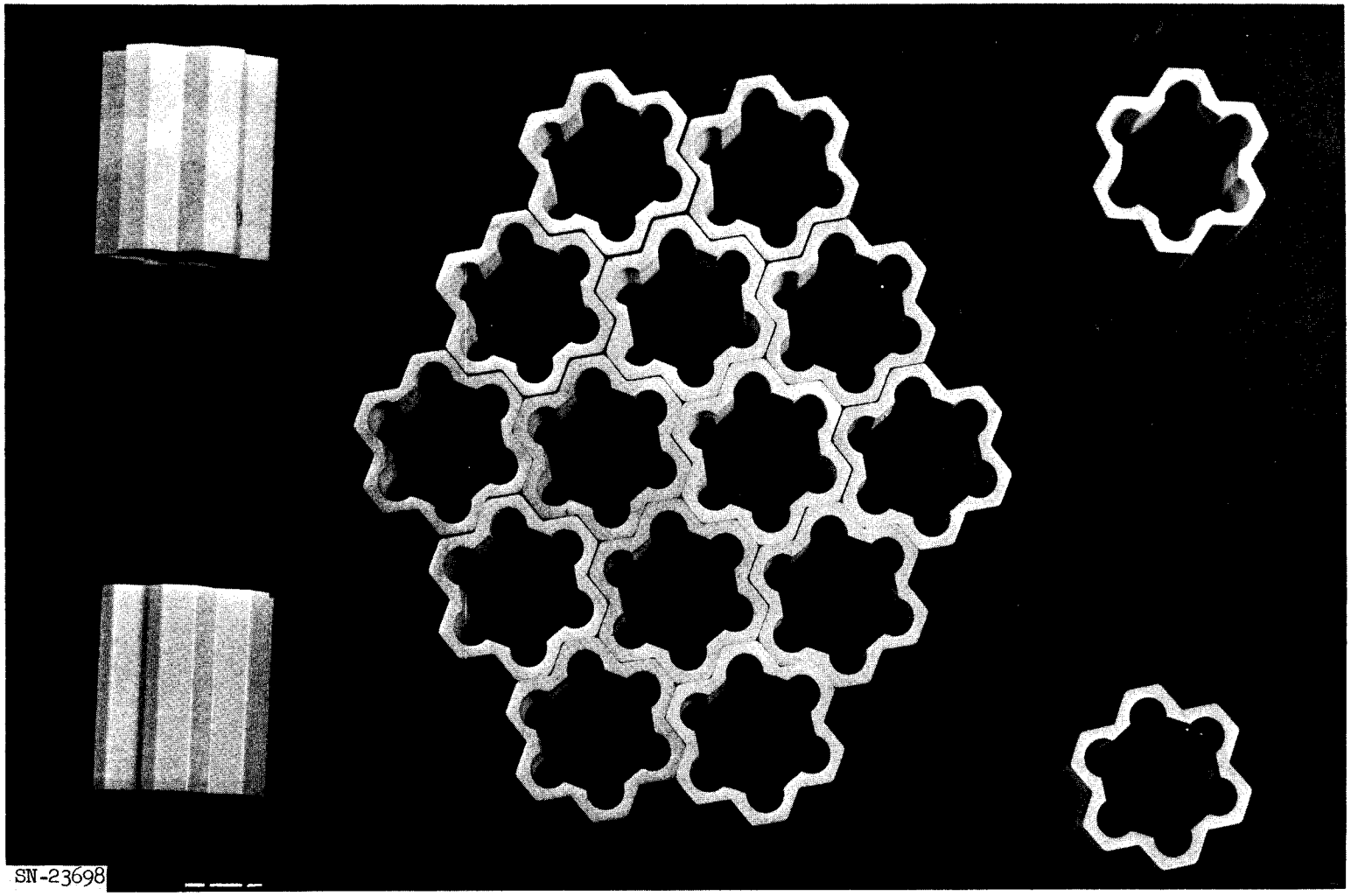

Fig. III-51. BeO insert for Tory II-C hot flow module assembly. Fabricated from a hot-pressed and sintered blank by diamond grinding and core drilling. The part exactly replaces seven hexagonal tubes.

fabricated by the Intraform process and the second group was produced by a conventional drawing process. The Intraformed tubes met the required specification. Cracking to various degrees occurred in the drawn tubing. This has been attributed to a final sizing operation which was performed without annealing beforehand. It is expected that cracking can be prevented in drawn tubing by using an annealing treatment before final sizing.

Short-time tensile tests have been made on samples from these shipments. The as-received material was in a 1975°F water-quenched condition. Heat treatment on the test samples was 1950°F – 30 min – ac, followed by 1400°F – 16 hr – ac. Test results are reported in Table III-6. Photographs of the failed specimens are shown in Fig. III-52.

Table III-6. Static Test of R-235 Tension Tubing.
Test temperature = 1400°F
Strain rate = 0.005 in. per min

		Ult. strength	Elongation
Intraformed:	As received	101,000 psi	15%
		84,000	15
	Heat treated	113,000	12
		118,000	12
Drawn :	Heat treated	101,000	6
		99,000	--

II. TEST VEHICLE

Design and development of the test vehicle and its components are being performed by American Car & Foundry Industries and The Marquardt Corporation under LRL direction.

The status of the test vehicle is summarized below:

A. Mobile Support System

This system includes the flat car and running gear and the duct support structure. Preliminary layouts and stress calculations have been completed for the flat car. The overall length of the car is 35 ft. Trucks and brakes are identical to those used with the Tory II-A car. Detail design of the duct supports

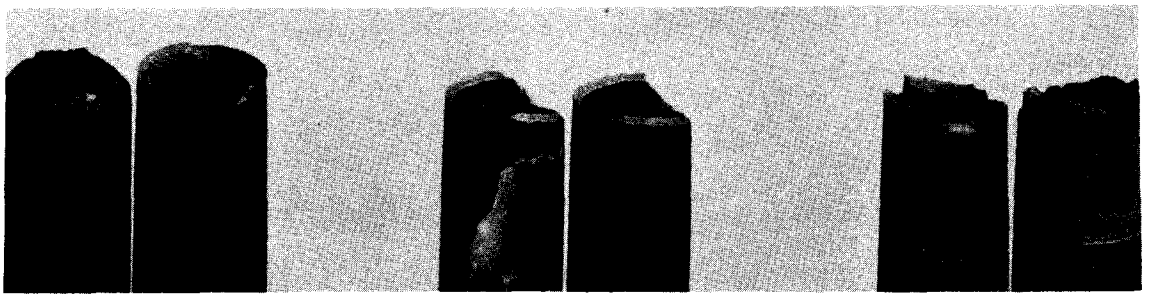

1
INTRAFORMED PROCESS ANNEALED

2
INTRAFORMED PROCESS ANNEALED

3
INTRAFORMED PROCESS AGED

SN-23909

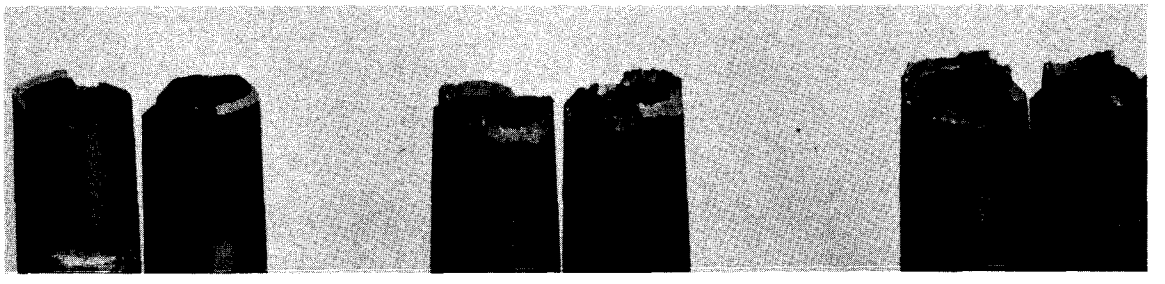

4
INTRAFORMED PROCESS AGED

5
DRAWN TUBING AGED

6
DRAWN TUBING AGED

SN-23910

Fig. III-52. Hastelloy R-235 tubing after test.

is in progress. As yet, little consideration has been given to vibration characteristics of the duct and support configuration. A computer program is being modified to solve for bending modes and resonant frequencies. Pending confirmation of vibration studies, it is planned to locate two supports under the support duct just forward of the reactor assembly and a third support under the aft reactor duct just forward of the nozzle flange. The overall layout is shown in Fig. III-53.

B. Duct Coupling

A 16-segment V-band type coupling has been designed.

C. Diffuser Grid

The diffuser grid design is complete. Some change in flow area is to be expected when reactor performance is finally specified. The grid is to be made from a single piece of A-286, 39 in. diam × 5 in. thick.

III. EXPERIMENTS

A. Slice Test

In order to better understand the results of the Slice Test, some preliminary testing is under way. The load-deflection characteristics of an array of hexagonal ceramic tubes have been studied.

Two rectangular arrays (≈ 6 × 12 in.) of ≈ 4-in.-long hexagonal ceramic tubes were subjected to load-deflection tests. Each array contained 1000 tubes. One array contained Tory II-A fuel elements ($BeO-UO_2$) while the other contained the steatite tubes which are to be used in the Tory II-C Slice Test.

The BeO tubes had a 63 microinch rms surface finish while the steatite tubes had a 108 to 149 microinch rms surface finish.

The tubes were stacked in a holder (see Figs. III-54 and III-55) and mounted in a universal testing machine. A loading rate was selected and the load was increased to about 600 lb (equivalent to 30 psi). Load rates were varied from 30 lb/min to 1000 lb/min with no marked effect on load-deflection characteristics. After a number of runs the holder was rapped to "loosen" the tubes and the sequence was repeated.

The results indicate some similarity between the BeO and steatite arrays. For each material there were two distinct load-deflection curves. One curve was followed for the first run after rapping, i.e., when the stack was

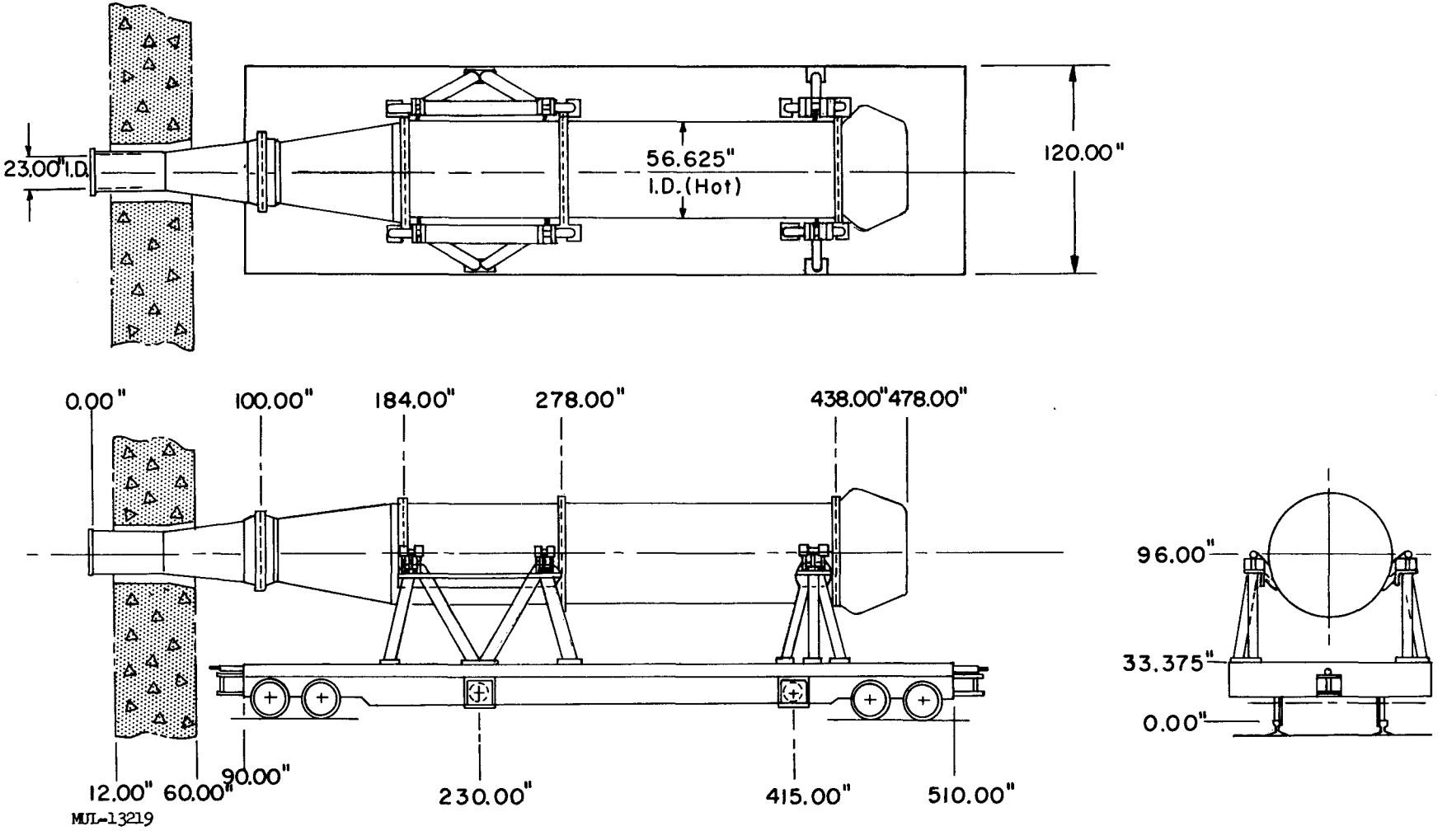

Fig. III-53. Tory II-C test vehicle.

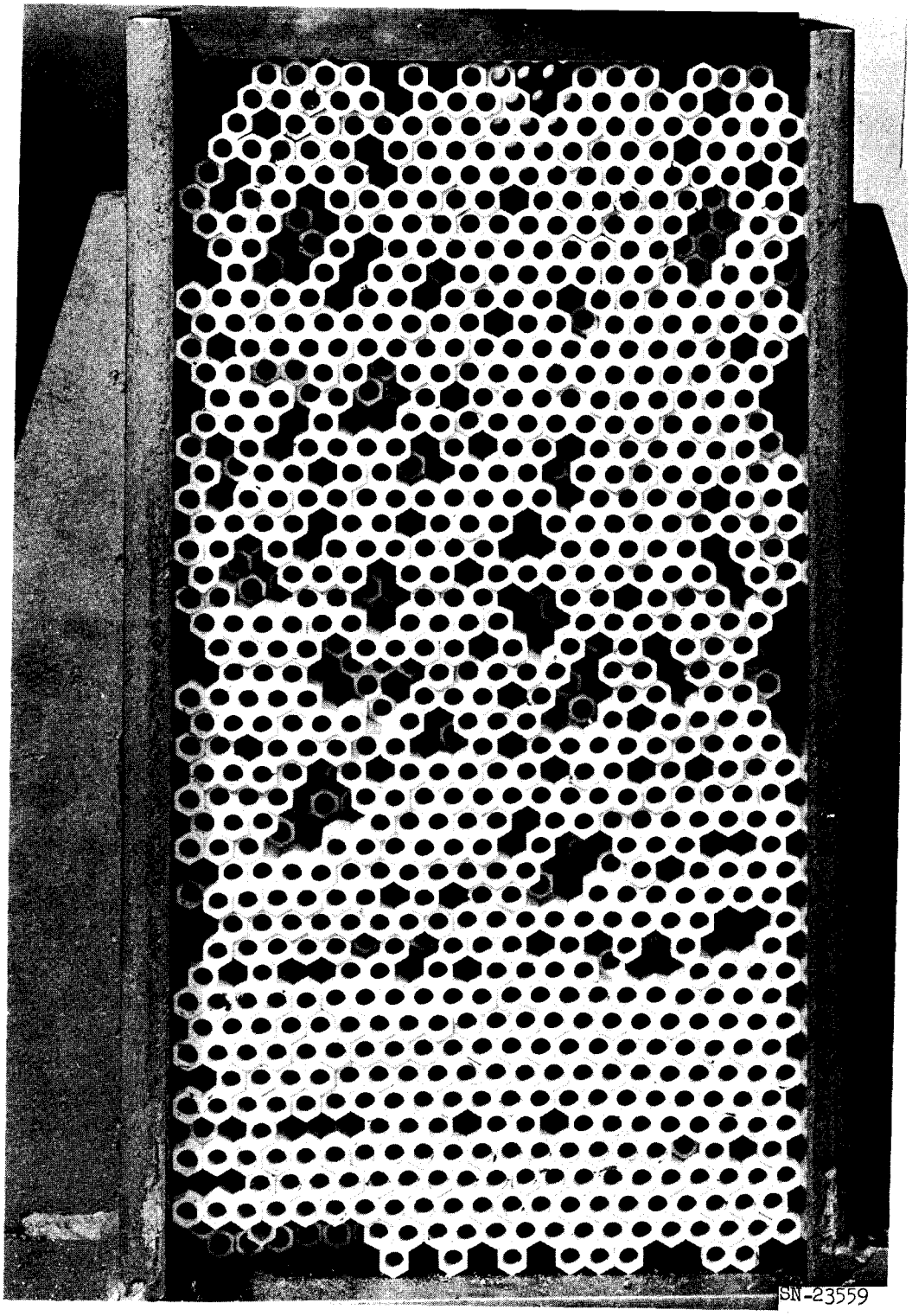

Fig. III-54. Tapered holders.

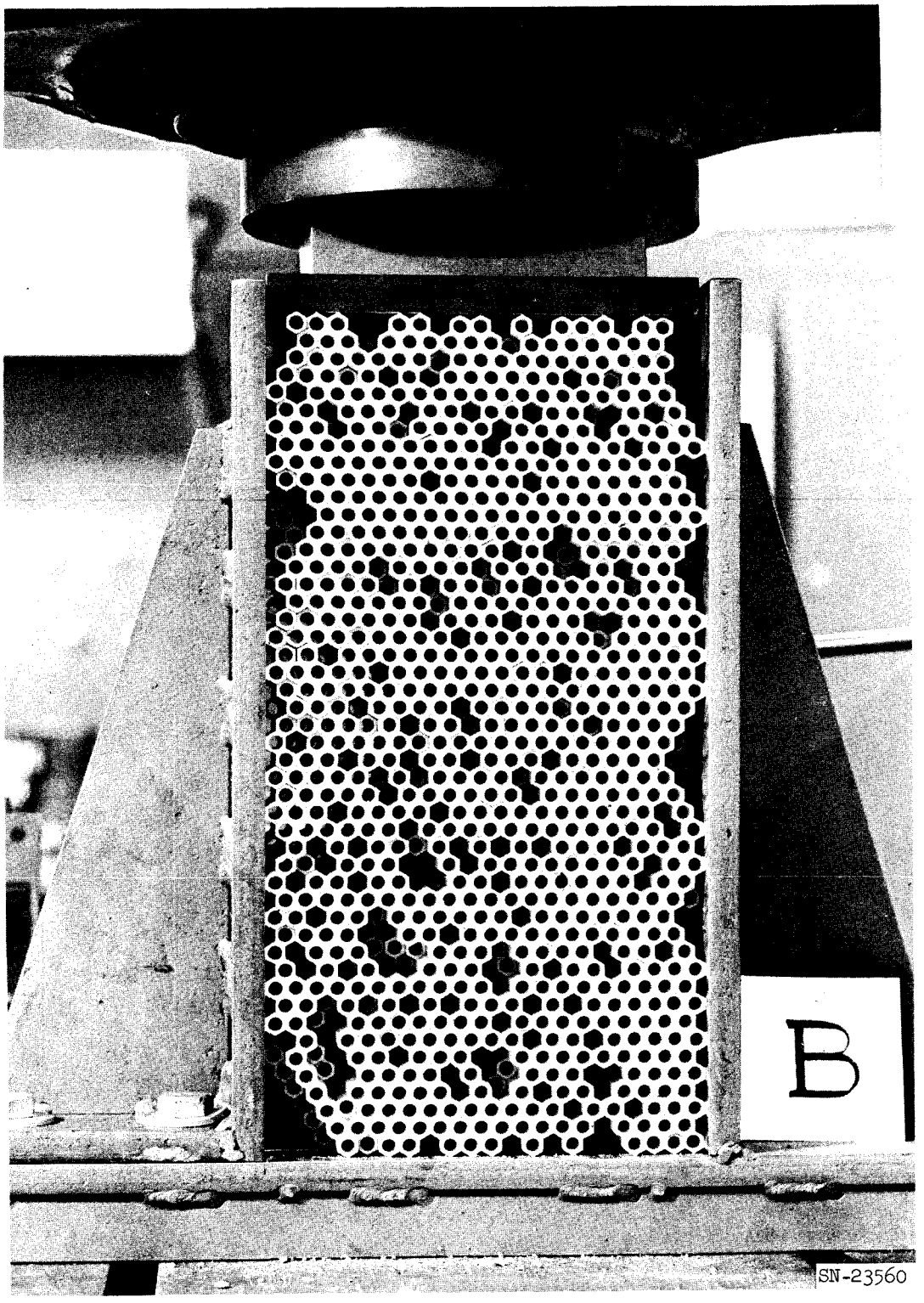

Fig. III-55. Adjusted holder.

"loose"; the second curve, for the "tight" stack, was followed in all subsequent runs. The arithmetic means of the experimental data points can be closely approximated by a parabola. Thus:*

$$P = Ay + By^2 ,$$

where $A \approx$ linear coefficient

$B \approx$ "stacking" coefficient

$P \approx$ load

$y \approx$ deflection.

The values of A and B can be evaluated from the experimental results and yield the following results (see Fig. III-56):

	BeO	Steatite
"Loose"	$P = 13.9y + 1.82y^2$	$P = 0.65y + 0.25y^2$
"Tight"	$P = 42y + 1.82y^2$	$P = 2.25y + 0.52y^2$
$\frac{A_{loose}}{A_{tight}}$	$\frac{13.9}{42} = 0.33$	$\frac{0.65}{2.25} = 0.29$

The smoother surfaces and perhaps the rounded corners of the BeO tubes, as well as the greater camber present in the steatite tubes, may account, in part, for the greater stiffness of the BeO stack. The differences in Young's modulus and length account for only a 40% greater stiffness of the BeO stack. The ratio of linear coefficients between the "loose" and "tight" condition should be an index of the increased stability of the stack, or "nesting" effect. This "nesting" is about the same for the two stacks if the ratio of linear coefficients is used as its measure. The similarity of coefficients in the second degree terms in the two BeO cases implies that the number of tubes which participate in either the tight or the loose case is the same. With the greater degree of freedom afforded by camber in the steatite array, the number of tubes which participate could reasonably be expected to change.

The number of tubes which were not supporting a load was determined in two cases for the steatite stack. Initially the stack holder was double tapered

---

*Note that this implies that the number of tubes, N, which participate in supporting the load is proportional to the deflection, at least for small deflections.

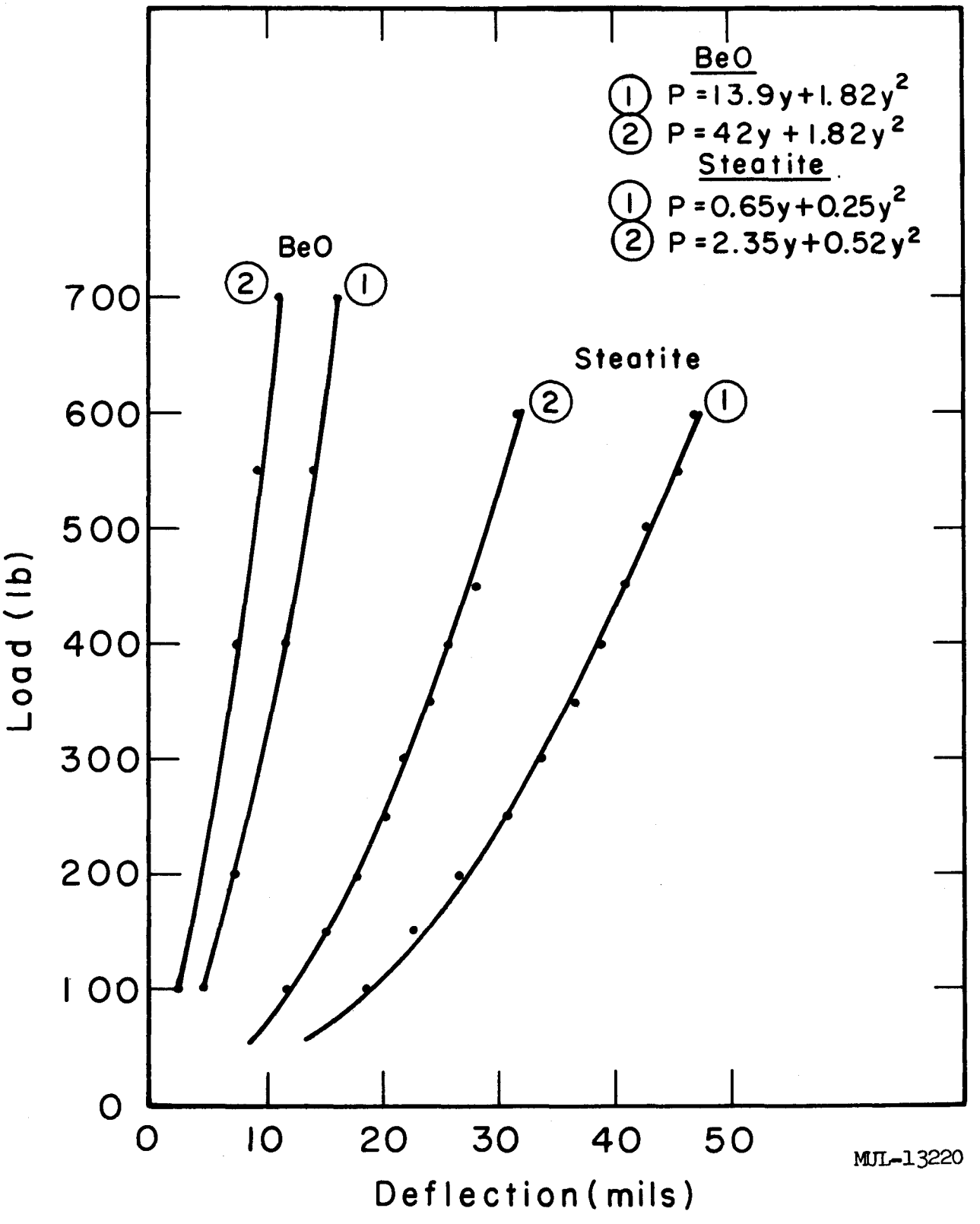

Fig. III-56. Load vs deflection for 1000-tube stack, 6-1/4 in. wide, 12 in. high. Loaded in 12-in. axis. Room temperature.

about 0.030 in. vertically (opening upwards) and 0.020 in. horizontally. Several runs were made this way and the holder was then readjusted to remove this taper. No marked effect on the load-deflection curve was observed.

In each case the unloaded tubes were found by loading the stack to 600 lb and pushing each tube with a pencil. The unloaded tubes slid out partially.

	No. of loose tubes	Distribution
Case A: Tapered holder	210	Group shift
Case B: Adjusted holder	202	Many single shifts

The tapered holder exhibited small groups of loose tubes while the adjusted holder included a majority of single loose tubes (see Figs. III-54 and III-55).

Some general characteristics of small groups of hexagonal tubes containing intentional twist and camber are pictured in Figs. III-57 and III-58. Elements having camber tend to form stable ring-like configurations as in Fig. III-57. When a circumferential load is applied to such a group, the unloaded elements may be found by probing. These elements will slide out. Elements having twist will form a radial array, as in Fig. III-58. It is obvious from the figures that in the case of twist more tubes participate in supporting the load.

From the above preliminary results, the following tentative conclusions may be drawn:

1. A large array of tubes is likely to exhibit a parabolic load-deflection character.

2. Smoother and straighter tubes improve load distribution among the tubes.

3. As many as 20% of the tubes may support no load.

4. Camber promotes a ring or "arch" type stability, whereas twist induces a radial load distribution.

5. The "nesting" of the elements, defined as the ratios of linear coefficients, is the same for both materials. This supports the view that "nesting" is primarily geometry-dependent.

6. The distribution of unloaded elements in a large array may be sensitive to boundary configuration and tolerance.

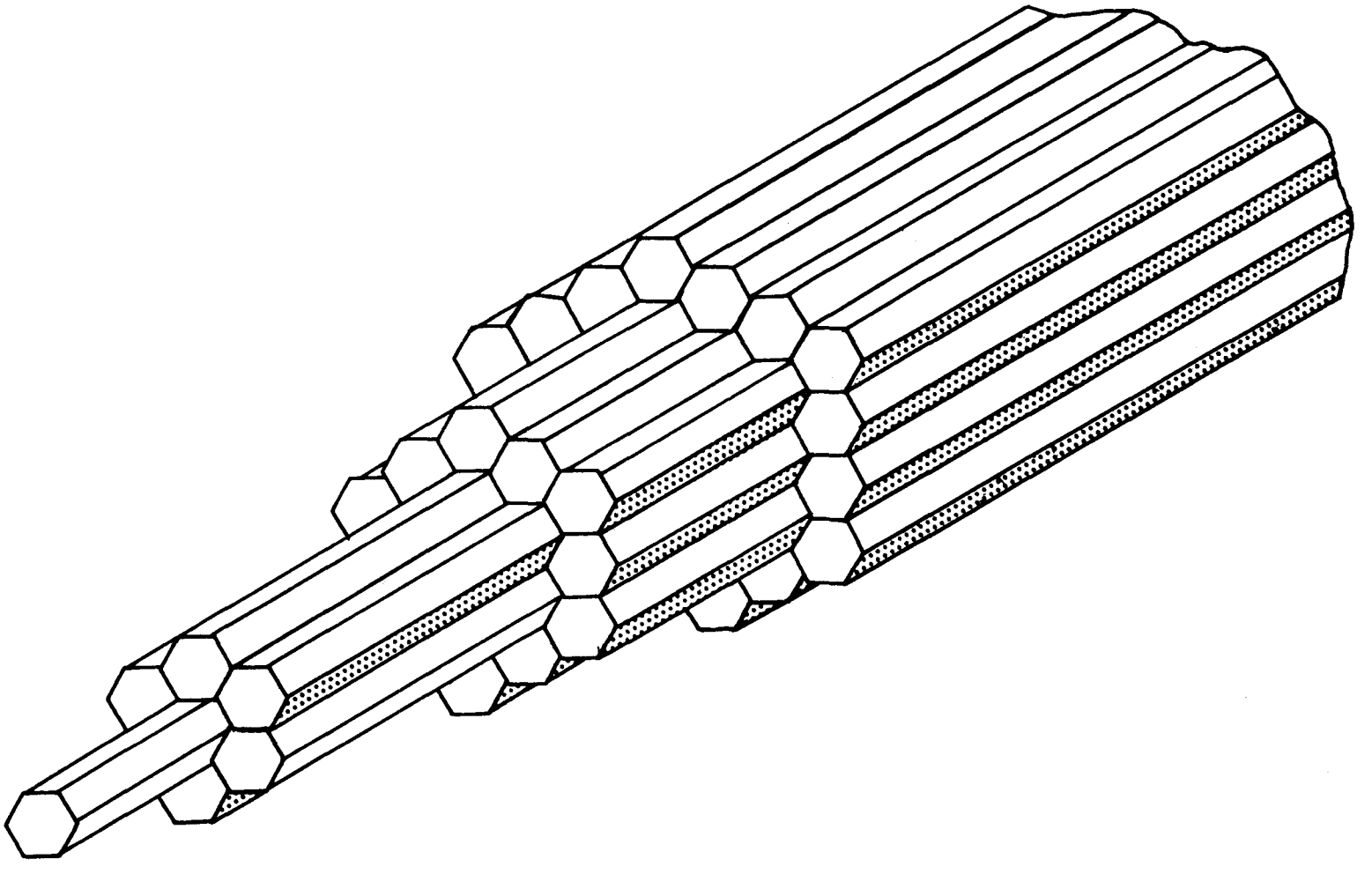

MUL-13221

Fig. III-57. Ring stability of cambered tubes. The elements in the outer ring are supporting nearly the whole load. Projecting elements are free to move.

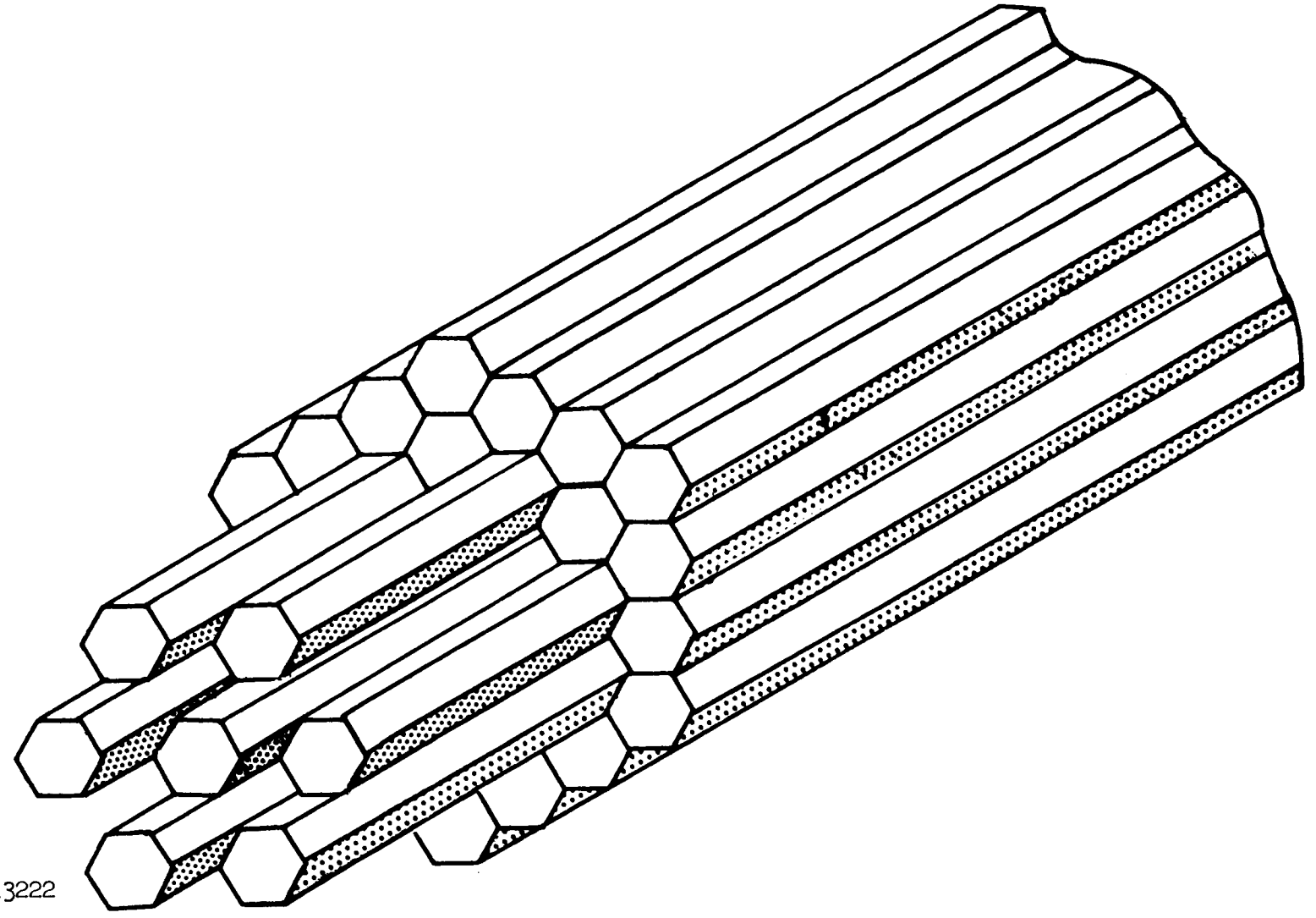

MUL-13222

Fig. III-58. Radial stability of twisted tubes. Each projecting tube is free to move.

B. Transition Losses

In order to minimize the number of flow passages in the base block (for strength and arrangement requirements), it is necessary to have flow from some number of reactor passages converge into one passage. The pressure losses attendant in these transitions are being investigated.

Four transition sections (7 to 1) (Fig. III-59) have been tested at the LRL blowdown facility. Test results are reported as percent of total pressure loss as a function of the Mach number at the exit of the tube section. The pressure losses include those across the transition and base-plate sections and the sudden expansion loss at the exit of the base plate. Losses were measured with static pressure taps between points 1 and 2 (see Fig. III-60) and calculated between points 3 and 4.

The spacing of the tubes and the ratio of diameters between the simulated base plate and the plenum represented a 52% porosity. The flow area of the simulated base plate was the same as the flow area of seven tubes. However, all transition sections had some increase in flow area within their length. The test sections were pinned together to give radial and rotational alignment.

The data are shown in Figs. III-61 through III-65. The transition for Run No. 237, which had the greatest porosity, showed the least loss by a small margin over the range of Mach numbers. It is interesting to note that Runs 234 and 235 gave identical results. The only difference between these two transition sections was that one had the points removed where the seven holes converge.

Test conditions:

Temperature of inlet air:	Ambient
Static pressure at point 1 for all data points:	Approx. 100 psia

C. Dome Strength

Tests on small domes (3.45 in. diam) have continued with one GRB silicon carbide and two KT silicon carbide domes being tested. Test conditions are given in Table III-7.

Figure III-66 is a sketch of the apparatus and modifications used for the series of tests. The initial design was used in Tests 1 and 2. No damage to the dome was observed after Test 1 other than some edge chipping caused by the test fixture disassembly.

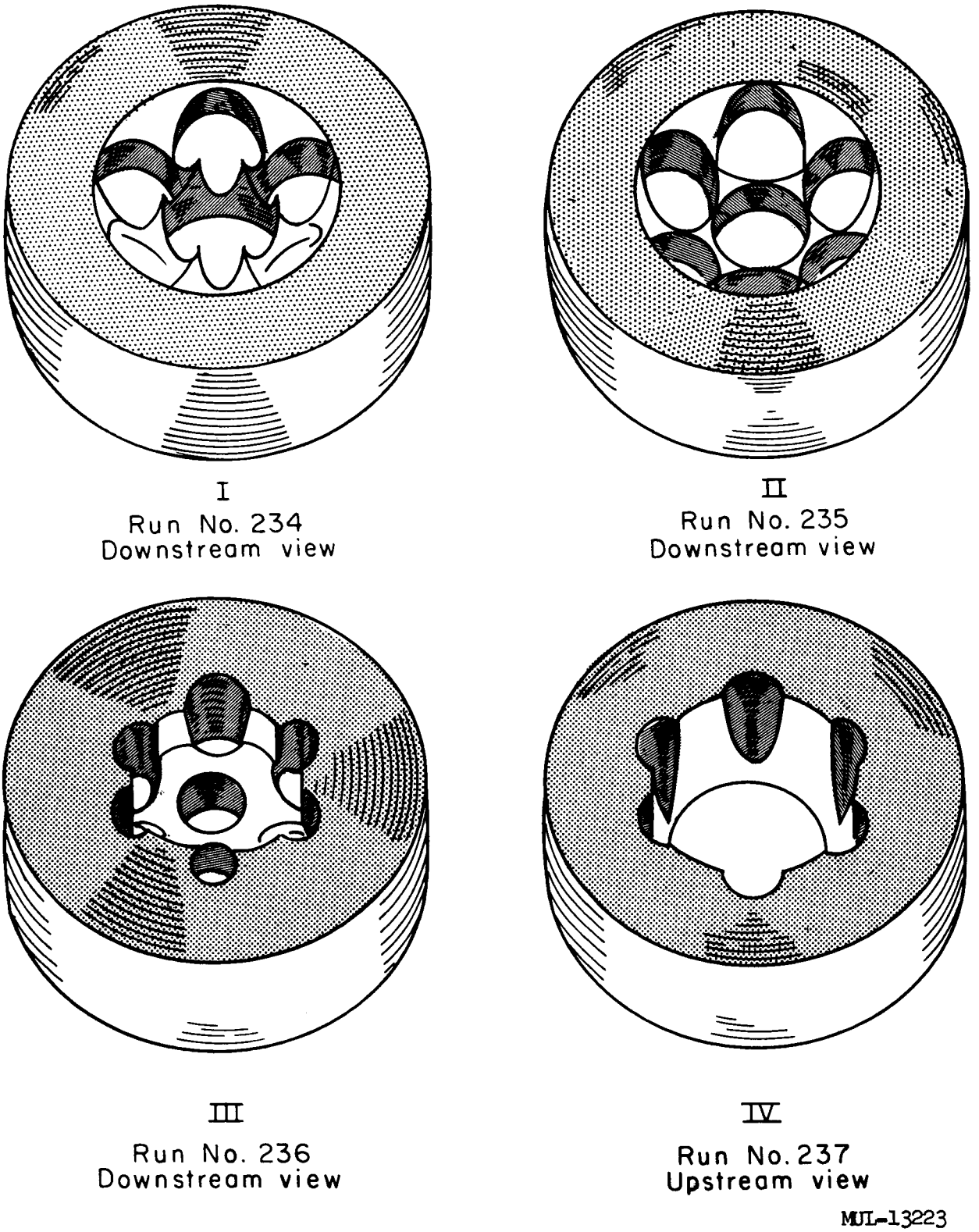

Fig. III-59. Transition geometries.

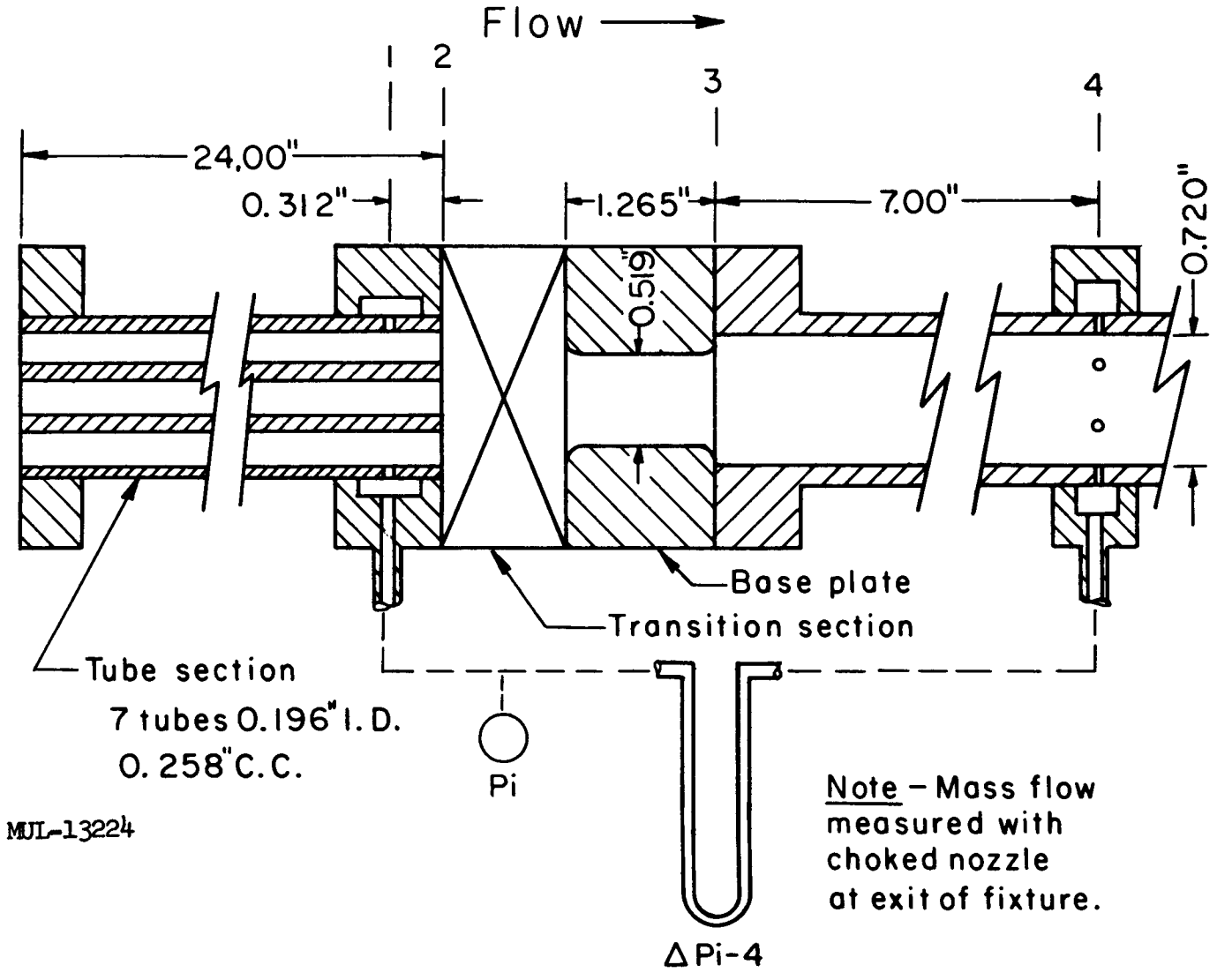

Fig. III-60. Test fixture for transition losses.

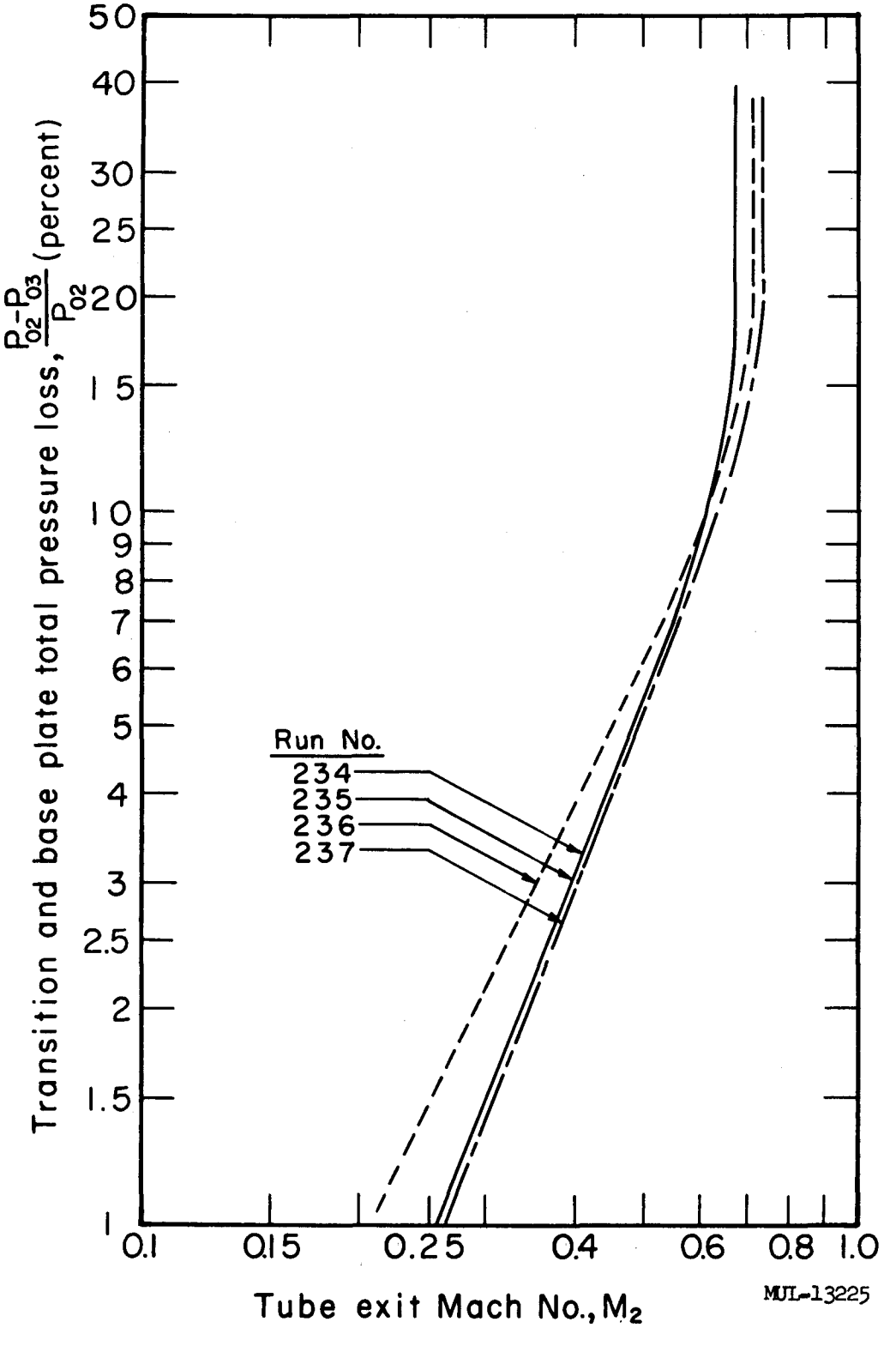

Fig. III-61. Transition test results, all four runs.

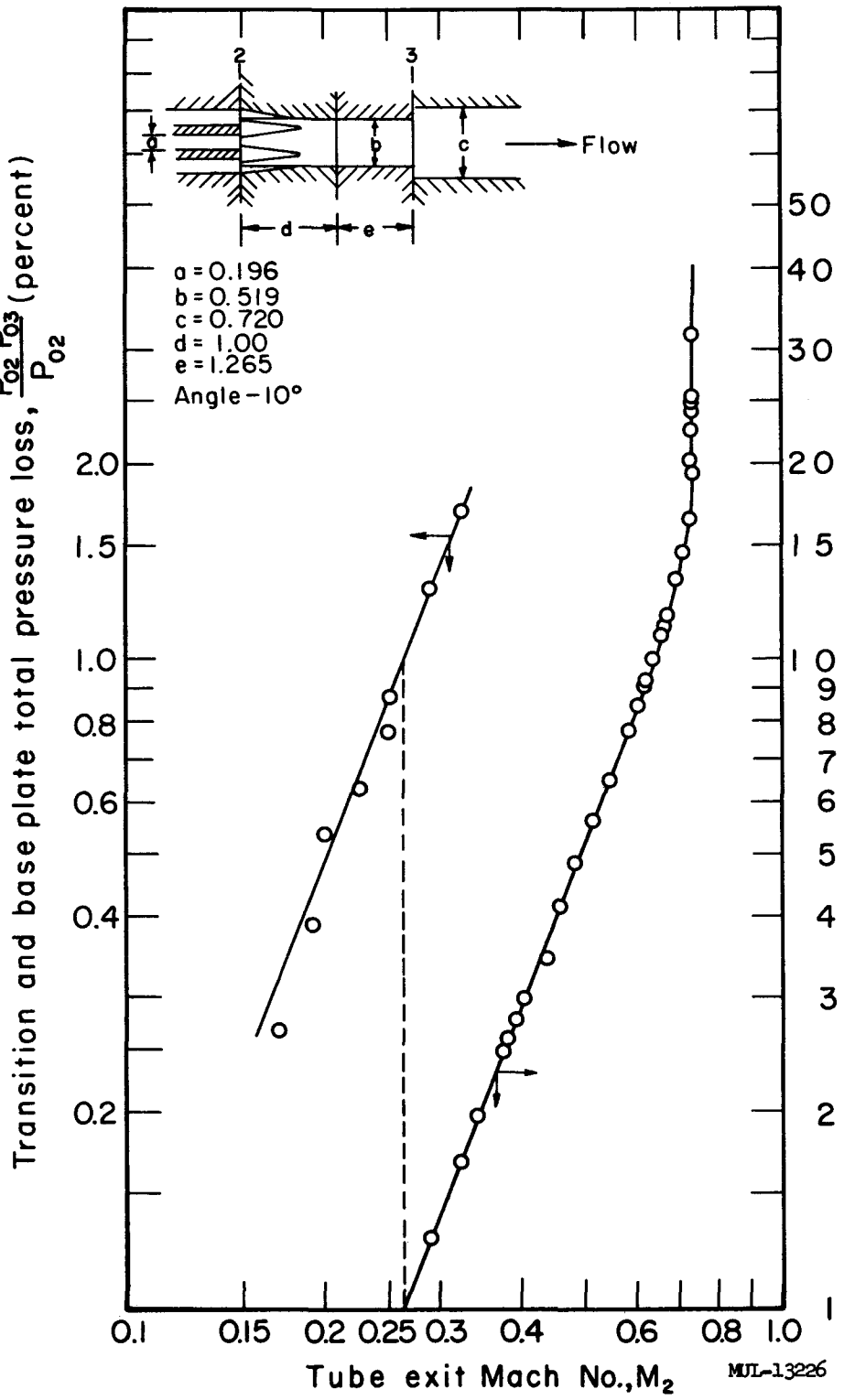

Fig. III-62. Run No. 237.

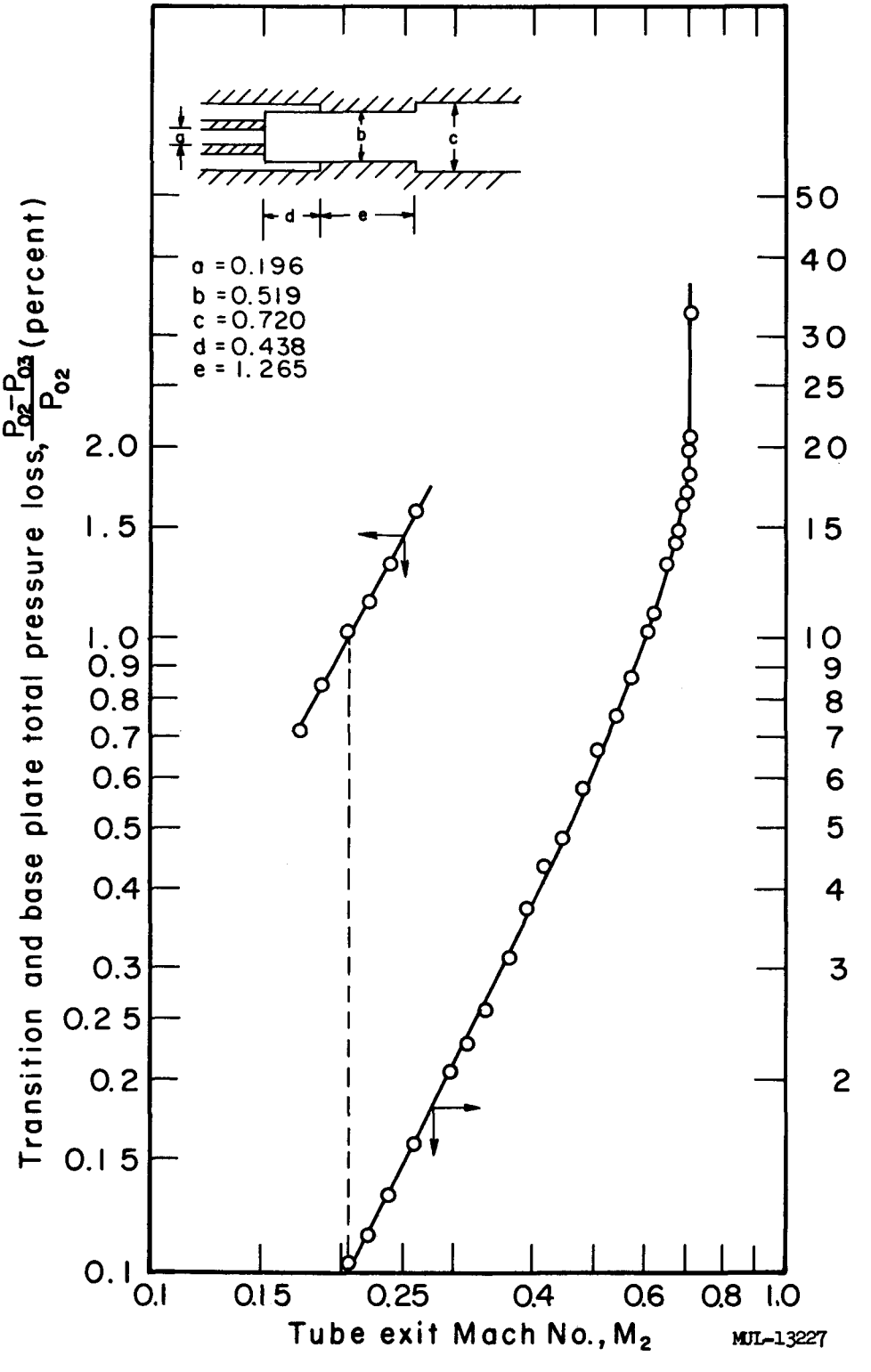

Fig. III-63. Run No. 236.

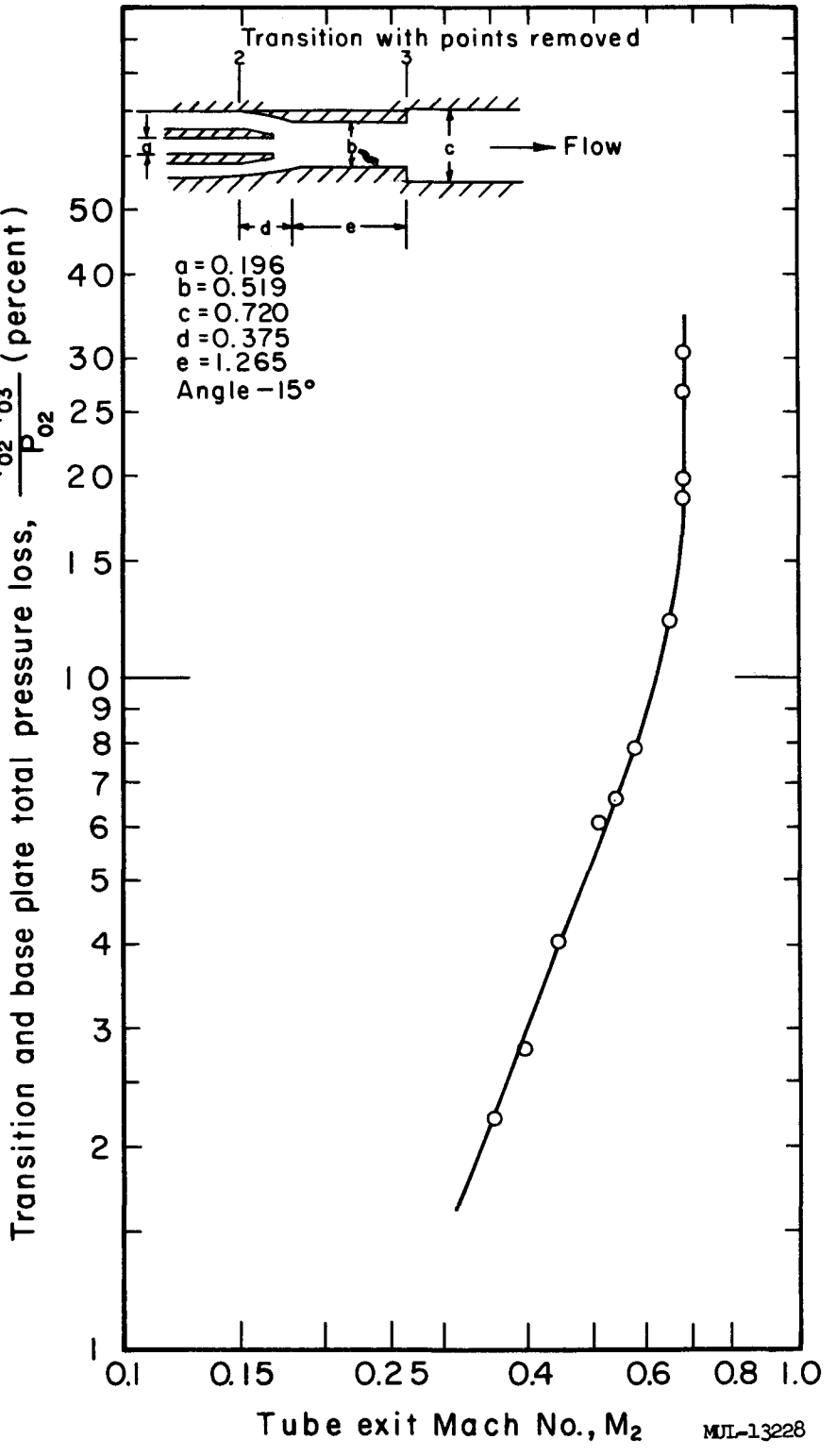

Fig. III-64. Run No. 235.

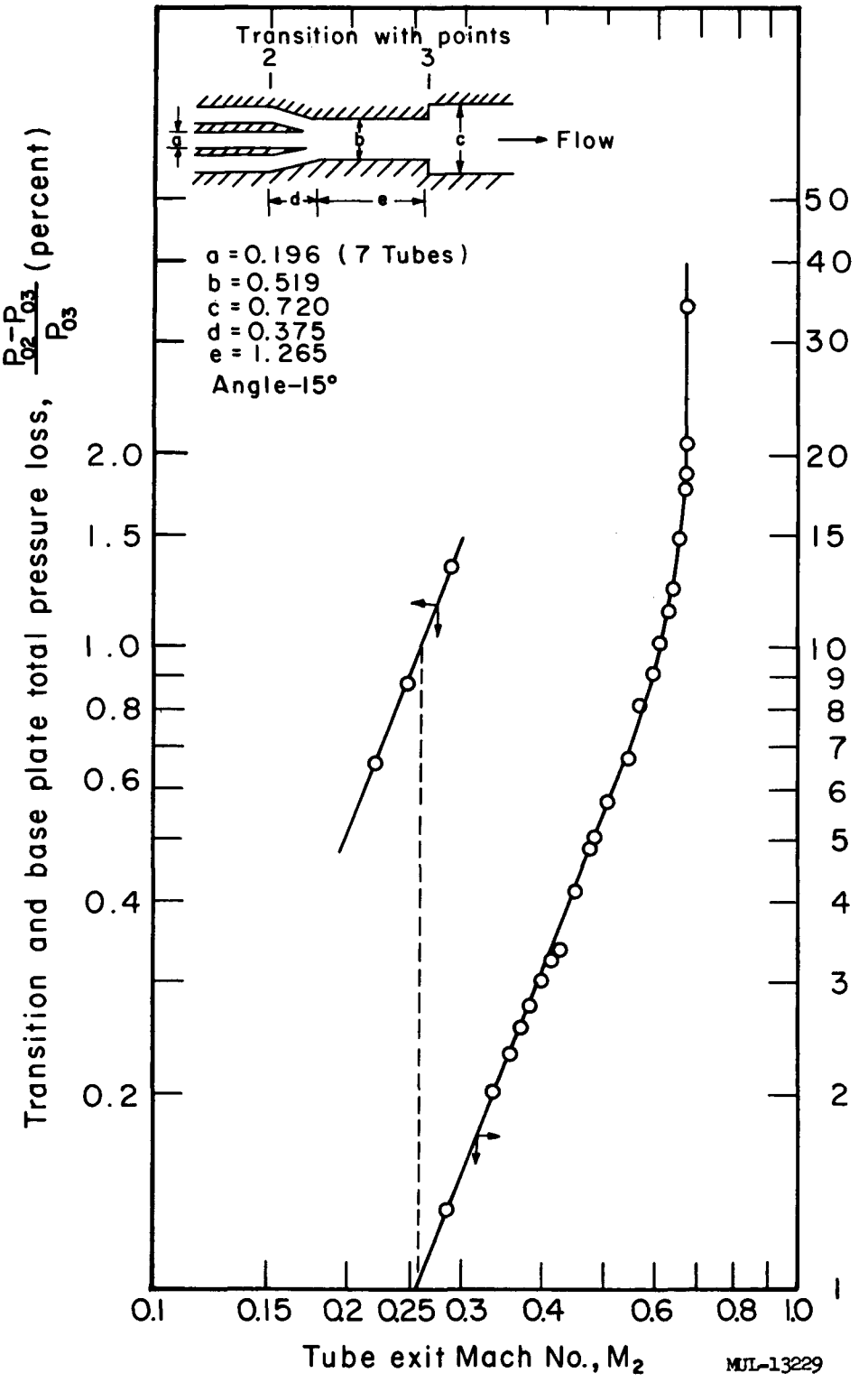

Fig. III-65. Run No. 234.

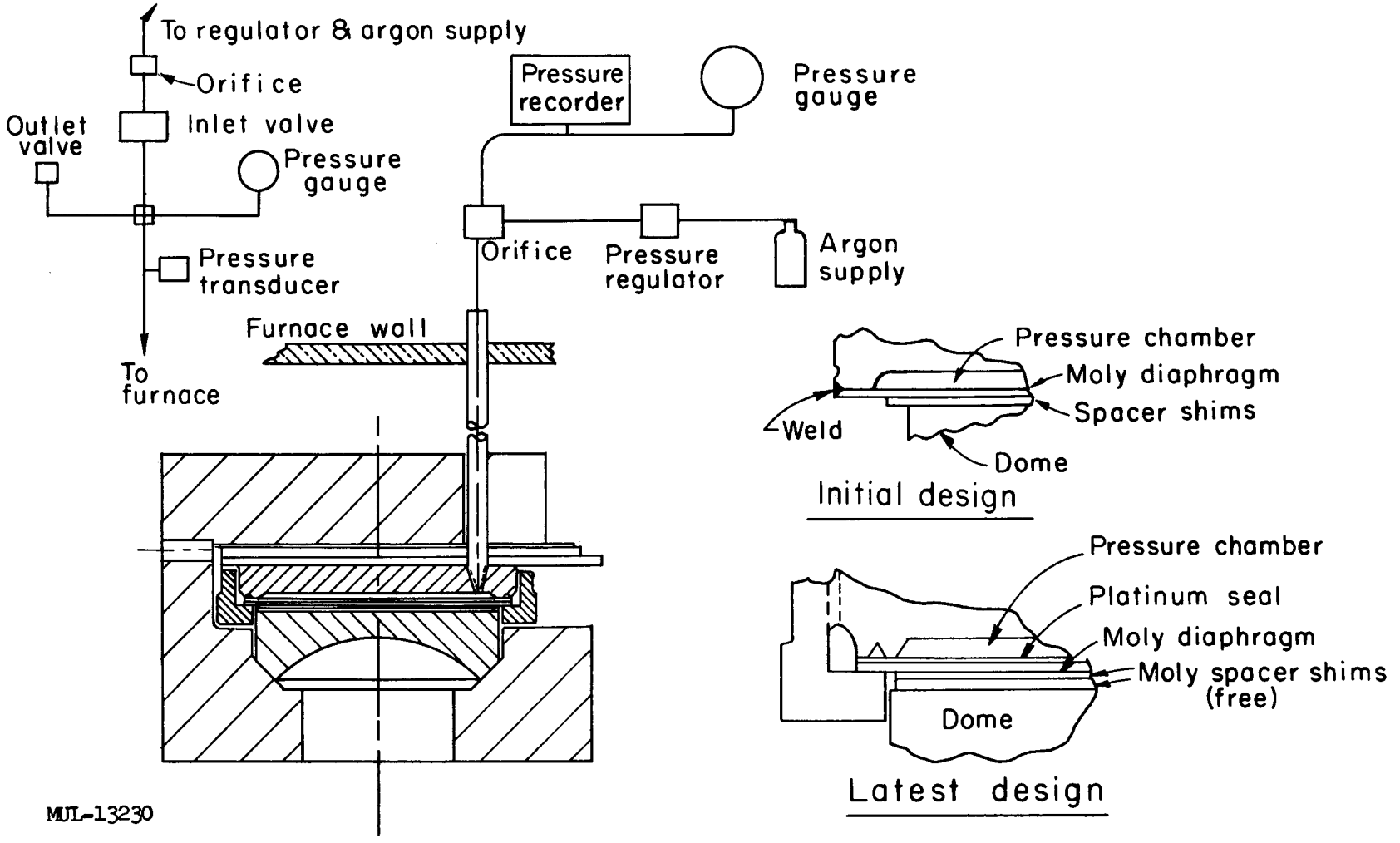

Fig. III-66. Diagram of apparatus used in dome strength tests.

Three tests were performed on two KT silicon carbide domes. The latest test fixture design was used in Tests 3 and 4.

Table III-7.

Test	Dome	Temp* (°F)	Pressure* (psi)	Time*	No. of pressure cycles at temp	Remarks
1	GRB SiC	2200	1000	2 hr-31 min	2	Pressure raised to 1120 psi, diaphragm ruptured
2	KT SiC (#1)	2350	1000	2 hr-19 min	2	
3	KT SiC (#1)	2400	1000	24 hr-26 min	3	
4	KT SiC (#2)	2400	0-1000, 30-sec cycle, see Fig. III-73	10 hr-43 min	1200+	

*Typical requirements: 2300°F, 3-10 hr, 150 psi.

At the conclusion of Test 2, the dome showed some cracking as shown in Figs. III-67 and III-68, but complete structural integrity was maintained. After Test 3 more extensive cracking was noted but the dome was still intact as shown in Figs. III-69, III-70, and III-71. It broke into three large and several small pieces two days later as shown in Fig. III-72.

In Test 4, pressure was cycled as shown in Fig. III-73. This cycle was repeated for 10 hr and 43 min, but after 3 hr a leak in the pressure supply pipe inside the furnace developed and caused the maximum pressure to slowly decrease to 420 psi at the conclusion of the test. Over 1200 complete pressure cycles were applied, the peak pressure dropping slowly as shown in Fig. III-74. The dome again maintained complete structural integrity while under load: Fig. III-75 shows the dome after removal from the test fixture. Ten days afterward it broke into four large pieces, as shown in Fig. III-76 (reproduced from Zyglo photographs).

During test-fixture disassembly after Test 2, considerable difficulty was encountered in removing the dome, which was firmly attached to the seat after the test. The pattern of circumferential cracks indicates that the dome was

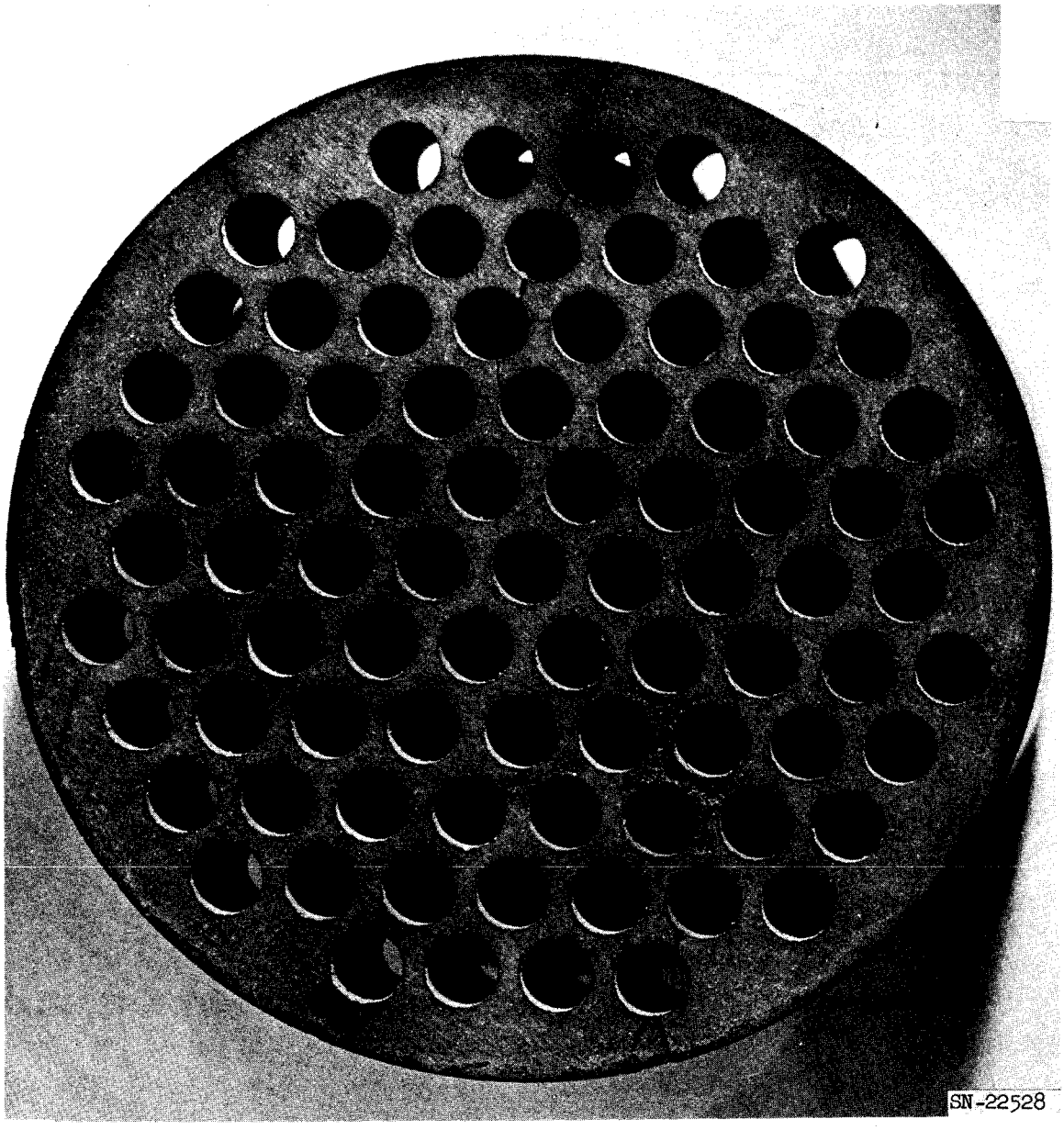

Fig. III-67. Dome after Test 2. Top.

Fig. III-68. Dome after Test 2. Side.

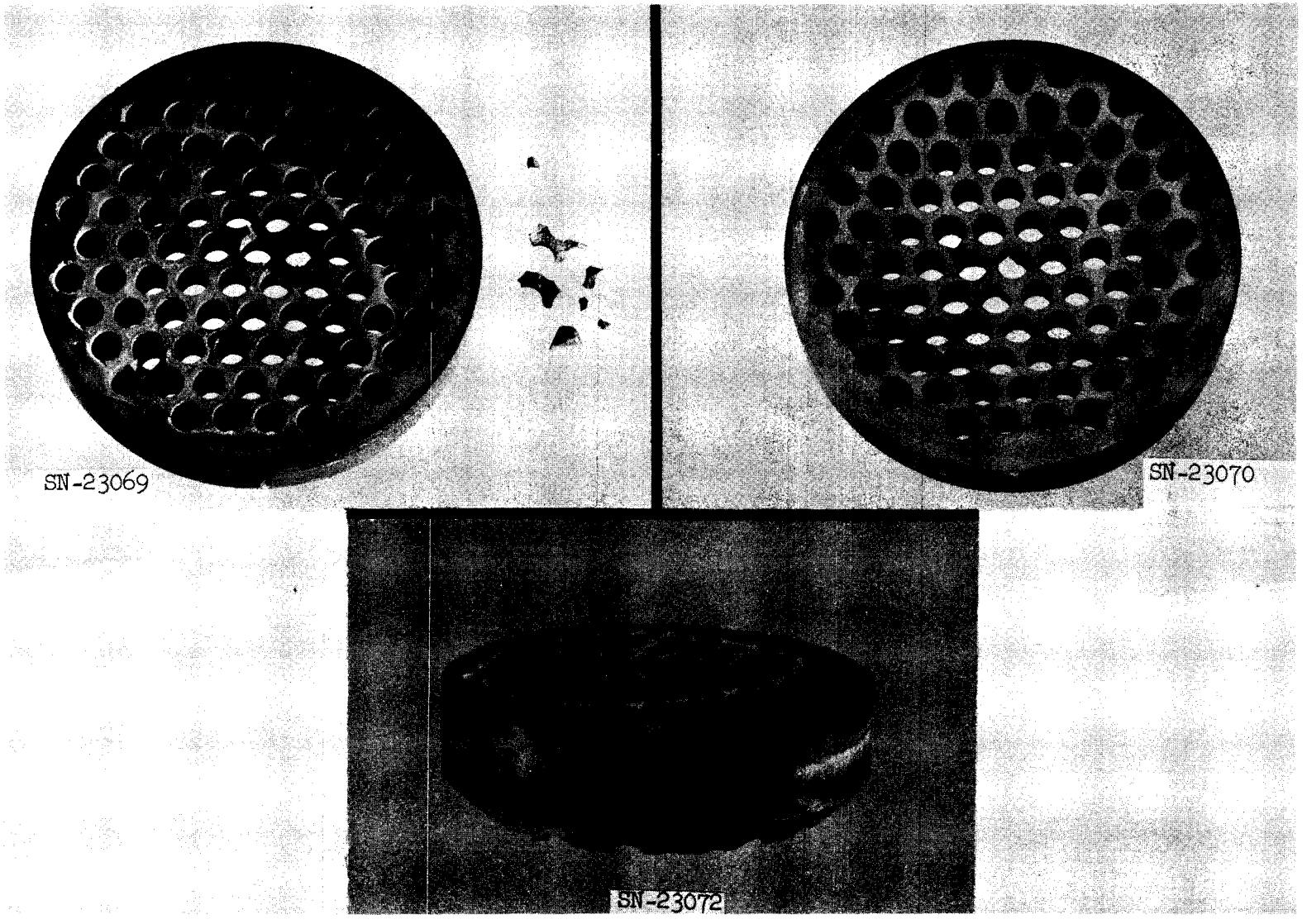

Figs. III-69, III-70, and III-71. Test 3 dome, immediately after removal from test fixture.

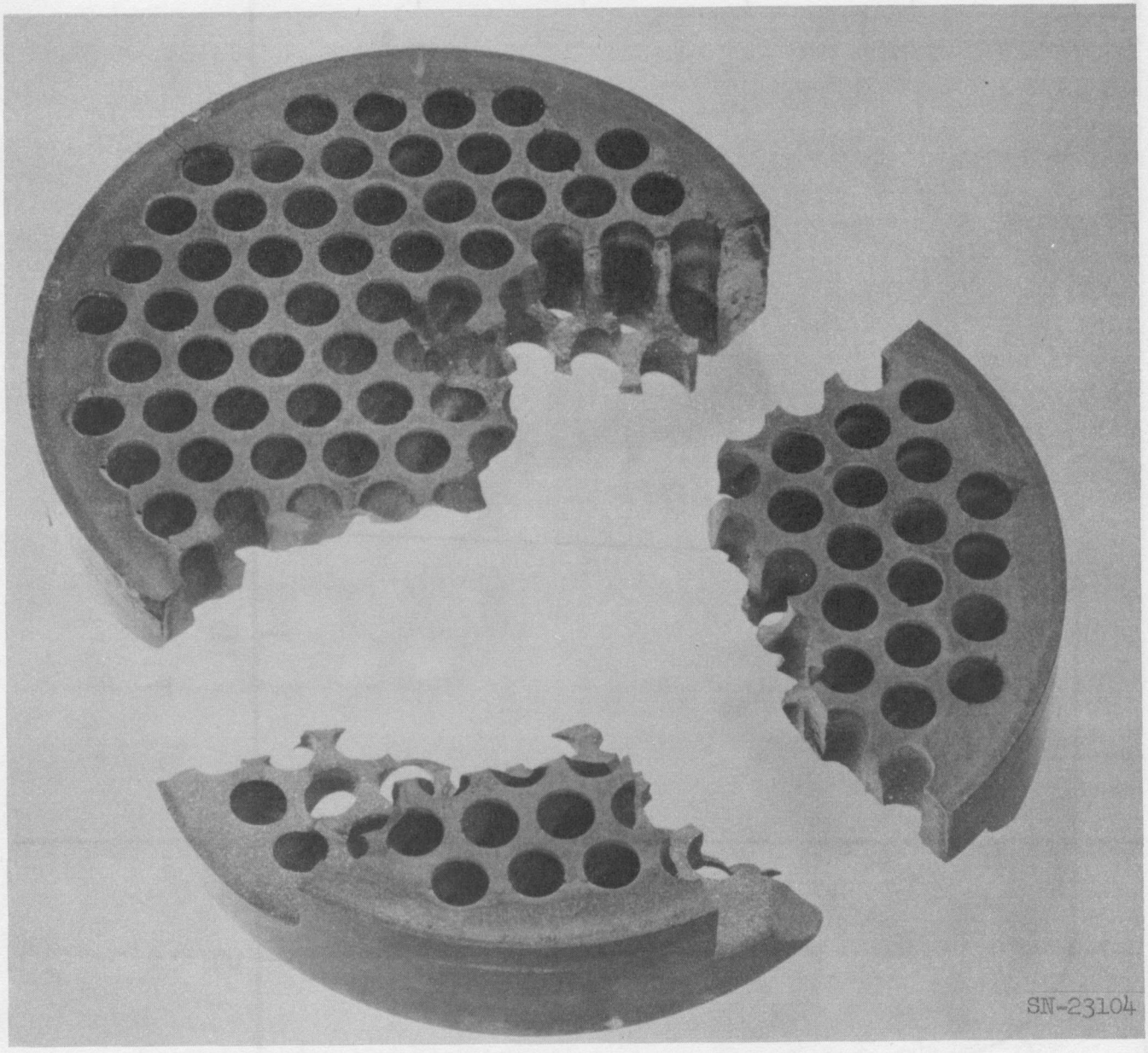

Fig. III-72. Test 3 dome two days after test.

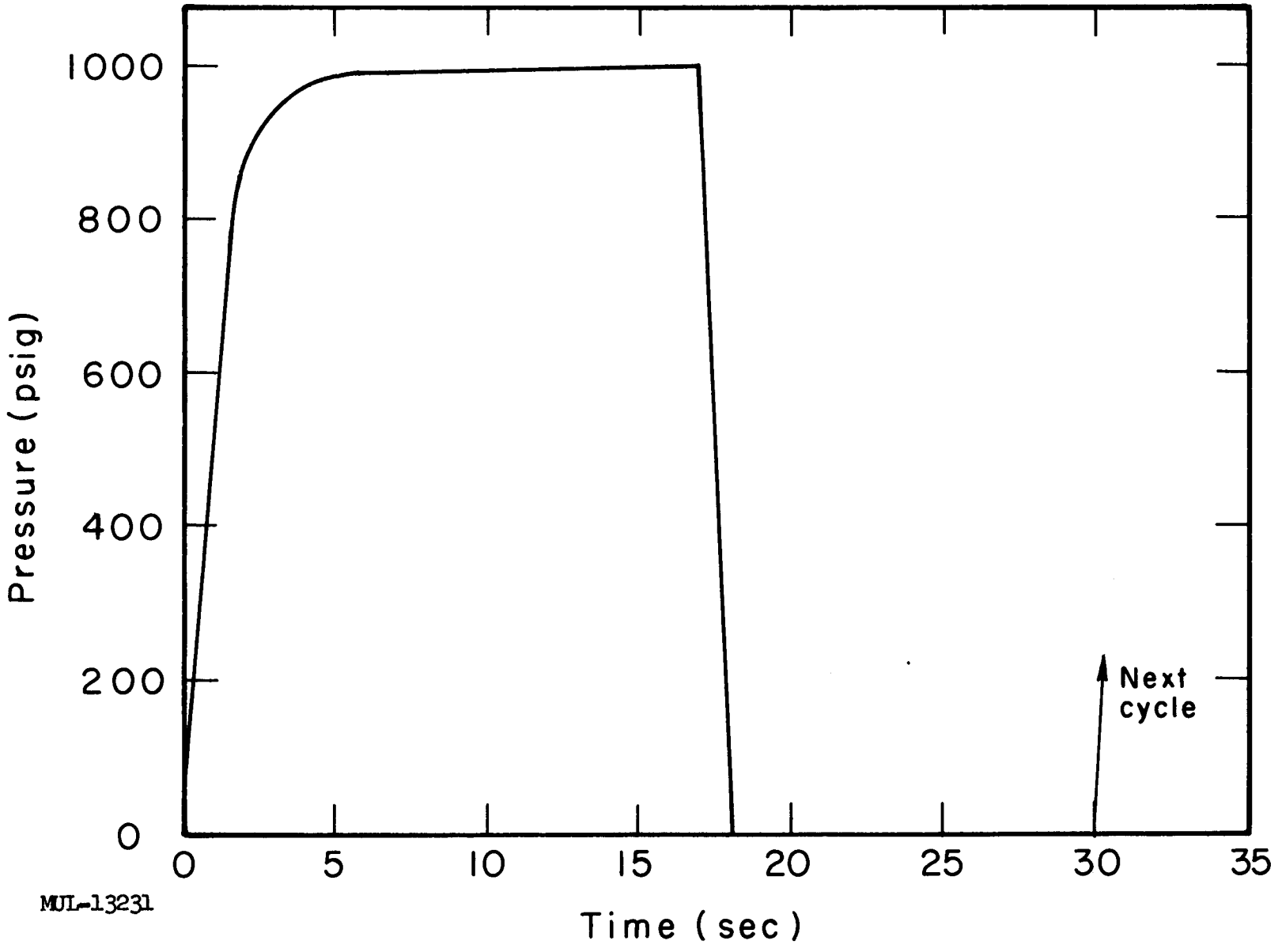

Fig. III-73. Dome Test 4.

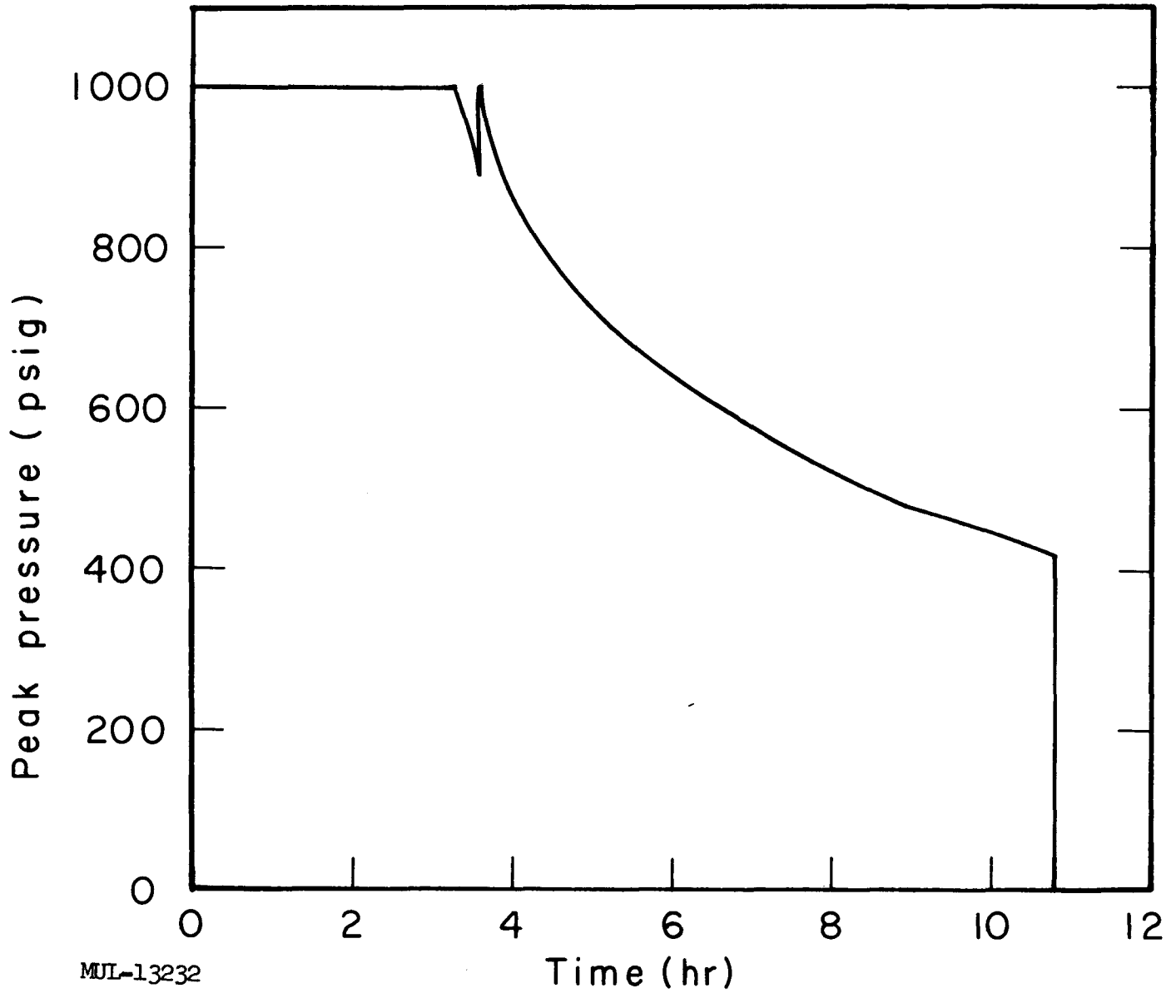

Fig. III-74. Dome Test 4.

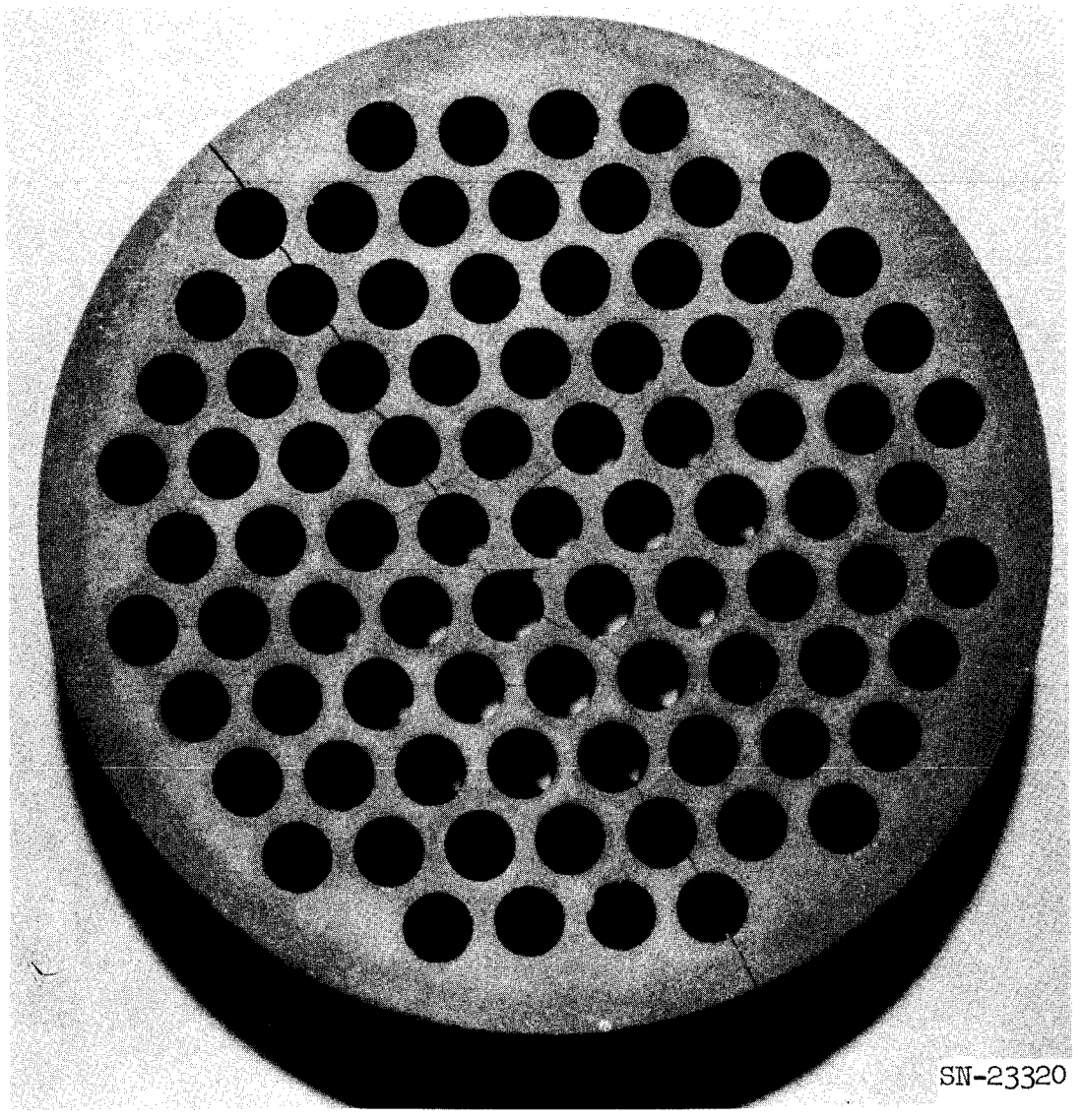

Fig. III-75. Test 4 dome after test.

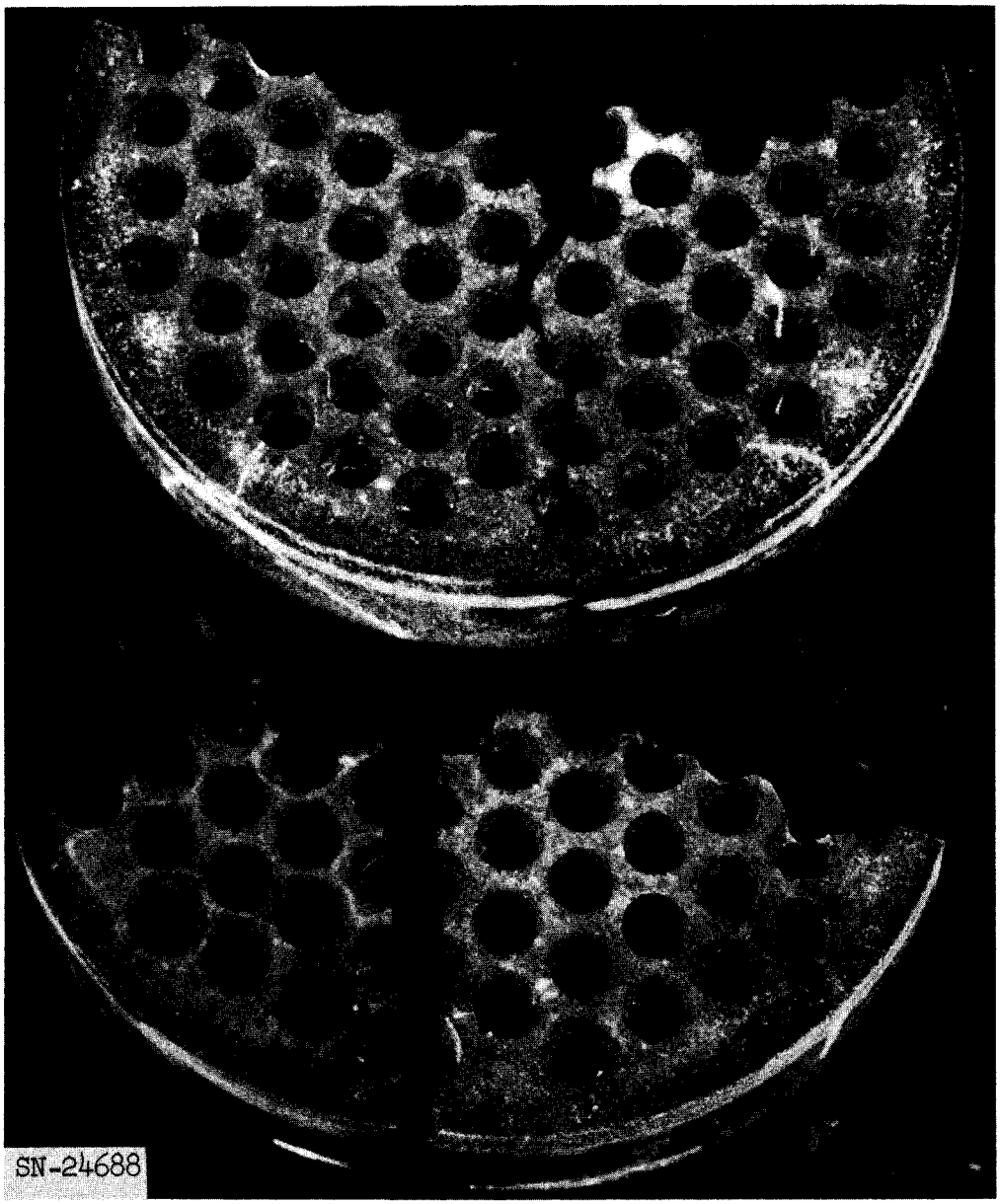

Fig. III-76. Test 4 dome 10 days after test.

rigidly retained in the fixture and heavy loads were imposed during cooldown by the different thermal expansion coefficients of molybdenum and silicon carbide. This difficulty was encountered to a lesser degree after Test 3, but another temperature cycle to 2400°F with no load on the dome caused it to fall free. A coating of milk of magnesia (to form MgO) was used on the dome seat for Test 4 and no difficulty was encountered. The difference in crack patterns (no circumferential cracks in Test 4 dome) indicates that the hypothesis regarding fixture retention was true and the failure pattern of Test 4 is more representative of a full-scale dome.

Stresses in the dome were calculated by several methods and result in a maximum compressive stress of about 14,000 psi for the 1000 psi applied over the top face. No wholly adequate theory has been derived but attempts are being made to correlate photoelastic studies, test results, and various theories.

Test 4 was considered the most severe as the pressure is about seven times the design load and the complete unloading could allow slippage between broken parts to take place. No slippage was evident and complete structural integrity and load-carrying ability was maintained.

D. Fabrication Development of SiC Dome Shapes

Fabrication development work is continuing on large perforated shapes of KT silicon carbide, suitable for use in reactor base domes. In general green machining has been done at LRL. Briefly, the material process is as follows:

1. Mechanically mix granular silicon carbide, powdered graphite, and a plastic binder.
2. Cold press the mix and cure the plastic binder. The plastic binder gives strength in the unfired state and allows handling and machining.
3. Machine the piece in the "green" or unfired state.
4. Fire the piece in a predominantly inert atmosphere in a graphite induction-heated furnace in the following stages.
    a. Burn the plastic binder away leaving carbonaceous residue.
    b. At a temperature of about 2100°C and in the presence of some silicon vapor, convert the carbon to silicon carbide.

The body thus produced consists of 90% (min) SiC with the remainder being largely free silicon. The shrinkage from the green state is less than 1%. Density is about 3.1 g/cm^3.

The first major obstacle encountered in the process was obtaining sound unfired bodies. The plastic initially used was a phenolic which required oven curing. Upon removal from the mold, cold-pressed cylinders, 18 in. diam by 16 in. long, would expand about 3/4 in. Mold-wall friction produced a nonuniform springback, resulting in large cracks in the interior of the cylinder. The plastic binder has been changed to an epoxy resin which largely cures at room temperature. This allows maintaining pressure on the green slug until it has gained strength. There is a consequent reduction of springback to about 1/16 in. The combination of this change and that of maintaining a partial vacuum in the pressing mold has solved the problem of producing sound unfired bodies. A mold is being made for pressing 29-in.-diam cylinders with about the same thickness.

Machining of the unfired material is possible with various cutting materials, but wear of the cutter has been generally excessive in all cutting materials tried except in diamond tools. Figure III-77 shows a green body during machining of the spherical contour, with a diamond wheel on the center segment of a 7-piece, 3-ft-diam dome. Figure III-78 shows the core drill (tip diameter is 9/16 in.). Figure III-79 shows the drill-press operation.

Firing studies were continued by a subcontractor. Some cracking has occurred in firing. The pieces have until recently been fired in the bottom of the furnace. Post-firing observations suggested that despite the absence of a logical explanation of its presence, a layer of silicon vapor accumulates in the bottom of the furnace to a depth which is less than the thickness of the piece. The resulting difference in siliconization rate through the piece may cause cracking. Recent firing of the piece where it is held at a level above this apparent layer has substantially reduced the cracking problem.

The fired material can be machined, though somewhat slowly, using diamond tools.

Figure III-80 shows two fired pieces having geometry similar to the center segment of a 7-piece, 3-ft dome. These were fired prior to the conclusion that firing should be done away from the bottom of the furnace. The slots are saw cuts which were made in the green state in an effort to eliminate cracking during firing.

Pieces of a 7-piece, 3-ft-diam dome are presently being processed. It is intended to conduct both cold and hot static and dynamic tests on the complete test dome.

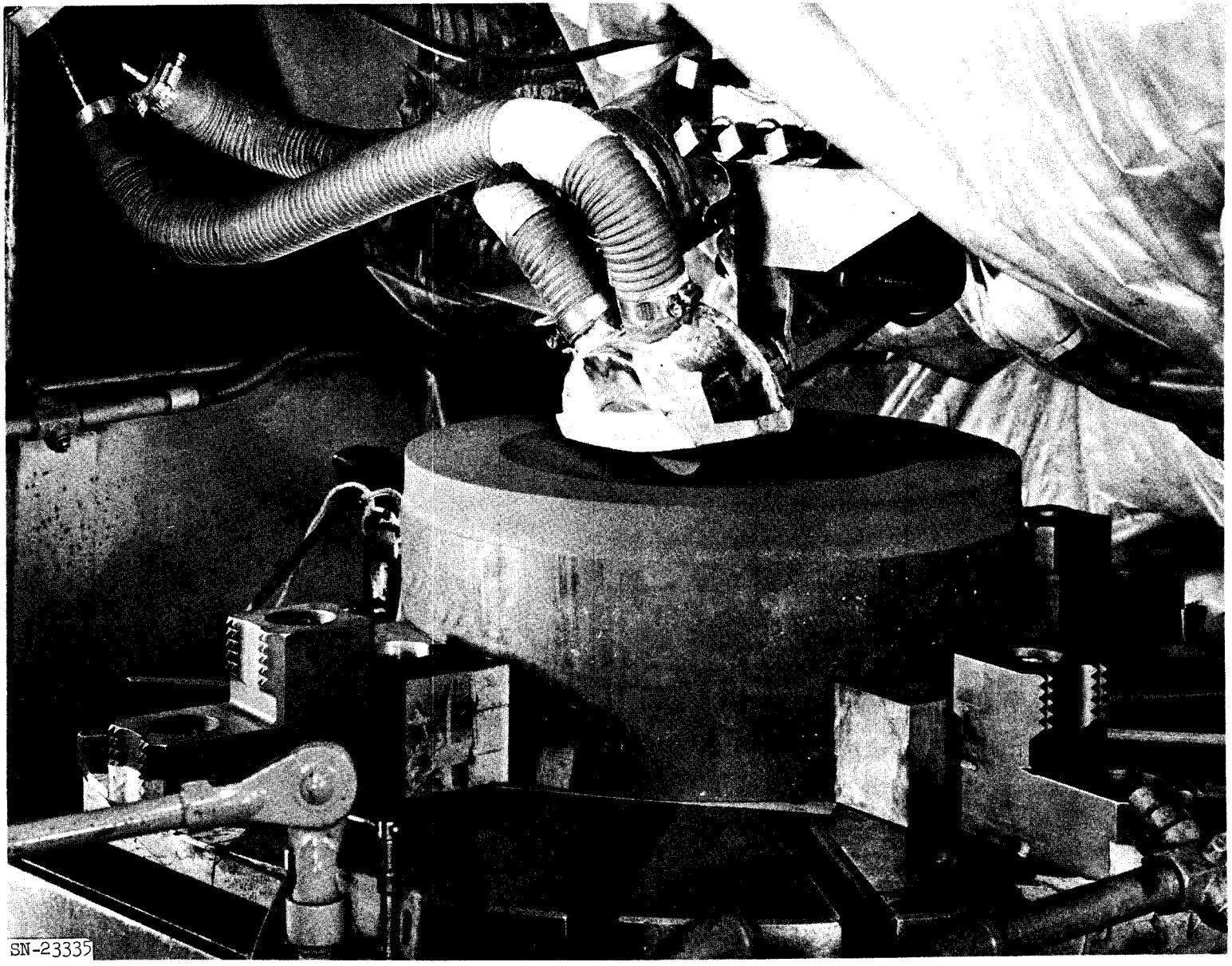

Fig. III-77. Machining of center segment of dome.

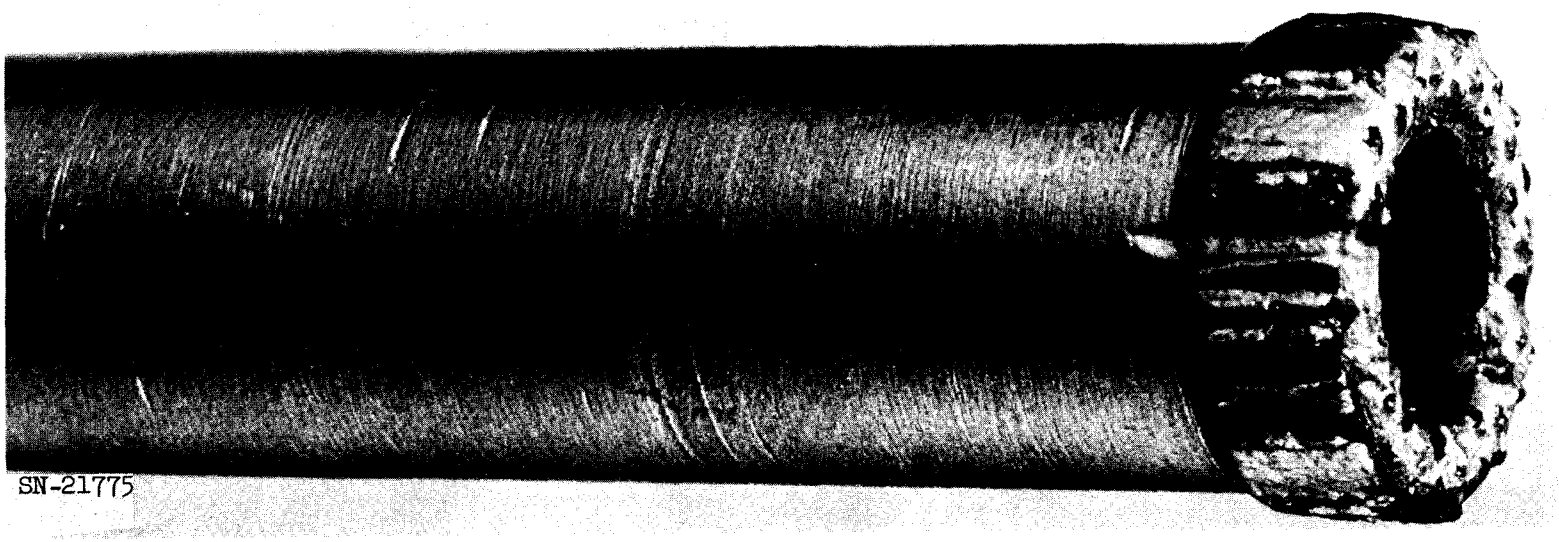

Fig. III-78. Diamond core drill.

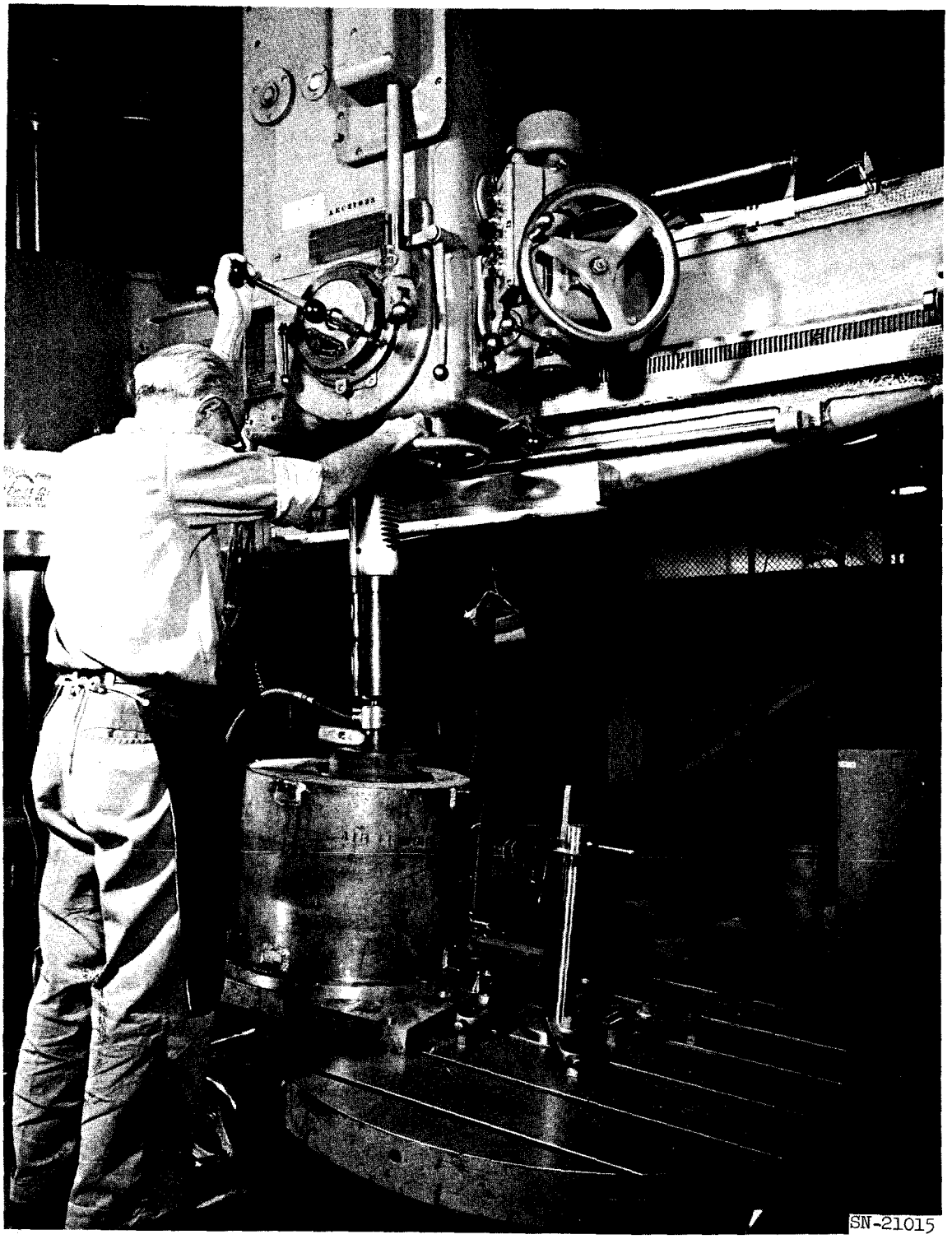

Fig. III-79. Drill-press operation on dome.

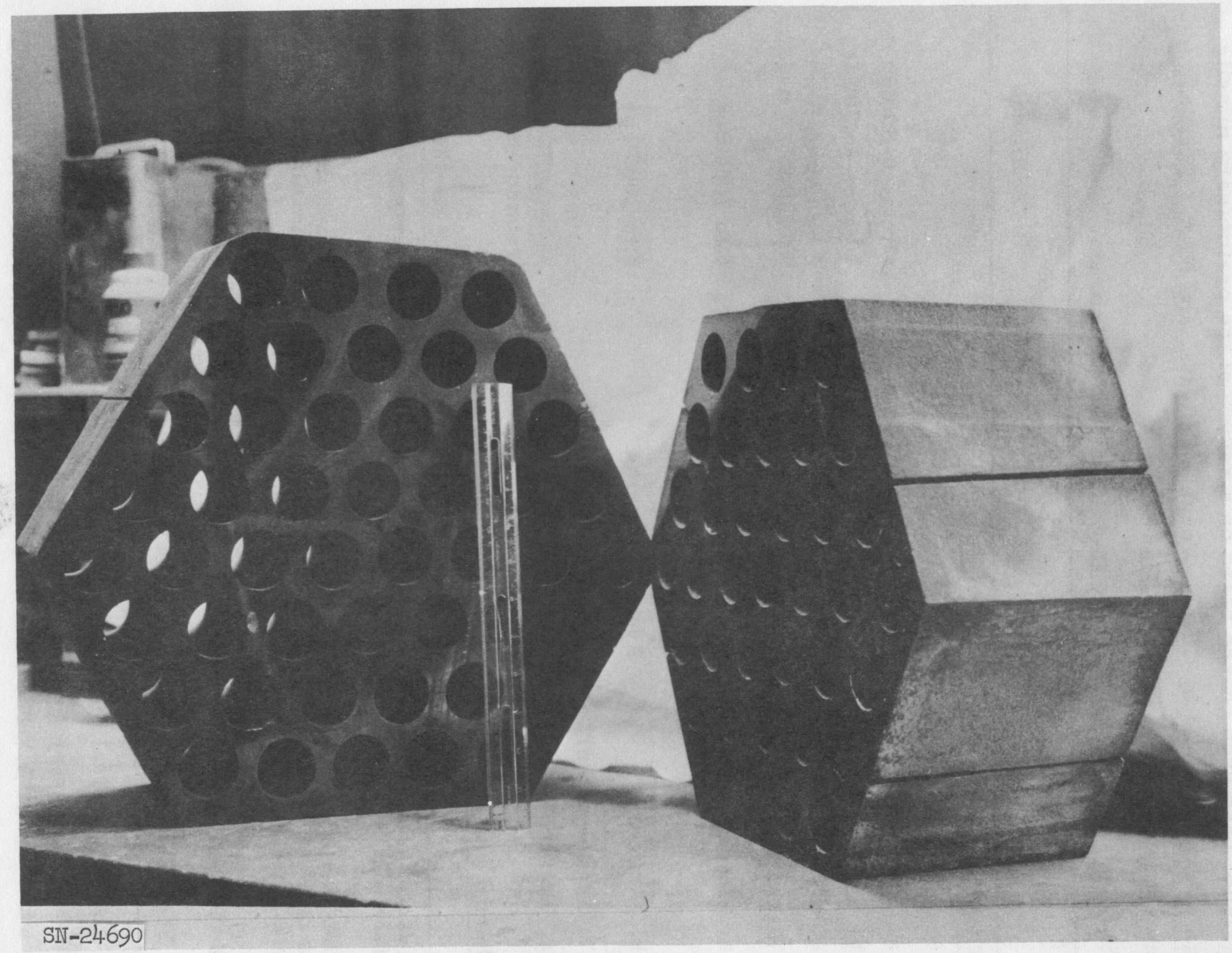

Fig. III-80. Two fired dome pieces.

IV. ANALYSIS OF TORY II-C LOAD DESIGN CRITERIA

The current ground and flight loads to which the Tory II-C reactor is to be designed have been chosen based on a review of the preliminary missile design work performed by Chance-Vought, Convair, and NAA. This load environment is presented in Table III-8 below:

Table III-8. Tory II-C Load Design Criteria.*

	N_x	N_y	N_z	$\left(N_x^2 + N_y^2\right)^{1/2}$	Conditions
A. Flight Loads					
1. Steady state†					
a. Launch	+3.0				1 min, 0-30,000 ft
b. Deceleration	-2.0				10 sec, 30,000 ft
c. Cruise		±5.0	±5.0	±5.0	2 hr, Mach 3 < 1000 ft
2. Vibration environment					
a. Launch-boost	Avg. 3 g rms in all directions (180 db)				5 to 2000 cps
b. Cruise (boundary-layer noise)	Avg. 2.25 g rms in all directions (164 db)				5 to 2000 cps
c. Bomb ejection			±0.5 total		At missile bending frequencies
B. Ground Loads†	±1.5	±2.25	±3.0	±3.0	-65 to 140°F

*A factor of safety has not been included in the numbers listed. The factor of safety will be applied to the material properties in design.

†The load factors listed are maximums. They do not act continuously, but fluctuate in an unknown manner. The times listed are the maximum time periods in which the loads can act and will be used for design.

V. MATERIALS

A. Thermal Expansivity of $BeO-UO_2$

The longitudinal thermal expansion of $BeO-UO_2$ fuel elements fabricated at LRL has been remeasured. Three fuel concentrations were studied: 5.17, 3.53, and 7.49 wt %. The instantaneous coefficient was found to be constant above 1000°F and equal to 5.00, 5.25, and 5.05×10^{-6} per °F, respectively, for the three concentrations.

The test fuel element (see Fig. III-81) was placed in an air atmosphere furnace. Measurements were taken with a precision cathetometer. The height of the top of the lever arm and the top of the quartz tube were measured. Allowance for the thermal expansion of fused quartz was made. In addition, checks were made using direct reading, rather than the lever-arm method.

The results are plotted in Figs. III-82, III-83, and III-84. The instantaneous thermal expansion coefficient is derived from the slope of the absolute expansion curve and is therefore approximate.

The observed expansion is lower than that generally found in the literature for pure BeO. However, it is consistent with other measurements at LRL on longitudinal expansion of extruded BeO-UO_2 fuel elements.

B. Influence of Phase Instability on Mechanical Properties of LRL Fuel Elements

The urania phase instability in the BeO-UO_2 system has been discussed in the General Chemistry section in this and in the previous quarterly report. This phenomenon showed first in a single modulus of rupture test in 1959 but was unrecognized at the time. Identification of the behavior came from strain studies by a subcontractor and from thermal stress studies in the Chemistry Blowpipe at Livermore.

LRL is sponsoring tests to determine strain characteristics of LRL fuel elements in air. The apparatus utilizes four-point loading and measures deflection at the midpoint. During preliminary tests to determine the temperature at which to begin programmed strain tests, high strain rates were observed at relatively low temperatures. One tube was held at a load equivalent to approximately 1000 psi elastic stress on the outer fibers as it was brought to 1400°F during a 3-hr period. After 20 hr at 1400°F about 1% strain was observed. Using the same procedure as above, another tube was brought to 1800°F. After 20 minutes at 1800°F this tube showed about 1% strain. Cracks on the parts may be visually observed as fine black lines. The cracking pattern is most dense at the surface initially under maximum tension. Adjacent to the surface under maximum compression is a thin layer largely free from cracks.

This may indicate that as the test progressed different creep behavior in tension and compression caused the neutral axis to shift upward to the lower boundary of the relatively uncracked layer near the top surface (about 0.010 to 0.015 in. deep).

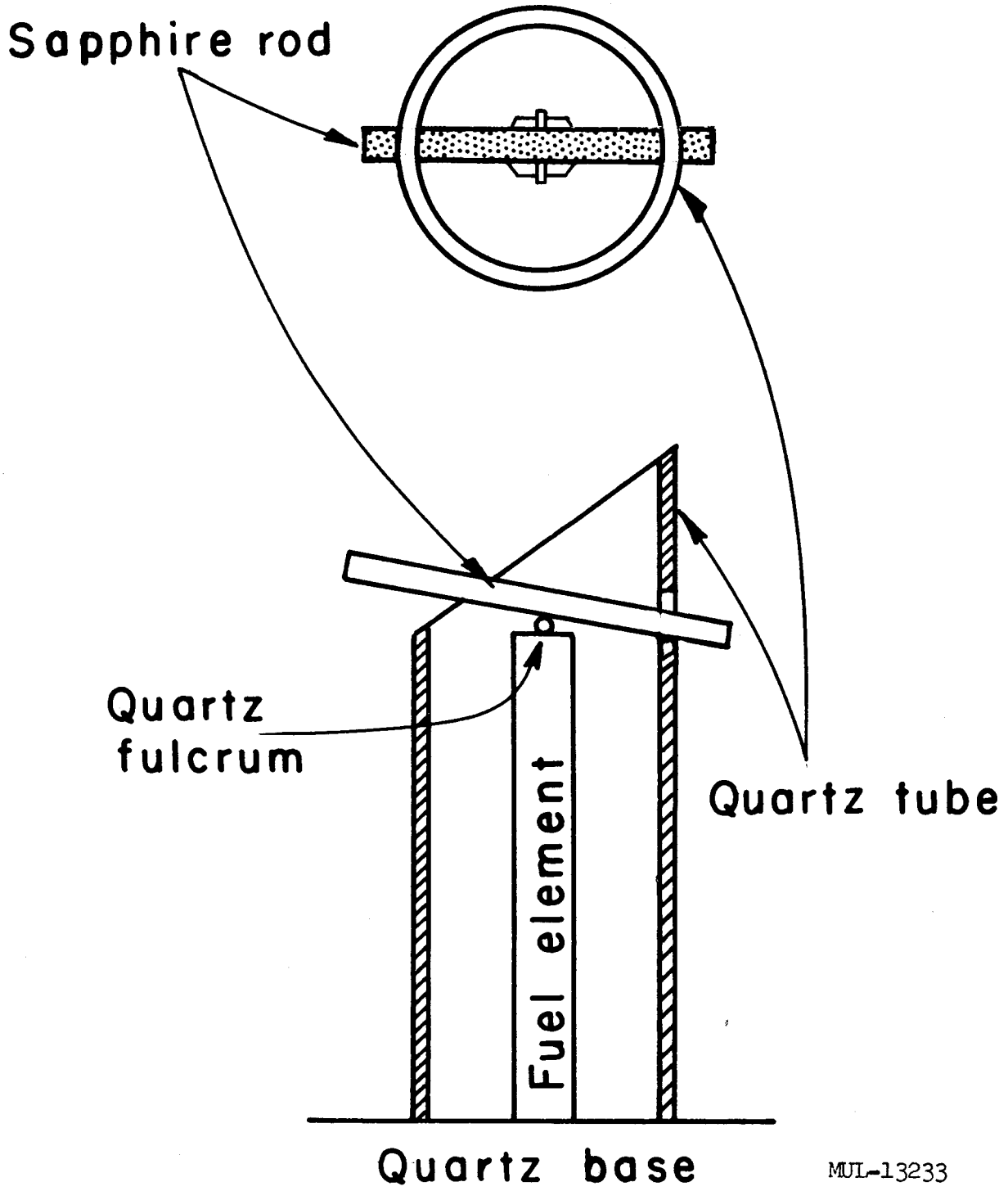

Fig. III-81. Thermal expansion test apparatus.

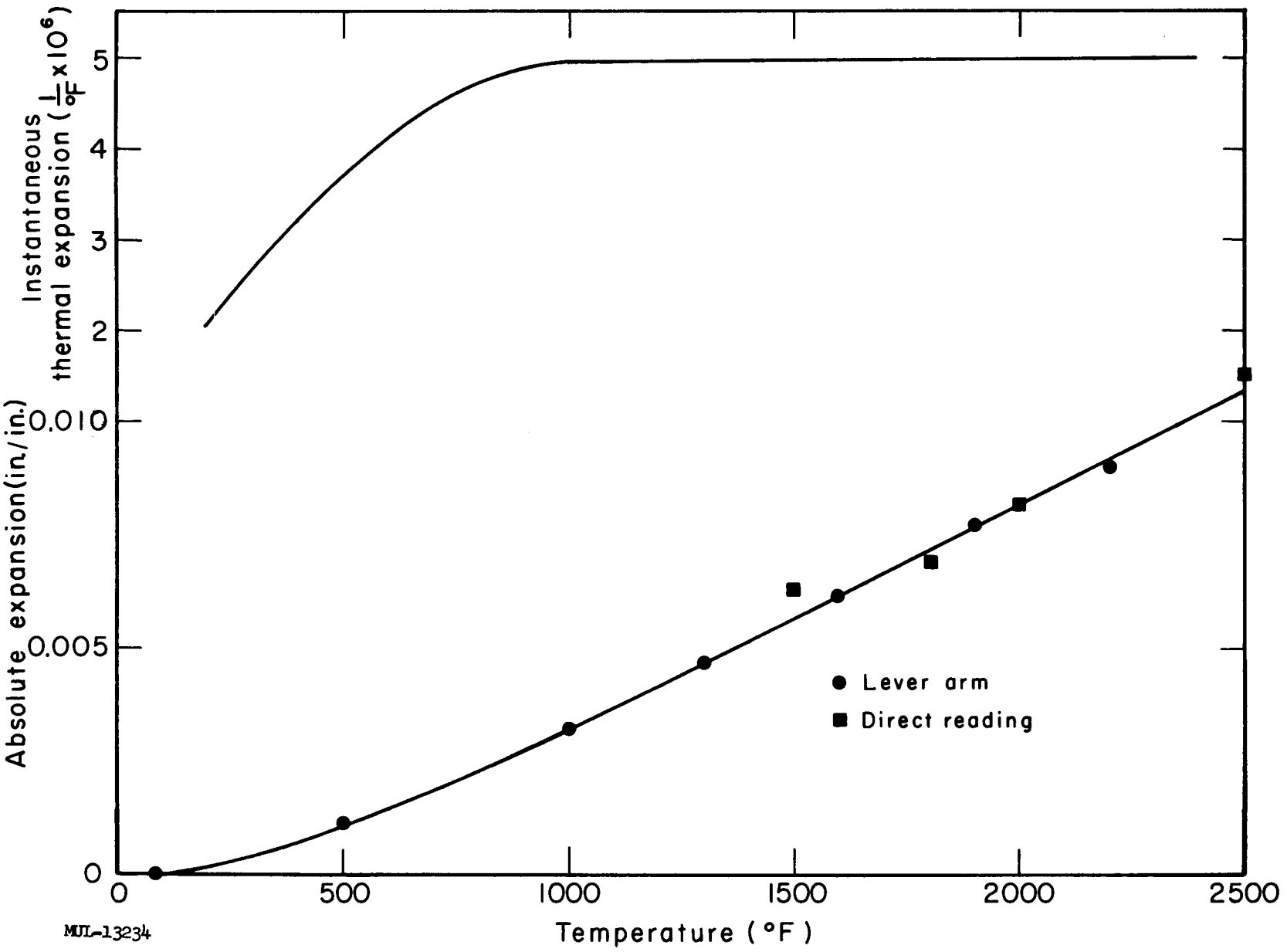

Fig. III-82. Longitudinal thermal expansion of BeO-5.17 w/o UO_2. Test in air at atmospheric pressure.

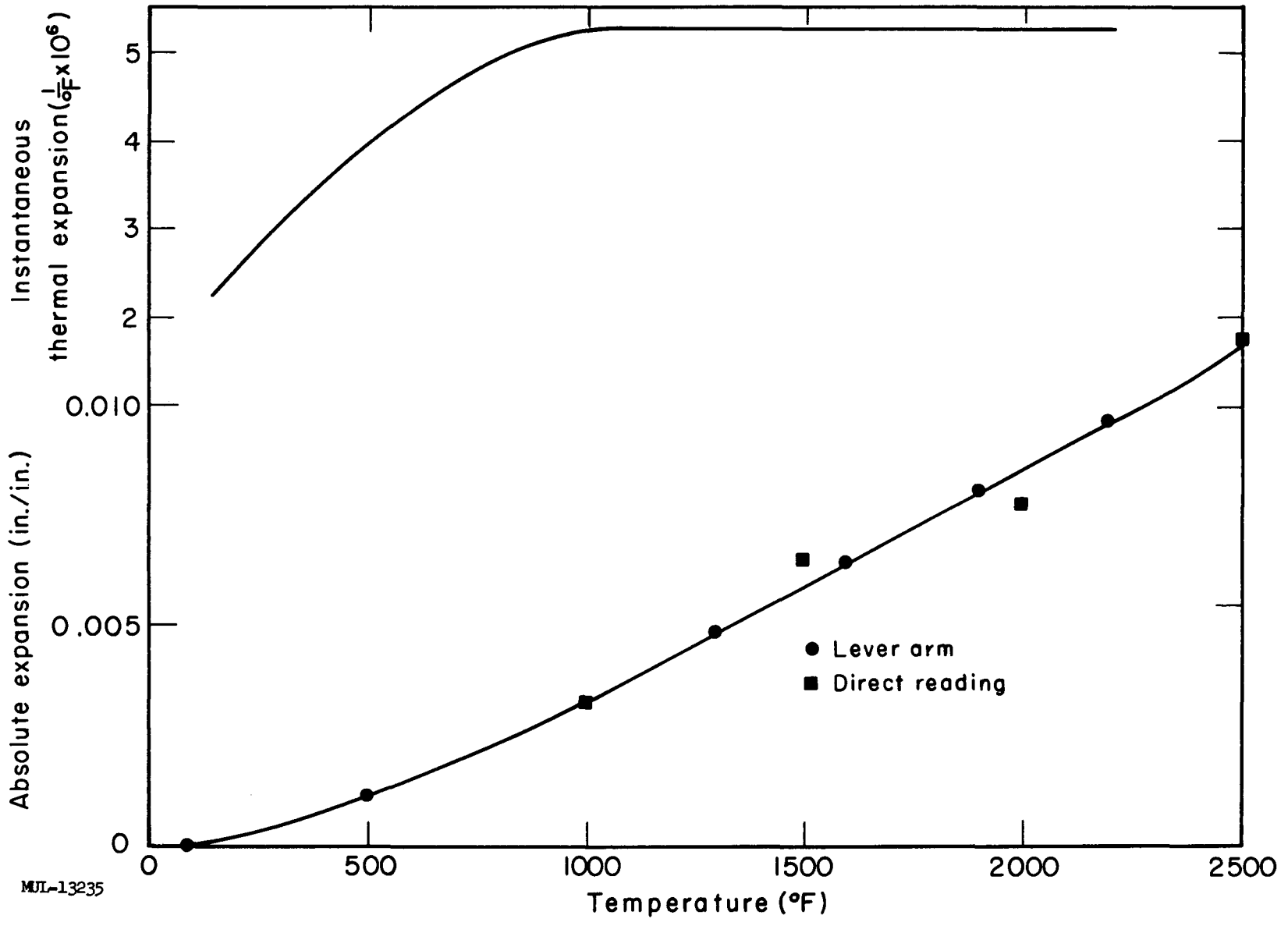

Fig. III-83. Longitudinal thermal expansion of BeO-3.53 w/o UO_2. Test in air at atmospheric pressure.

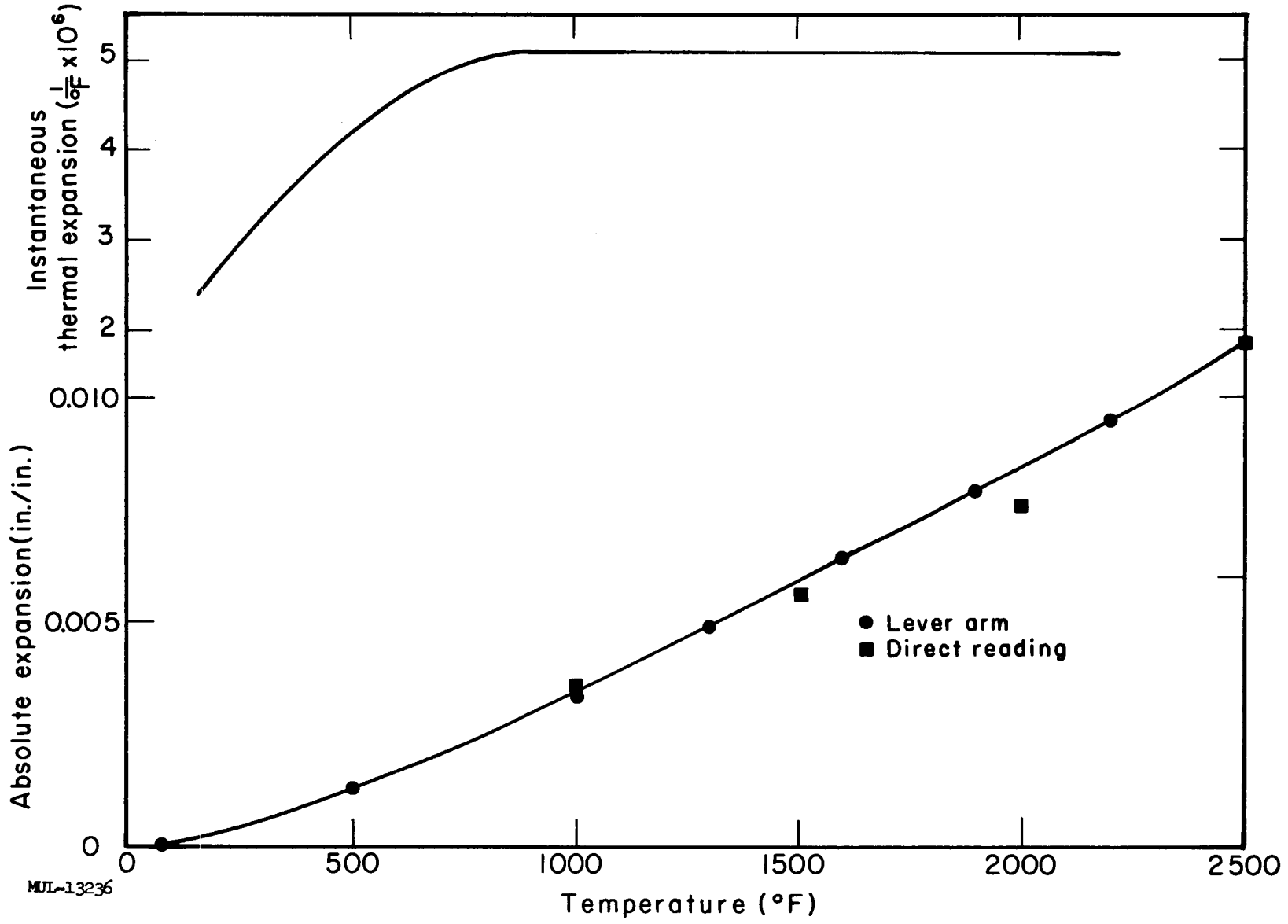

Fig. III-84. Longitudinal thermal expansion of BeO-7.49 w/o UO_2. Test in air at atmospheric pressure.

A further test has been run at 1800°F in a glo-bar air furnace at LRL where the deflection of an LRL tube under three-point loading could be measured with a cathetometer. The applied load was 1400 psi equivalent elastic stress on the outer fibers. The specimen was an LRL 10% UO_2 tube. It was brought to temperature in an argon atmosphere with only the weight of the loading rod applied. At temperature the full load was applied and held for 4 hours. No significant deflection was noted. At this point the atmosphere was changed from argon to air. After 30 minutes of air atmosphere, 0.013 in. deflection was measured. Between 45 and 55 minutes in air, deflection reached a maximum of 0.064 in., then the specimen began to straighten. After 1 hour and 20 minutes in air, the total deflection was 0.051 in., i.e., the tube had straightened 0.013 in. from its point of maximum deflection. The specimen continued to support the load with no change of deflection until the test was stopped after another 30 minutes. Subsequent fluorescent-penetrant examination indicated cracking on the compressive side. It is thought that after the point of maximum deflection was reached the uranium oxide transformation, accompanied by cracking and volumetric expansion, caused linear expansion of the compressive side relative to the tensile side, resulting in the straightening of the specimen. This may indicate that compression and tension have different effects on the rate of the uranium oxide transformations.

/md